Generation and Validation of Transmitochondrial Cybrid and Platelet Models to Investigate the Effect of Mitochondrial Genotype upon Drug-Induced Liver Injury

Thesis submitted in accordance with the requirements of the University of Liverpool for the degree of Doctor of Philosophy

By

Amy Louise Ball

November 2018

Declaration

This thesis is the result of my own work. The material contained within this thesis has not been presented, nor is currently being presented, either wholly or in part for any other degree or qualification.

Amy Louise Ball

This research was carried out in the Department of Molecular and Clinical Pharmacology, University of Liverpool, UK, in collaboration with GlaxoSmithKline.

CONTENTS

ABSTRACT

Idiosyncratic drug-induced liver injury (DILI) is a major concern for patient health and the pharmaceutical industry. Idiosyncratic DILI is characterised by a complex dose-response relationship, lack of predictivity from the primary pharmacology of a drug and significant interindividual variability, all of which contribute towards the limited preclinical prediction of these reactions.

Drug-induced mitochondrial dysfunction is implicated in the onset of DILI, supported by the fact that 50 % of drugs with a black box warning for hepatotoxicity also contain a mitochondrial liability. Mitochondria are also a source of the interindividual variation which underpins idiosyncratic DILI; mitochondria contain multiple copies of their own genome, mitochondrial DNA (mtDNA), which has been found to induce changes in mitochondrial function. Currently, there is limited incorporation of interindividual variation into preclinical models of mitochondrial dysfunction and DILI. This may contribute towards drug attrition.

The overall aim of this research was therefore to generate and characterise a personalised *in vitro* hepatic model which can be used for the preclinical assessment of the effect of mtDNA variation upon mitochondrial function and susceptibility to dysfunction induced by compounds associated with idiosyncratic DILI.

HepG2 transmitochondrial cybrids, an *in vitro* hepatic model, were generated for the first time by the fusion of platelets from volunteers of known mitochondrial genotype, with HepG2 rho zero cells (devoid of mtDNA). This cell line was selected as HepG2 cells are the most commonly used cell line during preclinical hepatotoxicity testing, therefore the personalisation of this model has great utility.

Following the assessment of HepG2 cell mitochondrial dysfunction induced by test compounds associated with idiosyncratic DILI (flutamide and tolcapone) alongside non-hepatotoxic structural analogues (bicalutamide and entacapone) and metabolites (2-hydroxyflutamide), 384 volunteers were recruited for whole mitochondrial genome sequencing. From this cohort, 30 participants from 4 common UK mitochondrial haplogroups (H, J, T, and U) were recruited to donate platelets for mitochondrial (dys)function testing using extracellular flux analysis. Subsequently, HepG2 transmitochondrial cybrids were generated from volunteers of haplogroups H and J prior to the assessment of basal mitochondrial function and compound-induced dysfunction. Taken together, extracellular flux analysis, ATP content assays and studies of mitochondrial dynamics in cybrids indicated

a differential susceptibility to mitochondrial dysfunction dependent on mitochondrial haplogroup. Specifically, haplogroup J conferred an increase in susceptibility to mitochondrial perturbations associated with tolcapone whereas haplogroup H appeared to confer a degree of protection.

To conclude, HepG2 transmitochondrial cybrids are able to provide preclinical representation of the mtDNA variation which may contribute towards the idiosyncrasy of some cases of DILI. The identification of mitochondrial haplogroups associated with differential susceptibility to mitochondrial dysfunction bodes well for future study plans which aim to differentiate individuals at the subhaplogroup level. When considered alongside other factors implicated in the onset of idiosyncratic DILI, continued work in this area has potential future clinical utility in the identification of patients whom can be safely and effectively treated with compounds such as tolcapone, which are currently withdrawn due to the risk of idiosyncratic DILI.

ACKNOWLEDGEMENTS

I would firstly like to thank my supervisors, Dr Amy Chadwick, Dr Ana Alfirevic and Dr Jon Lyon as well as the MRC and GSK, for giving me the opportunity to undertake this PhD project and for your guidance throughout. A special thanks must go to Amy. You've always been just a knock on the door away and you've given me the freedom to make this project my own whilst also being there to support and guide me, thank you.

I would like to extend this thanks to all past and present members of Team Bioenergetics: James, Oisin, Ross, Sammie, Sophie, Laleh and Carol. You have all supported me, whether it be by comforting me when my cybrids failed for what felt like the millionth time, bringing along some gluten free snacks to the lab meeting, or just making me laugh when I really needed it. Sophie, thank you for letting me stay with you in Liverpool while I finished writing this thesis, you have no idea how many M6 traffic jams you've saved me from. You're a star.

There is a long list of people in Liverpool I'd like to thank for the last four years. To everyone (especially Abby), who has engaged in highly inappropriate conversation with me over lunch, those 30 minutes away from the lab (almost) everyday have kept me sane and certainly informed me on a wide range of subjects. To all who have shared labs with me, thanks for not objecting to me having Radio City 2 on at full blast to get me through my Seahorse experiments. A special mention must also go to Sammie, to share a lab group and flat with someone for three years is quite something and I don't think there's a bond quite like it.

It would be impossible to thank my Mum enough, you've always worked so hard to give me every opportunity and I appreciate you more than you will ever know. To Susannah, the original Dr Ball, you always know the right thing to say, having you at the end of the phone over these past few years has been invaluable. Mark, you haven't always known the right thing to say, but thank you for always being there. George, despite being 200 miles away for most of my PhD you have been right by my side throughout. Thank you for being so patient with me and doing your best to understand the trials and tribulations of cybrids, you're a gem. To Grandma and Grandpa, a good chat about Brexit, cup of coffee and a wedge of cake with you both at the weekend is just what the doctor ordered, thank you.

Finally, I would like to dedicate this thesis to my late Grandad, Ivan Davies, Poppom. You have always nurtured the inquisition in me and to know we graduate from the same University, albeit 64 years apart, is an honour. I know you would have read this thesis from start to finish and I hope I have made you proud.

PUBLICATIONS

A.L. Ball, L. Kamalian, A. Alfirevic, J.J. Lyon, A.E. Chadwick, Identification of the Additional Mitochondrial Liabilities of 2-Hydroxyflutamide When Compared With its Parent Compound, Flutamide in HepG2 Cells, Toxicol Sci. (2016). doi:10.1093/toxsci/kfw126.

A.L. Ball, L. Kamalian, C.E. Jolly, A.E. Chadwick, Evaluating Mitotoxicity as Either a Single or Multi-Mechanistic Insult in the Context of Hepatotoxicity, Mitochondrial Dysfunct. Caused by Drugs Environ. Toxicants. (2018). doi:10.1002/9781119329725.ch6.

A.L. Ball, A. Alfirevic, J.J. Lyon, A.E. Chadwick, Assessment of Mitochondrial Function in Platelets Derived from Healthy Volunteers of Known Mitochondrial Genotype. *Manuscript in preparation* (2019).

A.L. Ball, A. Alfirevic, J.J. Lyon, A.E. Chadwick, The Role of MtDNA Variation in Drug Response: a Systematic Review**.** *Manuscript in preparation* (2019)

A.L. Ball, C.E. Jolly, A. Alfirevic, J.J. Lyon, A.E. Chadwick, Protocols: The Generation of HepG2 Transmitochondrial Cybrids. *Manuscript in preparation* (2019).

A.L. Ball, A. Alfirevic, J.J. Lyon, A.E. Chadwick, *In vitro* assessment of differential susceptibility to drug-induced mitochondrial dysfunction between mitochondrial haplogroups H and J. *Manuscript in preparation* (2019).

ABBREVIATIONS

ADP	Adenosine diphosphate
AIF	Apoptosis-inducing factor
AMP	Adenosine monophosphate
ANT	Adenine nucleotide translocator
Apaf-1	Apoptotic protease activating factor 1
ATP	Adenosine triphosphate
BCA	Bicinchoninic acid
BP	Buffering power
BSA	Bovine serum albumin
BSEP	Bile salt export pump
BWA	Burrows-Wheeler alignment tool
C_0t	Cycle to normalise amounts of PCR amplicons
CamK	Ca^{2+}-calmodulin dependent kinase
cAMP	Cyclic adenosine monophosphate
CAT	Carnitine acyltransferase
C_{max}	Maximum serum concentration of a drug after dosing
CoA	Coenzyme A
Complex I	Nicotinamide adenine dinucleotide-ubiquinone oxidoreductase
Complex II	Succinate dehydrogenase
Complex III	Ubiquinol-cytochrome *c* oxidoreductase
Complex IV	Cytochrome *c* oxidase
Complex V	Adenosine triphosphate synthase
CoQ	Ubiquinone
$CoQH_2$	Ubiquinol
COX	Cytochrome *c* oxidase
CPT	Carnitine palmitoyltransferase
C_t	Cycle threshold
CuA/B	Copper centre associated with cytochrome *a*

CYP450	Cytochrome P450
Cyt *a*/*b*/*c*1	Cytochrome *a*/*b*/*c*1
DAMP	Damage-associated molecular pattern
DILI	Drug-induced liver injury
DMEM	Dulbecco's modified Eagle's medium
Drp1	Dynamin-related protein 1
dsDNA	Double-stranded DNA
EC_{150}	Concentration of compound which causes a 50 % increase in the variable of interest compared to control
EC_{50}	Concentration of compound which causes a 50 % decrease in the variable of interest compared to control
ECACC	European Collection of Cell Cultures
ECAR	Extracellular acidification rate
EDTA	Ethylenediaminetetraacetic acid
EGTA	Ethylene glycol-bis(β-aminoethyl ether)-N,N,N',N'-tetraacetic acid
ER	Endoplasmic reticulum
EtBr	Ethidium bromide
ETC	Electron transport chain
$FADH_2$	Flavin adenine dinucleotide
FAM	Carboxyfluorescein
FAO	Fatty acid oxidation
FAT	Fatty acid translocase
FBS	Foetal bovine serum
FCCP	Carbonyl cyanide 4-(trifluoromethoxy) phenylhydrazone
FDA	US Food and Drug Administration
Fe-S	Iron-sulphur
FHH	Freshly isolated human hepatocytes
Fis1	Mitochondrial fission 1 protein
FMN	Flavin mononucleotide
GATK	Genome analysis toolkit

GTP	Guanosine triphosphate
H_20_2	Hydrogen peroxide
HEPES	4-(2-hydroxyethyl)-1-piperazineethanesulfonic acid)
HIF-1α	Hypoxia-inducible factor 1-alpha
HLA	Human leukocyte antigen
Hsp70	Heat shock protein 70
HSP	Heavy strand promoter
iDILI	Idiosyncratic drug-induced liver injury
IFC	Integrated fluidics circuit
IM space	Intermembrane space
INT	Iodonitrotetrazolium
KDa	Kilo Daltons
LDH	Lactate dehydrogenase
L-OPA1	Long fragment optic atrophy 1
LSP	Light strand promoter
MAPK	Mitogen-activated protein kinase
MAS	Mitochondrial assay solution
MFF	Mitochondrial fission factor
MGB	Minor groove binder
MIDD	Mitochondrially inherited diabetes and deafness
m-MPI	Mitochondrial membrane potential indicator
MPTP	Mitochondrial permeability transition pore
MRCA	Most recent common ancestor
mtDNA	Mitochondrial DNA
N/A	Not applicable
N/D	Not determined
NADH	Nicotinamide adenine dinucleotide
ND	NADH dehydrogenase
NF-κB	Nuclear factor kappa-light-chain-enhancer of activated B cells
Nrf1/2	Nuclear factor E2-related factor 1/2

NS	Non-synonymous
$O_2^{-\cdot}$	Superoxide radical
OCR	Oxygen consumption rate
O_H	Origin of heavy strand replication
O_L	Origin of light strand replication
OMA1	Metalloendopeptidase
OXPHOS	Oxidative phosphorylation
PAM	Presequence-translocase-associated motor
PCR	Polymerase chain reaction
PEG	Polethylene glycol
PGC1α	Peroxisome proliferator-activated gamma coactivator-alpha
PGE_2	Prostaglandin E_2
PGI_2	Prostaglandin I_2
PINK1	Phosphatase and tensin homolog-induced putative kinase 1
PKA	Protein kinase A
POLRMT	Mitochondrial RNA polymerase
PPR_{gly}	Glycolytic proton production rate
PRP	Platelet-rich plasma
PTEN	Phosphatase and tensin homolog
PVA	Polyvinyl alcohol
Q	Coenzyme Q
QH_2	Reduced Coenzyme Q
Q_N	$CoQH_2$ binding site (N/matrix side)
Q_P	$CoQH_2$ binding site (P/intermembrane space side)
qPCR	Quantitative polymerase chain reaction
rCRS	Revised Cambridge reference sequence
RET	Reverse electron transport
RNase P	Ribonuclease P RNA component H1
RNS	Reactive nitrogen species
ROI	Region of interest

ROS	Reactive oxygen species
RT-PCR	Real-time PCR
SAM	Sorting and assembly machinery
SAM	Sequence alignment/map
SDHA/B	Succinate dehydrogenase subunit A/B
SDS-PAGE	Sodium dodecyl sulphate-polyacrylamide gel electrophoresis
SEM	Standard error of the mean
SNP	Single nucleotide polymorphism
SOD 1/2	Superoxide dismutase 1/2
S-OPA1	Soluble fragment optic atrophy 1
$T_{1/2}$	Time taken for the concentration of the drug in the plasma to be reduced by 50 %
TAMRA	6-carboxytetramethyl-rhodamine
TBS-T	Tris-buffered saline-tween
TCA	Tricarboxylic acid
TERT	Telomerase reverse transcriptase
TFAM	Mitochondrial transcription factor A
TFB2M	Mitochondrial transcription factor B2
TIM	Translocase of the inner membrane
TMPD	N,N,N',N'-tetramethyl-*p*-phenylenediamine
TOM	Translocase of the outer membrane
UCP4	Uncoupling protein 4
UDP	Uridine diphosphate
VCF	Variant calling format
VIC	2'-chloro-7'phenyl-1,4-dichloro-6-carboxy-fluorescein
WT	Wild-type
XF	Extracellular flux
$\Delta\psi_m$	Mitochondrial membrane potential
ρ0	Rho zero

Chapter 1

General Introduction

CONTENTS

1.1 INTRODUCTION

Adverse drug reactions such as drug-induced liver injury (DILI) are a significant risk to patient health as well as a burden to the pharmaceutical industry, regulatory authorities and health services. Although DILI is considered to be rare (19.1 cases per 100 000 inhabitants), it is a major cause of drug withdrawal due to its associated morbidity and mortality (Leise *et al.*, 2014). The true incidence of DILI is difficult to determine due to the lack of a simple objective test and the high number of patients whom are prescribed multiple medications; this is problematic when identifying the causative drug (Pandit *et al.*, 2012; Regev, 2014).

DILI can be broadly divided into two categories; idiosyncratic and intrinsic injury. Intrinsic DILI is more common than idiosyncratic DILI (iDILI) but is less likely to lead to drug withdrawal from the market due to its dose-dependent nature and relative predictivity from the primary pharmacology of the drug (Russmann *et al.*, 2009). iDILI however, is characterised by a complex dose-response relationship, lack of predictivity from the primary pharmacology of a drug and significant interindividual variability. This means that despite being less common, iDILI can be viewed as far more costly, both in terms of patient health and from an economic perspective (Fontana, 2014).

Despite a limited understanding of the exact mechanisms that underlie cases of iDILI, it is agreed to be a product of interactions between the environment, host factors and the drug (Figure 1.1). All of these converge at the common point of hepatocyte death, with this manifesting clinically as hepatocellular injury and/or cholestasis (Yuan and Kaplowitz, 2013).

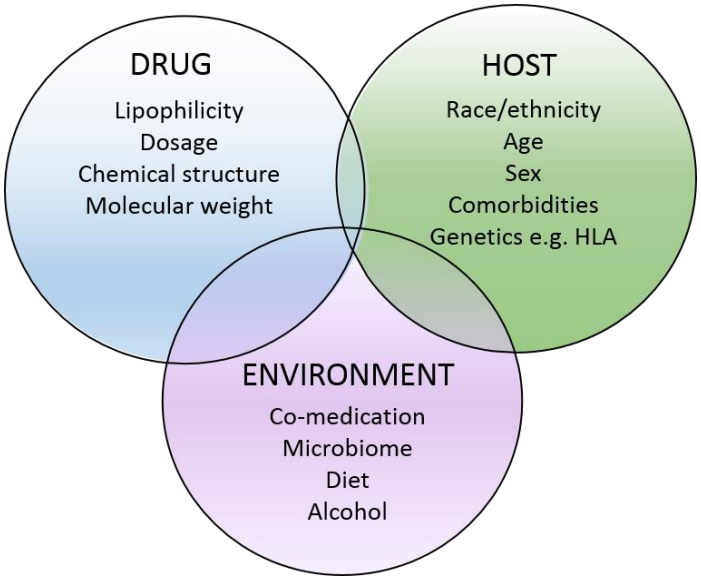

Figure 1.1. Idiosyncratic drug induced liver injury is a complex interplay of drug, host and environmental factors. Abbreviations: HLA, human leukocyte antigen (Maddukuri and Bonkovsky, 2014)**.**

Mitochondria are ubiquitous intracellular organelles whose main function is to produce energy in the form of adenosine triphosphate (ATP) (Kühlbrandt, 2015). Drug-induced mitochondrial dysfunction is implicated in the onset of DILI, supported by the fact that 50 % of drugs with a black box warning for hepatotoxicity also contain a mitochondrial liability, with many of these drugs associated specifically with iDILI (Table 1.1) (Dykens and Will, 2007). Mitochondria may also be a source of the interindividual variation which underpins iDILI; mitochondria contain multiple copies of their own genome, mitochondrial DNA (mtDNA) which has been found to induce changes in mitochondrial function (more information in Table 1.3) (Kenney *et al.*, 2014; Gómez-Durán *et al.*, 2010; Gomez-Duran *et al.*, 2012).

Table 1.1. Compounds evidenced to cause idiosyncratic drug-induced liver injury which have mitochondrial liabilities.

Compound	Class	Mitochondrial perturbation(s)	FDA status	Reference
Amiodarone	Antiarrhythmic	OXPHOS uncoupler and FAO inhibition	Boxed warning	(Fromenty *et al.*, 1990; Kennedy *et al.*, 1996; Begriche *et al.*, 2011)
Buspirone	Anxiolytic	ETC inhibition	Available	(Dykens *et al.*, 2008)
Diclofenac	Anti-inflammatory	OXPHOS uncoupler	Boxed warning	(Lim *et al.*, 2006; Begriche *et al.*, 2011)
Didanosine	Antiviral	MtDNA depletion	Boxed warning	(Walker *et al.*, 2004; Labbe *et al.*, 2008)
Flutamide	Anticancer	ETC inhibition	Boxed warning	(Coe *et al.*, 2007; Fau *et al.*, 1994)
Ketoconazole	Antifungal	ETC inhibition	Boxed warning	(Rodriguez and Acosta, 1996)
Nefazodone	Antidepressant	ETC inhibition	Boxed warning	(Dykens *et al.*, 2008)
Perhexiline	Antianginal	ETC and FAO inhibition	Withdrawn	(Kennedy *et al.*, 1996; Begriche *et al.*, 2011)
Pioglitazone	Antidiabetic	ETC inhibition	Boxed warning	(Garcia-Ruiz *et al.*, 2013)
Stavudine	Antiviral	MtDNA depletion	Boxed warning	(Walker *et al.*, 2004)
Tamoxifen	Anticancer	ETC and FAO inhibition	Boxed warning	(Larosche *et al.*, 2007; Begriche *et al.*, 2011)
Tolcapone	COMT inhibitor	ETC uncoupler	Withdrawn	(Korlipara *et al.*, 2004)
Troglitazone	Antidiabetic	OXPHOS uncoupler and ETC inhibition	Withdrawn	(Scatena *et al.*, 2004)
Valproic acid	Antiepileptic	FAO inhibition	Boxed warning	(Begriche *et al.*, 2011)
Zalcitabine	Antiviral	MtDNA depletion	Withdrawn	(Walker *et al.*, 2004)

Abbreviations: COMT, Catechol-methyl transferase; ETC, electron transport chain; FAO, fatty acid oxidation; mtDNA, mitochondrial DNA; FDA, US Food and Drug Administration; OXPHOS, oxidative phosphorylation.

Currently, there is limited incorporation of interindividual variation into the preclinical models used to test the hepatotoxic potential of compounds, this may contribute towards the limited preclinical prediction of this costly adverse drug reaction.

This thesis describes the generation of a novel *in vitro* hepatic model which is postulated to be able to account for interindividual variation in the mitochondrial genome. In addition, the utility of this model in identifying altered susceptibility to mitochondrial dysfunction induced by compounds associated with iDILI has been investigated.

1.2 MITOCHONDRIAL STRUCTURE AND FUNCTION

1.2.1 The origin of mitochondria

Mitochondria are present in almost all eukaryotic cells and according to the endosymbiotic theory, originate from free-living bacteria which were engulfed by cells from which a symbiotic relationship developed. Following the merger of these glycolytic cells with oxidative mitochondria, it is thought that most of the mtDNA was transferred to the nuclear DNA, with the mtDNA only retaining the genetic code for a selection of core mitochondrial proteins. Mitochondria can therefore be considered as semiautonomous (Whelan and Zuckerbraun, 2013).

1.2.2 Mitochondrial structure

Each mitochondrion contains two highly specialised membranes, the inner and outer mitochondrial membranes. These create two separate mitochondrial compartments, the matrix which is surrounded by the inner mitochondrial membrane, and the intermembrane space, which lies between the inner and outer mitochondrial membranes (Figure 1.2). The outer membrane has a similar phospholipid content to the cell surface membrane and is rich in voltage-dependent anion channels, allowing compounds < 5 KDa to pass freely. Resultantly, the intermembrane space is almost of chemical equivalence to the cytosol (Kühlbrandt, 2015; Wojtczak and Zabłocki, 2008).

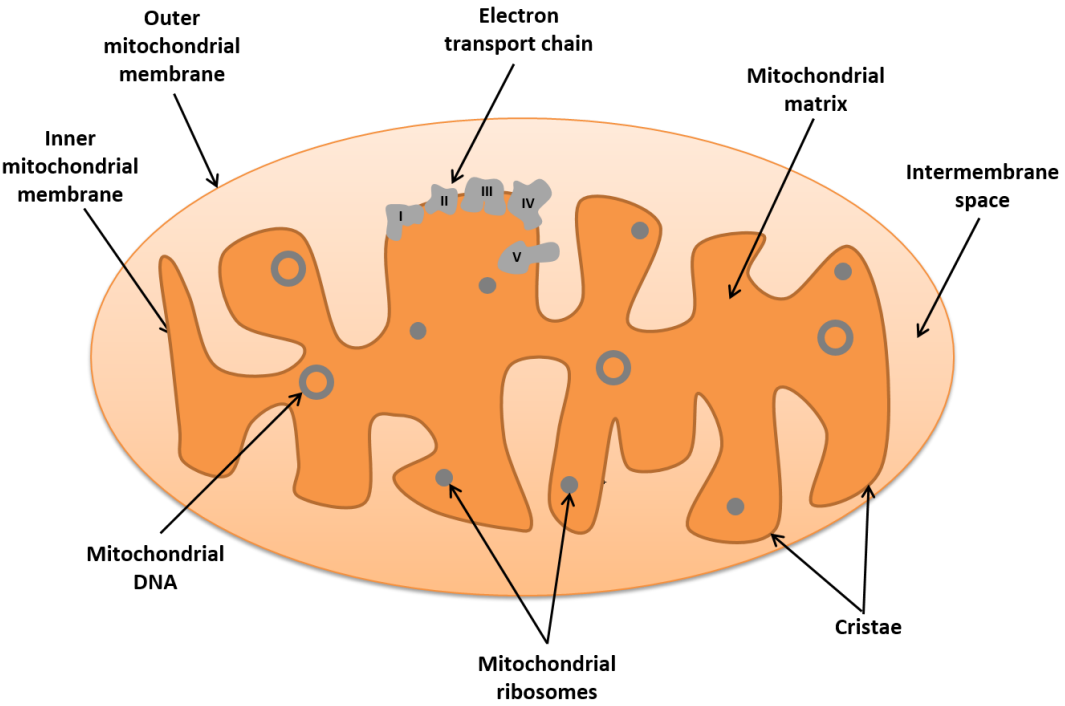

Figure 1.2. Schematic representation of key mitochondrial structures. Mitochondria are host to four main entities: the outer membrane, intermembrane space, inner membrane and matrix, each with a distinct composition. The mitochondrial matrix contains a dynamic mix of enzymatic proteins, as well as multiple copies of the mitochondrial genome and ribosomes required for the translation of mitochondrial DNA-encoded proteins.

Conversely, the inner mitochondrial membrane is extremely impermeable which can be attributed to its high proportion of proteins in comparison to phospholipids. This is crucial for the generation of a proton gradient and a voltage difference of up to 180 mV across the 100 nm-wide membrane (Wojtczak and Zabłocki, 2008). Maintenance of a proton gradient is also aided by the abundance of cardiolipin in this membrane which confers a negative surface charge. Cardiolipin has also been found to participate in the biogenesis and assembly of electron transport chain (ETC) components, and the function of adenine nucleotide translocators (ANTs). Unlike the outer mitochondrial membrane, the inner membrane is highly convoluted, forming cristae which project into the matrix and provide an increased surface area (Figure 1.2) (Paradies *et al.*, 2014).

The mitochondrial matrix is bound by the inner mitochondrial membrane and harbours the majority of mitochondrial proteins including a variety of enzymes involved in the tricarboxylic acid (TCA) cycle, fatty acid oxidation (FAO) and haem synthesis. The matrix also harbours multiple copies of mtDNA along with the necessary replicative machinery. By contrast, the intermembrane space contains less proteins than the matrix, the most prominent of which

is cytochrome *c* (tethered to the inner mitochondrial membrane) which induces apoptosis upon its release into the cytosol (Stein and Imai, 2012; Wojtczak and Zabłocki, 2008).

1.2.3 Oxidative phosphorylation

1.2.3.1 Introduction

Oxidative phosphorylation is the primary source of cellular ATP generation and consists of two coupled processes, the oxidation of reduced substrates and the phosphorylation of adenosine diphosphate (ADP). The latter is an energy consuming process performed by F_o/F_1 ATPase (ATP synthase) which relies upon the energy released from the oxidation of reduced substrates in the ETC. This coupling is highly dependent on the impermeability of the inner mitochondrial membrane and generation of a proton motive force. This drives the translocation of protons from the intermembrane space into the matrix via ATP synthase (Figure 1.3). This process enables approximately 15-fold more ATP to be produced than by glycolysis alone (Hüttemann *et al.*, 2007; Wojtczak and Zabłocki, 2008).

The ETC is composed of over 85 proteins assembled into 4 complexes: NADH (Nicotinamide adenine dinucleotide)-ubiquinone oxidoreductase (complex I), succinate dehydrogenase (complex II), ubiquinol-cytochrome *c* oxidoreductase (complex III) and cytochrome *c* oxidase (complex IV). Together, these complexes, along with the mobile electron carriers, ubiquinone and cytochrome *c*, catalyse the electron transfer from reduced donors, NADH and flavin adenine dinucleotide ($FADH_2$) to molecular oxygen (Figure 1.3).

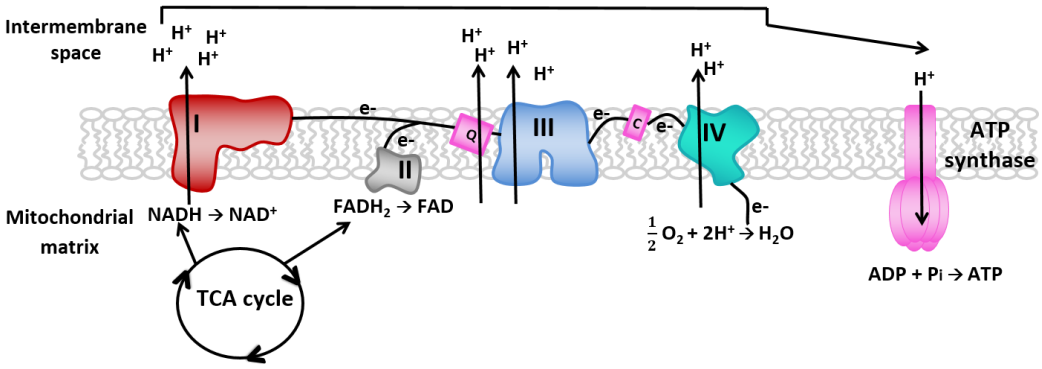

Figure 1.3. Oxidative phosphorylation. A schematic overview of oxidative phosphorylation. The mitochondrial respiratory chain comprises five protein complexes (I-IV and ATP synthase (V)) embedded in the inner mitochondrial membrane. Electrons from NADH and $FADH_2$ are transferred to complexes I and II respectively. These electrons are transferred via a series of electron donors and acceptors to the final electron acceptor, O_2. This electron flow is associated with a significant release of free energy which is used to pump protons across the inner mitochondrial membrane into the intermembrane space. This generates an electrochemical gradient which is used to drive ATP synthesis

and release (Nicholls and Ferguson, 2003). Abbreviations: $FADH_2$, flavin adenine dinucleotide; NADH, nicotinamide adenine dinucleotide; TCA, tricarboxylic acid.

Complex I is the primary entry point for low-potential, high free energy electrons from NADH. As electrons travel down the ETC their free energy decreases alongside the steady increase in the redox potential of their carriers, ending with oxygen which has the highest redox potential. The free energy released during this process enables the thermodynamically unfavourable active pumping of protons from the mitochondrial matrix to the inter-membrane space to take place (Miller *et al.*, 2002). The mechanism of proton pumping by complexes I, III and IV is not well understood however it is proposed that the millisecond reduced state of iron-sulphur (Fe-S) clusters in the complexes initiates a conformational change in lysine residues allowing channel formation (Sack, 2006).

1.2.3.2 Generation of an electrochemical gradient

1.2.3.2.1 Complex I

Reaction: $NADH + H^+ + CoQ \rightarrow NAD^+ + CoQH_2$

Protons pumped into intermembrane space: 4

Complex I binds NADH and two electrons from this are transferred to the flavin mononucleotide (FMN) of complex I to produce NAD^+ and $FMNH_2$. Electrons are then transferred to Fe-S complexes (at least seven are known to be present in complex I) and to coenzyme Q (ubiquinone/CoQ), one at a time (Figure 1.4A). For every two electrons transferred from NADH to CoQ, there is the active transport of four H^+ ions into the intermembrane space (Grover, 2006).

1.2.3.2.2 Complex II

Reaction: Succinate + CoQ → fumarate + $CoQH_2$

Protons pumped into intermembrane space: 0

Complex II offers an alternate point of electron entry into the ETC and is the only enzyme of the TCA cycle which is also an integral membrane protein. Here, the oxidation of succinate to fumarate in the TCA cycle is catalysed and $FADH_2$ is produced as a result. Two electrons (one at a time) are transferred from $FADH_2$ to the Fe-S centres, generating FAD and reducing $2Fe^{3+}$ to $2Fe^{2+}$. The electrons are then transferred to CoQ to generate $CoQH_2$ (ubiquinol; Figure 1.4B). In contrast to complex I, the transfer of electrons from $FADH_2$ to CoQ in complex II does not result in the pumping of protons into the intermembrane space, so the amount of ATP produced via complex II entry is less than with complex I (Berg *et al.*, 2002).

1.2.3.2.3 Complex III

Reaction: QH_2 + 2 cytochrome *c* (Fe^{III}) + 2 H^+_{in} → Q + 2 cytochrome *c* (Fe^{II}) + 4 H^+_{out}

Protons pumped into intermembrane space: 4

$CoQH_2$ diffuses through the lipid bilayer to the $CoQH_2$ binding site (Q_p) in complex III. One electron is transferred from $CoQH_2$ to the Rieske protein (a Fe-S protein) which then transfers the electron to cytochrome *c*1 and reduces the first molecule of cytochrome *c*. This allows the transport of two protons into the intermembrane space whilst $CoQH_2$ (now $CoQH\bullet^-$) remains bound to the Q_p site (Figure 1.4C).

The second electron is then transferred to a B_L haem, converting $CoQH\bullet^-$ to CoQ which now diffuses away from the Q_p binding site. The B_L haem then transfers its electron to the B_H haem and to a second molecule of $CoQH_2$ which is bound at the Q_N site to generate a second $CoQH\bullet^-$ which remains bound at the Q_N site (Figure 1.4C).

A third molecule of $CoQH_2$ then binds to the Q_p site, one electron from this is transferred to the Rieske protein which is transferred to cytochrome *c*1 and is picked up by cytochrome *c*. This releases another two protons into the intermembrane space (Figure 1.4D).

The second electron is then transferred to the B_L haem to generate a second molecule of reoxidised CoQ. The B_L haem then transfers its electrons to $CoQH\bullet^-$ at the Q_N site via the B_H haem. This generates CoQ, which after the uptake of two protons from the matrix is reduced to $CoQH_2$ and diffuses from the Q_N binding site (Figure 1.4D) (Grover, 2006).

1.2.3.2.4 Complex IV

Reaction: 4 cytochrome *c* (Fe^{2+}) + $4H^+$ + O_2 → 4 cytochrome *c* (Fe^{3+}) + 2 H_20.

Protons pumped into intermembrane space: 2

Reduced cytochrome *c* diffuses through the intermembrane space and transfers its electron to CuA (associated with cytochrome *a*) to enable cytochrome *c* dissociation. CuA then transfers the electron to CuB (associated with cytochrome *a3*) (Figure 1.4E). A second cytochrome *c* then binds and transfers its electron to cytochrome *a3*, which now has two electrons bound, allowing the binding of molecular oxygen (Figure 1.4E).

A third electron from another cytochrome *c* is then passed to cytochrome *a3* and this electron, together with two protons taken up from the matrix leads to cleavage of the O=O bond and the generation of a Fe^{4+} centre (Figure 1.4F). The fourth electron from a fourth cytochrome *c* molecule flows through to the cytochrome *a*3 CuB centre, reducing the Fe^{4+}=O to Fe^{3+}, with the oxygen atom picking up two protons simultaneously, to generate H_20 (Figure 1.4G) (Grover, 2006).

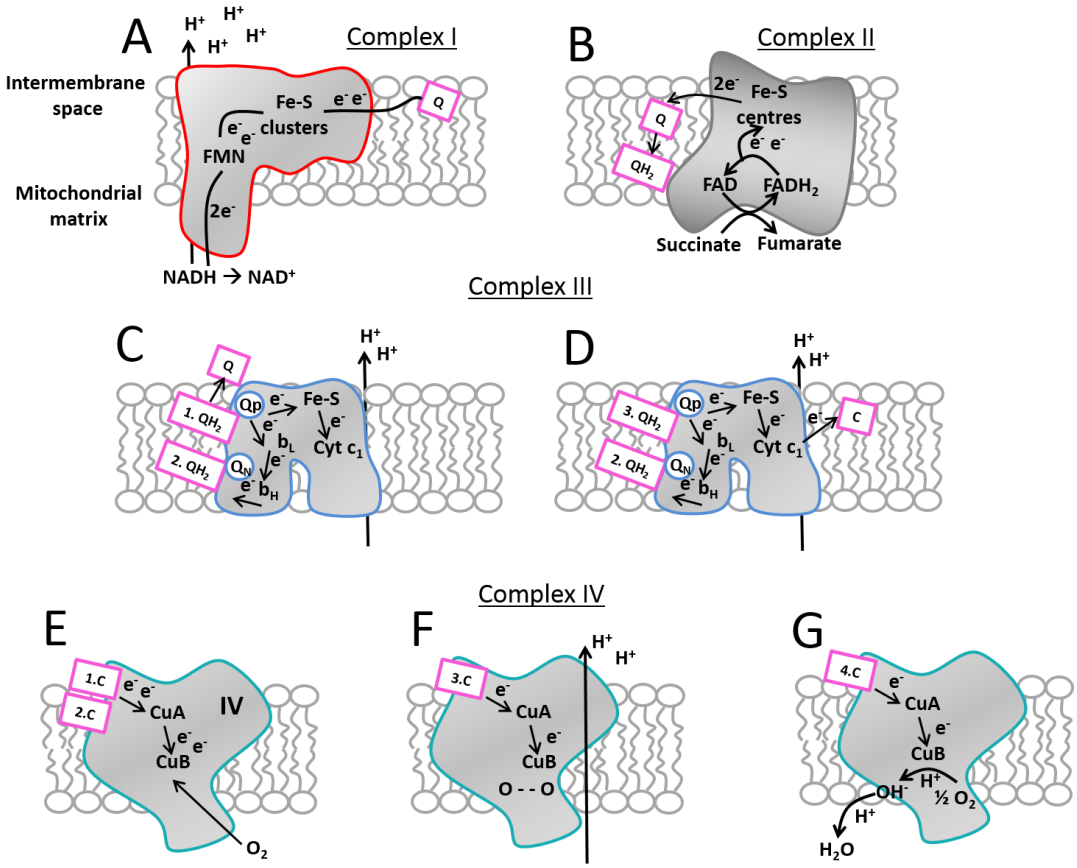

Figure 1.4. Electron flow in the electron transport chain. Abbreviations: b_H, haem b_H; b_L, haem b_L; C, Cytochrome *c*; CuA, copper centre associated with cytochrome *a*; CuB, copper centre associated with cytochrome *a3*; Cyt c_1, cytochrome *c1*; Fe-S, iron-sulphur cluster; FMN, flavin mononucleotide; Q, coenzyme Q; QH_2, reduced coenzyme Q; Q_N, $CoQH_2$ binding site (N/matrix side); Q_P, $CoQH_2$ binding site (P/intermembrane space side) (Grover, 2006).

1.2.3.3 ATP generation

During oxidative phosphorylation, protons pumped into the intermembrane space diffuse into the matrix via the F_O portion of ATP synthase which forms a proton channel (Figure 1.5A). This flow of protons is aided by the contrasting properties of the negative, alkaline matrix and the positive, acidic protons, enabling the generation of an electrochemical gradient. The energy of the electrochemical gradient is then used to constrain conformational changes in catalytic subunits of the F_1 portion of ATP synthase which enables the release of ATP. The translocation of 10 protons is required to generate 3 molecules of ATP (Figure 1.5B) (Sack, 2006).

1.2.3.4 Regulation of oxidative phosphorylation

Regulation of mitochondrial functions such as oxidative phosphorylation occurs through both long-term transcriptional changes and short-term post-transcriptional responses such as phosphorylation.

All components of the ETC can be phosphorylated, including the mobile electron carrier, cytochrome *c*. For example, increased intracellular cyclic adenosine monophosphate (cAMP) can stimulate the phosphorylation of respiratory complexes by protein kinase A (PKA) (Hüttemann *et al.*, 2007). This post-transcriptional modification is emerging as a central mechanism in the regulation of mitochondrial ETC function.

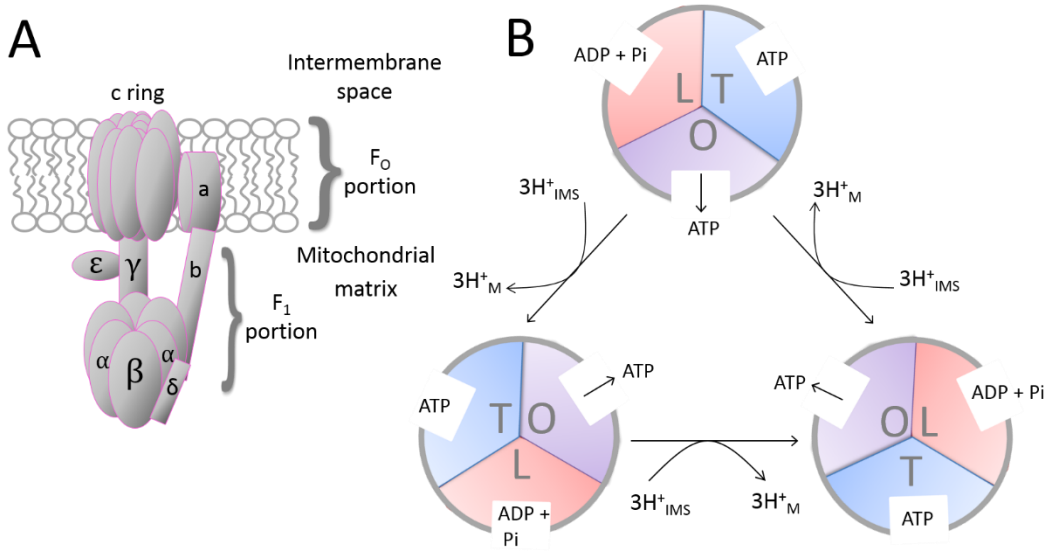

Figure 1.5. ATP generation by ATP synthase. A: ATP synthase consists of two functional domains, the F_O portion and F_1 portion. The F_O portion is bound to the inner mitochondrial membrane whereas the F_1 portion is soluble and is situated in the matrix. F_O consists of a 10 subunit c ring which forms the central proton selective channel and subunits *a* and *b*, the latter of which extends from the membrane to connect F_O to F_1. F_1 is composed of three copies of α and β subunits and one copy of subunits γ, ε and δ. Subunits α and β are positioned alternately around subunit γ which connects the cluster of α and β subunits with the F_O membrane portion. B: The three catalytic centres of ATP synthase are situated on β subunits and can assume three different conformations: O, low affinity for ATP; L, loosely binds ADP and Pi; T, tightly binds ADP and Pi. Proton entry to the matrix via F_O forces subunit γ to rotate whilst α and β subunits remain stationary. For one 360° turn, 10 protons return to the matrix and 3 molecules of ATP are released. Abbreviations: IMS, intermembrane space; M, mitochondrial matrix (Jonckheere *et al.*, 2012; Wojtczak and Zabłocki, 2008; Devlin, 2011).

Oxidative phosphorylation is also heavily regulated by increased Ca^{2+} in the mitochondrial matrix; cytosolic Ca^{2+} transported by the Ca^{2+} uniporter activates the TCA cycle enzymes,

pyruvate dehydrogenase, α-ketoglutarate dehydrogenase and isocitrate dehydrogenase, important for the supply of electron donors $NADH_2$ and FADH. Ca^{2+} can also activate ATP synthase by the release of inhibitor proteins and cytochrome *c* oxidase by Ca^{2+}-dependent dephosphorylation. More recent findings have also shown that cytosolic Ca^{2+} is able to regulate oxidative phosphorylation by the control of glutamate transport into mitochondria (Gellerich *et al.*, 2010).

Dynamic organisation of the respiratory complexes provides additional regulation of oxidative phosphorylation (Acin-Perez and Enriquez, 2014). Originally, respiratory complexes were proposed to be closely packed to increase the efficiency of electron transport. This was later replaced by the fluid model in which each respiratory complex was viewed as an independent entity embedded in the inner mitochondrial membrane. Since, the plasticity model has generally replaced both proposals, predicting that respiratory complexes exist and function both as single complexes and together as supercomplexes. The mechanisms by which the distribution and organisation of supercomplexes are regulated remains poorly understood, nevertheless, this plasticity within the inner mitochondrial membrane is agreed to enable the short term regulation of metabolism and optimised fuel utilisation when required (Porras and Bai, 2015).

1.2.4 Additional features of mitochondria

1.2.4.1 Apoptosis

Apoptosis, often termed “programmed cell death” is a process to eliminate cells when their natural biological function has ended or when damage is to such an extent that it is deleterious to the organism as a whole. Apoptosis can proceed along either the intrinsic (mitochondrial) or extrinsic pathway (Elmore, 2007).

Intrinsic apoptosis is triggered by the permeabilisation of the outer mitochondrial membrane, which can occur by the opening of the mitochondrial permeability transition pore (MPTP) (Saelens *et al.*, 2004).

The MPTP is a multi-protein complex which spans both mitochondrial membranes and allows the passage of molecules < 1.5 KDa between the cytoplasm and mitochondrial matrix. The MPTP is triggered to open by mitochondrial reactive oxygen species (ROS) and Ca^{2+} accumulation; it is thought to be formed by several proteins including cyclophilin D, ANT and porin (Wojtczak and Zabłocki, 2008; Taddeo *et al.*, 2014; Halestrap, 2009; Giorgio *et al.*, 2009). Ca^{2+} accumulation is often as a result of stress-induced release of Ca^{2+} from ER stores.

1.2.4.2 Reactive oxygen species production

The majority of electrons which enter the ETC are used in the four-electron reduction of O_2 to H_2O at complex IV. However, electron leakage at prior sites in the ETC is predicted to account for much of the O_2 that undergoes only a one-electron reduction to form superoxide radicals ($O_2^{\bullet-}$) (Murphy, 2009).

Complex I is the primary site of $O_2^{\bullet-}$ generation in isolated mitochondria. $O_2^{\bullet-}$ generation is often a consequence of reverse electron transport (RET), which occurs when the CoQ pool is reduced in the presence of a significant proton motive force. This forces electrons back from $CoQH_2$ to complex I and so reduces NAD^+, increasing the NADH/NAD^+ ratio and leading to a reduced FMN site and $O_2^{\bullet-}$ production (Andreyev *et al.*, 2005; Kussmaul and Hirst, 2006; Kushnareva *et al.*, 2002). Known physiological roles of ROS include regulation of autophagy via the stabilisation of hypoxia-inducible factors (Poillet-Perez *et al.*, 2015).

1.2.4.3 Fatty acid oxidation

Mitochondrial FAO is the principal pathway for the oxidation of fatty acids and is significant in the production of ATP (Kunau *et al.*, 1995). In order for fatty acids to be oxidised in the mitochondria, they must first be transformed to enable passage across the mitochondrial membrane (Figure 1.6). One cycle of β-oxidation of long chain acyl CoA results in the production of one acetyl CoA which can enter the TCA cycle to produce NADH/$FADH_2$ which can donate electrons to the ETC, thereby generating ATP (Section 1.2.3.1) (Figure 1.6) (Miller *et al.*, 2002). The β-oxidation which occurs in the mitochondria enables the complete degradation of fatty acids, unlike α and Ω oxidation which occur in peroxisomes (named according to the carbon of the fatty acid which is oxidised) (Wanders *et al.*, 2011).

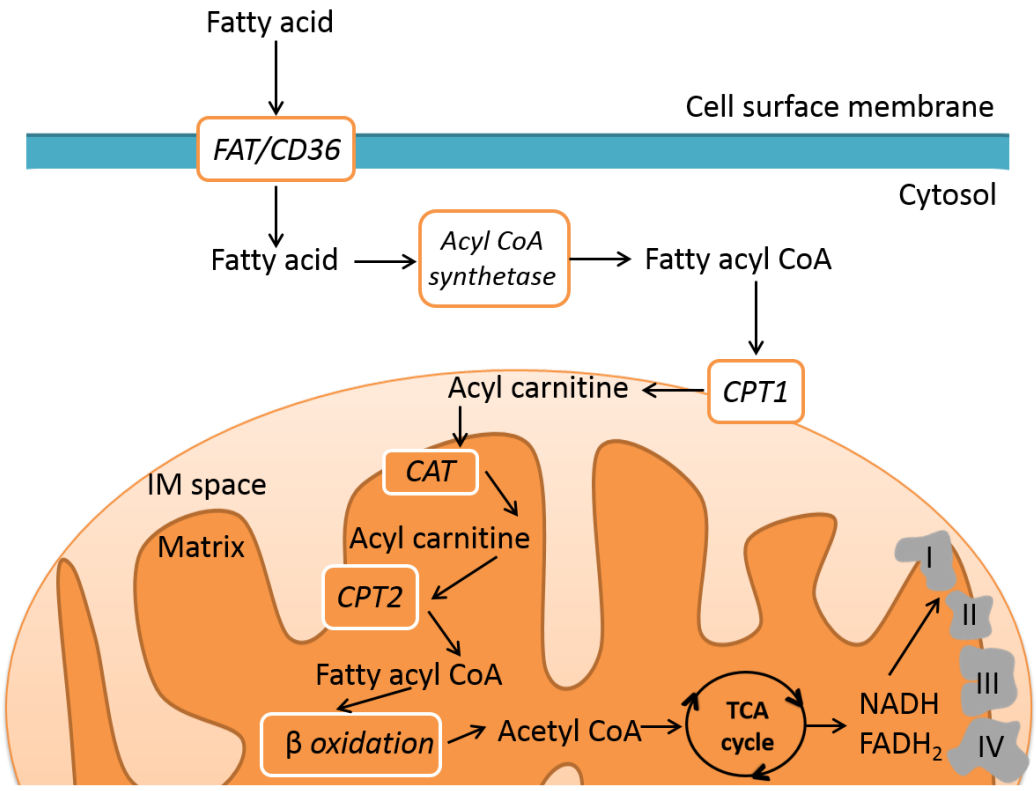

Figure 1.6. Fatty acid oxidation. Fatty acids primarily enter the cell via cell surface transporters including fatty acid translocase. Once in the cytosol, the fatty acids are activated by conjugation with coenzyme A in a reaction catalysed by acyl CoA synthetase, forming long-chain acyl CoA. Long-acyl CoAs are then converted to long-chain acylcarnitines by carnitine palmitoyltransferase 1. This enables the fatty acid moiety to be transported across the inner mitochondrial membrane via carnitine translocase which exchanges long-chain acylcarnitines for carnitine. An inner mitochondrial membrane carnitine palmitoyltransferase II then converts the long-chain acylcarnitine back to long-chain acyl CoA which can be metabolised via β-oxidation. The resultant acetyl CoA then enters the tricarboxylic acid cycle, generating NADH and $FADH_2$ which donate electrons to the electron transport chain (Fillmore *et al.*, 2011). Abbreviations: CAT, carnitine acyltransferase; CoA, coenzyme A; CPT, carnitine palmitoyltransferase; FAT, fatty acid translocase; IM space, intermembrane space; TCA, tricarboxylic acid.

1.2.5 Mitochondrial dynamics

1.2.5.1 Introduction

Mitochondria are extremely dynamic organelles undergoing cytoskeletal movement as well as fusion and fission. Cytoskeletal movement is mediated by mitochondrial localisation to microtubules, this is thought to enable long movement via motor protein transport, namely kinesins (anterograde) and dyneins (retrograde). Conversely, actin localisation is thought to enable tethering and shorter movements. This movement, alongside fusion and fission

determines the degree to which mitochondria form a network in the cell. The rates of these processes are influenced by both pathogenic and metabolic conditions and are important in the maintenance of a healthy mitochondrial network (Wu *et al.*, 2013).

1.2.5.2 Fission

Fission generates discrete mitochondria and is often the more active process in situations of low energy demand or when the removal of damaged mitochondria is required. Fission occurs when the guanosine triphosphate (GTP)ase, dynamin-related protein 1 (Drp1) is activated and translocates from the cytosol to the outer mitochondrial membrane where it oligomerises to form a "fission apparatus" guided by mitochondrial fission factor (MFF) and mitochondrial fission 1 protein (Fis1) (Figure 1.7). This initial activation of Drp1 is thought to be triggered by multiple sources such as phosphorylation by the Ca^{2+}-calmodulin dependent kinase (CamK). CamK is stimulated by an influx of Ca^{2+} from the extracellular environment as a result of oxidative stress (Ermak and Davies, 2002). Mitochondrial dynamics proteins 49 KDa and 51 KDa which are located in the outer mitochondrial membrane then form division-induced rings around mitochondria associated with oligomerised Drp1 which constrict and divide the organelle (Figure 1.7).

1.2.5.3 Fusion

Mitochondrial fusion generates an interconnected mitochondrial network and allows the mixing of matrix content (including mtDNA), metabolites and enzymes, as well as enhancing communication with the ER. This enhanced communication and spread of products throughout the entire mitochondrial compartment serves to optimise mitochondrial function, with fusion required for cells to reach maximal respiratory capacity (Westermann, 2012).

Fusion is mediated by mitofusin 1 and 2 in the outer mitochondrial membrane, these large GTPases transverse the outer mitochondrial membrane twice, with both the amino and carboxy termini facing the cytoplasm. Mitofusins bind to those on adjacent mitochondria in a process referred to as "tethering". Mitofusin 2 is also located in the ER where it promotes ER-mitochondrial tethering, thereby enhancing mitochondrial Ca^{2+} uptake. For inner membrane fusion, the dynamin-related GTPase, optic atrophy 1 (l-OPA1) can be cleaved into a shorter, soluble fragment (s-OPA1) by the ATP-dependent metalloprotease (YME1L) and, in response to stress, by zinc metallopeptidase (OMA1). This proteolytic cleavage stimulates mitochondrial inner membrane fusion. The exact mechanism by which GTP hydrolysis

triggers a mitofusin shape change to initiate the merging of membranes is still unknown (Figure 1.7) (Archer, 2013; Chen *et al.*, 2003).

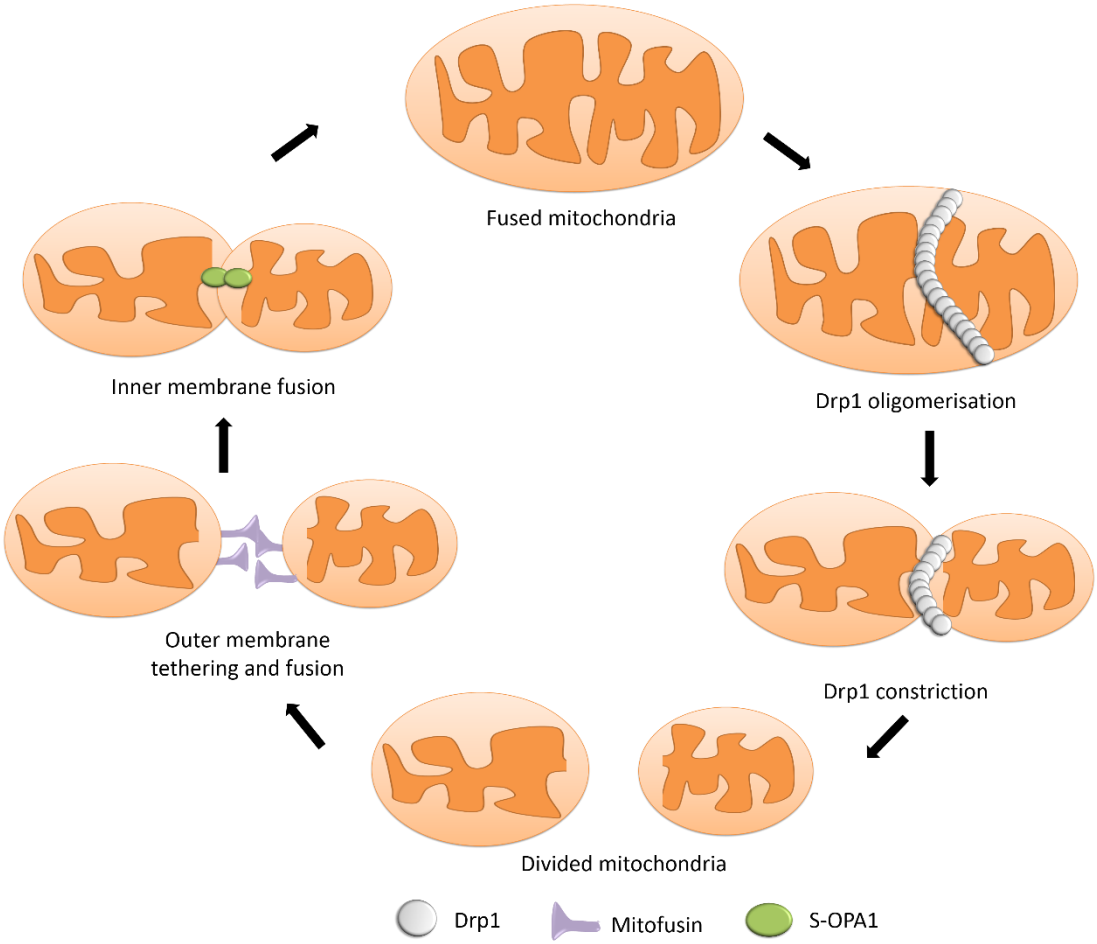

Figure 1.7. Schematic summary of mitochondrial fission and fusion. Mitochondria are dynamic organelles. An ongoing mitochondrial fusion–fission cycle allows mitochondrial functional and genetic complementation. Drp1 constriction enables mitochondrial fission, a prerequisite for mitophagy. Mitochondrial fusion occurs in two stages, firstly via the fusion of the outer membranes, mediated by mitofusins 1 and 2, followed by s-OPA1-mediated inner membrane fusion. Abbreviations: Drp1, dynamin-related protein 1; s-OPA1, soluble optic atrophy 1.

1.2.5.4 Mitophagy

Mitophagy is the selective removal of damaged mitochondria by autophagosomes and subsequent catabolism by lysosomes, therefore a distinction between damaged and healthy mitochondria is required. The hallmark of damaged mitochondria is the depolarisation of the mitochondrial membrane potential ($\Delta\psi_m$). Depolarisation of $\Delta\psi_m$ enables the accumulation of phosphatase and tensin homolog (PTEN)-induced putative kinase 1 (PINK1) on the outer membrane where it triggers the recruitment of the E3 ubiquitin ligase, Parkin. Following its recruitment, Parkin ubiquitinates multiple outer mitochondrial membrane proteins for targeting by the ubiquitin-binding adaptor, p62 which interacts with autophagosome-

associated LC3, to recruit autophagosomes to the mitochondria. Subsequent fusion of autophagosomes with lysosomes enables mitochondrial degradation (Ding and Yin, 2012).

In-line with this, mitochondria with low $\Delta\psi_m$ have been found to have low levels of optic atrophy 1 (OPA1), reducing fusion and increasing the likelihood of mitophagy (Duvezin-Caubet *et al.*, 2006).

Both fission and fusion are key in the segregation of damaged mitochondria and the maintenance of a healthy mitochondrial population. The implication of mitophagy deficiency in multiple neurodegenerative diseases has emphasised the importance of mitochondrial quality control in cellular homeostasis (Scheibye-Knudsen *et al.*, 2014).

1.2.6 Mitonuclear communication

1.2.6.1 Retrograde and anterograde signalling

Since oxidative phosphorylation is performed by proteins encoded in both the nuclear and mitochondrial genomes, the nucleus and mitochondria must coordinate the transcription and translation of mitochondrial proteins.

Mitochondrial function is controlled by the nucleus through anterograde signals, primarily mediated by several transcription factors which regulate the expression of the nuclear-encoded mitochondrial proteome, namely nuclear factor E2-related factor 1/2 (Nrf1 and Nrf2). Nrf1 and 2 stimulate the transcription of genes encoding cytochrome *c*, nuclear-encoded subunits of complexes I-V, transcription factor a, mitochondrial (TFAM), as well as a number of mitochondrial ribosomal proteins and tRNA synthetases (Gleyzer *et al.*, 2005).

These anterograde signals are activated by upstream sensors that detect changes in metabolic conditions. A decrease in ATP synthesis for example, increases the cellular ratio of adenosine monophosphate (AMP)/ATP, causing the activation of AMP-activated protein kinase. This in-turn increases cellular NAD^+ which leads to activation of the NAD^+-dependent deacetylase, sirtuin 1, which positively regulates the transcriptional co-activator, peroxisome proliferator-activated gamma coactivator-alpha (PGC1α). This is known to activate Nrf1 and Nrf2 to induce mitochondrial biogenesis (Fernandez-Marcos and Auwerx, 2011).

Conversely, mitochondrial changes can generate a retrograde response to signal to the nucleus to express genes required to modify mitochondrial and/or cell function. Multiple mitochondrial stressors, such as the depletion of mtDNA or perturbations of oxidative phosphorylation can trigger the loss of $\Delta\psi_m$ and the subsequent release of Ca^{2+} into the cytosol (Amuthan *et al.*, 2002; Luo *et al.*, 1997; Srinivasan *et al.*, 2015). Increased cytosolic

Ca^{2+} activates the phosphatase, calcineurin which activates the transcription factor, nuclear factor kappa-light-chain-enhancer of activated B cells (NF- κB) which promotes the synthesis of proteins involved in Ca^{2+} transport and storage, as well as glycolytic and gluconeogenic enzymes (Biswas *et al.*, 2003; Lim *et al.*, 2006).

1.2.6.2 Mitochondrial import of nuclear-encoded proteins

As the majority of mitochondrial proteins are encoded by the nuclear DNA, an import mechanism for these proteins is required. Nuclear mRNAs are translated on cytosolic ribosomes to generate precursor proteins with a positively charged N-terminal, capable of forming a basic, amphipathic alpha helix; this enables translocation across both the inner and outer mitochondrial membranes, aided by the $\Delta\psi_m$, heat shock protein 70 (hsp70) and translocases. This presequence is then cleaved and folded with the aid of molecular chaperones. Although this is the best understood pathway, multiple pathways exist, with their use dependent on the destination mitochondrial compartment (Jornayvaz and Shulman, 2010).

1.3 THE MITOCHONDRIAL GENOME

1.3.1 Introduction

The first publication citing the presence of "DNA-like" structures within mitochondria came in 1963 (Nass and Nass, 1963). For a period of time afterwards, mitochondrial genetics were considered to be outside of mainstream genetics, with many differences between nuclear DNA and mtDNA becoming apparent, not least the difference in codon rule between the two. In the 50 years since this initial discovery there has been a vast increase in investigations to understand the molecular basis of mtDNA, its inheritance and replication, as well as its implication in multiple disease states. More recently, its effect upon mitochondrial function and susceptibility to adverse drug reactions has been studied.

MtDNA resides in the mitochondrial matrix and is a 16 569 base pair, circular DNA comprising a heavy strand (guanine-rich) encoding 2 rRNAs, 14 tRNAs and 12 polypeptides, and a light strand (guanine-poor) encoding 8 tRNAs and 1 polypeptide. The 13 polypeptides encoded comprise integral subunits of the ETC (Figure 1.8). The remaining ~1500 mitochondrial proteins are encoded in the nuclear DNA (Calvo and Mootha, 2010).

MtDNA is packaged into protein-DNA ensembles termed nucleoids in order to maintain, protect and allow efficient replication of the mitochondrial genome. Without these structures, of which the main structural protein is TFAM, a naked mtDNA molecule would

stretch up to 2 µm inside the mitochondrion, as opposed to the 70 nm diameter of a single nucleoid. On average each nucleoid contains 1.4 copies of mtDNA (Kukat *et al.*, 2011).

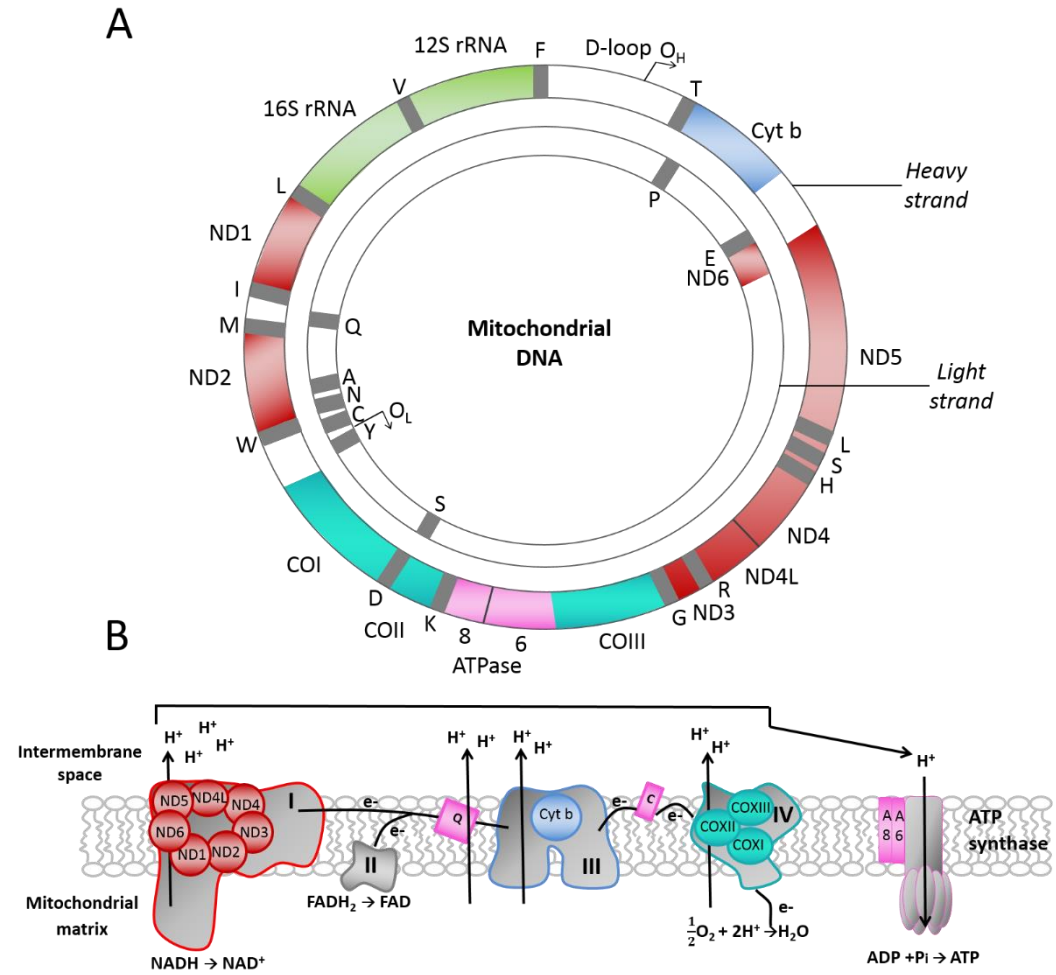

Figure 1.8. Mitochondrial DNA structure and proteome. A: Heavy and light strand structure of mitochondrial DNA B: Schematic diagram of the electron transport chain with mitochondrial DNA-encoded subunits shown in colour and nuclear DNA-encoded subunits in grey. Abbreviations: c, cytochrome *c*; COX, cytochrome *c* oxidase; cyt b, cytochrome *b*; ND, NADH dehydrogenase; O_H, origin of heavy strand replication; O_L, origin of light strand replication; Q, coenzyme Q (Schon *et al.*, 2012).

1.3.2 Mitochondrial and nuclear DNA: a comparison

Unlike nuclear DNA, mtDNA lacks intronic sequences and only has one regulatory region, the displacement (D)-loop, which provides a site of interaction for nuclear-encoded mtDNA replicative machinery. MtDNA does not encode any of the proteins required for its own replication, transcription or translation into protein. Although there is significant cell-cell variation in-line with energy demand (generally), the average mtDNA copy number is estimated at approximately 1000 per cell. This high copy number means that mutations in

the mitochondrial genome do not exert a cellular effect until the proportion of mutated mtDNA reaches a critical threshold. This high copy number also means that there can be many different mtDNAs within a single cell, a state referred to as heteroplasmy (Table 1.2) (Stewart and Chinnery, 2015; Scheffler, 2008; Dickinson *et al.*, 2013).

Table 1.2. Comparison of nuclear and mitochondrial genomes.

Nuclear DNA	Mitochondrial DNA
3 billion base pairs	16 569 base pairs
Linear and segregated into chromosomes	Circular
Histones	No histones: nucleoids
Replicates ∝ mitosis	Replicates independently of mitosis
One copy per cell	Thousands of copies per cell
Mendelian inheritance	Maternal inheritance
~93 % non-coding sequence	~3 % non-coding sequence
Follows universal codon usage rules	Some triplet codons do not follow the universal codon usage rules

1.3.3 Replication

Unlike nuclear DNA, which replicates only once during cell division, mtDNA is continuously replicated independently of the cell cycle and also in non-dividing cells (Bogenhagen and Clayton, 1977; Holt and Jacobs, 2014).

There are currently two predominant models of mtDNA replication, the strand-coupled and strand-displacement models. The latter is more widely accepted and describes the unidirectional initiation of replication from the heavy strand origin (O_H). As the replication of the leading strand continues, passage of the leading strand replication fork exposes the light strand origin (O_L) site in a single-stranded form which initiates synthesis of the lagging strand. Each of these strands is replicated by a set of core proteins, which includes DNA polymerase γ, mitochondrial helicase, mitochondrial single stranded DNA-binding protein and mitochondrial RNA polymerase.

Despite the high fidelity of DNA polymerase γ, the mutation rate of the mammalian mitochondrial genome is reported to be higher than the nuclear genome (Song *et al.*, 2005). This is proposed to be due to an imbalance of nucleotides in the mitochondria which is known to cause replication errors. For example in rat mitochondria, guanine was found to comprise 37-91 % of mitochondrial nucleotides but only 5-10 % of the nuclear pool (Flintoft, 2005; Song *et al.*, 2005).

1.3.4 Heteroplasmy

Heteroplasmy is defined as the presence of multiple distinct mitochondrial sequences within an individual and can be inter or intra-mitochondrial. Heteroplasmy is constantly changing, as unlike chromosome segregation during mitosis, the segregation of mtDNA is random. This means that daughter cells do not necessarily receive identical copies of mtDNA, a process referred to as vegetative segregation (Figure 1.9). This process can cause rapid changes in heteroplasmy if one daughter cell receives more copies of mutant DNA than another (Stewart and Chinnery, 2015).

Changes in the heteroplasmy level of mtDNA molecules which confer a bioenergetic defect are unlikely to be phenotypically observable until a critical threshold of mutant mtDNA is reached. This critical threshold has been estimated at 60-80 % though it varies dependent on the tissue origin and also on the severity of the mutation(s) (Wallace and Chalkia, 2013; Stewart and Chinnery, 2015). This threshold has been demonstrated by presence of the same mutations in patients with primary mtDNA disease and at a lower level in healthy individuals (Larsson and Clayton, 1995).

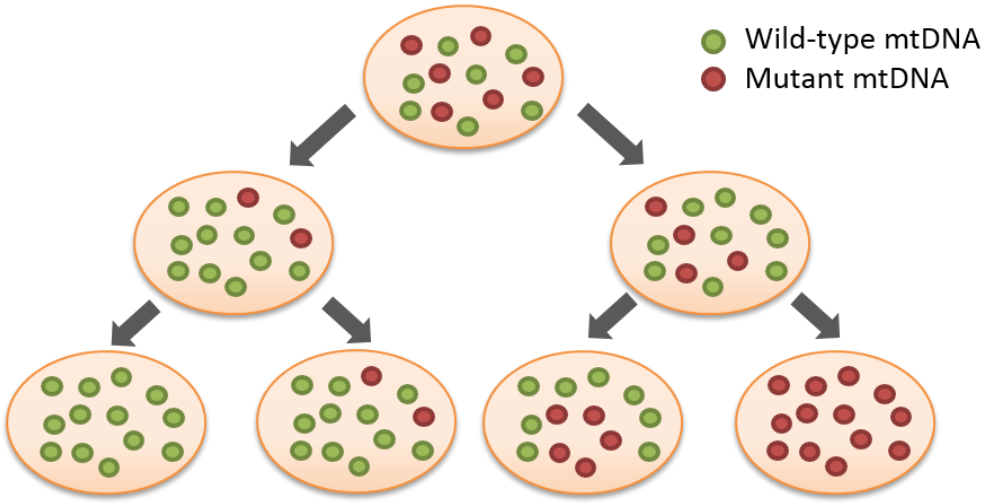

Figure 1.9. Vegetative segregation. Daughter cells receive different proportions of wild-type and mutant mitochondrial DNA (mtDNA).

1.3.5 Mitochondrial haplogroups

Mitochondrial haplogroups are the product of region-specific mtDNA sequence variation as a result of genetic drift and/or adaptive selection for environment-favoured mitochondrial function (Figure 1.10) (Ruiz-Pesini *et al.*, 2004). Single nucleotide polymorphisms (SNPs) are a significant source of mtDNA variation and are often inherited together, forming

haplotypes. Groups of similar patterned and related descendant haplotypes sharing a common ancestor culminate in a haplogroup (Hutchinson, 2010).

The high sequence evolution rate of the mitochondrial genome is a product of both a high mutation rate and a high mutation fixation rate. The high mutation rate results in part from the absence of histones associated with the mitochondrial genome and inefficient repair. The high fixation rate is due to the efficient intracellular sorting of mutant molecules in the female germ line and the rapid genetic drift of mtDNAs in the general population. The lack of recombination of mtDNA means that mtDNA sequences only change by the sequential accumulation of mutations along maternal lineages (Mishmar *et al.*, 2003; Michikawa *et al.*, 1999).

It is thought that ultimately, all mtDNA types in the human gene pool can be traced back to a common matrilineal ancestor that lived in Africa approximately 200 000 years ago (Van Oven and Kayser, 2009; Wallace, 2015).

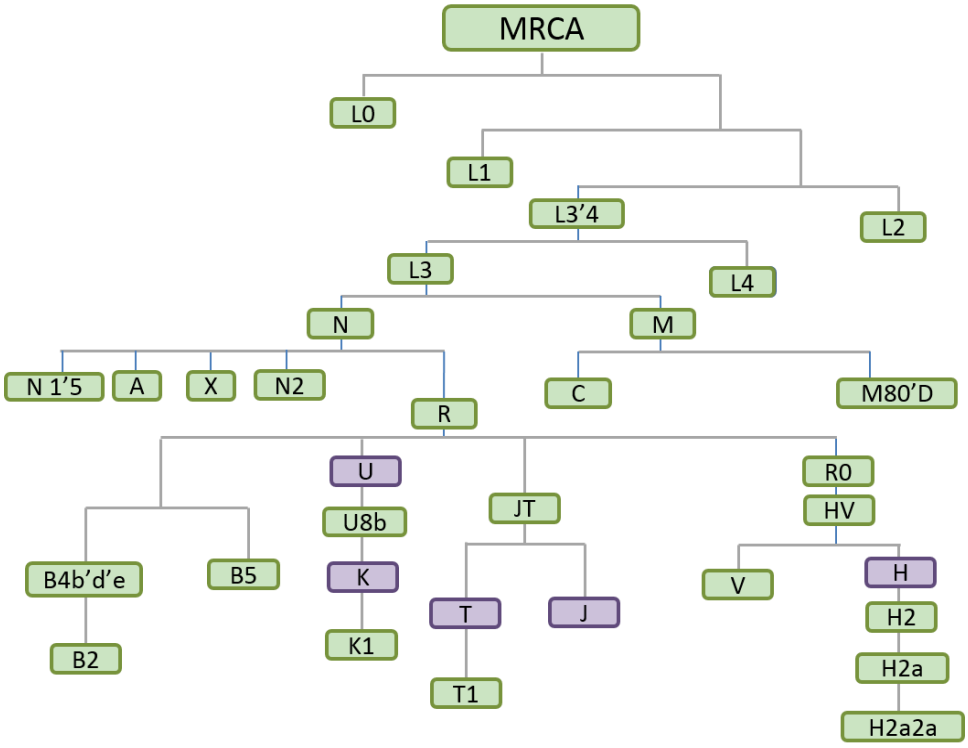

Figure 1.10. MtDNA haplogroup evolution. Phylogenetic tree of the evolution of mitochondrial macrohaplogroups (including L0, L3'4, N and M) and haplogroups (most common UK haplogroups are shown in purple: H, U, T, J, K) from the MRCA (most recent common ancestor) (Van Oven and Kayser, 2009).

1.3.6 Transcription and translation

The basic human mitochondrial transcription machinery consists of three components: mitochondrial RNA polymerase (POLRMT), TFAM and mitochondrial transcription factor B2 (TFB2M).

Transcription of human mtDNA is directed by two promoters, the LSP (light strand promoter) and the HSP (heavy strand promoter), located in opposing mtDNA strands. This produces two long transcripts, one originating from the LSP and the other from the HSP. These two long transcripts are processed by the mitochondrial RNA-processing machinery in order to release individual tRNAs, rRNAs, and mRNAs (Hallberg and Larsson, 2014; Morozov *et al.*, 2014).

Translation of mitochondrial proteins occurs on mitochondrial ribosomes in the mitochondrial matrix, tethered to the inner mitochondrial membrane (Figure 1.2). The basic mitochondrial translation machinery comprises mtDNA-encoded rRNAs and tRNAs as well as many proteins encoded in the nuclear genome: initiation, elongation and termination translation factors; mitochondrial ribosomal proteins, mitochondrial aminoacyl-tRNA synthetases and methionyl-tRNA transformylase (Smits *et al.*, 2010).

1.3.7 Mitochondrial DNA variation and mitochondrial function

Given that the mitochondrial genome encodes core subunits of the ETC, it is no surprise that multiple studies have shown differences in mitochondrial function and expression patterns dependent upon mtDNA variation. For example, a recent study found haplogroup L to have higher expression of some mtDNA-encoded genes, decreased ATP turnover rates and lower levels of ROS compared to haplogroup H (Kenney *et al.*, 2014). Many of these studies have been conducted using transmitochondrial cybrids, an *in vitro* model (Table 1.3) (Section 1.5.2.5).

Table 1.3. Mitochondrial DNA variation associated with a change in mitochondrial function.

Haplogroup association	Research model	Reference
Haplogroup L has lower ATP turnover and lower ROS compared to haplogroup H	Cybrid	(Kenney *et al.*, 2014)
Haplogroup H and Uk have significantly different complex IV activity	Cybrid	(Gómez-Durán *et al.*, 2010)
Haplogroup J has reduced oxygen consumption and $\Delta\psi_m$ compared to haplogroup H	Cybrid	(Gómez-Durán *et al.*, 2012)
There are no differences between haplogroup H and T bioenergetics	Cybrid	(Amo *et al.*, 2008)

There are no respiratory enzyme activity differences between haplogroup H and T	Cybrid	(Mueller, 2012)

Abbreviations: $\Delta\psi_m$, mitochondrial membrane potential; cybrid, transmitochondrial cybrid; ROS, reactive oxygen species.

1.3.8 Mitochondrial DNA variation and disease

Mitochondrial diseases have a variety of phenotypic origins due to the universal abundance of mitochondria. This variety can make it difficult to attribute mtDNA mutation(s) to a certain condition, meaning that the number of diseases associated with mtDNA mutations could in fact be underestimated. It should also be noted that many mitochondrial diseases originate from nuclear DNA mutations.

The heterogeneous nature of many mtDNA diseases means that many patients cannot be diagnosed with a specific clinical syndrome. Nonetheless there are established mtDNA diseases including MIDD (mitochondrially inherited diabetes and deafness) as well as multiple disorders, including neurogenic weakness, ataxia and retinitis pigmentosa, Leigh syndrome and myoclonic epilepsy (Table 1.4). Beyond this, a range of links between mtDNA haplogroup and diseases which are not typically classified as mitochondrial in nature continue to be elucidated, such as Alzheimer's disease and Parkinson's disease (Van den Ouweland *et al.*, 1999, 1992).

Table 1.4. Mitochondrial DNA variation associated with disease.

Indication	Haplogroup association	Reference
Breast cancer	K: increased risk U: decreased risk	(Bai *et al.*, 2007)
Osteoporosis	X: increased risk	(Guo et al., 2011)
AIDS	J, U5a: increased risk Uk, H3, IWX: decreased risk	(Hendrickson *et al.*, 2008)
Sepsis	HV, H: decreased risk	(Jimenez-Sousa *et al.*, 2015)
Metabolic syndrome	N9a, D5,G1: decreased risk	(Tanaka *et al.*, 2007)
Age-related diseases	K: decreased risk	(Thaker *et al.*, 2016)
Sepsis	R: decreased risk	(Yang *et al.*, 2008)
Peripheral neuropathy	T: increased risk	(Canter *et al.*, 2007)

1.4 DRUG-INDUCED MITOCHONDRIAL DYSFUNCTION

1.4.1 Introduction

Mitochondria are host to a myriad of critical cellular processes, meaning that mitochondrial toxins can cause severe damage, particularly those which have multiple mitochondrial targets.

Mitochondria are frequently cited as a target when defining the mechanism of an adverse drug reaction. This can be rationalised by the multiple structural and functional features of mitochondria which provide a wealth of potential targets for drug-induced dysfunction (Figure 1.11).

One of the hallmark features of the mitochondria is the -180 mV potential across the inner mitochondrial membrane, this enhances the accumulation of cationic amphiphilic drugs in the mitochondrial matrix (Boelsterli and Lim, 2007). Another feature associated with localised dysfunction to the mitochondria is the high cardiolipin content of the inner mitochondrial membrane, a stark contrast to most cholesterol-rich membranes. Many drugs bind cardiolipin, bringing them in close proximity to the ETC with the potential for inhibition. Cardiolipin is also rich in unsaturated bonds, thereby increasing the risk of oxidation by ETC-derived ROS. ETC-derived ROS may damage the mtDNA and perturb the function of ETC proteins, this may cause further ROS generation, thereby generating a vicious cycle. This theory is the subject of debate however, based on a lack of experimental evidence and knowledge of the protection of mtDNA conferred by nucleoids (Wiesner *et al.*, 2006; Alexeyev, 2009).

1.4.2 Mechanisms of drug-induced mitochondrial dysfunction

1.4.2.1 Oxidative phosphorylation uncoupling

Oxidative phosphorylation uncoupling (mitochondrial uncoupling) is any process by which electron transport and substrate oxidation are not used to drive ATP synthesis (Mookerjee *et al.*, 2010).

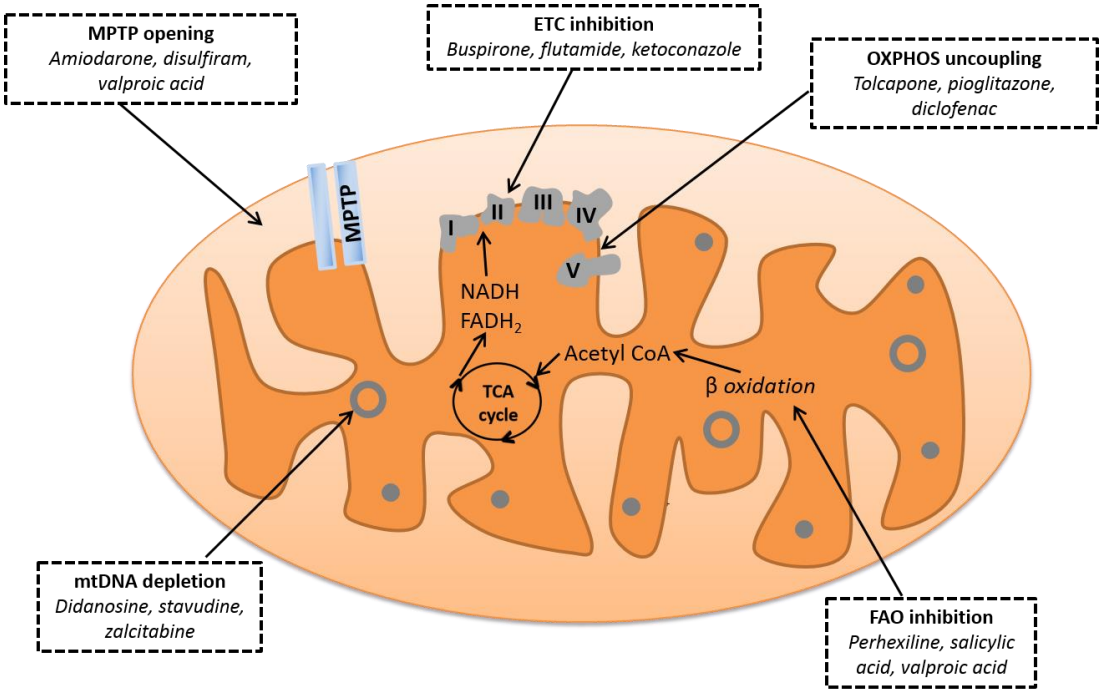

Figure 1.11. Common sites of mitochondrial dysfunction. There are multiple sites where a compound may perturb mitochondrial function. Examples of compounds associated with each mechanism are stated, however it is not uncommon for a compound to induce mitochondrial dysfunction via more than one mechanism, for example amiodarone is known to uncouple OXPHOS as well as inhibit FAO. Abbreviations: ETC, electron transport chain; FAO, fatty acid oxidation; MPTP, mitochondrial permeability transition pore; mtDNA, mitochondrial DNA; OXPHOS, oxidative phosphorylation; TCA, tricarboxylic acid.

Uncoupling of substrate oxidation from ADP phosphorylation (to generate ATP) is characterised by proton leak across the inner mitochondrial membrane. In healthy mitochondria, the activity of uncoupling proteins e.g. UCP1 can confer a proton leak which can comprise up to 30 % of the basal metabolic rate. This is proposed to be beneficial via reducing ROS generation (Jastroch *et al.*, 2010).

In contrast, drug-induced uncoupling tends to be beyond any physiological benefit. Generally, potent uncouplers have an acid-dissociable group, lipophilic group and a strong electron-withdrawing moiety. This provides solubility in lipid membranes, stability of the ionised form in a membrane and the ability to release and bind a proton (Wallace 2000).

These compounds can cycle across the inner mitochondrial membrane multiple times, catalysing the transport of protons and concomitantly short-circuiting the proton circuit whereby protons go back down their electrochemical gradient via ATP synthase (Figure 1.3). Concordantly, the generation of a proton motive force becomes uncoupled from ATP synthesis (Palmeira and Rolo, 2004).

1.4.2.2 Electron transport chain inhibition

The formation of a proton gradient used to drive ATP synthesis can also be impaired via the inhibition of one or more of the multiple enzyme complexes required for electron transport.

Of all the respiratory chain complexes, complex I (function described in Section 1.2.3.2.1) is the most vulnerable to chemical-induced dysfunction; more than 60 natural and synthetic compounds are known to inhibit its activity. Inhibitors vary in specificity and can be put into three categories: the first inhibits at the level of NADH-flavin interaction, but also inhibits a variety of dehydrogenases not specific to complex I. Quinole antagonists are the second category, these are inhibitors of both complex I and CoQ and therefore inhibit quinol binding. The third group of inhibitors is specific to complex I and includes rotenone (Wallace and Starkov, 2000).

1.4.2.3 Fatty acid oxidation impairment

Inhibition of mitochondrial FAO is a primary mechanism in the onset of drug-induced hepatic steatosis, the abnormal retention of lipids in the liver (Fromenty and Pessayre, 1995). Inhibition of FAO can be via the direct inhibition of enzymes for FAO (Deschamps *et al.*, 1994; Baldwin *et al.*, 1998) or secondary inhibition, for example via decreased availability of cofactors (Fromenty and Pessayre, 1995). MtDNA depletion by inhibition of DNA polymerase γ or oxidative damage which induces strand breaks and subsequent degradation by endonucleases may also result in FAO impairment (Lewis *et al.*, 1996; Rachek *et al.*, 2009).

1.4.3 The role of mtDNA variation in idiosyncratic drug-induced liver injury

The study of the effect of mitochondrial genome variation upon mitochondrial function and disease has paved the way for studies into the effect of mtDNA variation upon the incidence of adverse drug reactions, though these remain few and far between (Table 1.5) (Wallace, 2015). Nonetheless, clear evidence of 1) the effect of mtDNA upon mitochondrial function alongside 2) the implication of mitochondrial dysfunction in the onset of DILI, suggests that the direct assessment of the effect of mitochondrial genotype upon susceptibility to DILI is

worthwhile, a view point also put forward by Pacheu-Grau *et al.,* and Boelsterli and Lim (Pacheu-Grau *et al.*, 2012; Boelsterli and Lim, 2007).

Table 1.5. Mitochondrial DNA variation associated with adverse drug reactions.

Compound	Clinical manifestation	Haplogroup/ polymorphism	Reference
Streptomycin	Ototoxicity (deafness)	D5a	(Chen *et al.*, 2007)
HAART	Lipoatrophy	H	(Hendrickson *et al.*, 2009)
Antiretroviral therapy	Peripheral neuropathy	L1c	(Canter *et al.*, 2010)
HAART	Increased atherogenic risk	JT and T	(Micheloud *et al.*, 2011)
Stavudine-containing antiretroviral therapy	Peripheral neuropathy	L0a2	(Kampira *et al.*, 2013)
Linezolid	N/A (*in vitro*)	m.3018A	(Pacheu-Grau *et al.*, 2012)

Abbreviations: HAART, highly-active antiretroviral therapy.

Heteroplasmy, the co-existence of wild-type (WT) and mutant mtDNA has been a key feature in establishing a link between mitochondrial dysfunction and DILI. It is thought that the proportion of mutant mitochondria must surpass a critical threshold before phenotypically detectable damage occurs, this is in-line with the clinical symptoms of DILI in that there is often a delayed but severe onset (Boelsterli and Lim, 2007).

Age has also been cited as supporting evidence of the link between mitochondrial injury and DILI, supported by the classification of age as a major risk factor for both DILI and increased mtDNA damage/oxidative injury (Boelsterli and Lim, 2007). There are many reasons for the association of aging with increased susceptibility to DILI however, including the higher probability of polypharmacy and unknown drug-drug interactions, therefore this link is tenuous.

DILI as a result of mitochondrial dysfunction is also supported by the number of DILI cases which do not abate following treatment cessation. This implies that it is a problem of cumulative drug damage as oppose to drug accumulation and could be proposed to be the result of cumulative drug-induced dysfunction of a large population of mitochondria (surpassing a critical threshold) (Boelsterli and Lim, 2007).

It is important to acknowledge that *in vitro* mitochondrial liabilities are often only visible at drug concentrations which greatly exceed human plasma concentrations (commonly 100-fold greater) (Xu *et al.*, 2008). In addition, the factors discussed which implicate

mitochondrial dysfunction in the onset of DILI are only hazards, and these hazards manifest as DILI in only a small number of patients. This idiosyncrasy is the basis of the aim of the research described in this thesis, to begin to elucidate if abnormalities in mtDNA may be the "missing link" in the idiosyncrasy of some cases of DILI, by increasing susceptibility to drug-induced mitochondrial dysfunction in a subset of patients.

1.5 TECHNIQUES TO ASSESS MITOCHONDRIAL DYSFUNCTION IN THE CONTEXT OF DRUG-INDUCED LIVER INJURY

1.5.1 Mitochondrial models

1.5.1.1 Introduction

The study of mitochondrial function *in vitro* has classically used either isolated mitochondria or whole cells. Each method has its advantages and disadvantages; most notably isolated mitochondria allow the direct application of substrates but have limited physiological relevance, whereas intact cells have greater physiological relevance but are impermeable to many mitochondrial substrates (Figure 1.12) (Salabei *et al.*, 2014; Brand and Nicholls, 2011). In order to select the most suitable model for a specific mitochondrial study, one must therefore consider both the chemical characteristics of the drug being studied and the overall aim of the study. By understanding the potential benefits and limitations of the experimental set up, the results can be correctly interpreted in a chemical and clinical context.

1.5.1.2 Isolated mitochondria

Isolated mitochondria have long been a model of choice for the assessment of drug-induced mitochondrial dysfunction. However, practical limitations of this set up include the high number of cells (estimated at 200 x 10^6) required, as well as the risk of structural disruption and limited function following isolation (Kuznetsov *et al.*, 2008). In addition, isolation means that there is no consideration of mitochondrial dynamics nor interactions with other cellular compartments (Perry *et al.*, 2013).

Both fission and fusion are important in the maintenance of a healthy mitochondrial population, with increased fusion enabling mitochondria to "share the load" when under stress, whilst defective mitochondria undergo fission prior to mitophagy (Section 1.2.5.4). When mitochondria are isolated, these protective mechanisms are lost, potentially causing artefactual toxicity (Archer, 2013). Conversely, testing using isolated organelles also increases the likelihood of drug-induced dysfunction remaining undetected in situations

where multiple mechanisms of dysfunction or the xenobiotic activation of a compound is required to produce a toxic species.

1.5.1.3 Whole cells

The impermeability of the cell surface membrane to many mitochondrial substrates means that whole cell models can often only be used for the indirect assessment of mitochondrial function, such as the measurement of cellular ATP levels. These assessments do however require a fraction of the cells that are associated with isolated mitochondria studies. Importantly, whole cells also provide increased physiological relevance as the mitochondria are in an *in situ* environment. This enables continued interaction with other mitochondria, as well as the continuation of anterograde/retrograde signalling and other cytosolic communications (Brand and Nicholls, 2011).

1.5.1.4 Permeabilised cells

The disadvantages of isolated mitochondria and whole cell model systems can be alleviated in-part by the use of permeabilised cells. This method enables many mitochondria-associated proteins and organelles to remain intact, particularly the ER. This increases physiological relevance in comparison to isolated mitochondria, whilst still enabling substrate access to the mitochondria. In this way, cell permeabilisation permits assays which investigate the site of compound-mediated ETC inhibition, which often requires the use of substrates which are impermeable to the cell surface membrane. Far fewer cells are required than would be needed for comparable studies using isolated mitochondria and any bias occurring due to sub-selection of the mitochondrial population during isolation and limitations in quality due to the time taken for isolation can be avoided (Kuznetsov *et al.*, 2008; Brand and Nicholls, 2011).

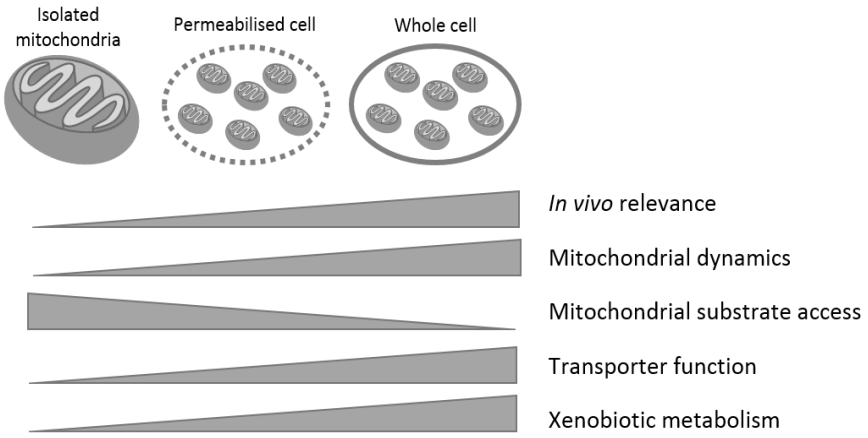

Figure 1.12. Comparison of isolated mitochondria, permeabilised and whole cells for the assessment of drug-induced mitochondrial dysfunction. The impermeability of the cell surface membrane to

many mitochondrial substrates has required the use of isolated mitochondria in many *in vitro* studies. Advanced permeabilisation methods have now enabled the use of permeabilised cells as a way to study mitochondria whilst bypassing many of the caveats associated with isolated mitochondria and whole cells.

1.5.2 *In vitro* hepatic models

1.5.2.1 Introduction

Hepatocytes constitute approximately 80 % of liver volume and are highly differentiated epithelial cells that perform xenobiotic, protein, steroid and fat metabolism, as well as vitamin and iron storage (Arias *et al.*, 2011; Bacon *et al.*, 2006). Generally, hepatocytes have an abundance of mitochondria (occupying approximately 20 % of cell volume, 1-2000/cell) and rough and smooth endoplasmic reticulum (ER). Hepatocytes are also highly polarised, with distinct differences between the sinusoidal and canalicular membranes. This allows the multiple functions of hepatocytes to be performed simultaneously (Alberts *et al.*, 2002).

The development of *in vitro* models to recapitulate this complex liver architecture is vital in improving the prediction of DILI preclinically. Freshly isolated human hepatocytes (FHH) are the gold standard for *in vitro* hepatotoxicity testing, providing xenobiotic metabolism and expression of a multitude of xenobiotic transporters, including the bile salt export pump (BSEP). Nonetheless, current protocols do not enable the maintenance of this function for more than a few hours as FHHs are subject to rapid dedifferentiation (Godoy *et al.*, 2013; Hewitt *et al.*, 2007). FHHs may also be used to study the effects of interindividual variation, however, whilst representative of the clinical situation, this effect can reduce the reproducibility of results. These limitations have necessitated the use of hepatocellular carcinoma cell lines such as HepG2 cells, which circumvent issues of availability, but come with their own set of restrictions which are discussed in more detail below (Figure 1.13).

1.5.2.2 HepG2 cells

HepG2 cells constitute the most widely used preclinical model for the assessment of DILI (LeCluyse *et al.*, 2012). This immortalised cell line permits long-term culture and reproducible results (though largely due to the absence of interindividual variation). They do however have restricted hepatocyte functionality, with a limited expression of phase I CYP450 enzymes, reducing their suitability for the study of metabolite-mediated dysfunction and potentially the propensity for ROS generation. This, coupled with an expression level of phase II detoxification enzymes similar to that of FHH could lead to an underestimation of drug-induced dysfunction (Westerink and Schoonen, 2007; Gerets *et al.*, 2012).

Differences between HepG2 cells and FHH also include key transporters, such as the BSEP, for which there is a 16-fold reduction in expression in HepG2 cells. This severely reduces the ability of HepG2 cells to detect synergistic dysfunction arising from compounds with liabilities in both mitochondria and the BSEP (Sison-Young *et al.*, 2015).

One of the most important considerations when using HepG2 cells as a model for both mitochondrial dysfunction and DILI assessment is the difference in the bioenergetics of this cell line compared to FHHs. The ability of HepG2 cells to increase glycolytic ATP production following a mitochondrial insult can reduce their utility in the detection of direct mitochondrial dysfunction. As a result, HepG2 cells require manipulation to increase their ability to detect direct mitochondrial dysfunction. This is easily achieved via long-term or acute galactose conditioning of HepG2 cells; the use of galactose as a substrate drastically reduces the ability of glycolysis to compensate for perturbation(s) in oxidative phosphorylation, thus making mitochondrial dysfunction easier to detect (Marroquin *et al.*, 2007; Kamalian *et al.*, 2015).

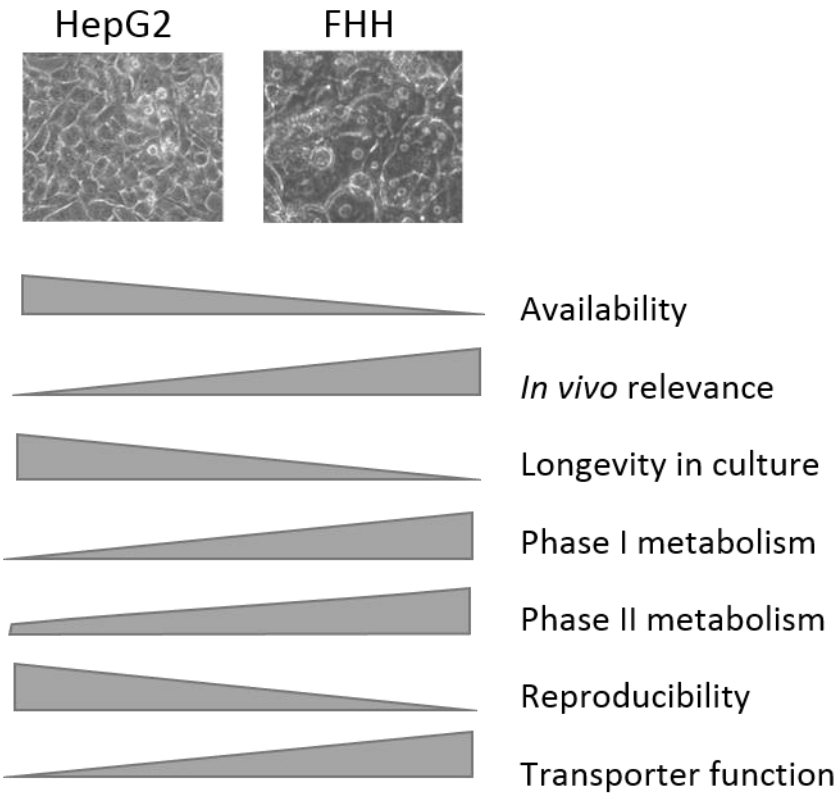

Figure 1.13. Comparison of HepG2 cells and freshly isolated human hepatocytes (FHH) for preclinical studies of drug-induced liver injury. FHHs are superior to HepG2 cells in terms of *in vivo* relevance, however their lack of longevity in culture requires the use of carcinoma cell lines such as HepG2 cells.

1.5.2.3 Rho zero cells

1.5.2.3.1 Introduction

Rho zero (ρ0) cells lack a mitochondrial genome and do not have a functional ETC; therefore they offer a negative control for the assessment of mitochondrial dysfunction. Multiple ρ0 cell lines have been reported (Table 1.6) though not from a hepatic parental cell line. Despite the absence of a functional ETC, ρ0 cells have an abundance of mitochondria, evidence of the multiple critical roles of the mitochondria beyond ATP generation. The maintenance of this mitochondrial population however requires multiple adaptations and specific cell culture conditions detailed below (Chevallet *et al.*, 2006; Schon *et al.*, 2012).

Table 1.6. Reported rho zero (ρ0) cell lines. Since first reported by King and Attardi in 1989, ρ0 cell lines have been generated from multiple parental cells, however none of hepatic or hepatocarcinoma origin have been reported to date.

Cell line	Cell type	Method of mtDNA depletion	Reference
143B206	Osteosarcoma	EtBr	(King and Attardi, 1989)
HeLa	Cervical carcinoma	EtBr	(Attardi *et al.*, 1991)
U937	Promonocytic leukaemia	EtBr	(Gamen *et al.*, 1995)
64/65	Neuroblastoma	EtBr	(Miller *et al.*, 1996)
HL60	Promyelocytic leukaemia	EtBr	(Herst *et al.*, 2004)
$143BTK^-$	Osteosarcoma	Transfection with restriction enzyme	(Schubert *et al.*, 2015)

Abbreviations: EtBr, ethidium bromide; mtDNA, mitochondrial DNA.

1.5.2.3.2 ATP synthesis

As previously discussed, ρ0 cells are unable to synthesise ATP by the generation of a proton motive force. Instead, ATP is generated entirely through glycolysis and is hydrolysed via the functional F_1 ATPase portion of ATP synthase. Despite the absence of mtDNA-encoded F_O subunits ATP6 and 8, the ATPase generates Pi and ADP^{3-} which is exchanged for ATP (from glycolysis) by the adenine dinucleotide carrier. This exchange generates a sufficient $\Delta\psi_m$ to prevent apoptosis and allows the import of nuclear-encoded proteins into the mitochondria. Concordantly, oligomycin (F_O ATP synthase inhibitor) does not change the $\Delta\psi_m$ of ρ0 cells and ρ0 cells are resistant to ETC inhibitors such as rotenone which ordinarily induce apoptosis (Ferraresi *et al.*, 2008; Chevallet *et al.*, 2006).

1.5.2.3.3 Pyruvate and uridine auxotrophy

P0 cells are auxotrophic for both uridine and pyruvate. This can be explained by the reliance of these cells upon ATP produced by glycolysis so they require pyruvate as a hydrogen acceptor to regenerate NAD^+ (in a WT cell this would be generated at complex I of the ETC). Reliance on uridine is due to the key reaction in *de novo* pyrimidine synthesis performed by mitochondrial dihydroorotate dehydrogenase (Figure 1.14). This enzyme requires an intact respiratory chain for its function and so in ρ0 cells, uridine must be provided to bypass this ETC-dependent step in the pyrimidine synthesis pathway (Gregoire *et al.*, 1984; Chevallet *et al.*, 2006).

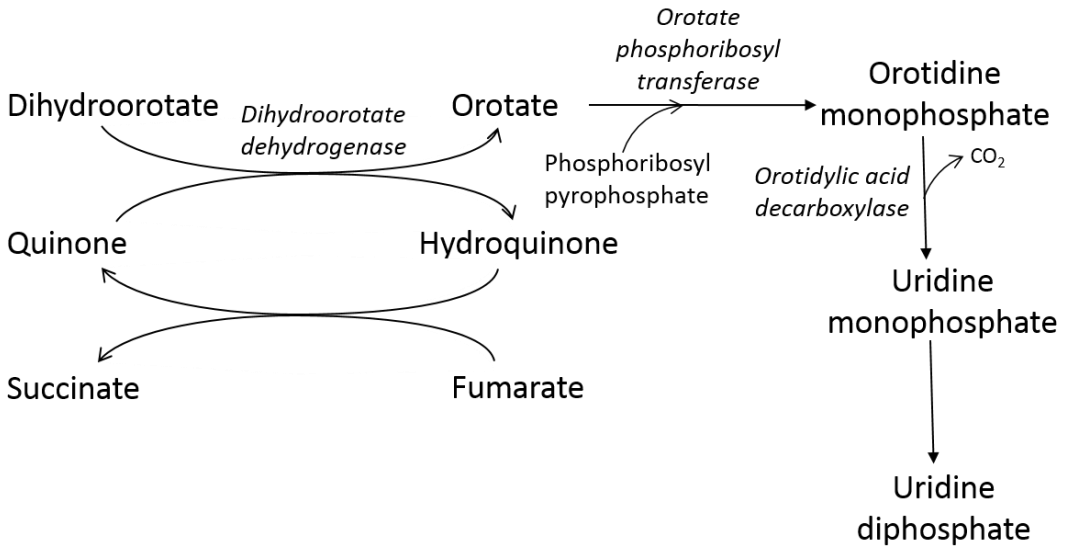

Figure 1.14. Generation of uridine by dihydroorotate dehydrogenase. Dihydroorotate dehydrogenase is required for pyrimidine synthesis and is located on the matrix side of the inner mitochondrial membrane. A functional respiratory chain is required for this enzyme to function.

1.5.2.4 Platelets

Platelets are small, anucleate cell fragments which are abundant in the bloodstream. They therefore provide a source of mtDNA which can be collected using minimally invasive techniques and without interference from the nuclear genome (Patel *et al.*, 2005). Nonetheless, the differences between platelets and hepatocytes must be understood in order to account for this variation when using platelets as an *in vitro* hepatic model.

Adults produce an average of 10^{11} platelets per day. Platelets are derived from megakaryocytes, which themselves are generated from haematopoietic stem cells in the bone marrow (Machlus and Italiano, 2013). Once developed, megakaryocytes can develop pseudopods, temporary cytoplasm-filled projections which give rise to proplatelets. This continues to the extent that the whole megakaryocyte cytoplasm is transformed into an

interconnected network of proplatelets. During this, the cell is filled with a high concentration of ribosomes which facilitate the production of platelet-specific proteins and DNA is amplified by as much as 64-fold (endomitosis) to generate a multi-lobed nucleus. Platelet-sized swellings develop at proplatelet ends and are the main source of platelet assembly and release (Patel *et al.*, 2005; Machlus and Italiano, 2013).

1.5.2.5 Transmitochondrial cybrids

Evaluation of the contribution that mtDNA variants have upon cellular behaviour is challenging in the presence of the nuclear genome. However, without the presence of a nuclear genome, anucleate cell fragments such as platelets have limited relevance to nucleated cells such as hepatocytes and cannot be cultured using traditional methods.

Transmitochondrial cybrids address these issues by providing a controlled nuclear background upon which to study the effects of variants in the mitochondrial genome in isolation.

The generation of cybrids was first reported in 1974 by Bunn *et al*., whom proposed the term "cybrid"; it was designed to be distinguishable from the term "hybrid" which implies the mixture of two nucleated cells. Commonly, cybrid cell lines are created by fusing ρ0 cells (Section 1.5.2.3) with mitochondria-rich platelets (anucleate) or cytoplasts (enucleated cells) from individuals (Figure 1.15), but this method was not reported until 1989 (King and Attardi, 1989). In either case, the resultant cybrids should have identical nuclei but contain the mitochondrial genome of the cytoplasts/platelets (Vithayathil *et al.*, 2012; Wilkins *et al.*, 2014; Kenney *et al.*, 2014).

To-date there is no evidence of cybrid generation using human hepatic cell lines as nuclear donor cells (ρ0 cells). The majority of studies use the 143BTK$^-$ ρ0 cell line, presumably due to the absence of thymidine kinase in these cells. This enables ρ0 cells which fail to fuse to be eliminated from culture via incubation with bromodeoxyuridine. Details of some of the cybrid cell lines reported to date are in Table 1.7.

Table 1.7. A selection of rho zero cells used to generate transmitochondrial cybrid cell lines.

Nuclear donor/ rho zero cell	Cell type	Reference
SH-SY5Y	Neuroblastoma	(Jeong *et al.*, 2015; Swerdlow *et al.*, 1996)
NT2	Teratoma	(Arduíno *et al.*, 2015)
143B-87	Osteosarcoma	(Trounce *et al.*, 1994)
143BTK$^-$	Osteosarcoma	(King and Attardi, 1989)

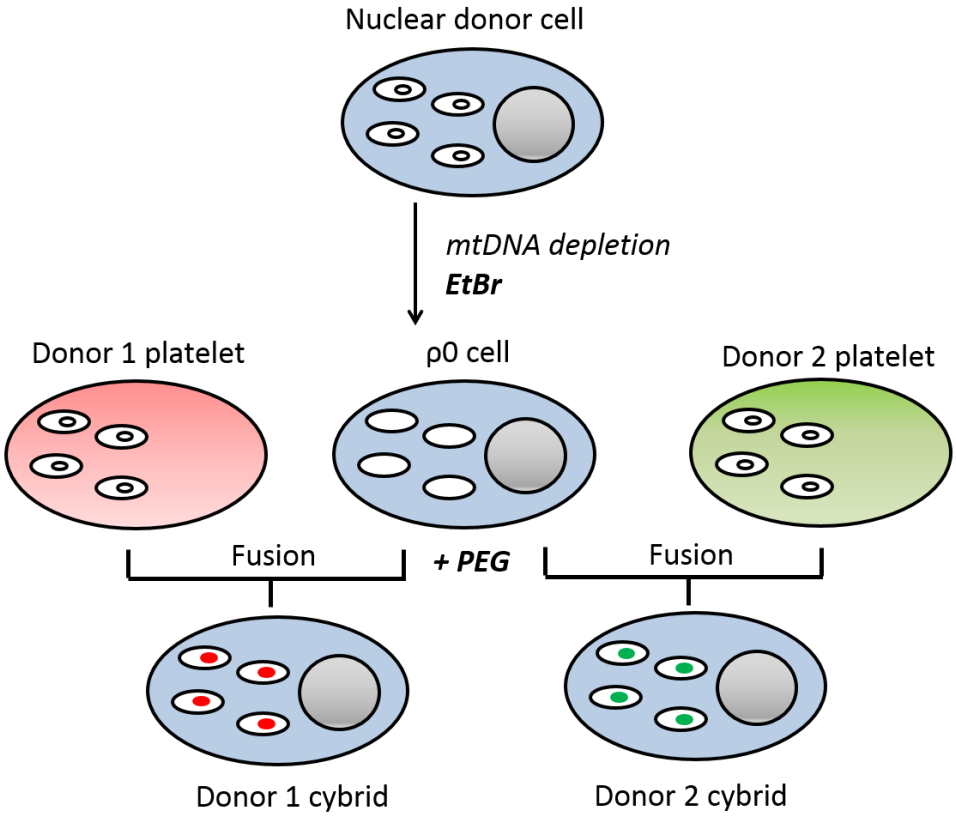

Figure 1.15. A reported method of transmitochondrial cybrid generation. A nuclear donor cell is depleted of its mitochondrial genome by treatment with the DNA intercalator, ethidium bromide (EtBr) to generate a rho zero (ρ0) cell. This is then fused with mitochondrial donor cells (in this case, platelets) using polyethylene glycol (PEG) to generate transmitochondrial cybrids. Both donor 1 and donor 2 cybrids have the nuclear genome of the nuclear donor cell, but the mtDNA of the platelets which have been fused.

1.6 HYPOTHESIS, AIMS AND OBJECTIVES

The research described in this thesis arose from evidence of the effect of mitochondrial genotype upon mitochondrial function and the role of mitochondrial dysfunction in the onset of drug-induced liver injury. Together, this evidence was used to formulate the hypothesis that variation in mitochondrial genotype confers an altered mitochondrial function which in-turn alters susceptibility to iDILI.

The overall aim of this research therefore, was to generate an *in vitro* hepatic model which can be used for the preclinical assessment of the effect of mtDNA variation upon mitochondrial function and mitochondrial dysfunction caused by compounds associated with iDILI. In order to achieve this, the following objectives were created:

Objective 1: To determine the mechanisms of mitochondrial dysfunction induced by compounds associated with iDILI in HepG2 cells (test compounds detailed in Table 1.8).

Objective 2: To sequence the whole mitochondrial genome of a cohort of healthy volunteers.

Objective 3: To generate and characterise HepG2 cells devoid of mtDNA (ρ0 cells).

Objective 4: To generate and characterise HepG2 transmitochondrial cybrids.

Objective 5: To use *ex vivo* (platelets) and *in vitro* models (transmitochondrial cybrids) to test the effect of mtDNA variation upon susceptibility to drug-induced mitochondrial dysfunction induced by compounds associated with iDILI (test compounds detailed in Table 1.8).

Table 1.8. Summary of DILI-associated compounds. These multi-mechanistic compounds were used to assess the ability of HepG2 cells to differentiate mechanisms of mitochondrial dysfunction. These compounds were also used to determine the effect of mitochondrial genome variation upon drug-induced mitochondrial dysfunction.

Compound	Structure	Pharmacology	Metabolism	Clinical toxicity	Mitochondrial liability	Reference
Flutamide	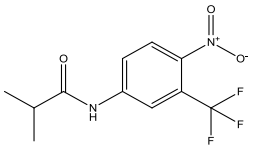	**Indication: prostate cancer** Flutamide is a non-steroidal antiandrogen which blocks the binding of 5α-dihydrotestosterone to androgen receptors. It is most commonly used in combination with gonadotropin-releasing hormone agonists (combined androgen blockade).	**C_{max}: 72.2 nM** **$T_{1/2}$: 7.8 h** Flutamide undergoes rapid first-pass metabolism, primarily via CYP1A2 to generate 2-hydroxyflutamide (C_{max}: 4.4 μM), prior to glucuronidation before excretion. Other routes of metabolism include hydrolysis to 3-trifluoromethyl-4-nitroaniline (C_{max}: 1.31 μM).	**Clinical usage: boxed warning** Flutamide was first-marketed in 1989, cases of iDILI were subsequently reported, with cases of hospitalisation or death in 0.03 % of flutamide-treated patients, primarily presenting with cholestatic hepatitis.	Complex I inhibitor. Possible uncoupling at low concentrations.	(Coe, 2008; Schulz *et al.*, 1988; Chu *et al.*, 1998; Wysowski and Fourcroy, 1996; Shet *et al.*, 1997; Boelsterli and Lim, 2007; Gao *et al.*, 2006)
Bicalutamide	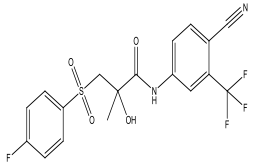	**Indication: prostate cancer** Bicalutamide is a nonsteroidal antiandrogen given as a racemic mixture. Its antiandrogenic activity resides almost exclusively in the (R)-enantiomer. It is most commonly used in combination with gonadotropin-releasing hormone agonists.	**C_{max}: 1.7 μM** **$T_{1/2}$: 6 days** (R)-Bicalutamide is hydroxylated primarily via CYP3A4 prior to glucuronidation. The (S)-enantiomer is metabolised by direct glucuronidation.	**Clinical usage: in use** Bicalutamide therapy is associated with mild, asymptomatic and transient elevations in serum aminotransferase levels in approximately 6 % of patients.	Suggested to deplete mtDNA during prolonged exposure.	(Cockshott, 2004; Coe, 2008; Hussain *et al.*, 2014)
Tolcapone	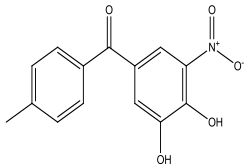	**Indication: Parkinson's disease** Levodopa (L-dopa) is commonly used to treat Parkinson's disease, yet its methylation by catechol-methyl transferases to 3-o-methyl dopa reduces the amount of L-dopa reaching the brain. Catechol-methyl transferase inhibitors such as tolcapone and entacapone prevent the methylation of L-dopa and so increase its elimination half-life.	**C_{max}: 16.5 μM** **$T_{1/2}$: 3.5 h** Tolcapone primarily undergoes direct glucuronidation by glucuronyltransferase, with a smaller proportion undergoing oxidation by CYP3A4.	**Clinical usage: withdrawn** Tolcapone has been reported to cause serum aminotransferase elevations above three times the upper limit of normal in 1-5 % of patients. It has been implicated in several cases of severe, clinically apparent acute liver injury and at least three cases of death from acute liver failure which arose 1-5 months after the start of treatment.	Uncoupler of oxidative phosphorylation.	(Keränen *et al.*, 1994; Jorga *et al.*, 1999; Khetani *et al.*, 2013; Korlipara *et al.*, 2004)
Entacapone	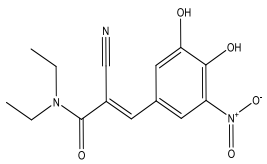		**C_{max}: 3.9 μM** **$T_{1/2}$: 0.7 h** Entacapone is almost entirely metabolised by isomerisation to the inactive *cis*-isomer, followed by glucuronidation before excretion. The parent compound also undergoes direct glucuronidation.	**Clinical usage: in use** Entacapone therapy has been associated with asymptomatic and transient serum aminotransferase elevations in 0.3-0.5 % of patients. Isolated instances of hepatotoxicity have been reported 2-6 weeks after the start of treatment but with rapid recovery upon treatment cessation.	Uncoupler of oxidative phosphorylation at higher concentrations than tolcapone.	(Khetani *et al.*, 2013; Naven *et al.*, 2012; Korlipara *et al.*, 2004)

Abbreviations: C_{max}, maximum serum concentration of a drug after dosing; CYP450, cytochrome P450; L-dopa, levodopa; iDILI, idiosyncratic drug-induced liver injury; $T_{1/2}$, time taken for the concentration of the drug in the plasma to be reduced by 50 %.

Chapter 2

Investigation of Drug-induced Mitochondrial Dysfunction Using HepG2 Cells

CONTENTS

2.1 INTRODUCTION

Hepatoma-derived HepG2 cells are frequently used as a model for the identification of compounds with hepatic liabilities in the early stages of drug development due to their wide availability and reproducibility (Gerets *et al.*, 2012).

As an acknowledged factor in the onset of iDILI, mitochondrial dysfunction forms an integral part of screening for compound-induced hepatotoxicity in most pharmaceutical companies (Will and Dykens, 2014). It is generally accepted that HepG2 cells have utility in first tier screening to identify compounds with a mitochondrial liability, yet there is little evidence of the use of HepG2 cells for the determination of mitochondrial dysfunction mechanisms (Kamalian *et al.*, 2015). It was hypothesised that with the application of appropriate manipulations, HepG2 cells can be used to identify multiple mechanisms and potencies of drug-induced mitochondrial dysfunction.

The research described in this chapter therefore aimed to determine the mechanisms of HepG2 cell mitochondrial dysfunction induced by a panel of compounds with a range of previously reported mitochondrial liabilities (Table 1.8). Ultimately, this would provide baseline information which could be used to guide the testing of drug-induced mitochondrial dysfunction in personalised HepG2 cells (personalised HepG2 cell generation described in Chapter 5). The compounds selected were flutamide and tolcapone, alongside non-hepatotoxic structural analogues, bicalutamide and entacapone (Table 1.8). In addition, the limited expression of many enzymes required for xenobiotic metabolism in HepG2 cells, alongside knowledge of the rapid first-pass metabolism of flutamide meant its primary metabolite, 2-hydroxyflutamide was also included in the panel of compounds (Sison-Young *et al.*, 2015; Shet *et al.*, 1997).

When cultured in glucose media, HepG2 cells are capable of overcoming (at least in part) drug-induced mitochondrial dysfunction via the upregulation of glycolysis to generate ATP. This adaptation greatly reduces the ability of HepG2 cells to identify compound-induced mitochondrial dysfunction via the measurement of cellular ATP alone. This effect may be circumvented via the replacement of glucose in media with galactose. This decreases the ATP yield of glycolysis, thereby increasing reliance upon mitochondrial oxidative phosphorylation; thus compounds which interfere with mitochondrial respiration can be identified (Marroquin *et al.*, 2007). Concordantly, measurements of ATP following compound treatment were performed in acutely galactose-conditioned as well as glucose-cultured HepG2 cells.

Following the use of acute galactose-conditioning to identify direct mitochondrial dysfunction, assessment of oxygen consumption rate (OCR) in intact and permeabilised HepG2 cells using extracellular flux (XF) analysis enabled in-depth assessment of the nature of compound-induced mitochondrial dysfunction. Subsequently, NAD^+/NADH ratio, $\Delta\psi_m$ and cellular superoxide levels were measured to provide quantification of the downstream impacts of mitochondrial dysfunction. The cofactor NAD^+ is produced at complex I of the ETC when NADH is oxidised to donate electrons to the ETC. Reduced production of NAD^+ and a low NAD^+/NADH ratio can therefore be particularly indicative of complex I dysfunction.

The final manipulation applied to HepG2 cells was the depletion of mtDNA to generate HepG2 ρ0 cells (Section 1.5.2.3). The absence of mtDNA and consequent lack of critical ETC subunits in these cells causes disrupted respiratory complex formation and overall ETC dysfunction (Schon *et al.*, 2012). Resultantly, if compound-induced dysfunction is evident in HepG2 cells but not HepG2 ρ0 cells, it supports a case of direct mitochondrial dysfunction. On the other hand if dysfunction is evident in HepG2 ρ0 cells then the compound in question must have other liabilities in addition to ETC perturbations. Application of this range of manipulations to HepG2 cells, alongside treatment with compounds host to different mitochondrial liabilities enabled the mitochondrial perturbations induced by the test compound panel to be investigated in this cell line.

2.2 MATERIALS AND METHODS

2.2.1 Materials

All forms of Dulbecco's Modified Eagle's Medium (DMEM), MitoSOX™ Red indicator and rat tail collagen I were purchased from Life Technologies (Paisley, UK). HepG2 cells were purchased from European Collection of Cell Cultures (ECACC, Salisbury, UK). NAD^+/NADH ratio assay kits were purchased from eEnzyme (MD, USA). Cytotoxicity detection kits were purchased from Roche Diagnostics Ltd (West Sussex, UK). All XF analysis consumables (except for compounds) were purchased from Agilent Technologies (CA, USA). Flat-bottomed 96-well plates were from ThermoFisher Scientific (Loughborough, UK). Mitochondrial membrane potential indicator (m-MPI) was purchased from Codex BioSolutions (MD, USA). All other reagents and chemicals were purchased from Sigma Aldrich (Dorset, UK) unless stated otherwise.

2.2.2 Cell culture

HepG2 cells were maintained in DMEM high-glucose media (glucose; 25 mM) supplemented with foetal bovine serum (FBS; 10 % v/v), sodium pyruvate (1 mM) and HEPES ((4-(2-hydroxyethyl)-1-piperazineethanesulfonic acid), 1 mM). HepG2 ρ0 cells were maintained in DMEM/F-12 GlutaMAX™ (glucose; 17 mM) supplemented with FBS (10 % v/v), sodium pyruvate (1 mM), uridine (500 µM) and HEPES (2 mM). All cells were incubated at 37 °C and 5 % CO_2. Cells were used up to passage 20.

2.2.3 Dual assessment of mitochondrial function (ATP content) alongside cytotoxicity (Lactate dehydrogenase release)

2.2.3.1 Metabolic manipulation using galactose media

Assessment of direct mitochondrial dysfunction in carcinoma cell lines such as HepG2 cells requires the use of galactose rather than glucose media. By culturing cells in a galactose medium, glycolysis must be initiated from galactose oxidation to pyruvate. This reduces the net generation of ATP and increases cell reliance upon oxidative phosphorylation. This enables detection of compounds which perturb mitochondrial function and is collectively known as the "glucose-galactose" assay (Figure 2.1) (Reitzer *et al.*, 1979; Marroquin *et al.*, 2007).

Long-term galactose culture has since been found to induce a range of additional effects, such as a reduction in mitochondrial fission (MacVicar and Lane, 2014). Concordantly, this method has since been adapted by Kamalian *et al*. Here, the acute conditioning of cells in galactose media 2 h prior to drug treatment and ATP assessment was found to be sufficient for identifying direct drug-induced mitochondrial dysfunction (Kamalian *et al.*, 2015).

When assessed alongside cytotoxicity, it can also provide information on whether the mitochondrial dysfunction is the cause or effect of cytotoxicity (Kamalian *et al.*, 2015). Direct mitochondrial dysfunction can be defined by a ratio ≥ 2 for the compound's cellular ATP content EC_{50} between glucose and galactose media (EC_{50}ATPglu/EC_{50}ATPgal ≥ 2). Drug-induced mitochondrial dysfunction prior to cell death is identified by EC_{150}CTgal/EC_{50}ATPgal ≥ 2; where EC_{150}CTgal refers to the concentration which is required to reach 150 % of control (Kamalian *et al.*, 2015b; Swiss *et al.*, 2013).

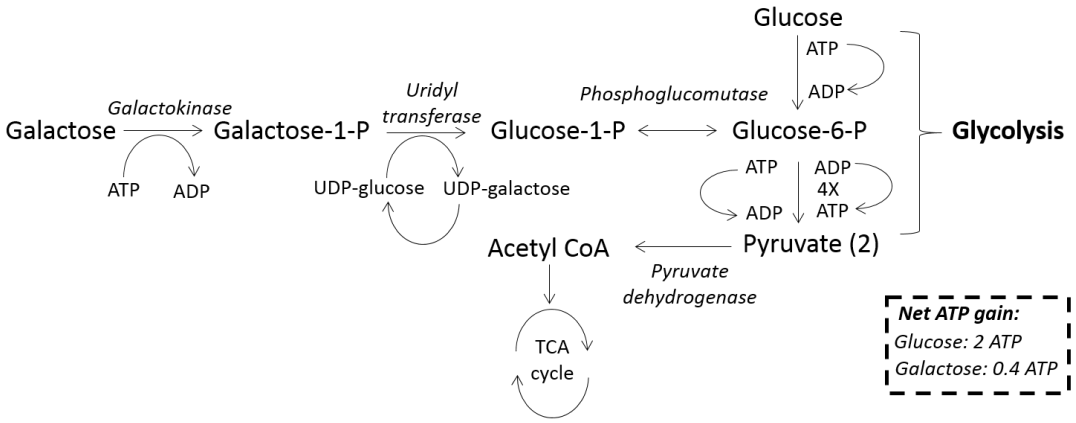

Figure 2.1. Glycolysis using galactose and glucose as substrates. At steady state because of inefficiencies in the pathway, the net ATP yield is 0.4 mol/mol galactose compared to 2 mol/mol glucose. This is sufficient for cells to become aerobically poised (Reitzer *et al.*, 1979). Abbreviations: CoA, coenzyme A; TCA, tricarboxylic acid; UDP, uridine diphosphate; 1/6-P, 1/6-phosphate.

2.2.3.2 Experimental set up

HepG2 cells or HepG2 ρ0 cells (devoid of mtDNA; generation described in Chapter 5) were collected by trypsinisation and seeded on a collagen-coated flat-bottomed 96-well plate in DMEM high-glucose media (20 000 cells/50 µL/well) and incubated (24 h, 37 °C, 5 % CO_2). Cells were then washed three times in serum-free glucose or galactose media (DMEM containing 25 mM glucose and 4 mM L-glutamine or 10 mM galactose and 6 mM L-glutamine respectively, plus supplements listed above) before addition of either glucose or galactose media (50 µL) and incubation (2 h, 37 °C, 5 % CO_2). Flutamide, 2-hydroxyflutamide, bicalutamide, tolcapone and entacapone stock solutions were prepared in DMSO and diluted further in the appropriate media. Each compound was serially diluted to generate a concentration range of 0.01 – 300 µM in both glucose and galactose media. Diluted compounds (50 µL) were then added to each well (total well volume; 100 µL) and cells were incubated (2 h, 37 °C, 5 % CO_2) before conducting assays to assess mitochondrial function and cytotoxicity. All assays used ≤ 0.5 % DMSO as a vehicle control. HepG2 ρ0 cells were tested using the same experimental set up but in glucose (not galactose) media only.

2.2.3.3 ATP bioluminescent assay

The ATP bioluminescent assay is based upon two reactions:

Reaction 1: D-luciferin + luciferase + ATP $Mg^{2+} \longrightarrow$ Luciferil adenylate complex +PP_i

Reaction 2: Luciferil adenylate complex + $O_2 \longrightarrow$ Oxyluciferin + AMP+ CO_2 + light

The luciferil adenylate complex formed in reaction 1 is subject to oxidation to oxyluciferin (reaction 2), this rapid loss of energy from oxyluciferin causes light emission at 550-570 nm, which is proportional to the ATP present when ATP is the limiting reagent.

ATP content was assessed by the addition of cell lysate (10 μL) and ATP standard curve solutions to a white-walled 96-well plate. ATP assay mix (40 μL; prepared according to the manufacturer's instructions) was then added and bioluminescence was measured (Varioskan, Thermo Scientific).

2.2.3.4 Lactate dehydrogenase assay

Lactate dehydrogenase (LDH) is a stable cytoplasmic enzyme present in most cells, however if the integrity of the cell surface membrane is sufficiently compromised then LDH is released into the surrounding supernatant (Figure 2.2).

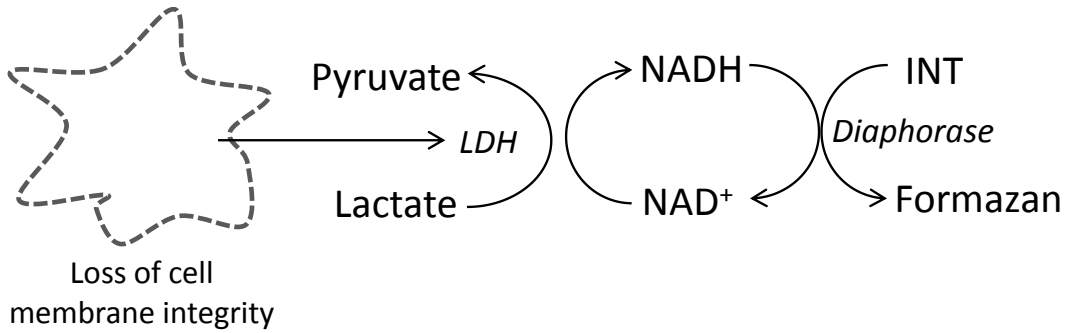

Figure 2.2. LDH release upon loss of cell membrane integrity enables the production of formazan which can be detected at 490-520 nm. Abbreviations: INT, iodonitrotetrazolium; LDH, lactate dehydrogenase.

LDH release was determined by the extraction of 25 μL supernatant and 10 μL cell lysate before use of a cytotoxicity detection kit and reading at 490 nm. LDH release was calculated as: LDH supernatant/(supernatant + lysate).

2.2.3.5 Bicinchoninic acid assay

The bicinchoninic acid (BCA) assay was used to normalise ATP results to protein content to reduce the heterogeneity of results due to cell number variability.

The BCA assay relies upon the following two reactions, in which the protein-mediated reduction of Cu^{2+} forms a stable complex with the BCA reagent, with the absorbance of this complex directly proportional to the amount of protein present.

Reaction 1: Protein + Cu^{2+} → Cu^{1+}

Reaction 2: Cu^{1+} + BCA → BCA- Cu^{1+} complex (purple)

Protein content was determined using cell lysate (10 µL) and protein standards (10 µL). BCA assay fluorescence was then measured at 570 nm.

2.2.4 Extracellular flux analysis

2.2.4.1 Extracellular flux analysis technology

The glucose-galactose assay has become the industry standard for the early assessment of compounds, however direct assessment of mitochondrial respiratory function is preferred if compounds are advanced in the drug-development pipeline based on a favourable safety profile (Will and Dykens, 2014).

The most commonly used commercial machine for this technique, the XFe96 analyser (Agilent Technologies) uses a 96-well cell culture microplate with a sensor cartridge for each well. On each sensor probe are two fluorophores, one sensitive to oxygen [O_2] and the other to protons [H^+]. Periodically, fibre optic bundles are lowered into the sensor cartridge, which emit light to excite the embedded fluorophores, a change in the emission of the fluorophore provides information on the changes in [O_2] and [H^+]. Importantly, this lowering also forms a transient microchamber (200 µm) above the cell monolayer which allows the rapid detection of changes in [O_2] and [H^+]. Following measurement the sensor cartridge is raised to allow mixing of the isolated micro chamber with the rest of the sample medium. Injection ports in the XFe96 analyser also enable the sequential addition of up to four compounds per well at user-defined intervals to determine multiple parameters of mitochondrial function (Figure 2.3) (Perry *et al.*, 2013; Agilent).

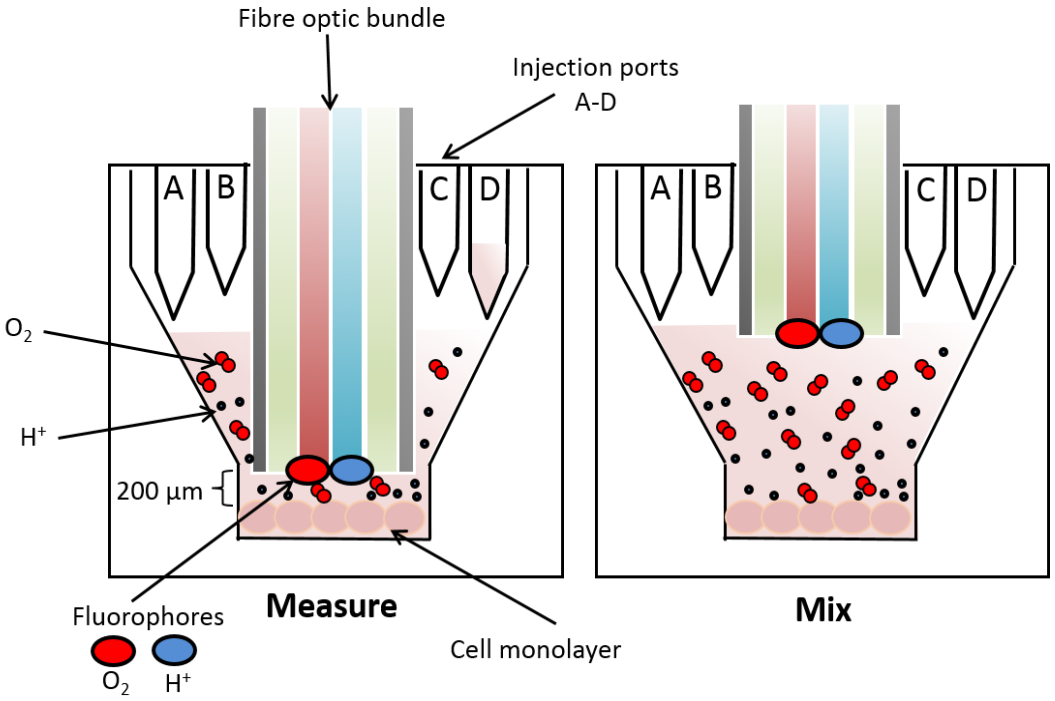

Figure 2.3. Schematic representation of the detection of [O_2] and [H^+] by the XFe96 analyser (Agilent Technologies). Measurement of changes in [O_2] and [H^+] occurs by the lowering of a sensor cartridge containing fluorophores into a microchamber containing a cell monolayer. The microchamber enables the rapid detection of changes in [O_2] and [H^+]. Following measurement, the sensor cartridge is lifted, enabling mixing of the microchamber contents with the remaining cell medium. Injection ports A-D enable the addition of substrates and inhibitors at up to four points during the assay.

2.2.4.2 Extracellular flux assay preparation and normalisation

HepG2 cells were collected by trypsinisation and seeded on a collagen-coated XFe96 cell culture microplate (25 000 cells/100 µL medium/well) and incubated (37 °C, 5 % CO_2) overnight. Following completion of XF assays, media were removed from all wells and somatic ATP releasing agent (20 µL) was added to each well before shaking for 1 min, transfer of lysates (10 µL) to a 96-well plate and performance of a BCA assay as described above (Section 2.2.3.5). Lysates of respiratory complex assays had protein content determined using a Bradford assay (Bio-Rad, Deeside, UK) due to cross-reactivity of substrates with the BCA reagent. Protein content per well was used to normalise OCR (OCR/µg protein). OCR/µg protein was then expressed as a % of the vehicle control value. All assays used ≤ 0.5 % DMSO as a vehicle control.

2.2.4.3 Mitochondrial stress test

Cells were incubated (1 h, 37 °C, 0 % CO_2) before replacement of culture medium with 175 µL of unbuffered XF base medium supplemented with glucose (25 mM), L-glutamine (2 mM), sodium pyruvate (1 mM), pre-warmed to 37 °C (pH 7.4). Following an equilibration period,

three measurement cycles (each cycle: 3 min mix and 3 min measure) were used to establish a baseline OCR prior to the acute injection of each of the five test compounds (7.8-500 µM). Following compound injection there were nine OCR measurement cycles (total: 54 min), a mitochondrial stress test was then performed consisting of sequential injections of oligomycin (ATP synthase inhibitor; 1 µM), carbonyl cyanide 4-(trifluoromethoxy) phenylhydrazone (FCCP) (uncoupler; 0.5 µM) and rotenone/antimycin A (complex I/III inhibitors respectively; 1 µM each), with three measurement cycles between each (Figure 2.4).

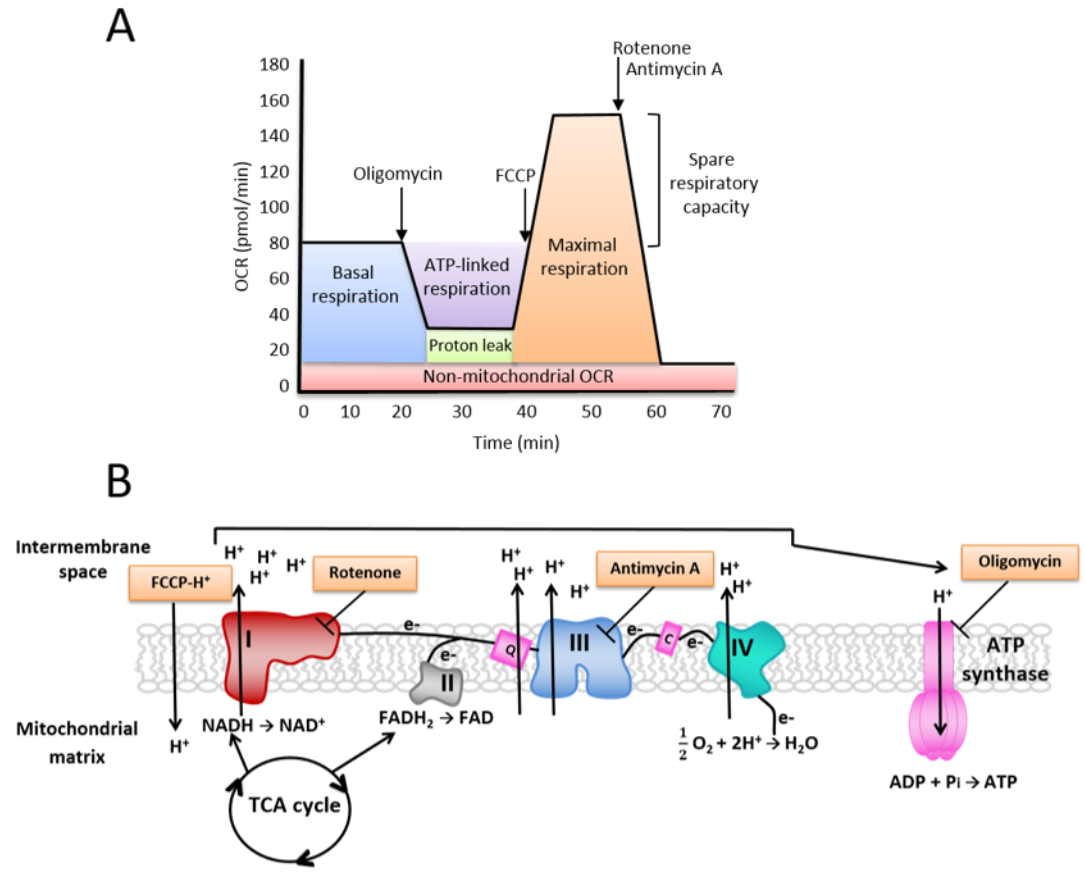

Figure 2.4. Mitochondrial stress test. A: Example trace of mitochondrial stress test with parameters derived: basal, ATP-linked and maximal respiration, proton leak and non-mitochondrial OCR. B: Site of action of ETC inhibitors used in mitochondrial stress test. Abbreviations: FCCP, carbonyl cyanide 4-(trifluoromethoxy) phenylhydrazone; OCR, oxygen consumption rate; TCA, tricarboxylic acid.

2.2.4.4 Respiratory complex assays (I-IV)

Culture medium was replaced with mitochondrial assay solution buffer (MAS: $MgCl_2$; 5 mM, mannitol; 220 mM, sucrose; 70 mM, KH_2PO_4; 10 mM, HEPES; 2 mM, ethylene glycol-bis(β-aminoethyl ether)-N,N,N′,N′-tetraacetic acid (EGTA); 1 mM; bovine serum albumin (BSA); 0.4 % w/v) containing constituents to permeabilise cells and stimulate oxygen consumption via

complex I (ADP; 4.6 mM, malic acid; 30 mM, glutamic acid; 22 mM, BSA; 30 µM, PMP; 1 nM), complex II (ADP; 4.6 mM, succinic acid; 20 mM, rotenone; 1 µM, BSA; 30 µM, PMP; 1 nM), complex III (ADP; 4.6 mM, duroquinol; 500 µM, rotenone; 1 µM, malonic acid; 40 µM, BSA; 0.2 % w/v, PMP; 1 nM) or complex IV (ADP; 4.6 mM, ascorbic acid; 20 mM, TMPD (N,N,N',N'-tetramethyl-p-phenylenediamine); 0.5 mM, antimycin A; 2 mM, BSA; 30 mM, PMP; 1 nM). Following a basal measurement (no equilibration period) of three cycles of mix (30 s), wait (30 s) and measure (2 min), flutamide or 2-hydroxyflutamide was injected (10-250 µM) followed by a mitochondrial stress test as detailed previously, only each measurement cycle was 3 min rather than 6 min. The site of action of complex-specific substrates and inhibitors is shown in Figure 2.5.

For assessment of complex IV activity, rather than injection of antimycin A/rotenone (complex I and III inhibitors respectively) to prevent mitochondrial respiration, potassium azide (complex IV inhibitor) was used. Importantly this also allowed the deduction of non-mitochondrial OCR as a result of the addition of TMPD/ascorbate in either assay. This active redox couple can "consume" oxygen within the medium of the well, producing a significant amount of background which could be mistaken for complex IV activity (Morgan and Wikstrom, 1991). Complex I, II, III or IV activity was defined as maximal respiration (as a % of basal respiration) as a % of vehicle control.

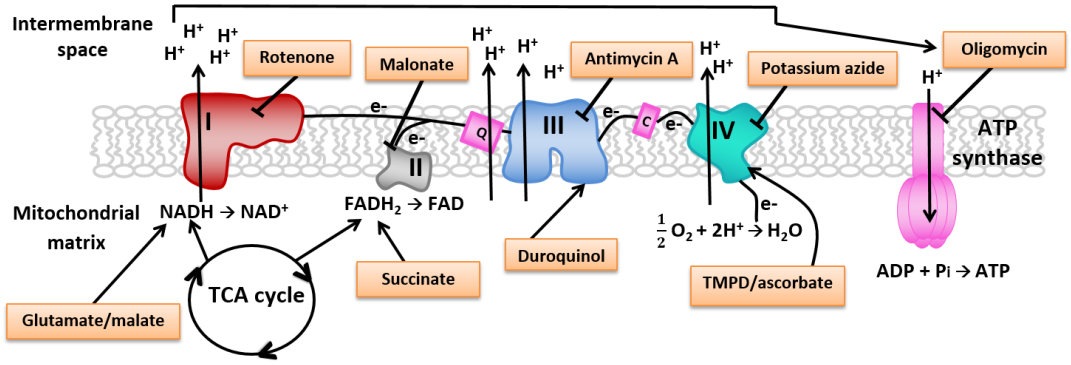

Figure 2.5. Site of action of substrates and inhibitors used in complex assays. Abbreviations: TCA, tricarboxylic acid; TMPD, N,N,N',N'-tetramethyl-*p*-phenylenediamine.

2.2.4.5 Complex V (ATP synthase) assays

Neither flutamide nor 2-hydroxyflutamide significantly affected complex IV activity, therefore ATP synthase activity was assessed by stimulating respiration via complex IV. Culture medium was replaced with MAS buffer containing constituents to stimulate oxygen consumption via complex IV activity (as described in 2.2.4.4). Injections consisted of MAS or FCCP (0.5 µM) followed by injection of flutamide or 2-hydroxyflutamide (10-250 µM) or

oligomycin (positive control; 1 µM) (Figure 2.6). ATP synthase activity was defined as the difference in compound-induced OCR change between coupled (MAS injection) and uncoupled (FCCP injection) cells compared to vehicle control.

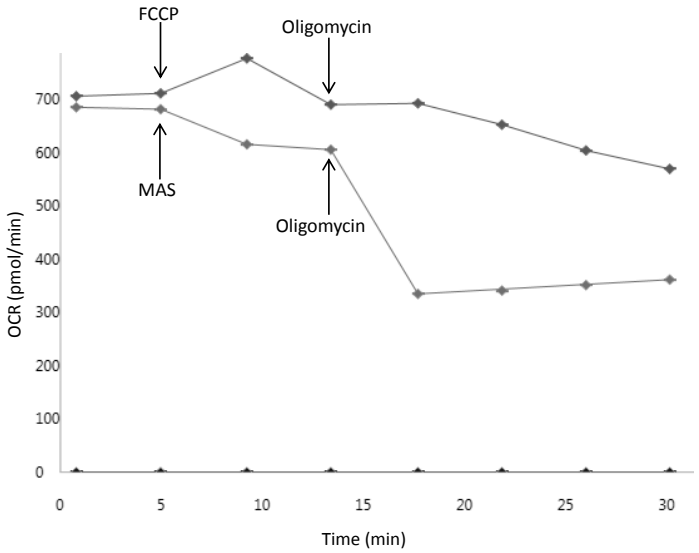

Figure 2.6. Proof of concept: Representative trace of complex V assay using the positive control, oligomycin (complex V/ATP synthase inhibitor). The impact of 2-hydroxyflutamide and flutamide on complex V activity was assessed following a proof of concept assay to test the ability of the experimental set up to identify a complex V (ATP synthase) inhibitor. Substrates to stimulate respiration via complex IV in permeabilised HepG2 cells were supplied, following this, half of the cells were treated with FCCP to cause uncoupling, the other half were treated with MAS and so remained coupled. All cells were then treated with oligomycin (positive control). In uncoupled cells, oligomycin did not change the OCR, whereas in cells which were still coupled, oligomycin induced a substantial decrease in OCR, demonstrating the ability of the assay to identify an ATP synthase inhibitor.

2.2.5 Assessment of NAD^+/NADH ratio

For the assessment of NAD^+/NADH ratio, HepG2 cells were collected by trypsinisation and seeded on a 24-well plate (450 000 cells/500 µL/well) and incubated overnight in glucose media (37 °C, 5 % CO_2). Cells were then treated with fresh glucose media containing 30-500 µM of each of the five test compounds and incubated (2 h, 37 °C, 5 % CO_2). Triplicate wells of all treated-cells were then lysed with NAD^+/NADH lysis buffer before extraction of NAD^+, NADH or both using the NAD^+/NADH ratio assay kit according to the manufacturer's instructions. Following the addition of NADH reaction mixture to all extractions and NADH standards, the reaction was incubated in the dark (1 h, room temperature) before monitoring fluorescence at excitation/emission 540/590 nm and comparison to standard values to calculate NAD^+/NADH ratio.

2.2.6 Assessment of cellular superoxide level

2.2.6.1 MitoSOX™ Red reagent

The MitoSOX™ Red reagent offers direct measurement of cellular superoxide in live cells where it selectively targets mitochondria (Figure 2.7). Here, it is rapidly oxidised by superoxide but not by other ROS or reactive nitrogen species (RNS), this oxidation causes emission of red fluorescence which can be measured using a standard plate reader assay (Perry *et al.*, 2013).

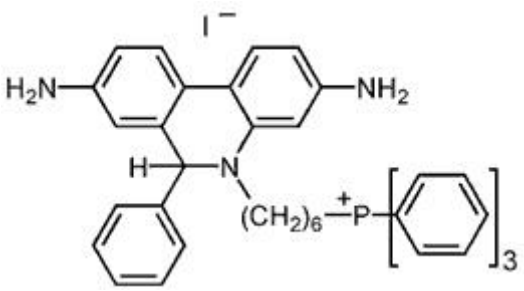

Figure 2.7. Structure of MitoSOX™ Red reagent. This reagent selectively targets mitochondria (where the vast proportion of cellular superoxide is produced) due to its positively charged phosphonium group.

2.2.6.2 Experimental set up

HepG2 cells were collected by trypsinisation and seeded on a 24-well plate (150 000 cells/500 µL/well) and incubated overnight in glucose media (37 °C, 5 % CO_2). Cells were then treated with fresh glucose media containing 15-500 µM of each of the five test compounds and incubated (2 h, 37 °C, 5 % CO_2). MitoSOX™ Red indicator was then added to each well (5 µL/well) and cells were incubated in the dark for 30 min (37 °C, 5 % CO_2). Cells were then collected by trypsinisation and measurements were made using a plate reader at excitation/emission 396/579 nm in a white-walled 96-well plate.

2.2.7 Measurement of mitochondrial membrane potential

2.2.7.1 Fluorescent dyes for the measurement of mitochondrial membrane potential

In healthy cells mitochondria are polarised, enabling the fluorescent cationic, lipophilic dye, m-MPI to accumulate in the mitochondrial matrix and form red fluorescent aggregates (termed J-aggregates). However, if the inner mitochondrial membrane becomes depolarised, m-MPI is unable to accumulate and remains in a monomeric form in the cytoplasm, which shows as green fluorescence (Figure 2.8). Resultantly the ratio of red/green emission can be used as a marker of mitochondrial polarisation, with a lower ratio indicating mitochondrial depolarisation/loss of $\Delta\psi_m$ (Perry *et al.*, 2011; Scaduto and Grotyohann, 1999).

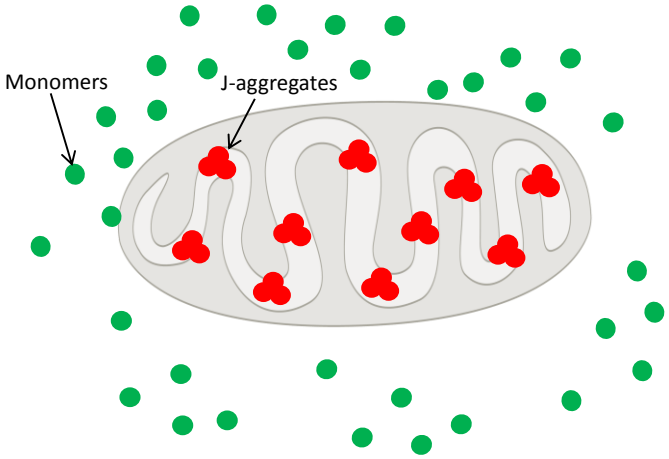

Figure 2.8. Schematic diagram of the formation of intra-mitochondrial J-aggregates in the mitochondria or cytosolic monomers during the membrane potential assay. If the inner mitochondrial membrane is polarised, the m-MPI dye is able to accumulate in the mitochondria and form J-aggregates, however if the mitochondria have become depolarised upon compound treatment, m-MPI remains in the cytoplasm in a monomeric form.

2.2.7.2 Experimental set up

For the measurement of mitochondrial polarisation, HepG2 cells were collected by trypsinisation and seeded on a black 96-well plate (35 000 cells/50 µL/well) and incubated overnight in glucose media (37 °C, 5 % CO_2). Cells were then treated with fresh glucose media containing 5-500 µM of flutamide, bicalutamide or 2-hydroxyflutamide or 31.3 µM-500 µM of tolcapone or entacapone and incubated (2 h, 37 °C, 5 % CO_2). m-MPI indicator was then added (50 µL/well) and cells were incubated in the dark (30 min, 37 °C, 5 % CO_2) before removal of supernatant and addition of m-MPI assay buffer and simultaneous fluorescence measurement at 485/530 nm (green fluorescence) and 485/590 nm (red fluorescence).

2.2.8 Statistical analysis

Data are representative of at least three independent experiments (n=3) and are expressed as mean ± standard error of the mean (SEM). EC_{50} data were determined by nonlinear regression analysis using GraphPad Prism 7.0. Normality was assessed using a Shapiro-Wilk test. Statistical significance was determined by a one-way ANOVA for parametric data and a Kruskal-Wallis test for non-parametric data followed by a Dunnett's post-hoc test using StatsDirect 2.7.9. Significance was determined from a $p\ value < 0.05$.

2.3 RESULTS

2.3.1 Identification of compound-induced direct mitochondrial dysfunction

To identify compound-induced mitochondrial dysfunction in HepG2 cells in the absence of significant cell death, the cellular ATP levels and LDH release from glucose- and acutely galactose-conditioned cells were simultaneously assessed. None of the test compounds (flutamide, 2-hydroxyflutamide, bicalutamide, tolcapone and entacapone) induced a significant increase in LDH release in glucose or galactose-conditioned cells after 2 h, however changes in ATP content varied significantly. Flutamide and 2-hydroxyflutamide induced an almost equipotent, concentration-dependent decrease in ATP content in glucose-conditioned cells, with galactose-conditioned cells demonstrating a more pronounced decrease in ATP content, which was significantly different to their glucose-conditioned counterparts (Figure 2.9A, B). Bicalutamide induced a significant decrease in ATP level but it was not significantly different between glucose- and galactose-conditioned cells (Figure 2.9C). Tolcapone induced a significant decrease in the ATP content of galactose-conditioned cells but not in glucose-conditioned cells (Figure 2.9D). Entacapone did not cause a significant decrease in ATP content in either glucose or galactose-conditioned cells (Figure 2.9E).

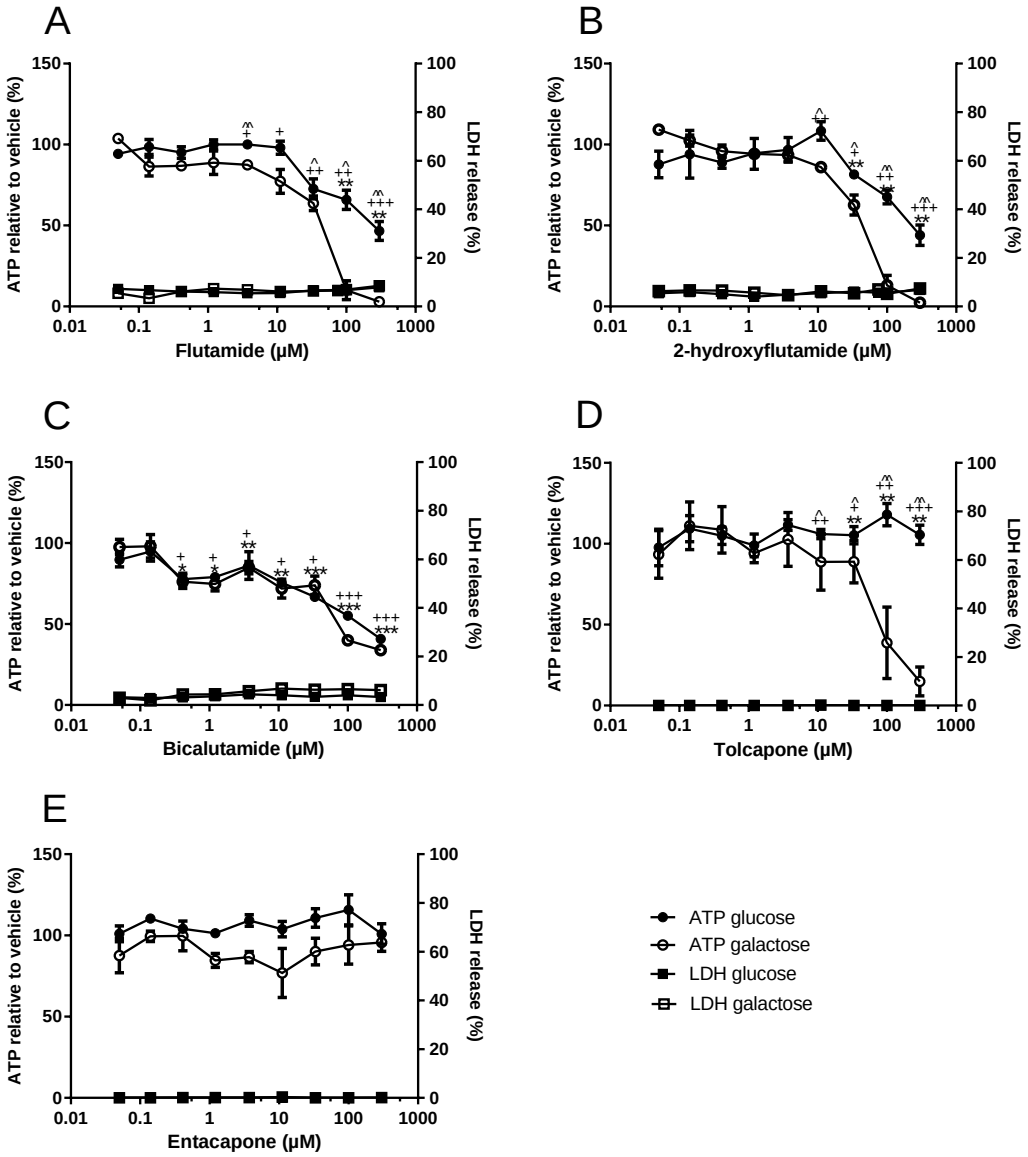

Figure 2.9. The effect of flutamide (A), 2-hydroxyflutamide (B), bicalutamide (C), tolcapone (D) and entacapone (E) exposure on ATP content and cytotoxicity. HepG2 cells were treated (2 h) with serial concentrations of compounds up to 300 μM in glucose or galactose media. ATP values are expressed as a percentage of those of the vehicle control. Lactate dehydrogenase (LDH) release is expressed as extracellular LDH as a % of total LDH. Statistical significance compared to vehicle control: glucose: * $p < 0.05$, ** $p < 0.01$, *** $p < 0.001$, galactose: $^{+}$ $p < 0.05$, $^{++}$ $p < 0.01$, $^{+++}$ $p < 0.001$, between glucose and galactose: ^ $p < 0.05$, ^^ $p < 0.01$, ^^^ $p < 0.001$. Data are presented as mean ± SEM of n=3 experiments.

Flutamide, 2-hydroxyflutamide and tolcapone exceeded the threshold for direct mitochondrial dysfunction (EC_{50}ATPglu/EC_{50}ATPgal ≥ 2) and induced mitochondrial dysfunction in the absence of cell death (Table 2.1). Whereas bicalutamide had an EC_{50}ATPglu/EC_{50}ATPgal < 2 and an EC_{50} value for entacapone was unable to be determined due to an absence of toxicity at the concentrations used (Table 2.1).

Table 2.1. The effect of flutamide, 2-hydroxyflutamide, bicalutamide, tolcapone and entacapone exposure on intracellular ATP content and cytotoxicity of HepG2 cells. HepG2 cells were treated (2 h) with serial concentrations of compounds up to 300 µM in glucose or galactose media.

Compound	EC_{50}ATP (µM)		EC_{150}CT (µM)		C_{max} (µM)	EC_{50}ATPglu/ EC_{50}ATPgal (*p* value[a])	EC_{150}CTgal/ EC_{50}ATPgal (*p* value[b])
	GLU	GAL	GLU	GAL			
Flutamide	255	43.9	>300	>300	0.0720	5.82 (0.03)	>11 (n/d)
2-hydroxyflutamide	267	48.5	>300	>300	4.40	5.51 (0.01)	>10 (n/d)
Bicalutamide	148	103	>300	>300	1.70	1.44 (0.22)	>4 (n/d)
Tolcapone	>300	74.1	>300	>300	16.5	>4.04 (n/d)	n/d
Entacapone	>300	>300	>300	>300	3.90	n/d	n/d

Abbreviations: C_{max}, peak human serum concentration; EC_{50}ATP, concentration of compound to cause a 50 % reduction in ATP compared to control; EC_{150}CT, concentration of compound to cause a 50 % increase in cytotoxicity compared to control; GLU, glucose medium; GAL, galactose medium; n/d, value unable to be determined. *P* value[a] indicates the significance of EC_{50}ATPglu compared to EC_{50}ATPgal. *P* value[b] indicates the significance of EC_{150}CTgal compared to EC_{50}ATPgal.

2.3.2 Extracellular flux analysis of compound-induced changes in mitochondrial function

Following the identification of mitochondrial liabilities, the effect of compounds on mitochondrial function was assessed using a mitochondrial stress test (Figure 2.10). Both flutamide and 2-hydroxyflutamide induced a significant concentration-dependent decrease in basal and maximal respiration whereas bicalutamide only caused a significant concentration-dependent decrease in maximal respiration (Figure 2.11A, 2.12A and B) Flutamide and 2-hydroxyflutamide also caused a significant increase in proton leak and a

significant decrease in spare respiratory capacity and ATP-linked OCR, changes which were not observed upon bicalutamide-treatment (Figure 2.12E, F and G).

A

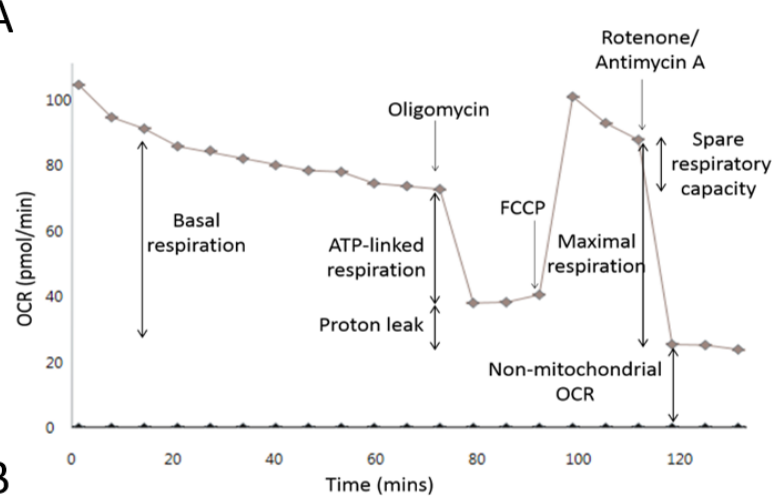

B

Parameter	Calculation
Basal respiration	Last OCR measurement before oligomycin injection - Non-mitochondrial respiration rate
Maximal respiration	Maximum OCR measurement after FCCP injection - Non-mitochondrial respiration rate
ATP-linked respiration	Last OCR measurement before oligomycin injection - Minimum OCR measurement after oligomycin injection
Spare respiratory capacity	Maximal respiration - Basal respiration
Proton leak	Minimum OCR measurement after oligomycin injection - Non-mitochondrial respiration
Non-mitochondrial OCR	Minimum OCR measurement after rotenone/antimycin A injection

Figure 2.10. Representative control mitochondrial stress test trace (A) and parameter definitions (B). Mitochondrial stress test assays consisted of a series of compound injections into the cell culture microplate. One of the five test compounds or vehicle control (shown) was first injected, followed by nine measurement cycles. Remaining injections consisted of oligomycin, FCCP and rotenone/antimycin A, with each followed by three measurement cycles. Each measurement cycle was a total of 6 min.

Both tolcapone and entacapone caused a concentration-dependent decrease in maximal respiration yet induced an increase in basal respiration, peaking at 62 µM and 250 µM respectively (Figure 2.11B, 2.12C and D). Tolcapone induced a significant increase in proton leak and concomitant decreases in spare respiratory capacity and ATP-linked OCR at

concentrations of 62.5 µM above. The same effect was seen with entacapone treatment, though not until cells were treated at a concentration of 250 µM (Figure 2.12H and I).

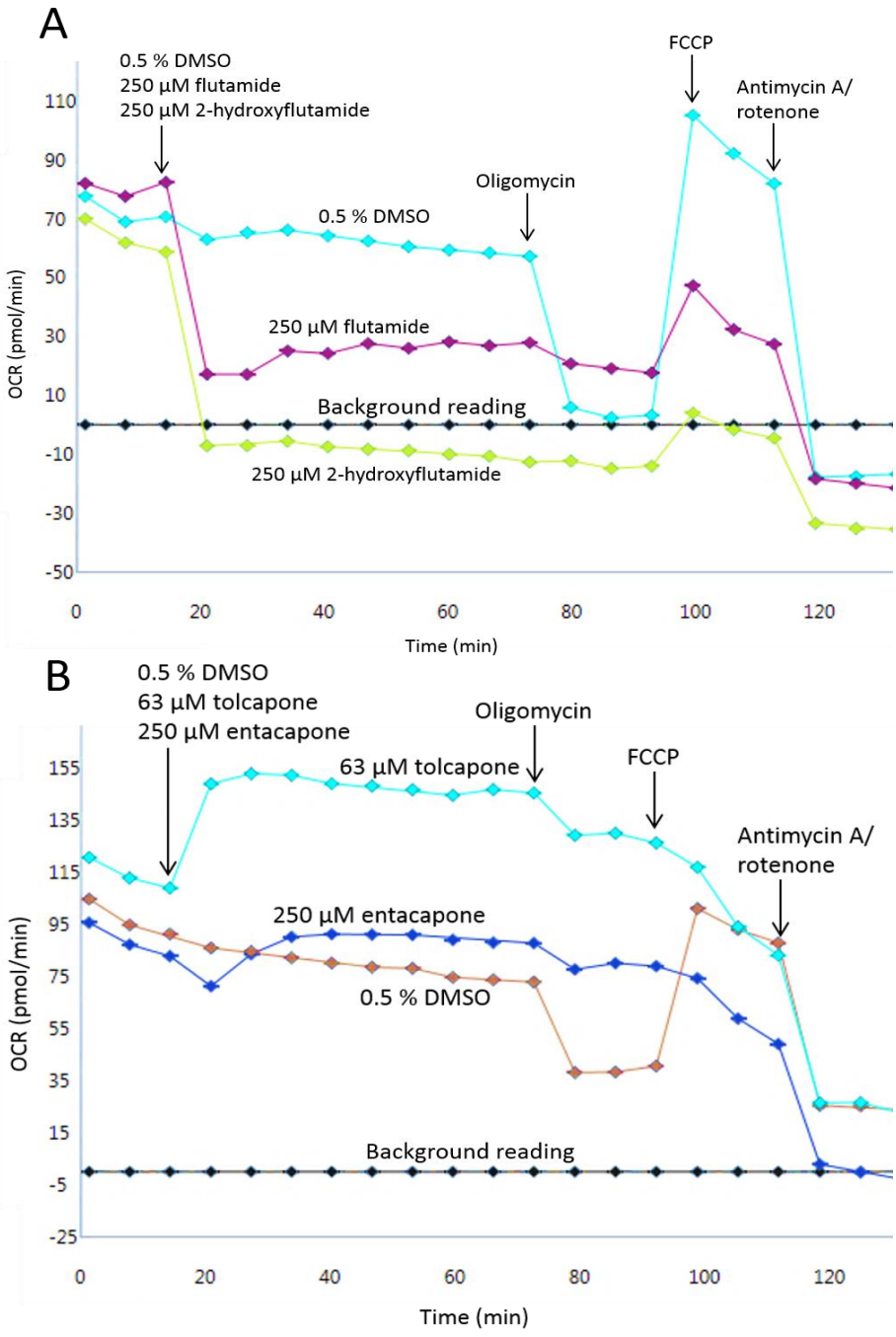

Figure 2.11. Mitochondrial stress test traces of vehicle control (A, B), flutamide (A), 2-hydroxyflutamide (A), tolcapone (B) and entacapone-treated (B) HepG2 cells. Following compound incubation (54 min), a mitochondrial stress test was performed consisting of sequential injections of oligomycin (ATP synthase inhibitor; 1 µM), carbonyl cyanide 4-(trifluoromethoxy) phenylhydrazone (FCCP) (uncoupler; 0.5 µM) and rotenone/antimycin A (complex I/III inhibitors respectively; 1 µM each). Vehicle control: 0.5 % DMSO.

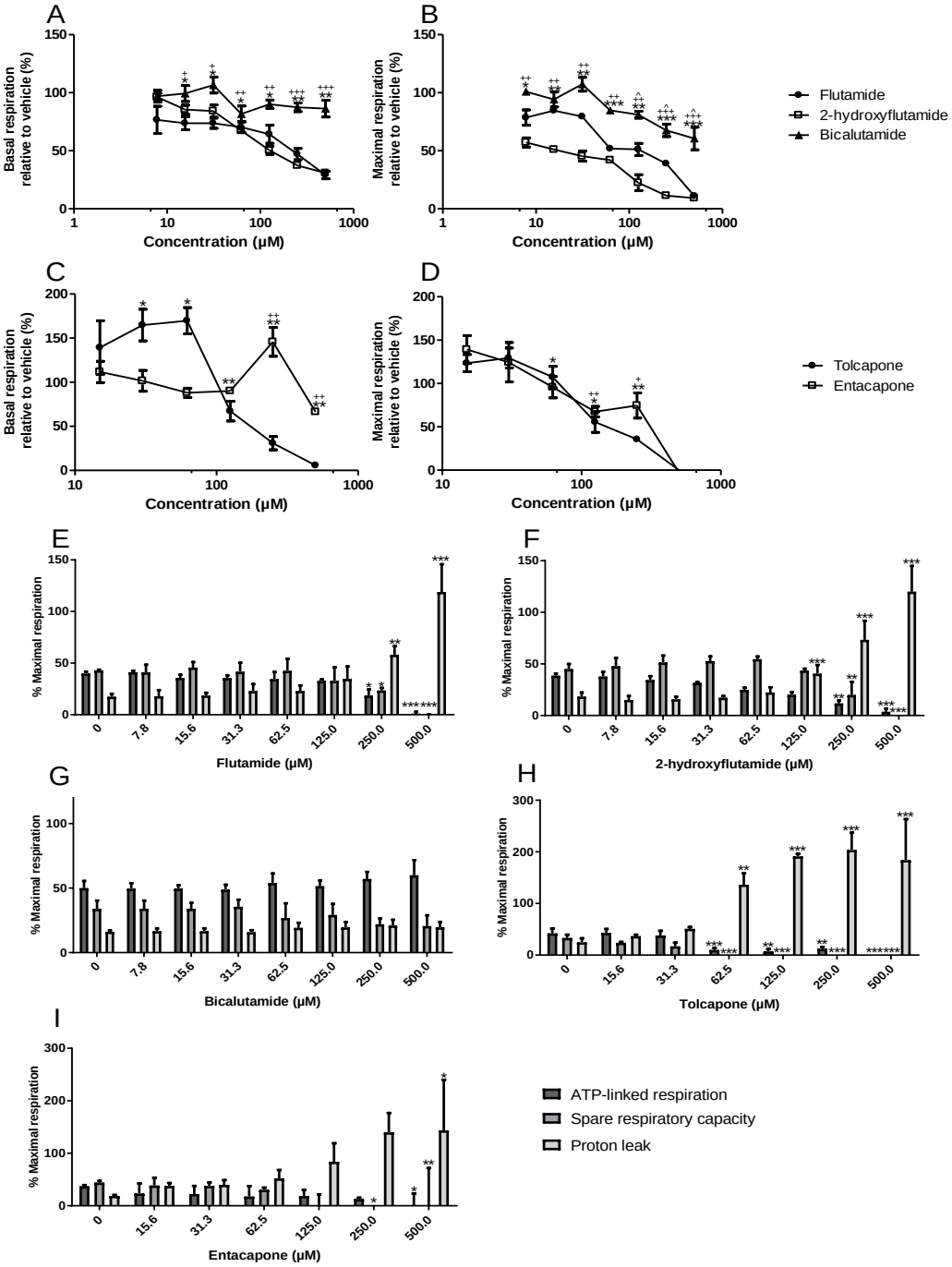

Figure 2.12. The effect of test compounds on mitochondrial respiration. HepG2 cells were acutely treated with serial concentrations of test compounds up to 500 μM before a mitochondrial stress test using extracellular flux analysis. A-D: changes in basal and maximal respiration. E-I: changes in proton leak, spare respiratory capacity and ATP-linked respiration induced by flutamide (E), 2-hydroxyflutamide (F), bicalutamide (G), tolcapone (H), entacapone (I). Statistical significance compared to vehicle control: A-D: flutamide and tolcapone: * $p < 0.05$, ** $p < 0.01$, *** $p < 0.001$, 2-hydroxyflutamide and entacapone: $^{+}p < 0.05$, $^{++}p < 0.01$, $^{+++}p < 0.001$ and bicalutamide: ^ $p < 0.05$, ^^ $p < 0.01$, ^^^ $p < 0.001$. E-I: * $p < 0.05$, ** $p < 0.01$, *** $p < 0.001$. Data are presented as mean ± SEM of n=3 experiments.

2.3.3 Assessment of compound-induced respiratory complex dysfunction

For the assessment of complexes I-IV, HepG2 cells were permeabilised in a solution containing substrates specific for the complex of interest. Cells were then treated with flutamide or 2-hydroxyflutamide followed by a mitochondrial stress test. A significant reduction in complex I activity was induced by both compounds at 125 µM and above (Figure 2.13A). Only 2-hydroxyflutamide and not flutamide induced a significant reduction in complex II activity (Figure 2.13B). Assessment of complex V/ATP synthase activity by comparison of compound-induced OCR change in uncoupled and coupled cells showed a significant reduction in complex V activity following treatment with 2-hydroxyflutamide at 125 µM and above, though this was not the case for flutamide (Figure 2.13E). Neither the parent compound nor metabolite significantly inhibited complex III or IV activity (Figure 2.13C, D).

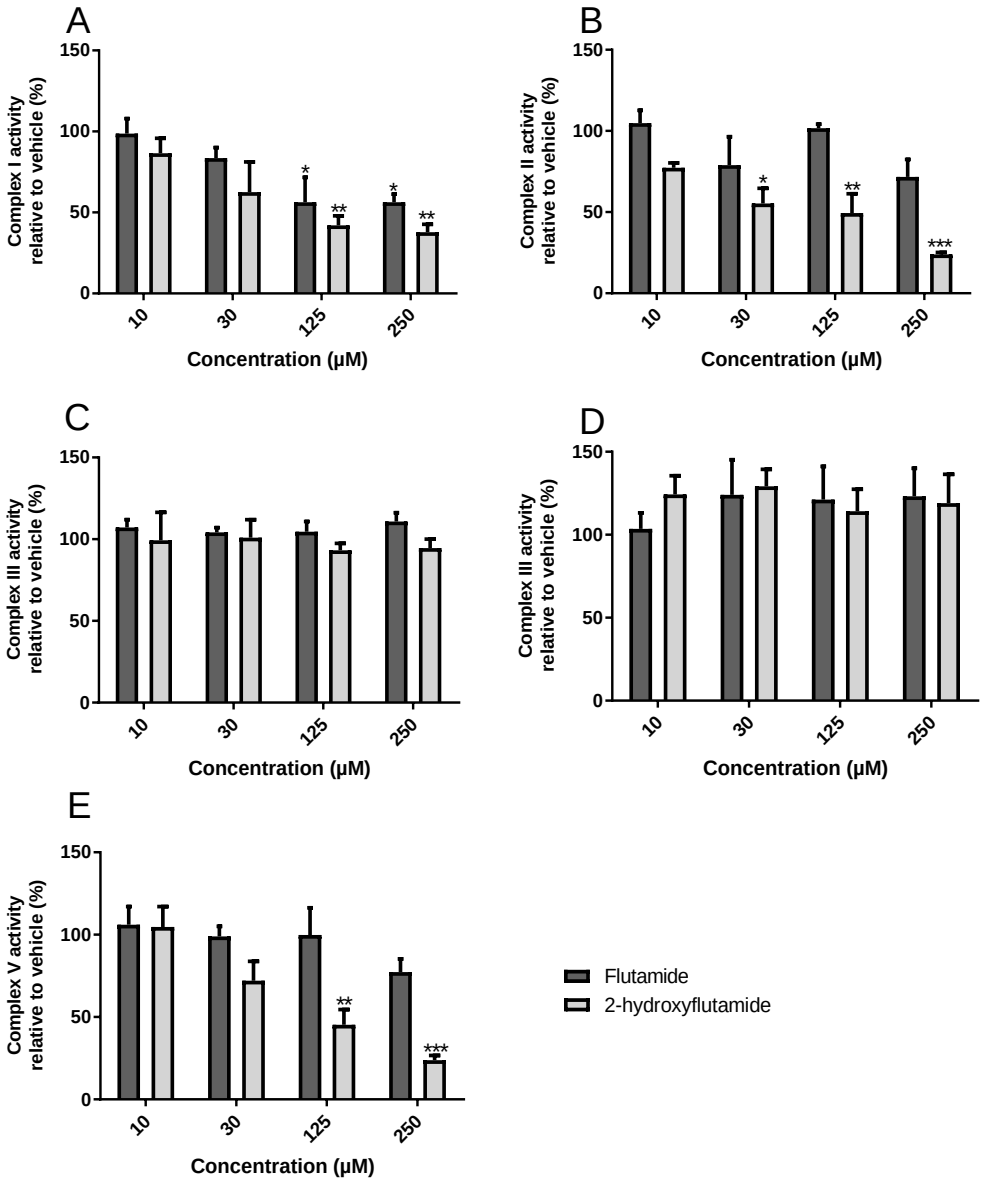

Figure 2.13. The effect of flutamide and 2-hydroxyflutamide exposure on the activity of mitochondrial respiratory complexes I-IV and ATP synthase (complex V). Permeabilised HepG2 cells provided with substrates for the complex of interest were acutely treated with flutamide or 2-hydroxyflutamide (10-250 μM) before a mitochondrial stress test using extracellular flux analysis. Complex I (A), II (B), III (C) or IV (D) activity was defined as maximal respiration (as a % of basal respiration) as a % of vehicle control. Complex V (E) activity was defined as the difference in compound-induced oxygen consumption rate (OCR) change between coupled and uncoupled cells relative to vehicle control. Statistical significance compared to vehicle control: * $p < 0.05$, ** $p < 0.01$, *** $p < 0.001$. Data are presented as mean + SEM of n=3 experiments.

2.3.4 Assessment of compound effects upon cellular NAD⁺/NADH ratio

Bicalutamide did not significantly change the ratio of NAD⁺/NADH in HepG2 cells, whereas flutamide and 2-hydroxyflutamide significantly decreased NAD⁺/NADH at 125 µM and above (Figure 2.14A). Tolcapone on the other hand increased this ratio at 125 µM and decreased the ratio at concentrations higher than this (Figure 2.14B). Entacapone also increased NAD⁺/NADH though not until 250 µM was used (Figure 2.14B).

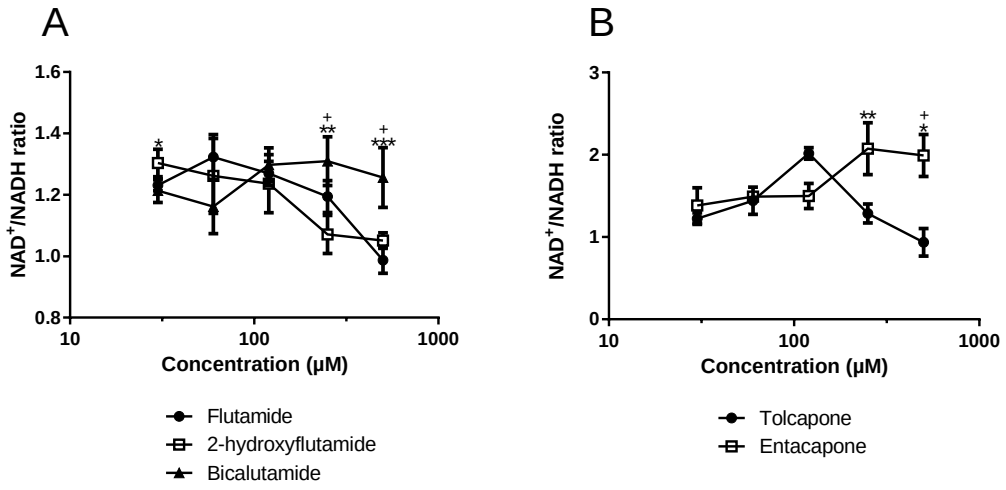

Figure 2.14. The effect of test compounds on NAD⁺/NADH ratio. HepG2 cells were treated (2 h) with test compounds up to 500 µM. Statistical significance compared to vehicle control: flutamide and tolcapone: * $p < 0.05$, ** $p < 0.01$, *** $p < 0.001$, 2-hydroxyflutamide and entacapone; $^{+}p < 0.05$, $^{++}p < 0.01$, $^{+++}p < 0.001$, bicalutamide; ^ $p < 0.05$, ^^ $p < 0.01$, ^^^ $p < 0.001$. Data are presented as mean ± SEM of n=3 experiments.

2.3.5 The effect of compounds on cellular superoxide level

Flutamide, 2-hydroxyflutamide, bicalutamide and tolcapone significantly increased cellular superoxide at 30 µM and above whereas entacapone did not induce a significant change at any of the concentrations used (Figure 2.15).

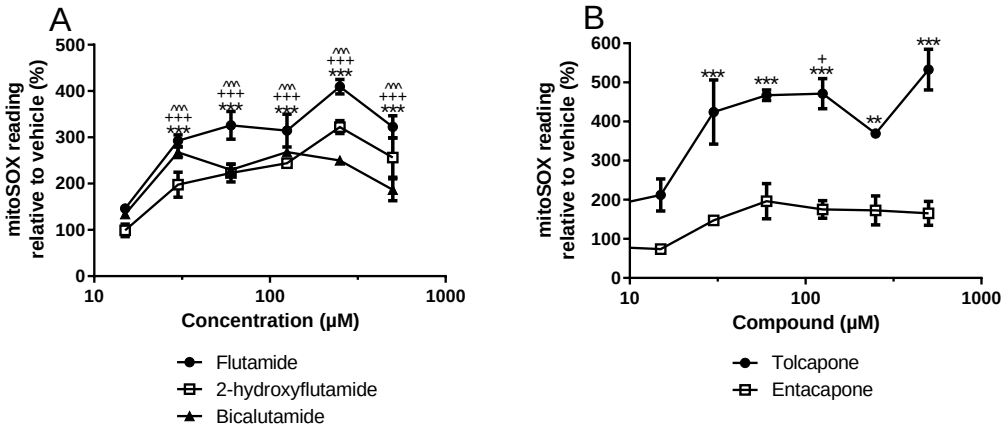

Figure 2.15. The effect of test compounds on superoxide levels. HepG2 cells were treated (2 h) with test compounds up to 500 µM. Statistical significance compared to vehicle control: flutamide and tolcapone: * $p < 0.05$, ** $p < 0.01$, *** $p < 0.001$, 2-hydroxyflutamide and entacapone: $^{+}p < 0.05$, $^{++}p < 0.01$, $^{+++}p < 0.001$, bicalutamide: $^{\wedge}p < 0.05$, $^{\wedge\wedge}p < 0.01$, $^{\wedge\wedge\wedge}p < 0.001$. Data are presented as mean ± SEM of n=3 experiments.

2.3.6 The effect of compounds on mitochondrial membrane potential

All anti-androgen compounds caused a significant decrease in red/green ratio at 10 µM and above, representative of a decrease in $\Delta\psi_m$ compared to control (Figure 2.16A). Tolcapone induced a significant reduction in $\Delta\psi_m$ at 30 µM and above, whereas entacapone did not induce a significant reduction until cells HepG2 cells were treated with 250 µM of the compound (Figure 2.16B).

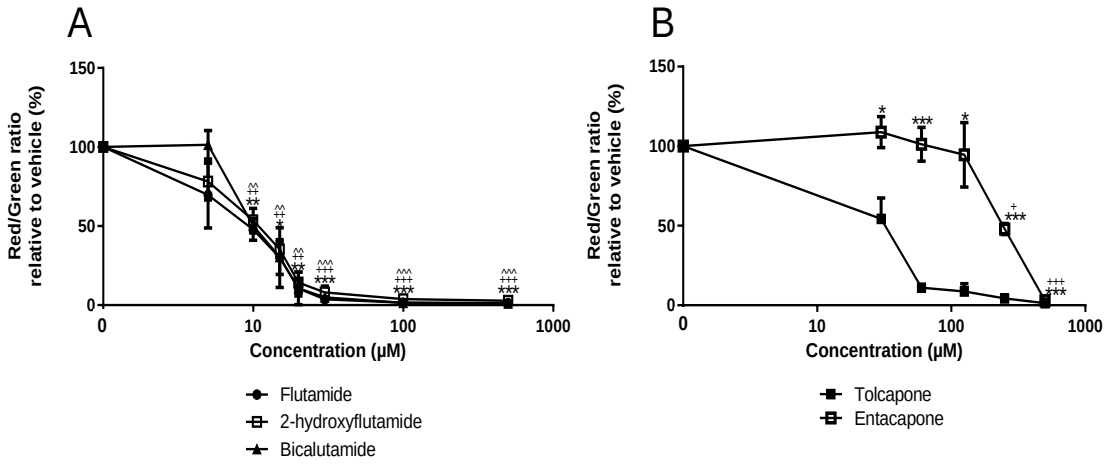

Figure 2.16. The effect of test compounds on mitochondrial membrane potential. HepG2 cells were treated (2 h) with test compounds up to 500 µM. Red/green fluorescence ratio was used as a measure of mitochondrial membrane potential. Statistical significance compared to vehicle control: flutamide and tolcapone: * $p < 0.05$, ** $p < 0.01$, *** $p < 0.001$, 2-hydroxyflutamide and entacapone: $^{+}p < 0.05$, $^{++}p < 0.01$, $^{+++}p < 0.001$, bicalutamide; $^{\wedge}p < 0.05$, $^{\wedge\wedge}p < 0.01$, $^{\wedge\wedge\wedge}p < 0.001$. Data are presented as mean ± SEM of n=3 experiments.

2.3.7 Assessment of the effect of compounds on cellular ATP and cytotoxicity in the absence of mitochondrial respiration

The absence of a functional ETC in rho zero cells (ρ0 cells; generation described in Section 5.2.3) provides an ideal model to identify dysfunction which is occurring independently of the ETC. None of the compounds induced a significant increase in cytotoxicity however flutamide and 2-hydroxyflutamide induced a significant decrease in cellular ATP, though not to the same extent seen in HepG2 WT cells (Figure 2.17A, B). Bicalutamide, tolcapone and entacapone however did not induce a significant decrease in ATP (Figure 2.17C, D, E).

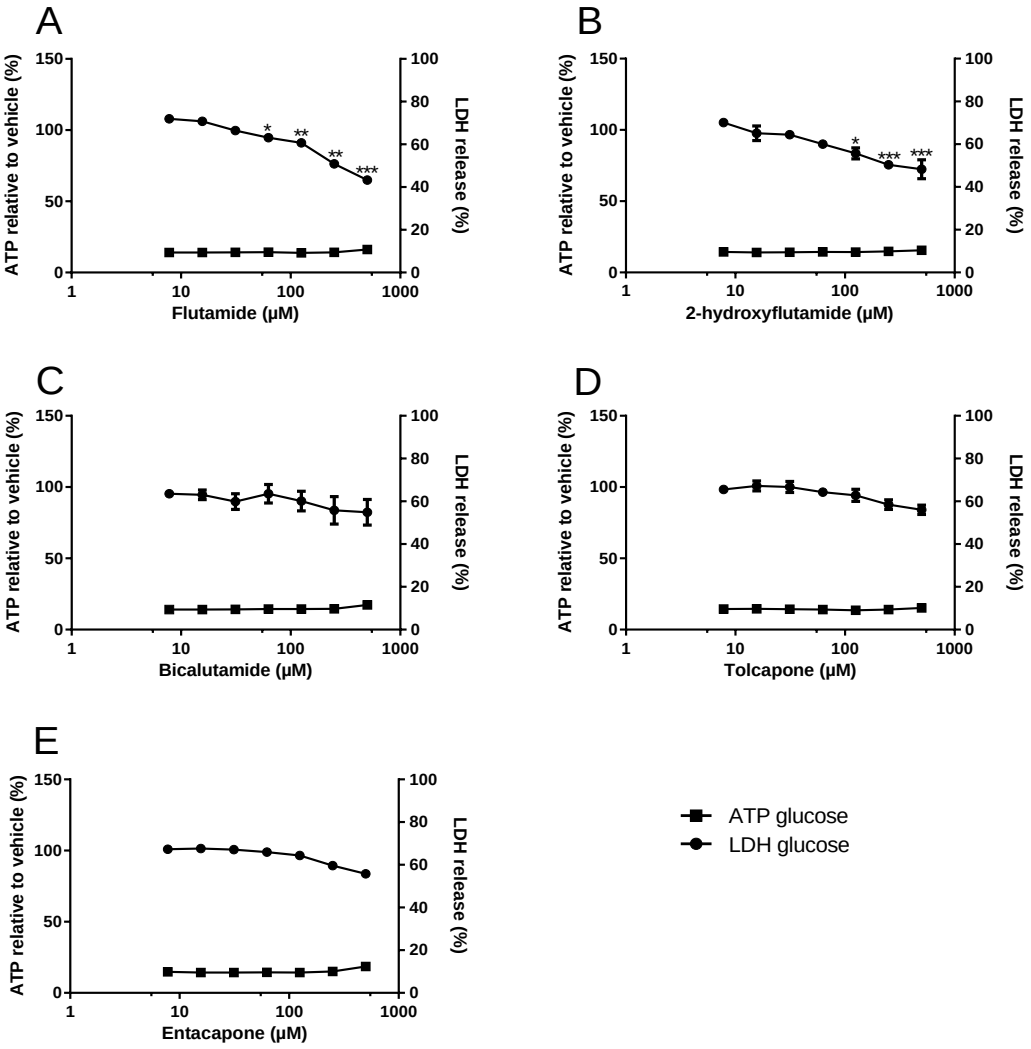

Figure 2.17. The effect of flutamide (A), 2-hydroxyflutamide (B), bicalutamide (C), tolcapone (D) and entacapone (E) exposure on ATP content and cytotoxicity of HepG2 rho zero (ρ0) cells (generation described in Section 5.2.3). HepG2 ρ0 cells were treated (2 h) with serial concentrations of compounds up to 500 μM in glucose media. ATP values are expressed as a percentage of those of the vehicle control. Lactate dehydrogenase (LDH) release is expressed as extracellular LDH as a % of total LDH. Statistical significance compared to vehicle control: * $p < 0.05$, ** $p < 0.01$, *** $p < 0.001$. Data are presented as mean ± SEM of n = 3 experiments.

2.4 DISCUSSION

HepG2 cells have previously shown utility for the detection of direct drug-induced mitochondrial dysfunction, however the findings described in this chapter have shown that this cell line can also provide mechanistic insight and differentiate between compounds which induce dysfunction of different severities.

Manipulation of HepG2 cell bioenergetics by substituting glucose for galactose in media increased HepG2 cell reliance upon oxidative phosphorylation for ATP production (Section 2.2.3.1). This was evident from the significantly greater decrease in cellular ATP content following flutamide, 2-hydroxyflutamide or tolcapone treatment of acutely galactose-conditioned cells vs glucose-cultured cells. Comparison of EC_{50} values in both media identified direct mitochondrial dysfunction induced by each compound, with simultaneous measurement of LDH release providing evidence that mitochondrial dysfunction was occurring independently of significant cytotoxicity, findings which echo those of Kamalian *et al.,* (Kamalian *et al.*, 2015). While ATP depletion in flutamide and 2-hydroxyflutamide-treated cells was more pronounced in galactose media, there was still significant ATP depletion in glucose-treated HepG2 cells and also in HepG2 ρ0 cells (absence of a functional ETC), implying that although direct mitochondrial dysfunction occurred, there were additional mechanisms by which these compounds depleted ATP.

Although ATP is a commonly used measure of mitochondrial function, it does not directly assess the effect of a compound upon mitochondrial respiration. For example, ATP may also be depleted due to the activation of cell defence mechanisms and may be maintained despite oxidative phosphorylation perturbations due to other ATP-generating cellular processes (Espinosa-Diez *et al.*, 2015). Resultantly, XF analysis to measure OCR in HepG2 cells was used to provide more in-depth information regarding the nature of any mitochondrial perturbations.

Despite flutamide, 2-hydroxyflutamide and tolcapone all inducing ATP depletion, they differed in their effect upon mitochondrial respiration; flutamide and 2-hydroxyflutamide significantly reduced the basal and maximal respiration of HepG2 cells, whereas tolcapone increased basal respiration. These characteristics indicated direct ETC inhibition by flutamide and its metabolite and uncoupling induced by tolcapone. Uncoupling of oxidative phosphorylation increases basal respiration as the rate-limiting step of ATP synthesis is no longer coupled to oxygen consumption, enabling the OCR to increase (Berg *et al.*, 2002). At the highest concentrations of tolcapone however, basal respiration was reduced, but given

the increase in basal respiration at lower concentrations of this compounds, this is suggestive of uncoupling to the extent that complete ETC dysfunction occurs at higher concentrations. These findings were reinforced by the increased proton leak and simultaneous decreases in spare respiratory capacity and ATP-linked respiration induced by tolcapone.

XF analysis of permeabilised HepG2 cells in the presence of respiratory complex-specific substrates identified flutamide as an inhibitor of complex I-mediated respiration (herein referred to as activity), in agreement with the findings of Coe *et al.,* (Coe *et al.*, 2007). A novel finding however, was the identification of 2-hydroxyflutamide as an inhibitor of complex I, II and V activity (Ball *et al.*, 2016). The identification of additional liabilities with 2-hydroxyflutamide highlighted areas of interest when determining individual susceptibility to flutamide-induced liver injury; interindividual variation in the glucuronidation-mediated clearance of 2-hydroxyflutamide and polymorphisms in complexes I, II and V (ATP synthase).

Downstream impacts of ETC inhibition, particularly of complex I include a decrease in cellular NAD^+/NADH, since complex I ordinarily catalyses NADH oxidation and so increases the cellular NAD^+/NADH ratio when functioning properly (Vinogradov and Grivennikova, 2016). An uncoupling mechanism and consequent increase in OCR would increase the rate of NADH oxidation at complex I (providing sufficient substrate availability) thereby increasing the ratio of NAD^+/NADH further (Berg *et al.*, 2002). Accordingly, flutamide and 2-hydroxyflutamide decreased NAD^+/NADH whereas tolcapone induced an increase in this ratio, supporting previous mechanistic conclusions from XF analysis of ETC inhibition and uncoupling respectively. Imbalances in NAD^+/NADH ratio have been shown to inhibit NAD^+-dependent enzymes, particularly sirtuin 3, leading to hyperacetylation of target protein lysine residues and dysregulation of mitochondrial homeostasis (Lombard *et al.*, 2007).

Oxidative stress, predominantly conferred by mitochondrially-produced ROS is a potentially deleterious product of ETC inhibition (Turrens, 2003). Flutamide and its metabolite induced a significant increase in cellular superoxide and given the complex I liabilities of these compounds, they may act similarly to the complex I inhibitor, rotenone. Rotenone enhances superoxide production via causing a backup of electrons on the FMN of complex I by blocking the CoQ binding site in complex I. These electrons are then able to react with molecular oxygen to produce superoxide (Li *et al.*, 2003; Brand, 2010).

Notably, upon flutamide or 2-hydroxyflutamide treatment, the peak superoxide level was reached after treatment with sub-maximal levels of compound. This could be due to a cessation of electron donation at the highest compound concentrations, reducing the

opportunistic interaction of electrons with molecular oxygen. It should be noted that due to the irreversible nature of the MitoSOX™ Red assay used, the results are insensitive to transient increases in superoxide. This meant it was not possible to distinguish increases in superoxide which were scavenged by cellular antioxidant systems from those which were not and subsequently would go on to have a more deleterious impact upon cells. It is conceivable that the increased superoxide could also be a result of increased RET, associated with a large change in $\Delta\psi_m$. A substantial decrease in $\Delta\psi_m$ was detected in all compound-treated cells, resultant RET may then force electrons back from $CoQH_2$ (reduced coenzyme Q) to complex I where NAD^+ can be reduced to NADH at the FMN site, this again increases the opportunity for electrons to react with molecular oxygen to produce superoxide (Murphy, 2009).

The aforementioned investigations were also performed using HepG2 cells treated with structural analogues of flutamide and tolcapone which are not associated with clinical hepatotoxicity, bicalutamide and entacapone respectively. Interestingly, despite its lack of clinical toxicity, the EC_{50} of bicalutamide in glucose media was substantially lower than that of flutamide (148 μM vs 255 μM). The induction of near equivalent ATP depletion in both glucose and galactose-conditioned bicalutamide-treated cells as well as ρ0 cells indicated that although negative for direct mitochondrial dysfunction, bicalutamide caused ATP depletion. Entacapone induced no significant ATP depletion in HepG2 ρ0 cells or HepG2 cells in either glucose or galactose media, implying an absence of mitochondrial dysfunction at the concentrations used, a difference between entacapone and tolcapone also found by Kamalian *et al.,* and others (Korlipara *et al.*, 2004; Longo *et al.*, 2016; Kamalian *et al.*, 2015).

XF analysis helped to elucidate the mechanisms underlying the differential hepatotoxic potentials of flutamide and bicalutamide; bicalutamide only reduced maximal respiration by 39.5 % in contrast to 2-hydroxyflutamide and flutamide which reduced maximal respiration by 88.9 and 90.8 % respectively. Following bicalutamide treatment, the spare respiratory capacity of cells was largely maintained, indicating that the mitochondria were still able to increase OCR upon FCCP (uncoupler) treatment, an adaptive ability which was severely compromised by flutamide or 2-hydroxyflutamide. The fact that bicalutamide did not erode spare respiratory capacity as flutamide or 2-hydroxyflutamide did may contribute to the absence of hepatotoxicity in bicalutamide-treated patients, despite the higher C_{max} and longer half-life (1.7 μM and 6 days respectively from a single 50 mg dose) of the active (R)-bicalutamide enantiomer compared to flutamide (Cockshott, 2004).

Entacapone caused a significant increase in basal respiration and proton leak although not until 250 µM (compared to the 62.5 µM tolcapone required), implying a less potent uncoupling mechanism. Together with the higher ATP EC_{50} and lower C_{max} of entacapone, this data may indicate why entacapone, unlike tolcapone is not associated with clinical hepatotoxicity (Grünig *et al.*, 2017).

The significant increase in proton leak induced by flutamide, 2-hydroxyflutamide, tolcapone and entacapone treatment is in stark contrast to the mild uncoupling which is generally seen as beneficial; mild uncoupling and a slight reduction of the proton motive force can in fact be used to prevent ROS production without deleteriously reducing ATP synthesis. Without this reduction in proton motive force, there would be a slow flow of electrons in the ETC, meaning there is an increased probability of interaction between electrons and molecular oxygen to form superoxide (Holmstrom and Finkel, 2014).

Observation of the downstream impacts of mitochondrial dysfunction found that bicalutamide induced no significant change in the ratio of NAD^+/NADH (supportive of a lack of ETC inhibition), but did induce an increase in cellular superoxide, pointing to an alternative mechanism of superoxide generation to that of flutamide, or a reduction in superoxide sequestration. Entacapone again, mirrored the effect of tolcapone on NAD^+/NADH and superoxide levels, although only at higher concentrations, reflecting the lack of clinical hepatotoxicity associated with entacapone.

2.5 CONCLUSION

The work described in this chapter has demonstrated that with appropriate manipulation, HepG2 cells can be used to determine whether drug-induced mitochondrial dysfunction is direct or indirect and to identify varying mechanisms and potencies of direct drug-induced mitochondrial dysfunction. The use of the primary metabolite of flutamide, 2-hydroxyflutamide has also enabled the identification of metabolite-specific mitochondrial liabilities despite the limited expression of many xenobiotic metabolism enzymes in HepG2 cells. Knowledge of the potential molecular targets of these compounds will be of use when designing the assessment of transmitochondrial cybrids, work described in subsequent chapters of this thesis. For example, the effect of flutamide/2-hydroxyflutamide upon cybrids harbouring variants in regions of mtDNA encoding complex I is of particular interest.

Chapter 3

Mitochondrial DNA Sequencing and Haplogroup Calling of 384 Healthy Volunteer Samples

CONTENTS

3.1 INTRODUCTION

The advent of next-generation sequencing has enabled the rapid evolution of pharmacogenomics, the branch of genetics concerned with determining the likely response of an individual to therapeutic drugs (Kalow, 2006). By definition, pharmacogenomics is inclusive of both the nuclear and mitochondrial genomes, although the latter has been studied considerably less as a basis for differential susceptibility to adverse drug reactions.

Mitochondrial dysfunction is implicated in the onset of multiple adverse drug reactions including hepatotoxicity, enteropathy, myotoxicity and lipodystrophy (Section 1.4.3) (Vuda and Kamath, 2016; Schirris *et al.*, 2015; Jing *et al.*, 2015). Studies have also associated some mtDNA haplogroups with altered mitochondrial function which may confer an increased risk of dysfunction. For example, Kenney *et al.,* found by *ex vivo* studies that haplogroup H conferred a significantly reduced spare respiratory capacity compared to haplogroup L (Kenney, et al., 2014). It can therefore be postulated that haplogroup H individuals (the most common European haplogroup) may be more likely to experience mitochondrial dysfunction following exposure to a compound known to reduce spare respiratory capacity.

Conversely, many studies have reported no significant difference in mitochondrial function between haplogroups (Amo *et al.*, 2008; Mueller, 2012). However, this may have arisen due to the limitations of the methodology employed, including Sanger sequencing and/or identification of only a handful of SNPs in the non-coding, D-loop region of mtDNA. Sanger sequencing is reported to only detect variants present in >10 % of mtDNA copies and often only enables the classification of an individual's mtDNA into common macrohaplogroups which encompass great variation (Kloss-Brandstatter *et al.*, 2015; Carr *et al.*, 2009; Amo *et al.*, 2008).

The research described in this chapter therefore aimed to utilise novel, next-generation sequencing and bioinformatics technologies to identify variation across the entire mitochondrial genome of 384 healthy volunteers. The resultant ability to assign an individual's sub- rather than macrohaplogroup may reduce intra-group disparities, thus improving the quality and specificity of examinations into the effect of mtDNA variation upon mitochondrial function.

DNA was isolated from the whole blood of 384 healthy volunteers prior to multiplex amplicon tagging (Fluidigm Access array) to enable simultaneous whole mitochondrial genome sequencing (Illumina MiSeq). Four methods of variant identification were then used and compared before variant input into HaploGrep2 for the classification of individual

samples into subhaplogroups. Results were also examined for differences in the quality of haplogroup calling between Caucasian and Asian Indian, Chinese and Black populations.

3.2 MATERIALS AND METHODS

3.2.1 Materials

Sample preparation for sequencing used Fluidigm reagents unless stated otherwise (Fluidigm, CA, USA). Sequencing used Illumina reagents unless stated otherwise (Illumina, CA, USA). Quality control used instruments from ThermoFisher unless stated otherwise (Thermo Fisher Scientific, MA, USA).

3.2.2 Cohort

The study was approved by the North West of England Research Ethics Committee and all participants gave written informed consent (REC reference number: 09/H1005/10). 384 samples were selected from a study by Faulkner *et al.,* in which 600 healthy volunteers were recruited from North West England and 100 mL of blood was collected for DNA extraction (Faulkner *et al.*, 2016). The most recently collected 384 samples were chosen for this project to maximise volunteer recall. Volunteer confidentiality was maintained by double-coding DNA samples and by restricting access to participant's personal data to trained clinical personnel.

Volunteers were eligible to take part in the study if they were healthy, aged between 18 and 60 years and willing to donate one or more blood samples. The following exclusion criteria were applied and volunteers were not recruited if they had: donated blood to transfusion services in the last four months, any medical problems; including asthma, diabetes, epilepsy or anaemia, taken medication or recreational drugs in the last six weeks. Women were also excluded if pregnant.

The volunteer cohort was 64 % female and 36 % male with a mean age of 29 years (range 18-60 years). The ethnicity of the volunteers also reflected regional diversity; primarily Caucasian (white north European ancestry; 84 %) with Asian Indians (6 %), Chinese (4 %) and Blacks (1 %) as minority populations.

3.2.3 DNA extraction

DNA was extracted from 384 whole blood samples using the Chemagen magnetic separation module 1 (PerkinElmer, Buckinghamshire, UK).

3.2.3.1 Method background

The Chemagen magnetic separation module 1 enables the capture of nucleic acids via highly specific binding to polyvinyl alcohol (PVA) magnetic beads. The magnetic separation of DNA from other contaminants is based on the lowering of metal rods into solutions containing the PVA beads and withdrawing the rods with the pelleted beads attached. The process was repeated multiple times in various wash and elution buffers, with the magnetism switched off at multiple steps to enable resuspension of the beads.

3.2.4 DNA quality control

Assessment of DNA quality was performed using nanodrop spectrophotometry (Thermo Fisher Scientific, Loughborough, UK), with minimum sample purity set at $A_{260/230}$ > 1.8 and $A_{260/280}$ > 1.9. Sample integrity was also tested using 2 % agarose e-gel electrophoresis (Invitrogen, UK) with reference DNA ladder, Quick-Load 1 Kb DNA ladder (New England BioLabs, MA, USA). Gels were visualised using a ChemiDoc system (Bio-Rad, CA, USA) to detect DNA bands in the absence of contaminants such as RNA, which would often appear as a smear of < 200 bp (Figure 3.1).

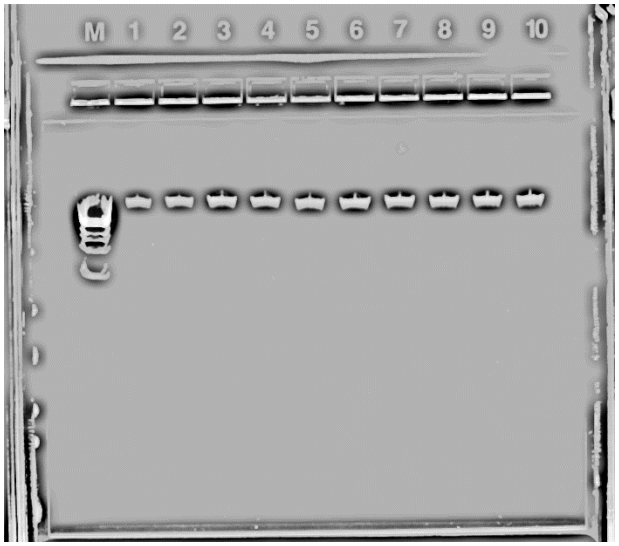

Figure 3.1. Representative image of DNA quality control using agarose e-gel electrophoresis. All samples (lanes 1-10) have intact DNA in the absence of contaminants. Lane M: Quick-Load 1 Kb DNA ladder.

3.2.5 DNA quantification

Sample DNA concentrations were quantified using the PicoGreen dsDNA Assay Kit (Invitrogen) according to the manufacturer's instructions, with samples compared to a DNA

standard curve. Samples were prepared at 100 ng/µL using DNA resuspension buffer (10 mM Tris, 0.1 mM ethylenediaminetetraacetic acid (EDTA), pH 8.0)

3.2.5.1 Method background

PicoGreen is a fluorescent probe which intercalates double-stranded DNA (dsDNA), this causes immobilisation of the probe and a >1000-fold increase in fluorescence compared to its free form (Dragan *et al.*, 2010).

3.2.6 Preparation of samples and primers for sequencing

3.2.6.1 Preparation of multiplex primer stock plates

Stock multiplex primer plates were prepared by the combination of six simplex stock primer plates of individual primer pairs (60 µM; Figure 3.2). Each well of the simplex primer plates had primer pairs (5 µL) transferred into the corresponding single column in the multiplex plate. This generated primer concentrations of 5 µM in the multiplex primer stock plate, with up to 12 forward and 12 reverse primers per well.

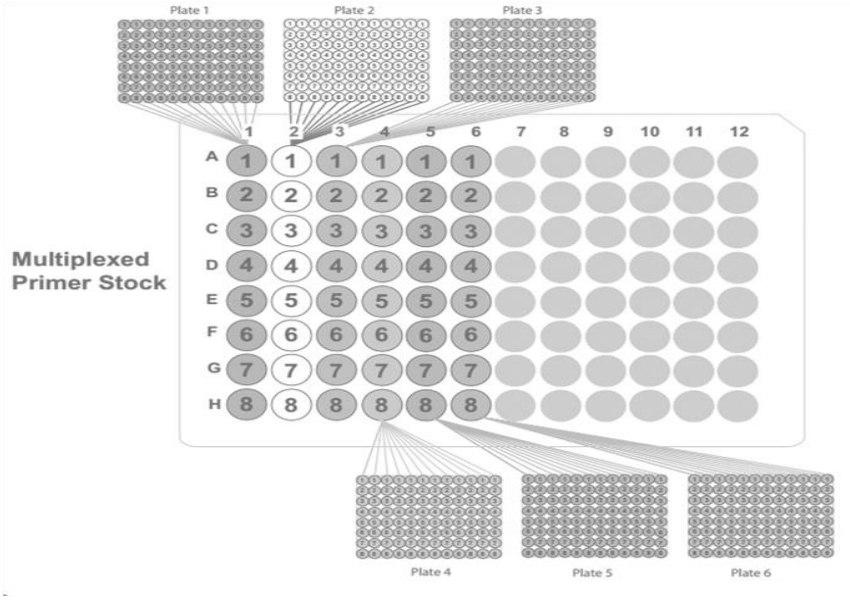

Figure 3.2. Generation of multiplex primer stock plates. Image adapted from Fluidigm user guide.

3.2.6.2 Preparation of working primer plates

In a 96-well plate, polymerase chain reaction (PCR)-grade water (75 µL) was combined with 20X Access array loading reagent (5 µL) and stock multiplex primer mix (20 µL; 5 µM) to generate a primer concentration of 1 µM. Multiple copies of this working plate were generated to reduce freeze-thaw cycles of the primers.

3.2.6.3 Preparation of the Access array integrated fluidic circuit

Before the loading of samples into the Access array integrated fluidics circuit (IFC), each sample (from 384 volunteers) (1µL of 100 ng/µL) was mixed with a sample pre-mix solution (4 µL; components listed in Table 3.1) in a 96-well plate.

Table 3.1. Sample pre-mix solution constituents.

Component	Volume per reaction (µL)	Final concentration
10X FastStart high fidelity reaction buffer without $MgCl_2$ (Roche)	0.500	1X
25 mM $MgCl_2$ (Roche)	0.900	4.5 mM
DMSO (Roche)	0.250	5 %
10 mM PCR grade nucleotide mix (Roche)	0.100	200 µM
5 units/µL FastStart high fidelity enzyme blend (Roche)	0.0500	0.05 units/µL
20X Access array loading reagent	0.250	1X
PCR-certified water	1.95	—

3.2.6.4 Access array integrated fluidics circuit loading

Following the combination of samples with pre-mix solution, the Access array IFC was loaded (Figure 3.3A). Following the loading of components, the IFC was placed into the pre-PCR IFC controller and the load mix script prime 151x was run (Figure 3.3B). During this, primers and samples were drawn from the inlets to the centre of the IFC (Figure 3.3A). Following this the IFC was placed in the FC1 cycler where protocol AA48x48 standard v1 was performed, with cycling conditions described in Table 3.2.

A

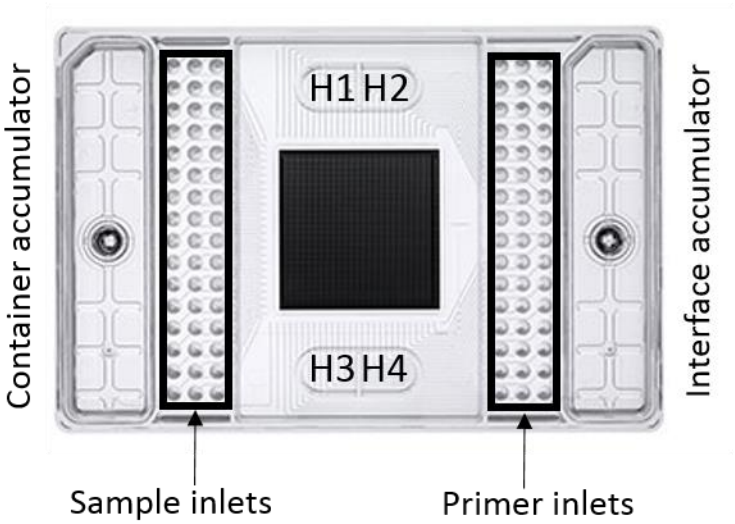

B

Location	Component	Volume (µL)
Accumulators	Control-line fluid	300
H1	1X Access array harvest solution	700
H2, H3	1X Access array harvest solution	500
H4	1x Access array hydration reagent v2	500
Primer inlets	20X primer solution	4
Sample inlets	Sample pre-mix	4

Figure 3.3. Loading the Access array integrated fluidics circuit (IFC). Each IFC (A) holds 48 samples and 48 groups of primers and must also be loaded with control-line fluid, harvest solution and hydration reagent (quantities stated in B).

Table 3.2. FC1 cycler protocol.

Stage	Temperature (°C)	Time (sec)	Cycles	Segment time (sec)
Thermal mix	50	120	1	1320
	70	1200		
Hot start	95	600	1	600
PCR	95	15	10	1050
	60	30		
	72	60		
C_0t cycle	95	15	2	270
	80	30		
	60	30		
	72	60		
PCR cycle	95	15	8	840
	60	30		
	72	60		
C_0t cycle	95	15	2	840
	80	30		
	60	30		
	72	60		
PCR cycle	95	15	8	840
	60	30		
	72	60		
C_0t cycle	95	15	5	675
	80	30		
	60	30		
	72	60		
Extension	72	180	1	180
Cool down	10	hold	—	—

Abbreviations: PCR, polymerase chain reaction; C_0t, cycle to normalise the amount of PCR amplicons.

3.2.6.5 Harvesting samples

Following PCR in the FC1 cycler, the IFC was removed and all remaining fluids in H1 to H4 were removed. Harvest solution was then added to H1 (700 µL) and H2-H4 (600 µL). 1X Access array harvest solution (2 µL) was also added to each of the sample inlets. Following this the IFC was placed into the post-PCR IFC controller and a script harvest (151x v7) run was performed. Once completed, the IFC was removed and the samples were harvested (approx. 10 -12 µL) from each sample inlet into a clean 96-well plate (harvest plate). These harvested products were then diluted 100-fold with water (99 µL water + 1 µL PCR product).

3.2.6.6 Preparation of harvest for sequencing

Sample pre-mix solution was prepared for the harvested sample (Table 3.3). This solution (15 µL) was then added to 1 of 384 Illumina barcodes (4 µL) and harvested PCR product pool (1

µL) to give a total volume of 20 µL in four 96-well plates. This was then placed into a PCR thermal cycler before running the PCR protocol described in Table 3.4.

Table 3.3. Sample pre-mix constituents.

Component	Volume per reaction (µL)	Final concentration
10X FastStart high fidelity reaction buffer without $MgCl_2$ (Roche)	2.0	1X
25 mM $MgCl_2$ (Roche)	3.6	4.5 mM
DMSO (Roche)	1.0	5 %
10 mM PCR grade nucleotide mix (Roche)	0.40	200 µM
5 units/µL FastStart high fidelity enzyme blend (Roche)	0.20	0.05 units/µL
20X Access array loading reagent (Fluidigm)	1.0	1X
PCR-grade water	7.8	—

Table 3.4. Polymerase chain reaction (PCR) thermal cycles. After harvesting the PCR products from the integrated fluidics circuit, the second PCR step was performed in a 96-well PCR plate which introduced a sample-specific barcode and Illumina adaptor sequences**.**

Temperature (°C)	Time (sec)	Cycles
95	60	1
95	15	15
60	30	
72	60	
72	3	1

3.2.6.7 PCR product purification

All barcoded amplified PCR products generated on the 48.48 Access array IFC underwent quality control using the Fragment Analyser and DNA was measured using a Qubit dsDNA HS kit.

3.2.6.7.1 Method background

The Fragment Analyser accelerates nucleic acid analysis workflow by the automation of key steps such as gel loading and sample injection. Each sample is injected into discrete, parallel capillaries which contain a pre-incorporated, intercalating fluorescent dye. During electrophoresis, nucleic acid fragments migrate based upon size and the dye binds. As fragments pass the detection window, the nucleic acid-bound fluorescent dye is excited by

the continuous light source and emits detectable fluorescent signal. Together, when compared to a known calibration ladder, the time required to pass the detection window and the relative emission signal can provide information on size and nucleic acid concentration respectively (Analytical, 2017).

3.2.6.8 Sample pooling

Samples were pooled using the Mosquito_X1 (TTP Labtech, Herts, UK), this enabled the rapid transfer of small volumes without the need for further dilution. For the pooling, PCR product (1 µL) was extracted from each of the 96 wells (from a total of four 96-well plates) to generate four pools (from each of the 96-well plates).

These libraries were then cleaned using Ampure beads (1:1) (Beckman Coulter, CA, USA). PCR amplicons bind to Ampure beads which enabled the removal of unincorporated dideoxynucleotides, primer dimers, primers and other contaminants as well as anything below 100 bp, whilst enabling the efficient recovery of DNA.

3.2.6.9 Further quality control

The quantity and quality of each pool was assessed by the Bioanalyzer (Agilent, CA, USA) and quantitative PCR (qPCR), the latter was performed using the Illumina Library Quantification Kit (Kapa Biosystems, CA, USA) on a Light Cycler LC480II (Roche, Basel, Switzerland) according to the manufacturer's instructions. The four pools were then combined in an equimolar ratio before sequencing.

3.2.6.9.1 Method background

The Bioanalyzer uses electrophoresis and flow cytometry to make assessments and consumes minimal sample. Only 1 µL of PCR product from each of the PCR reactions was required to determine if the PCR product pool had the expected size. Electrophenogram results of the samples were considered in-line with the size of incorporated barcodes (approx. 59 bp) to determine the expected product size range.

The Illumina Library Quantification Kit contains the engineered KAPA SYBR FAST DNA Polymerase which amplifies GC- and AT-rich DNA fragments of different lengths with similar efficiency, making it capable of accurate qPCR-based quantification of next-generation sequencing libraries.

3.2.7 Sequencing

Samples were denatured by the addition of non-denatured library (5 µL) to 0.1 M NaOH (5 µL) and 200 mM Tris-HCl pH 8.0 (5 µL). The library mix was then added to the MiSeq reagent

cartridge (Illumina) before loading of the flow cell and reagent cartridge into the MiSeq machine pre-filled with clustering and sequencing reagents sufficient for sequencing one flow cell. During the MiSeq run, libraries were automatically transferred to the flow cell, a single-lane glass-based substrate on which clusters were generated and the sequencing reaction was later performed.

Sequencing began with cluster generation during which single DNA molecules were bound to the surface of the flow cell and then bridge-amplified to form clusters. Clusters were then imaged in small areas of the flow cell called tiles. This used LED and filter combinations specific to each of the four fluorescently-labelled dideoxynucleotides. Following imaging of each tile, the flow cell was moved into place to expose the next tile. This process was repeated for each cycle of sequencing. Once imaging was complete, MiSeq Reporter software performed base calling, filtering and quality scoring.

3.2.8 Bioinformatics analysis

3.2.8.1 Alignment

The high volume of short reads generated by Illumina sequencing technology has required the use of fast and accurate read alignment tools. Sequencing reads were aligned to the revised Cambridge Reference Sequence (rCRS) (NC_012920) using the BWA-MEM algorithm (Burrows-Wheeler alignment tool) (v0.7.12) (Li and Durbin, 2009).

3.2.8.1.1 Method background

BWA is a modern fast read aligner software package which provides a tool for mapping sequences of low divergence against a reference genome. The latest version of BWA, BWA-MEM, was used as it has faster and more accurate performance than predecessors such as BW-backtrack for 70-100 bp illumina reads.

3.2.8.2 Variant calling

BWA-MEM generates outputs in the standard sequence alignment/map (SAM) format. SAMtools (v.01.18) was then used to provide data in the format required for variant calling. Variant calling was performed using the genome analysis toolkit (GATK v3.2.2) (with diploidy and tenploidy settings) (McKenna *et al.*, 2010) and VarScan (v2.3.9) (Koboldt *et al.*, 2009, 2012). GATK is widely considered to be the gold standard for variant calling, although not specifically in the context of the mitochondrial genome, therefore multiple methods were used so that a comparison could be performed. Each method produced a variant calling format (VCF) file which could then be input into haplogroup calling software.

3.2.8.3 Haplogroup calling

MtDNA haplogroups were determined using HaploGrep2 (v.2.1.0) (Weissensteiner *et al.*, 2016).

3.2.8.3.1 Method background

HaploGrep2 is a web application which provides fully automated determination of haplogroups according to the underlying phylogenetic tree (Van Oven and Kayser, 2009). Unlike its predecessor, HaploGrep(1), it enables the direct input of VCF files generated by variant calling softwares and provides the user with the 50 highest ranked haplogroups of their sample(s) (Weissensteiner *et al.*, 2016).

3.3 RESULTS

3.3.1 Phylogenetic distribution of samples

Failed amplification of one sample resulted in the collection of sequencing data for 383 samples. A representation of HaploGrep2 outputs is shown in Figure 3.4. As well as providing haplogroup classification and quality information, HaploGrep2 also provided the resultant phylogenetic tree of all samples (Appendix 1). A simplified version of this phylogenetic tree is displayed in Figure 3.5, featuring subclades of the five most common haplogroups in the cohort: H, U, J, T and K.

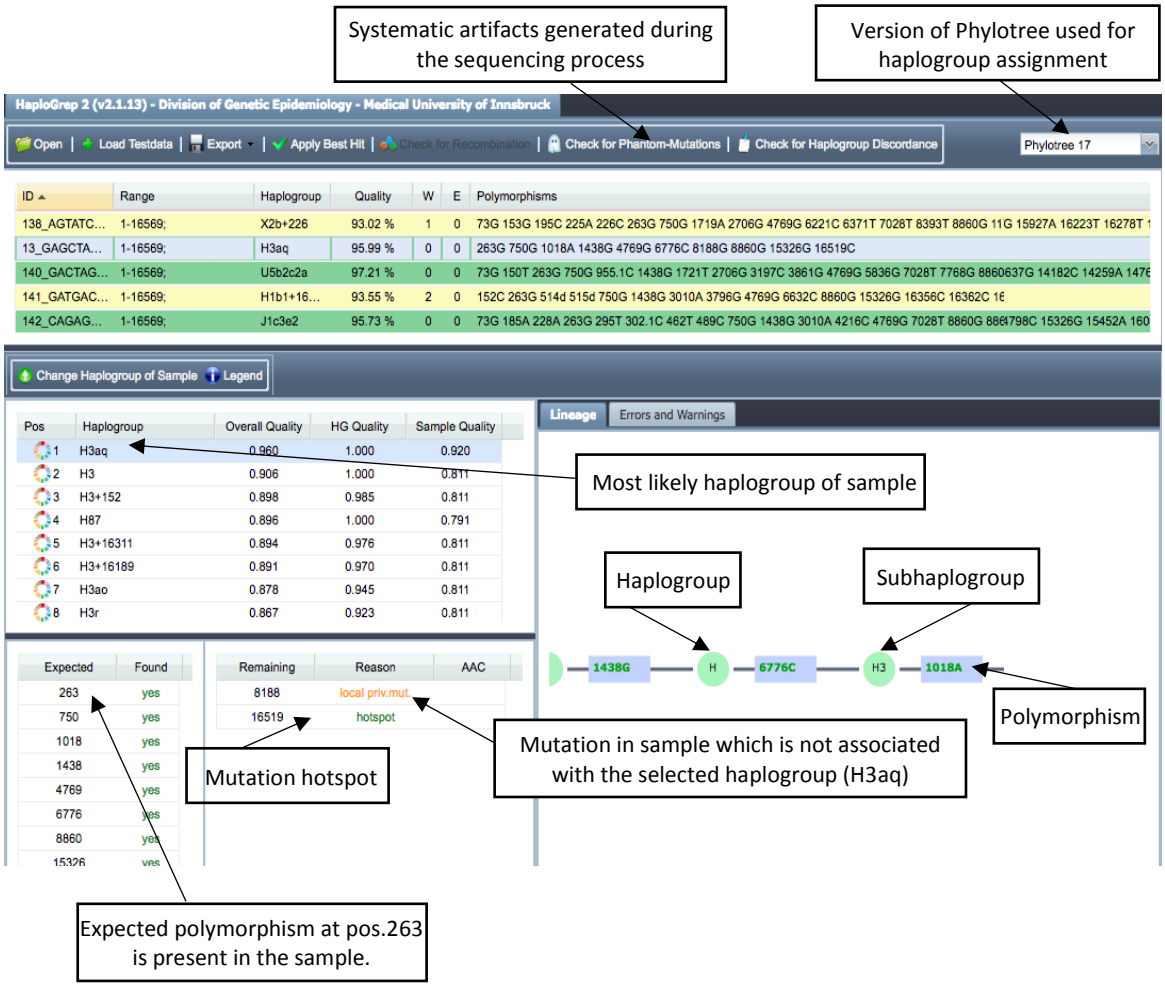

Figure 3.4. Annotated HaploGrep2 output. Variant calling format (VCF) files generated using genome analysis toolkit (GATK) tenploidy were input into HaploGrep2 to determine the quality of multiple haplogroup assignments.

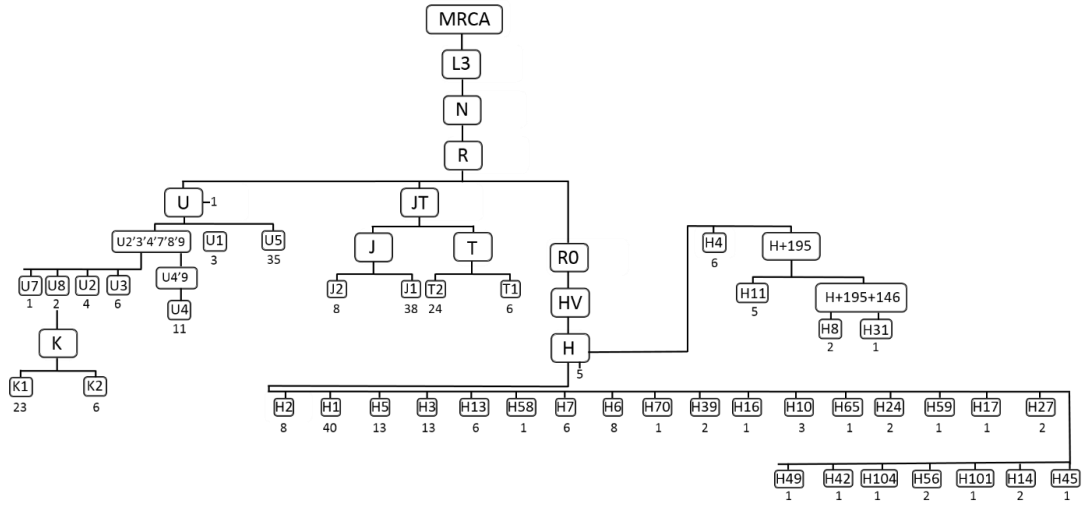

Figure 3.5. Simplified phylogenetic tree. 383 samples were classified into subhaplogroups, with the samples from the five most common haplogroups displayed here. Number of samples is displayed under each group. Abbreviations: MRCA, most recent common ancestor.

3.3.2 Comparison of haplogroup frequency to an online database

A comparison of the five most common haplogroups in the cohort to a database of haplogroups in an English population showed close agreement between the frequency of all haplogroups, with maximum deviation seen in haplogroup H with its frequency reduced by 5.6 % compared to the database (Table 3.5) (Eupedia, 2016). When non-Caucasian participants were removed there was still close agreement with haplogroup frequencies in the literature (Table 3.5).

Table 3.5. Comparison of haplogroup frequencies in this cohort with an online database (Eupedia, 2016). Comparisons were performed using the whole cohort and Caucasian participants only.

Haplogroup	Frequency (%)			
	All participants		Caucasian only	
	Study	Database	Study	Database
H	39.1	44.7	37.8	44.7
J	12.0	11.5	11.5	11.5
U	16.4	16.1	15.9	16.1
T	7.80	7.80	7.60	7.80
K	7.60	7.80	7.00	7.80

3.3.3 Comparison of variant calling tools

Prior to haplogroup calling, variants were identified using GATK (haploidy, diploidy and tenploidy) and VarScan variant calling tools. All variant calling tools had a concordance of ≥ 85 % with GATK tenploidy, with this concordance rising to > 97 % if results which had identical macrohaplogroups were included e.g. H1 vs. H1e2 (Figure 3.6A).

The entry of variant calling data into HaploGrep2 software in our study found that 1.0 % of VarScan results had a quality score of less than 70 %, compared to 0.0 % of GATK results (Figure 3.6B). On average, 77.7 % and 79.7 % of GATK and VarScan results respectively had a quality score of greater than 90 % when entered into HaploGrep2. The HaploGrep2 quality score of samples reflects the reliability of the haplogroup assignment, which is reduced if there are absent SNPs which are expected to be present in the designated haplogroup, or if there were additional SNPs present which are not characteristic of the assigned haplogroup.

A

Concordance to GATK tenploidy	Variant calling software		
	GATK haploidy (%)	GATK diploidy (%)	VarScan (%)
Match[a]	85.9	85.0	86.2
Match[b]	12.0	12.5	10.7

B

Quality score	Variant calling software			
	GATK haploidy (%)	GATK diploidy (%)	GATK tenploidy (%)	VarScan (%)
< 70 %	0.00	0.00	0.00	1.04
> 90 %	87.1	85.9	60.1	79.7
Average (%)	94.3	94.2	90.0	93.6

Figure 3.6. Comparison of variant calling softwares. A: Percentage of HaploGrep2 results from GATK haploidy, diploidy and VarScan which matched results from GATK tenploidy variant calling. Match[a] describes the percentage of samples which had identical haplogroup calling. Match[b] describes the number of samples which had matching haplogroups but not to the same level of detail e.g. H1a rather than H1a2a. **B:** Quality scores in HaploGrep2 when variants were input from GATK (haploidy, diploidy and tenploidy) and VarScan. Higher quality scores indicate increased confidence that the correct haplogroup has been assigned.

3.4 DISCUSSION

In this chapter, the whole mitochondrial genome sequencing of 384 volunteer DNA samples, followed by the comparison of multiple methods of variant calling and classification into mitochondrial subhaplogroups has been described (haplogroup classification of all samples is detailed in Appendix 2). Whole mitochondrial genome sequencing identified variation which would have been overlooked when only assigning macrohaplogroups. The quality of subhaplogroup classification in Caucasian and non-Caucasian participants was also compared, with reduced quality classification in samples from non-Caucasian participants compared to Caucasian participants.

GATK software is widely considered to be the gold standard for variant calling, but there is little evidence of the tailoring of this software to mitochondrial genome sequencing. For example, GATK does not completely account for the number of copies of mtDNA, which can range from hundreds to thousands per cell (Warden *et al.*, 2014). With this knowledge of the polyploidy nature of mtDNA, GATK variant calling was performed with multiple "ploidy" settings; haploidy, diploidy and tenploidy which assume one, two and ten copies of the

mitochondrial genome respectively. The lower the copy number assumed, the more likely it was that minor variants in a heterogeneous population of mtDNA would be incorrectly assigned as erroneous sequencing reads, therefore GATK tenploidy was used as the principal variant calling method in this work.

Since the completion of this work, MToolBox, a highly automated bioinformatics pipeline which can analyse mtDNA from high throughput sequencing data has become well established (Calabrese *et al.*, 2014). This pipeline includes a computational strategy to assemble mitochondrial genomes while assessing the heteroplasmic fraction of each variant allele and providing a related confidence interval. This would prove particularly useful for studies which have a high depth of sequencing (high number of reads at each base position) such as in the present research. High sequencing depths increase the likelihood that a heteroplasmic variant is read, so it is important to have bioinformatics tools which allow accurate measurements of this heteroplasmy. It should however be considered that mutated mtDNA must exceed a critical threshold of 60-80 % (dependent on the severity of the mutation) before an effect can be detected using established laboratory techniques, therefore the clinical relevance of identifying minor heteroplasmic mutations is debatable (Stewart and Chinnery, 2015).

The identification of SNPs from across the entire mitochondrial genome in this work demonstrates a progression from several previous projects. Many have been unable to determine mitochondrial subhaplogroups from the identification of only a handful of haplogroup-associated SNPs using technologies such as the Sequenom MassARRAY iPLEX platform (Guzman-Fulgencio *et al.*, 2014). Such methods may have contributed to the increased percentage of individuals in the most common haplogroup H in an online database compared to our own study (Table 3.5), though this could also have been affected by the population structure in the area our cohort was taken from; there may have been disparities due to the high prevalence of the Irish population in the North West of England (Irish population haplogroup H frequency: 38.5 %) (Khazaria, 2000).

Accordingly, the whole genome sequencing described here has enabled the identification of SNPs spanning the entire mitochondrial genome and classification into sub- rather than macrohaplogroups. This research identified just six samples which were not assigned a subhaplogroup (e.g. U and H rather than U1 and H2), exemplifying the vast number of SNPs present in addition to the select few which define macrohaplogroups. Importantly, this has allowed the SNPs in an individual's sample which are not characteristic of the assigned

macrohaplogroup to be acknowledged. This may be of particular interest if the SNP(s) are non-synonymous and the effect of mitochondrial genotype upon the structure/function of a specific protein is of importance to a study. Nonetheless, it should be acknowledged that the incorporation of this level of detail into applications such as personalised healthcare is unlikely in the near future; it would likely require an increased number of clinical trials participants to provide sufficient diversity, with the exact number dependent on the classification of individuals e.g. macrohaplogroup, subhaplogroup, individual SNPs etc.

The ethnicity of 39 volunteers in this study was recorded as non-Caucasian (Figure 3.7). Given previous statements of a lack of data regarding non-Caucasians in genetics studies it was of interest to identify any effects this had on the present work (Knerr *et al.*, 2011; Konkel, 2015). When variant calling using GATK tenploidy, only 28.5 % of samples from non-Caucasians achieved a HaploGrep2 quality score of >95 %, compared to 56 % in samples from Caucasian participants. This reduced quality score indicated that for the samples from non-Caucasians there were a higher number of unassigned or absent variants for the assigned haplogroup, creating less confidence that the true haplogroup of the sample had been allocated.

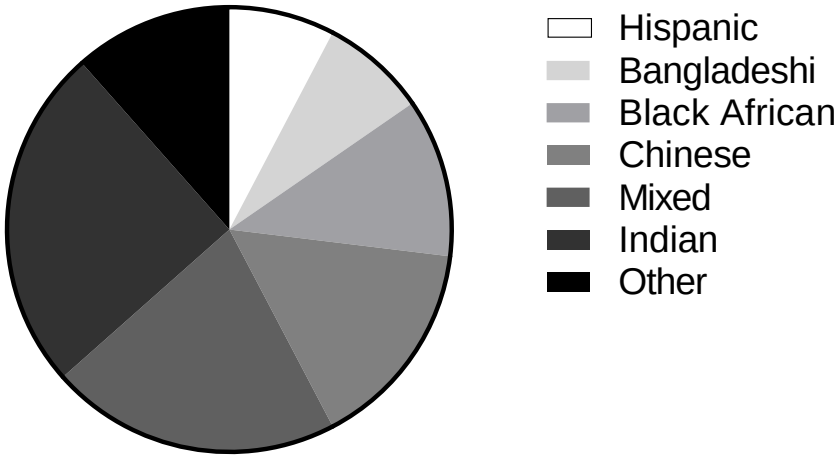

Figure 3.7. Ethnicities of non-Caucasian participants. Other: Arabic (1), Filipino (1), Turkish (1), Iranian (1), Malay (2). N = 39.

Similarly, the average number of global private mutations (mutations never observed before in the mitochondrial phylogenetic tree) per sample from non-Caucasians was 1.03, substantially higher than the average of 0.39 for samples from Caucasian participants. The data described in this chapter may therefore contribute towards the identification of novel mitochondrial subhaplogroups following incorporation into relevant databases. Data from

non-Caucasian samples is of particular value as there are currently less data entries for this group.

The identification of mtDNA subhaplogroup provides information which may be used to determine the effect of mtDNA variation upon mitochondrial function, but the ability for any person's genotype to change following subhaplogroup assignment has not been accounted for in this work. Vegetative segregation (Figure 1.9) of mtDNA during cell division has the propensity to increase the prevalence of mutated mtDNA, potentially increasing the ratio of "mutated" to "healthy" mtDNA to above the critical threshold and inducing a phenotypically observable effect on mitochondrial function as a consequence (Stewart and Chinnery, 2015). In light of this, a longitudinal study of a selection of participants in this study is planned in order to provide an insight into whether such changes are occurring at a significant level.

3.5 CONCLUSION

In conclusion, the successful next-generation mtDNA sequencing of 383 volunteers in this study has provided volunteer genotype information to enable the effect of mitochondrial subhaplogroup upon mitochondrial function to be studied in an *in vitro* model, work which is described in subsequent chapters of this thesis. For such studies to be optimally utilised, the variant calling software used should better account for the heteroplasmic nature of mtDNA. Furthermore, the results of increased incorporation of non-Caucasian mitochondrial genotypes into Phylotree and the results of the suggested longitudinal study should be used when available in order to provide a better understanding of the validity of future related studies.

Chapter 4

Assessment of the Impact of Mitochondrial DNA Variation upon Mitochondrial Function Using Freshly Isolated Platelets

CONTENTS

4.1 INTRODUCTION

Platelets are small (2-4 µm), discoid anucleate cell fragments which are highly abundant in the blood where they promote haemostasis. Platelets are derived from megakaryocytes present in the bone marrow which transfer cellular components including mitochondria to platelets, therefore platelets offer an abundant source of mtDNA in the bloodstream. Their anucleate nature also means that they can be used as a source of mtDNA without interference from the nuclear genome (Thon and Italiano, 2012).

Multiple studies describe the use of platelets for bioenergetic testing using XF analysis techniques (Kramer *et al.*, 2014; Chacko *et al.*, 2013; Ravi *et al.*, 2015) similar to those described in Section 2.2.4. At basal state, both oxidative phosphorylation and glycolysis are used to generate ATP in platelets (a high proportion of aerobic glycolysis), with glycolytic metabolism increasing upon platelet aggregation. In contrast to other blood cell types such as monocytes or lymphocytes, platelets dedicate over 50 % of their mitochondrial function to ATP synthesis (double that of monocytes) and platelet reserve capacity is approximately only 20 % of maximal mitochondrial respiration. Notably, both complex III and IV proteins are low in platelets (Kramer *et al.*, 2014; Wintrobe, 2009).

Given the exclusive abundance of the mitochondrial genome in platelets, coupled with evidence of their suitability for mitochondrial function testing using established laboratory techniques, it was hypothesised that platelets can provide a suitable *in vitro* model of interindividual variation in mtDNA and susceptibility to drug-induced mitochondrial dysfunction induced by compounds associated with iDILI.

The aim of the work described in this chapter was therefore to recruit volunteers of known mitochondrial genotype to donate platelets which could be used to determine if mitochondrial haplogroup conferred differential basal mitochondrial function and/or susceptibility to drug-induced mitochondrial dysfunction.

In total, 30 volunteers were recruited from mitochondrial haplogroups H, J, T and U (the four most common haplogroups in the cohort and in the UK, volunteer cohort described in Section 3.2.2). Platelets were isolated from the whole blood donated by volunteers and were subject to mitochondrial function testing using XF analysis. XF analysis consisted of a mitochondrial stress test (Section 2.2.4.3) with platelets at basal state and upon treatment with mitotoxic compounds associated with iDILI: flutamide, 2-hydroxyflutamide and tolcapone. Platelets were also permeabilised and supplied with respiratory complex-specific substrates to determine individual respiratory complex function (Section 2.2.4.4).

4.2 METHODS

4.2.1 Materials

All forms of PBS were purchased from Life Technologies (Paisley, UK) unless stated otherwise. All XF assay consumables were purchased from Agilent Technologies (CA, USA). All other reagents and chemicals were purchased from Sigma Aldrich (Dorset, UK) unless stated otherwise.

4.2.2 Cohort

Healthy volunteers (n=30) of mitochondrial haplogroups H, J, T and U were recruited from the cohort described in Section 3.2.2. Subhaplogroups and SNPs present in DNA isolated from each individual are described in Table 4.1. This project was approved by the North West of England Research Ethics Committee and all participants gave written informed consent. A cohort of two non-genotyped healthy volunteers was also used to investigate day-to-day variation in parameters of mitochondrial function (Section 4.3.5).

Table 4.1. MtDNA variation of 30 healthy volunteers whose platelets were used in this study.

Donor number	Macrohaplogroup	Assigned haplogroup	SNPs characteristic of assigned haplogroup	Additional SNPs
1	H	H1c	263G 477C 750G 1438G 3010A 4769G 8860G 15326G 16519C	16519C
2	H	H1c3	257G 263G 477C 750G 1438G 3010A 4769G 8473C 8860G 15326G	195C 12966T 16519C
3	H	H1bb	152C 263G 750G 1438G 3010A 4769G 8860G 11864C 15326G	16519C
4	H	H1a1	73G 263G 750G 1438G 3010A 4769G 6365C 8860G 15326G 16162G	152C 3483A 16360T 16519C
5	H	H1c	263G 477C 750G 1438G 3010A 4769G 8860G 15326G	10646A 16519C
27	H	H2a1e1a1	263G 575T 750G 751G 951A 8860G 15326G 16124C 16148T 16166G 16354T	—
28	H	H1	263G 750G 1438G 3010A 4769G 8860G 15326G 16189C	16218T 16519C
29	H	H3aq	263G 750G 1018A 1438G 4769G 6776C 8860G 15326G	8188G 16519C
6	J	J2b1g	73G 150T 152C 263G 489C 750G 1438G 4769G 5633T 7028T 8860G 9872G 10172A 10398G 11251G 11719A 12612G 13708A 14766T 15257A 15326G 15452A	2789T 13821T

			15812A 16069T 16126C 16193T	
7	J	J1c	73G 185A 228A 263G 295T 462T 489C 750G 1438G 3010A 4216C 4769G 7028T 8860G 10398G 11251G 11719A 12612G 13708A 14766T 14798C 15326G 15452A 16069T 16126C 16261T	4113A 6554T 10915C 16316G
9	J	J1c1c	185A 228A 462T 482C 489C 750G 1438G 3010A 3394C 4216C 4769G 7028T 8860G 10398G 11251G 11719A 13708A 14766T 14798C 15326G 15452A 16069T 16126C 16145A	188G 13943T 14552G
16	J	J1c1a	73G 228A 263G 295T 462T 482C 489C 750G 1438G 3010A 3394C 4216C 4769G 7028T 8860G 9635C 10398G 11251G 11623T 11719A 13708A 13899C 14766T 14798C 15326G 15452A 16069T 16126C	—
20	J	J1c2h	185A 188G 222T 228A 263G 295T 462T 489C 750G 1438G 3010A 4216C 4769G 7028T 8860G 10398G 11251G 11719A 12612G 13708A 14766T 14798C 15326G 15452A 16069T 16126C	16189C 16519C 16527T
30	J	J1c1e	185A 228A 263G 295T 462T 482C 489C 750G 1438G 3010A 3394C 4216C 4769G 7028T 8860G 10398G 10454C 11251G 11719A 12612G 13708A 14766T 14798C 15326G 15452A 16069T 16126C 16368C	13889A
8	T	T2b28	73G 263G 750G 930A 1438G 1888A 4216C 4769G 4917G 5147A 7028T 8697A 8860G 10463C 11176A 11251G 11719A 11812G 13368A 14233G 14766T 14905A 15326G 15452A 15607G 15928A 16126C 16294T 16296T 16304C	199C 11180A 16519C
10	T	T2b17a	73G 263G 709A 750G 930A 1438G 2706G 4216C 4688C 4769G 4917G 5147A 7028T 7891T 8697A 8860G 10463C 11251G 11719A 11812G 13368A 13692T 14233G	152C 16291T 16519C

			14766T 14905A 15326G 15452A 15607G 15928A 16126C 16294T 16296T 16304C	
11	T	T2b	73G 263G 750G 930A 1438G 4216C 4769G 5147A 7028T 8697A 8860G 10463C 11251G 11719A 11812G 13368A 14233G 14766T 14905A 15326G 15452A 15607G 15928A 16126C 16294T 16296T 16304C	5773A 16188T 16519C
13	T	T2b3	73G 263G 709A 750G 930A 4216C 4769G 4917G 5147A 7028T 8697A 8860G 10463C 10750G 11251G 11719A 11812G 13368A 14233G 14766T 14905A 15326G 15452A 15607G 15928A 16126C 16294T 16296T 16304C	152C 199C 5054A 16519C
14	T	T1a1	73G 152C 750G 1438G 4216C 4769G 7028T 8697A 9899C 10463C 11251G 11719A 13368A 14766T 14905A 15326G 15452A 15607G 15928A 16126C 16163G 16189C 16294T	14016A 16519C
21	T	T2a1a	73G 709A 750G 1438G 2850C 4216C 4769G 7022C 7028T 8697A 8860G 10463C 11251G 11719A 11812G 13368A 13965C 14233G 14766T 14905A 15326G 15452A 15607G 15928A 16126C 16294T	12490G 16519C
22	T	T2a1b1a	73G 263G 750G 1438G 1888A 2141C 4216C 4769G 4917G 7028T 8697A 8860G 9117C 10463C 11251G 11719A 11812G 13368A 13965C 13966G 14233G 14687G 14766T 14905A 15326G 15607G 15928A 16126C 16294T 16296T 16324C	498T 6710G 8152A 16240G 16519C
12	U	U5b1	73G 150T 263G 750G 1438G 3197C 4769G 7028T 7768G 8860G 9477A 11467G 11719A 12308G 12372A 13617C 14182C 14766T 15326G 16189C 16192T! 16270T	146C 16311C
15	U	U8b	73G 750G 1438G 2706G 4769G 7028T 8860G 9055A 9698C 11467G 11719A	146C 195C 310C 3432T 13135A 16362C 16519C

			12372A 14167T 14766T 15326G	
17	U	U4b1b1b	73G 146C! 152C 195C 263G 499A 750G 1811G 4646C 4769G 5999C 6047G 7028T 7705C 8308G 8860G 9389G 10819G 11332T 11339C 11467G 11719A 12372A 13528G 13565T 14620T 14766T 15326G 15373G 15693C 15758G 16356C	16519C
18	U	U3a1	73G 150T 263G 750G 1438G 1811G 2294G 2706G 3010A 4703C 4769G 6518T 7028T 9266A 10506G 11467G 11719A 12372A 13934T 14139G 14766T 15326G 15454C 16343G 16390A	10043T 13174C 16192T 16519C
19	U	U4b1a2b	73G 195C 263G 750G 1811G 2706G 3672G 4646C 4769G 5999C 6047G 7028T 7705C 8860G 11143T 11332T 11339C 11719A 12308G 12372A 12609C 13708A 14620T 14766T 15067C 15326G 15693C 16356C	16519C
23	U	U5a1a1	73G 150T 189G 228A 263G 750G 1438G 2706G 3197C 4769G 7028T 7226A 7768G 8860G 9196A 9477A 11467G 11719A 12308G 12372A 13617C 14182C 14766T 15326G 16192T 16270T	204C 15553A
24	U	U3a1c	73G 263G 750G 1438G 1811G 2294G 3010A 4703C 4769G 6518T 7028T 8860G 9266A 10506G 11467G 11719A 12372A 13934T 14139G 14766T 15326G 15454C 16343G 16356C 16390A	9615C 16519C
25	U	U2e2a1a	73G 152C 217C 263G 750G 1811G 2706G 3720G 3849A 4553C 4736C 4769G 5390G 5426C 6045T 6152C 7028T 8473C 8860G 10876G 11467G 11719A 12372A 12557T 13020C 13734C 14766T 15326G 15907G 16051G 16092C 16129C 16189C 16362C	514T 10649C 16075C
26	U	U5a1f1a1	73G 199C 750G 2706G 3197C 4769G 5585A 6023A 7569G 8251A 8860G 9477A 11467G 12308G 12372A 13617C 14766T 14793G 15218G	—

			15326G 16192T 16256T 16270T 16311C 16526A	

4.2.3 Blood collection and platelet isolation

20 mL blood was collected from each healthy volunteer and collected in EDTA vacutainers (BD Biosciences, US). A tourniquet was used to assist blood collection only when absolutely required and in each case was used for < 30 sec to minimise the risk of platelet activation. Within 30 min of collection, blood was layered on top of Optiprep™ density gradient medium (1.063 g/mL, Sigma Aldrich) using a Pasteur pipette before centrifugation (350 g, 15 min, no brake).

Following this, the top ¾ of platelet-rich plasma (PRP) was removed and the remaining ¼ (likely to be contaminated with red blood cells) was discarded (Figure 4.1). Prostaglandin I_2 (PGI_2) was added to the PRP to a final concentration of 1 µg/mL to prevent platelet activation. The PRP was then centrifuged (1500 g, 15 min, no brake) to generate a platelet pellet (Figure 4.1). The platelet pellet was subsequently resuspended in 10 mL Ca^{2+}-free PBS supplemented with PGI_2 (1 µg/mL) before centrifugation (1500 g, 15 min, no brake).

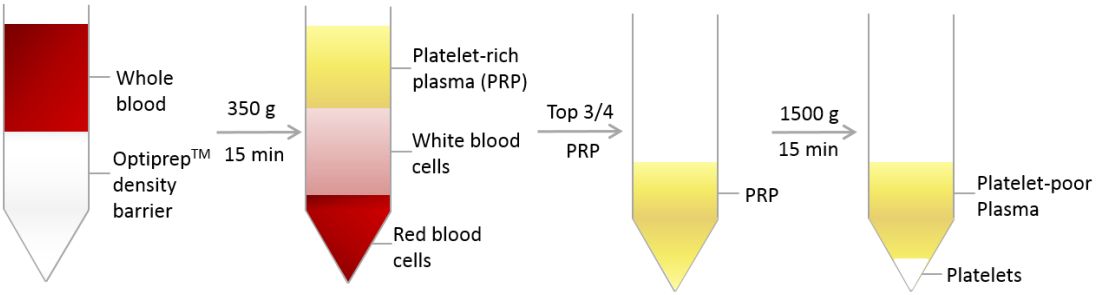

Figure 4.1. Platelet isolation. Schematic representation of the isolation of platelets from whole blood. Abbreviations: PRP, platelet-rich plasma.

4.2.3.1 Utility of prostaglandin I_2 to prevent platelet activation

When circulating through vessels with an intact and healthy endothelial lining, platelets remain inactivated. This is maintained by an absence of activating factors as well as the presence of PGI_2 (Thon and Italiano, 2012; Machlus and Italiano, 2013).

Platelet activation occurs when there is a break in the endothelium, bringing platelets into contact with activating factors such as collagen, thromboxane A2, ADP and thrombin. Upon this activation there is a rapid change in platelet morphology in which platelets transform from smooth discs into irregular spheroids and aggregate (Kramer *et al.*, 2014).

PGI_2 was used during platelet isolation for this work as it binds to prostacyclin receptors on platelets, acting as an antagonist of their activation. This binding causes an increase in intracellular cAMP which inhibits phospholipase C activation, and reduces Ca^{2+} mobilisation from intracellular stores. This calcium mobilisation would otherwise result in platelet activation and aggregation. Prevention of activation is especially important given evidence of mitochondrial release in the microparticles produced by activated platelets (Boudreau *et al.*, 2014).

4.2.4 Platelet quantification

Following generation of a platelet pellet (Figure 4.1), supernatant was removed and platelets were resuspended in 10 mL Ca^{2+}-free PBS supplemented with PGI_2 (1 µg/mL). This suspension was then diluted 10-fold (36 µL + 324 µL PBS) in triplicate in a 96-well plate before absorbance was read at 750 nm using a plate reader (Varioskan, Thermo Scientific). Absorbance data were input into the following equation to quantify platelets (Figure 4.2) (Walkowiak *et al.*, 1997).

$$\left(\frac{6.23}{2.016 - \left(k \times y \times \left(\frac{reading - blank}{800}\right)\right)} - 3.09 \right) x\ R = platelets\ x\ 10^8/mL$$

Figure 4.2. Equation to quantify platelets. Where k is a geometrical factor equal to 1.33 for a flat bottom 96-well microplate, y is the wavelength used (750 nm), R is the dilution factor of the sample.

4.2.5 Platelet extracellular flux analysis

4.2.5.1 Preparation

Following quantification, platelets were seeded in Ca^{2+}-free PBS in two CellTak (Corning™)-coated XF 96-well cell culture microplates, one for a mitochondrial stress test and one for a complex activity assay (1 x 10^7 platelets/50 µL/well). Plates were then centrifuged (200 g, 1 min, without brake) to enable platelet adherence.

4.2.5.2 Mitochondrial stress test

Mitochondrial stress tests were performed as described in Section 2.2.4.3. Briefly, PBS was removed from wells containing platelets and was replaced with supplemented XF base medium (175 µL/well), prior to incubation (1 h, 0 % CO_2, 37 °C). During the assay, flutamide, 2-hydroxyflutamide or tolcapone (30, 125 or 250 µM) were injected into each well prior to the sequential addition of oligomycin, FCCP, rotenone and antimycin A (concentrations detailed in Section 2.2.4.3).

4.2.5.3 Complex I-IV activity assays

Following washes in 1XPBS to check for platelet adherence, complex assays were performed as described in Section 2.2.4.4. Briefly, PBS was removed from wells containing platelets and was replaced with MAS buffer containing plasma membrane permeabiliser (1 nM) and constituents to stimulate oxygen consumption via complex I, II, III or IV (175 µL/well). During the assay, 2-hydroxyflutamide (15, 30, 125 or 250 µM) was injected, 9 min later oligomycin, FCCP, rotenone and antimycin A (potassium azide for complex IV activity assessment) were sequentially added (concentrations detailed in Section 2.2.4.4).

4.2.6 Statistical analysis plan

A data analysis plan was formulated based on the sub-hypotheses below, all analyses were performed blinded.

1) Platelets from donors of haplogroups H, J, T and U differ in mitochondrial function.
2) Platelets from donors of haplogroups H, J, T and U have differential susceptibility to drug-induced mitochondrial dysfunction.
3) Basal mitochondrial function can predict susceptibility to drug-induced mitochondrial dysfunction.

To address each question, donors of each haplogroup were pooled to give final n numbers of H (8), J (6), T (7) and U (9). For 1) and 2) results from mitochondrial stress tests and complex assays were to be assessed for statistically significant deviations from other haplogroups. The following parameters were selected for comparison based on findings from Chapter 2: basal, maximum and ATP-linked respiration, spare respiratory capacity, proton leak and complex I-IV activity (maximal respiration).

To address 3) Pearson's correlation coefficient was to be calculated for parameters of basal mitochondrial function: spare respiratory capacity, basal respiration and compared with outputs of dysfunction: EC_{50} ATP-linked respiration (flutamide, 2-hydroxyflutamide, tolcapone) and complex I/II activity (2-hydroxyflutamide only).

EC_{50} values were determined by nonlinear regression analysis using GraphPad Prism 7.0 following mean centering using SPSS v24 (to account for cases where the control value was 0 for the parameter of interest). Normality was assessed using a Shapiro-Wilk test. Statistical significance was determined by a one-way ANOVA for parametric data followed by a Dunnett's post-hoc test using StatsDirect 2.7.9. Differences were determined significant at $p < 0.05$.

4.3 RESULTS

4.3.1 Assessment of basal mitochondrial function in platelets of multiple haplogroups

Assessment of basal mitochondrial function using a mitochondrial stress test revealed no significant difference between each of the four haplogroups for each of the parameters quantified in this assay (Figure 4.3A). Similarly, when each parameter was considered as a proportion of maximal respiration, there was no significant difference between the ATP-linked respiration, spare respiratory capacity and proton leak in platelets of each haplogroup (Figure 4.3B-E).

Permeabilisation of platelets and addition of complex-specific substrates also enabled the determination of complex-specific differences between haplogroups. Complex I activity was significantly lower in platelets of haplogroup J (Figure 4.4A) and haplogroup U platelets exhibited significantly increased complex I and III activity (Figure 4.4A, C) compared to other haplogroups. There was no significant difference in complex II or IV activity between haplogroups (Figure 4.4B, D). Basal mitochondrial function data from individual donors is presented in Appendix 3 (3A: data points categorised as either genotypes or as samples which did or did not contain SNPs (16192T, 16189C, 295T) associated with increased mtDNA copy number, 3B: data points individually labelled for donors 1-30) (Ebner *et al.*, 2011; Suissa *et al.*, 2009).

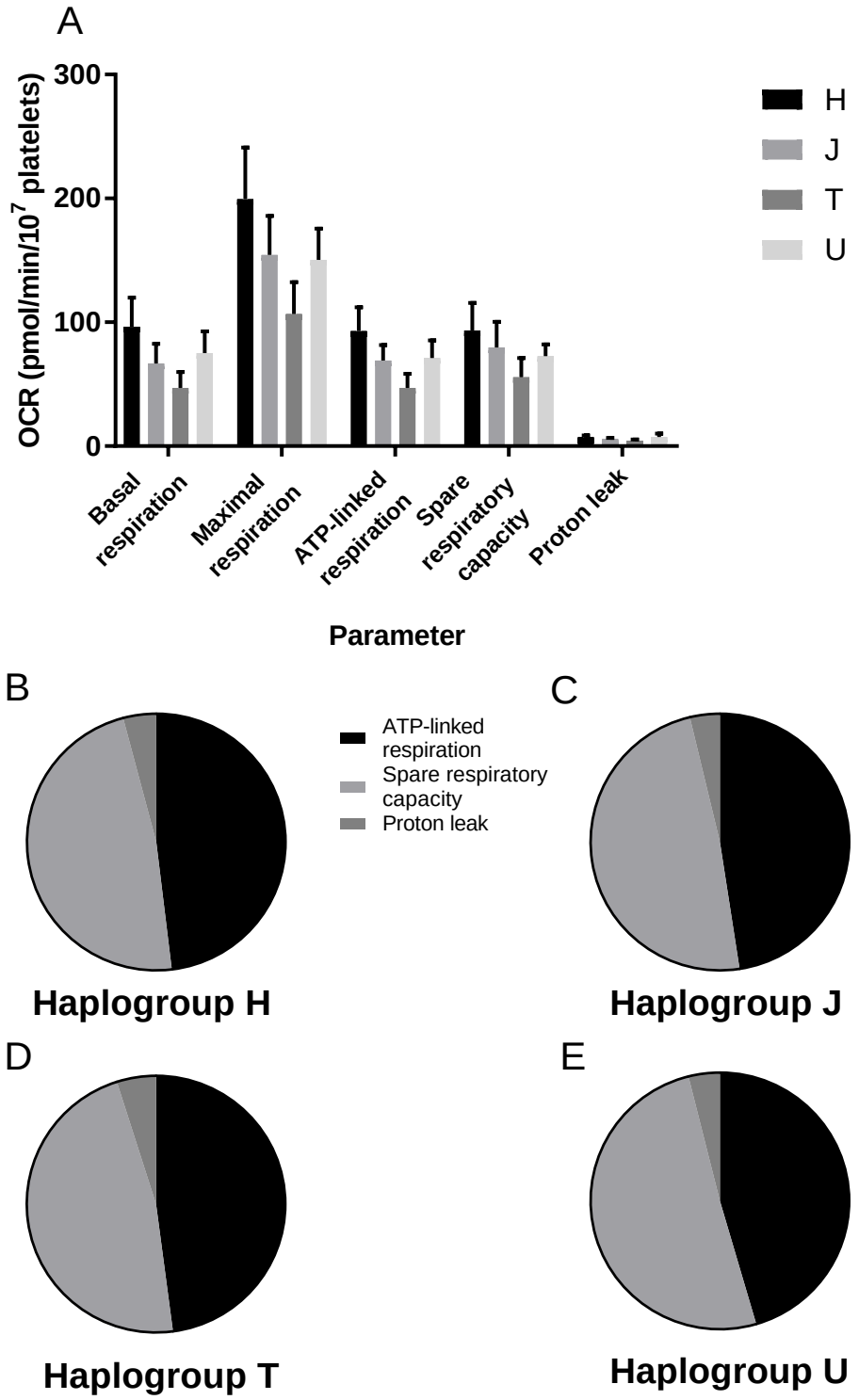

Figure 4.3. Basal mitochondrial function. Extracellular flux analysis of platelets from donors of haplogroups H, J, T and U were performed. A: basal, maximal and ATP-linked respiration, spare respiratory capacity and proton leak of platelets from each haplogroup. B-E: ATP-linked respiration, spare respiratory capacity and proton leak as a proportion of maximal respiration. Data are presented as mean + SEM of $n \geq 6$ experiments.

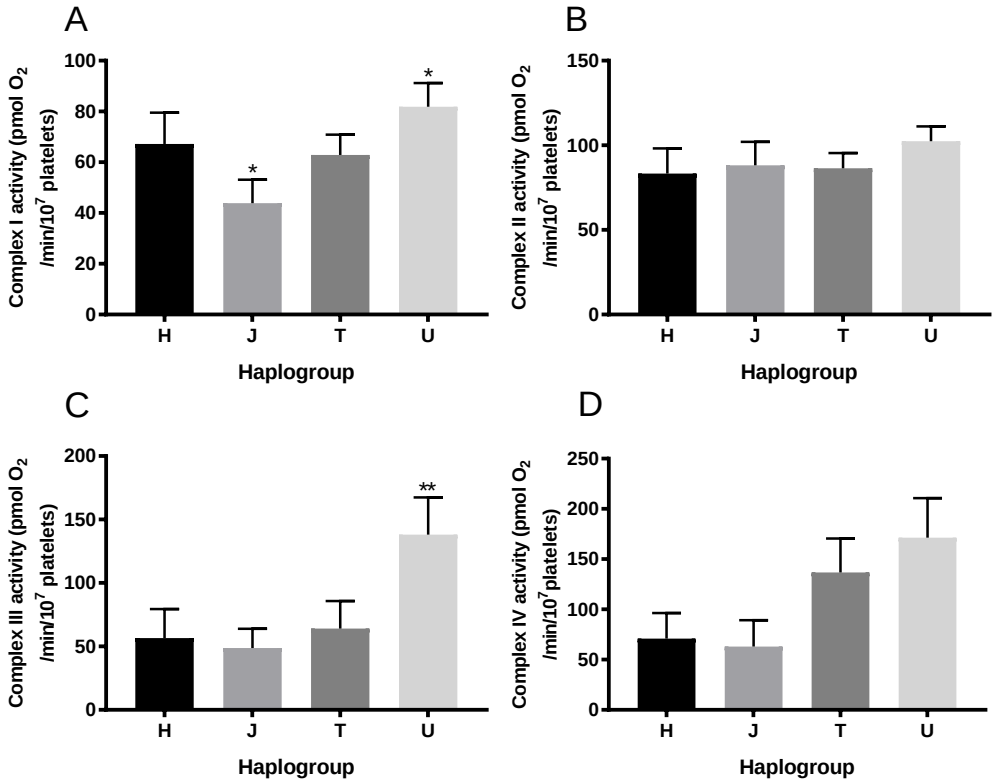

Figure 4.4. Basal complex activity. Extracellular flux analysis of platelets from donors of haplogroups H, J, T and U was performed under conditions of permeabilisation and addition of substrates specific to complexes I (A), II (B), III (C) or IV (D). Complex activity was defined as the maximal respiration when treated with substrates specific to the complex of interest. Statistical significance compared to other haplogroups e.g. H vs. non-H: * $p<0.05$, ** $p<0.01$, *** $p<0.001$. Data are presented as mean + SEM of $n \geq 6$ experiments.

4.3.2 Differential impact of flutamide, 2-hydroxyflutamide and tolcapone upon platelets of different mitochondrial haplogroups

When multiple parameters of mitochondrial function were measured following acute treatment with flutamide (Figure 4.5), 2-hydroxyflutamide (Figure 4.6) or tolcapone (Figure 4.7), no single haplogroup had a significantly different response to the remaining three haplogroups. Although not significant, differences were visible between haplogroups J and T vs H and U; with haplogroup JT platelets exhibiting significant functional differences at lower test compound concentrations than haplogroup H/U. When assessed for significance, macrohaplogroup JT was more susceptible to a reduction in maximal respiration induced by tolcapone (Figure 4.7).

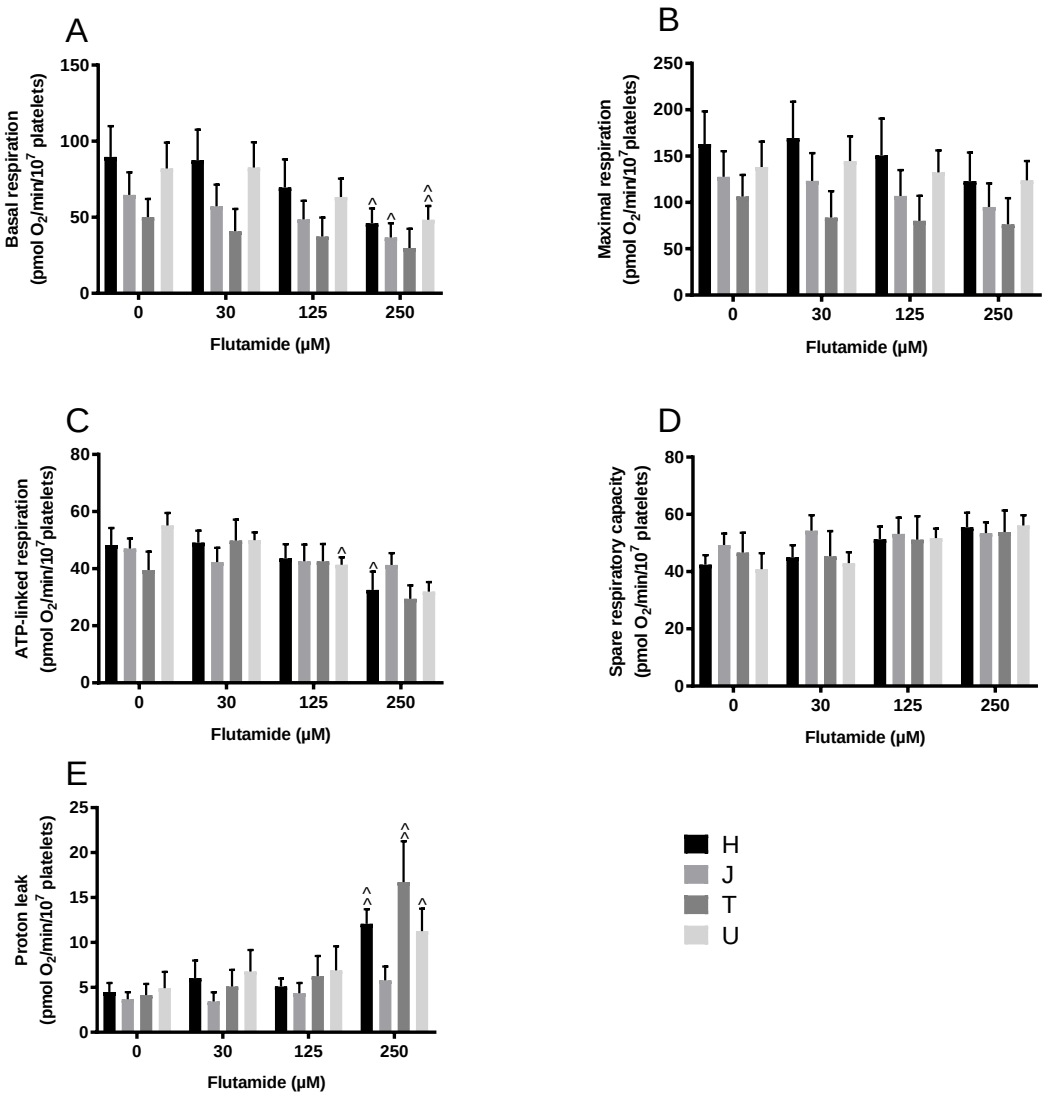

Figure 4.5. Mitochondrial function of flutamide-treated platelets. Extracellular flux analysis of platelets from donors of haplogroups H, J, T and U was performed following acute treatment with flutamide. A, B: changes in maximal and basal respiration, C-E: changes in ATP-linked respiration, spare respiratory capacity and proton leak. Statistical significance compared to vehicle control: ^ $p < 0.05$, ^^ $p < 0.01$, ^^^ $p < 0.001$. For clarity only the first point of significance is shown. Data are presented as mean + SEM of $n \geq 6$ experiments.

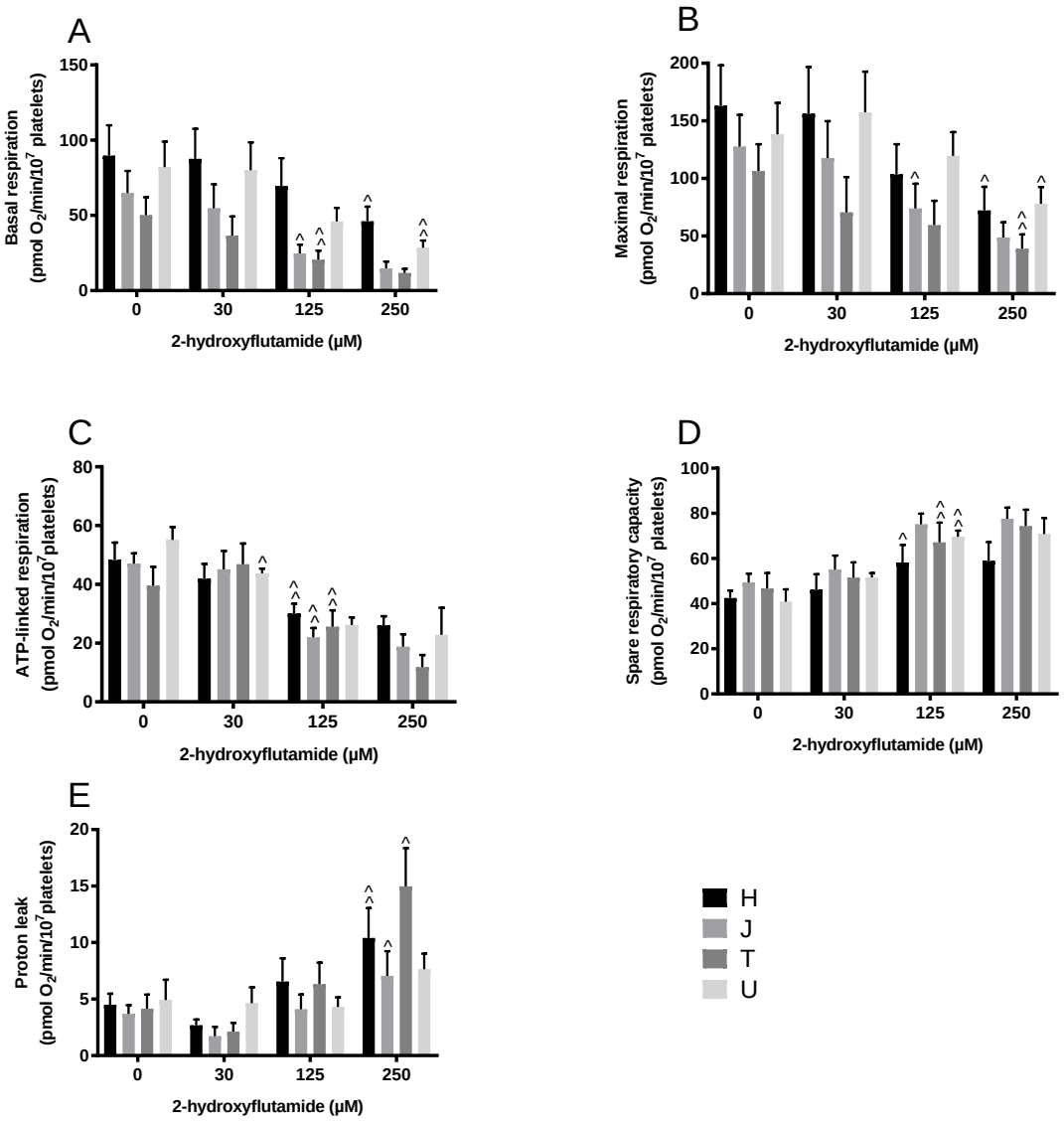

Figure 4.6. Mitochondrial function of 2-hydroxyflutamide-treated platelets. Extracellular flux analysis of platelets from donors of haplogroups H, J, T and U was performed following acute treatment with 2-hydroxyflutamide. A, B: changes in maximal and basal respiration, C-E: changes in ATP-linked respiration, spare respiratory capacity and proton leak. Statistical significance compared to vehicle control: ^ $p < 0.05$, ^^ $p < 0.01$, ^^^ $p < 0.001$. For clarity only the first point of significance is shown. Data are presented as mean + SEM of $n \geq 6$ experiments.

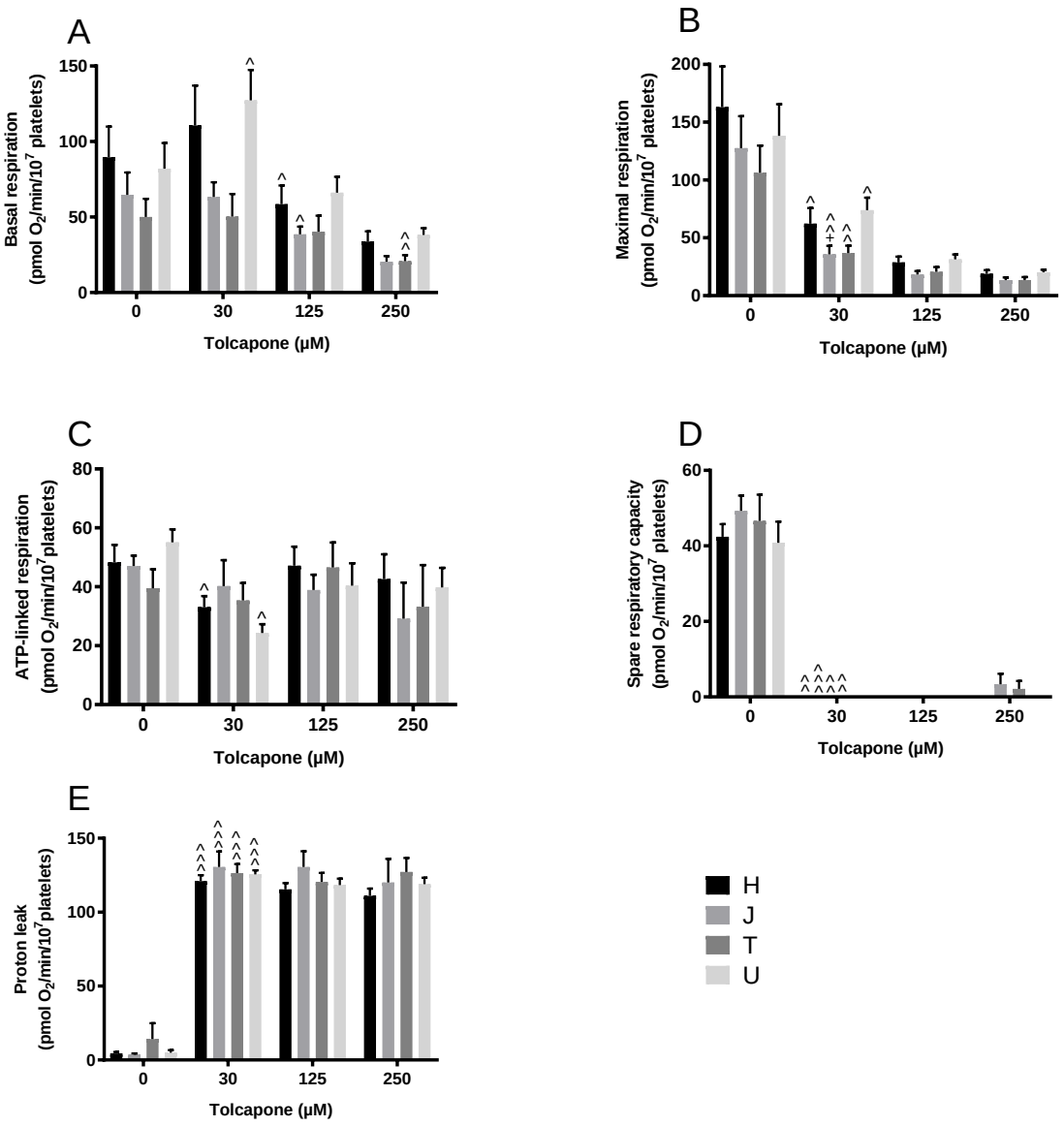

Figure 4.7. Mitochondrial function of tolcapone-treated platelets. Extracellular flux analysis of platelets from donors of haplogroups H, J, T and U was performed following acute treatment with tolcapone. A, B: changes in maximal and basal respiration, C-E: changes in ATP-linked respiration, spare respiratory capacity and proton leak. Statistical significance compared to vehicle control: ^ $p < 0.05$, ^^ $p < 0.01$, ^^^ $p < 0.001$. For clarity only the first point of significance is shown. Statistical significance of haplogroups J, T compared to other haplogroups; $^{+}p < 0.05$. Data are presented as mean + SEM of n ≥ 6 experiments.

4.3.3 Assessment of 2-hydroxyflutamide-induced respiratory complex dysfunction

Previous evidence of the complex I and II liabilities of 2-hydroxyflutamide (Section 2.3.3) prompted the investigation of these liabilities in platelets of different haplogroups. Haplogroup J was significantly more susceptible to complex I inhibition induced by 125 µM and 250 µM 2-hydroxyflutamide (Figure 4.8A). This was also reflected in the EC_{50} complex I

activity of 2-hydroxyflutamide in haplogroup J platelets, which was significantly less than the remaining haplogroups (Table 4.2). Notably, although no single concentration of 2-hydroxyflutamide was significantly more inhibitory of complex II activity in haplogroup J platelets, the EC_{50} complex II activity when exposed to 2-hydroxyflutamide was significantly less in haplogroup J platelets (Figure 4.8B, Table 4.2).

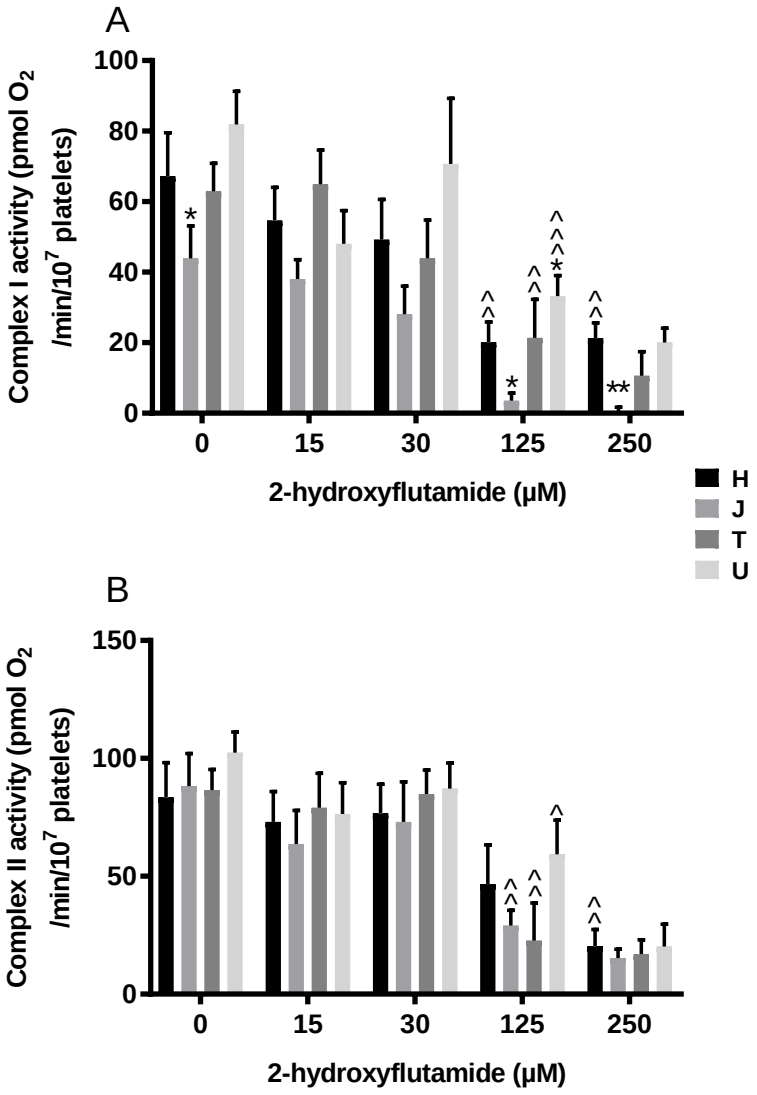

Figure 4.8. Complex I and II activity of 2-hydroxyflutamide-treated platelets. Extracellular flux analysis of platelets from donors of haplogroups H, J, T and U was performed under conditions of permeabilisation and addition of substrates specific to complexes I (A), II (B) followed by acute treatment with 2-hydroxyflutamide. Complex I/II activity was defined as maximal respiration upon treatment with substrates for complex I/II respectively. Statistical significance compared to vehicle control: ^ $p < 0.05$, ^^ $p < 0.01$, ^^^ $p < 0.001$. For clarity only the first point of significance is shown. Statistical significance compared to other haplogroups e.g. H vs. non-H: * $p < 0.05$, ** $p < 0.01$, *** $p < 0.001$. Data are presented as mean + SEM of n ≥ 6 experiments.

Table 4.2. EC_{50} complex I and II activity of 2-hydroxyflutamide in platelets from donors of haplogroups H, J, T and U.

Complex	EC_{50} complex activity (μM)			
	H	J	T	U
I	118 ± 16.2	49.3 ± 5.55 (0.0390)	69.0 ± 9.72	70.8 ± 9.47
II	144 ± 12.1	63.1 ± 3.92 (0.0200)	79.0 ± 8.96	110 ± 8.80

EC_{50} complex activity refers to the concentration of 2-hydroxyflutamide required to reduce complex I/II activity by 50 %. Data are presented as mean ± SEM (*p* value) of n ≥ 6 experiments. *P* value indicates statistical significance compared to other haplogroups and is only shown if < 0.05.

4.3.4 Correlations between basal and treated mitochondrial function

The ability of basal values of mitochondrial function to predict responses to compound treatment was assessed by the calculation of Pearson's correlation coefficient (Table 4.3). The spare respiratory capacity of untreated platelets provided the strongest positive correlation (*R* value nearest to +1) with the EC_{50} ATP-linked respiration of flutamide and 2-hydroxyflutamide but not tolcapone. Basal respiration and complex I/II activity failed to strongly correlate (*R* value near 0) with the EC_{50} of any of the test compounds.

Table 4.3. The correlation of basal mitochondrial function with function upon treatment with flutamide, 2-hydroxyflutamide and tolcapone.

Variable 1	Variable 2	*R*	*P* value
Complex I activity	2-hydroxyflutamide EC_{50} complex I activity	0.23	0.3356
Complex II activity	2-hydroxyflutamide EC_{50} complex II activity	0.33	0.4010
Spare respiratory capacity	Flutamide EC_{50} ATP-linked respiration	0.72	<0.0001
Spare respiratory capacity	2-hydroxyflutamide EC_{50} ATP-linked respiration	0.63	0.0002
Spare respiratory capacity	Tolcapone EC_{50} ATP-linked respiration	0.35	0.0602
Basal respiration	Flutamide EC_{50} ATP-linked respiration	0.17	0.3622
Basal respiration	2-hydroxyflutamide EC_{50} ATP-linked respiration	0.28	0.1278
Basal respiration	Tolcapone EC_{50} ATP-linked respiration	0.18	0.3446

Variable 1 and 2: functions of platelets in a basal and treated state respectively. R: Pearson's correlation coefficient. *P* value: statistical significance of correlation.

4.3.5 Day-to-day variation of platelet mitochondrial function

Parameters of mitochondrial respiration were compared between two individual platelet donors over a four day period. Overall, the values of the parameters measured were inconsistent over the time course (Figure 4.9). In particular, donor 2 platelets exhibited a

substantial increase in proton leak over the time course (Figure 4.9E), whereas the maximal respiration remained very similar in the same donor across this time course (Figure 4.9B).

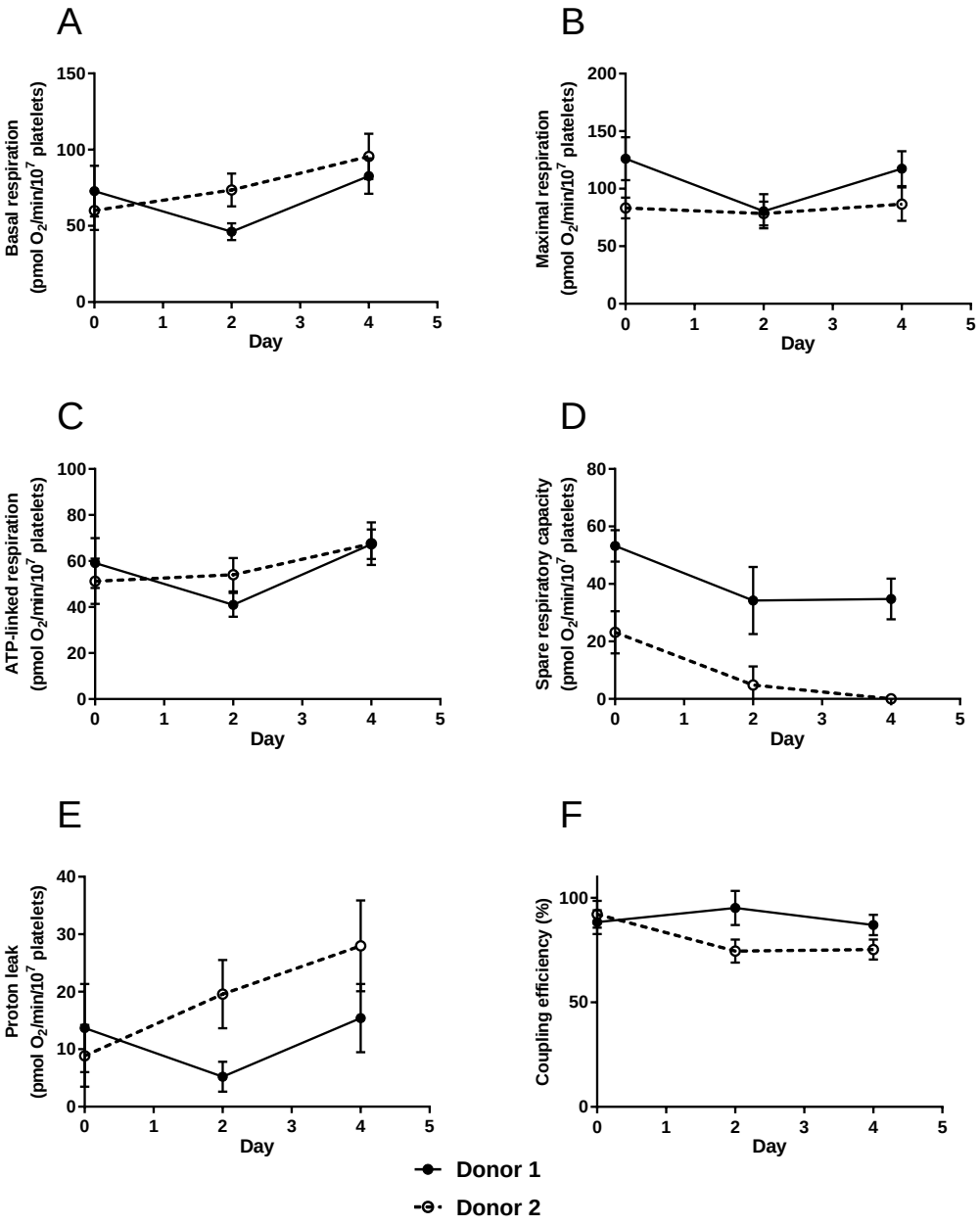

Figure 4.9. Day-to-day variation of platelet mitochondrial function. Two healthy volunteers (of unknown mitochondrial genotype) donated platelets for extracellular flux analysis on days 0, 2 and 4. The following parameters were assessed: basal respiration (A), maximal respiration (B), ATP-linked respiration (C), spare respiratory capacity (D), proton leak (E), coupling efficiency (F). Coupling efficiency calculation: (ATP-linked respiration/basal respiration)*100. Data are presented as mean ± SEM of n =1 experiments (30 technical replicates).

4.3.6 Comparison of HepG2 cell and platelet basal mitochondrial function

Indicators of basal mitochondrial health: ATP-linked respiration, spare respiratory capacity and proton leak were compared between HepG2 cells and platelets (Figure 4.10). On average, platelets had more spare respiratory capacity (+10.26 (±1.41) %) and ATP-linked respiration (+5.10 (±1.09) %) and less proton leak (-15.36 (±1.38) %) than HepG2 cells as a proportion of maximal respiration.

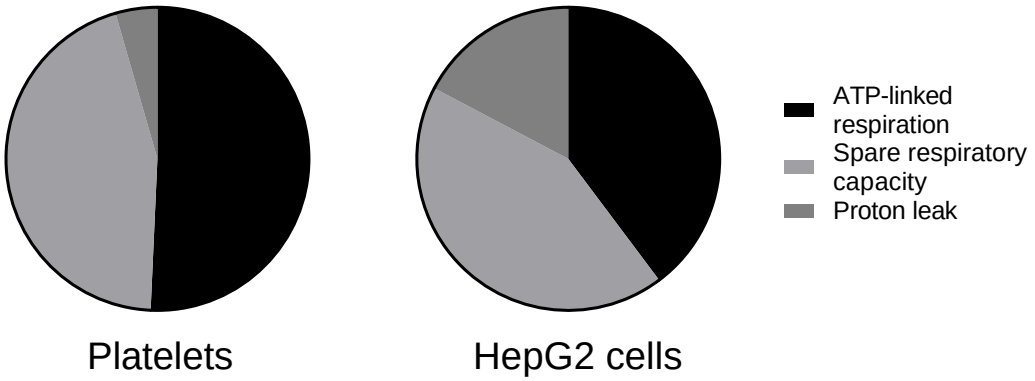

Figure 4.10. Comparison of parameters of mitochondrial function in platelets and HepG2 cells. ATP-linked respiration, spare respiratory and proton leak for platelets from each haplogroup were pooled for comparison with HepG2 cells. HepG2 cell values were derived from data described in Section 2.3.2. Values are displayed as a proportion of maximal respiration of the cell type.

4.4 DISCUSSION

Platelets have previously shown utility as an accessible cell type which is amenable to XF analysis for the assessment of mitochondrial function. This, together with the abundance of mtDNA and absence of nuclear DNA in platelets makes these cell fragments an ideal candidate for the assessment of mtDNA variation upon mitochondrial function and also highlights their potential as a surrogate cell type for the investigation of the effect of mtDNA variation in hepatocytes. The experiments described in this chapter have used platelets isolated from the whole blood of 30 healthy volunteers from mitochondrial haplogroups, H, J, T and U (the four most common haplogroups in the UK) and have demonstrated that platelets are suitable for the XF analysis of ETC function, as well as for the study of specific respiratory complexes via permeabilisation.

Differences in function conferred by haplogroup were particularly evident in XF analysis complex assays; compared to haplogroups H and T, haplogroup J had a reduced respiratory activity and haplogroup U had a higher respiratory activity, deviations which were evident at both basal state and upon 2-hydroxyflutamide treatment. The reduced complex I activity of haplogroup J platelets could be associated with the SNPs characteristic of this haplogroup

including A10398G (rs2853826) and G13708A (rs28359178) which are non-synonymous mutations in regions encoding complex I subunits, MT-ND3 and MT-ND5 respectively (Czarnecka *et al.*, 2010; Pignataro *et al.*, 2017). Three haplogroup J donor samples (9, 16 and 30) also contained the T3394C SNP within the region encoding MT-ND1 (complex I), characteristic of the J1c1 subhaplogroup (Liang *et al.*, 2009; MITOMAP). The impact of these amino acid substitutions upon complex I activity has not been assessed directly, but taken together, the multiple SNPs in regions encoding complex I of haplogroup J platelets and the concomitant decrease in complex I activity observed suggest that these polymorphisms may have a functional impact.

In contrast to complex I, complex II is entirely encoded in the nuclear genome, therefore in theory one would not expect to observe a difference between haplogroups, indeed this was the case in this work, with no significant difference in platelet complex II activity between haplogroups (Chinnery and Hudson, 2013). Despite variation in complex I activity, the primary entry point of electrons in the ETC, parameters of overall mitochondrial health upon 2-hydroxyflutamide treatment (including spare respiratory capacity and ATP-linked respiration) did not vary between haplogroups, this lack of variation should be confirmed in a more highly powered study, but it does pose the question: although there is a difference in respiratory complex function between haplogroups, is it physiologically relevant if there is no detectable impact upon total ETC function?

As well as identifying haplogroup-related differences in mitochondrial function, this research sought to assess the suitability of platelets for such studies. This was particularly important given a previous investigation by Chacko *et al.,* which concluded that platelets were not an optimal choice for the study of bioenergetic defects, based on their functioning at near maximal energetic capacity under basal conditions (Chacko *et al.*, 2013). By contrast, the investigation of basal platelet function described in this chapter found a significant spare respiratory capacity in platelets, similar to that of HepG2 cells and indicative of an ability to increase respiration above basal levels. This difference could be a result of the difference in platelet donors in each study; dependent on the platelet donor, the concentration of FCCP (uncoupler) required to stimulate maximal respiration could vary. Ideally, before XF analysis of each donor sample, the concentration of FCCP would be titrated to generate maximal respiration in the absence of cell death, but this is not always logistically possible. There were also considerable differences in parameters of mitochondrial respiration dependent on the day the experiments were performed which means that titration may be required for the same donor upon each platelet donation, which again may not be feasible.

In the context of the assessment of iDILI, the suitability of platelets also depends on concordance with current models of iDILI. Upon treatment with the uncoupler, tolcapone and respiratory complex inhibitors, flutamide and 2-hydroxyflutamide, considerable differences in response compared to HepG2 cells were evident. In HepG2 cells, tolcapone did not induce a substantial increase in proton leak until used at 62.5 µM, whereas in platelets significantly increased proton leak was evident at the lowest concentration used (30 µM) (Section 2.3.2) Contrastingly, there were no substantial changes in proton leak, spare respiratory capacity or ATP-linked respiration in platelets of any haplogroup upon 250 µM flutamide or 2-hydroxyflutamide treatment, but upon treatment with this concentration in HepG2 cells, there was a significant decrease in ATP-linked respiration and spare respiratory capacity, alongside a large increase in proton leak (Section 2.3.2).

The overall increased susceptibility to uncouplers in platelets compared to HepG2 cells may be explained in part by the relative hyperpolarisation of the mitochondrial membrane in cancer cells in comparison to primary cells. $\Delta\psi_m$ has been found on average to be -220 mV in cancer cells, compared to -140 mV in primary cells (Forrest, 2015). This may confer increased resistance to depolarisation of the membrane induced by uncouplers. Nonetheless, the significance of this effect is debatable given the constant fluctuation of $\Delta\psi_m$ dependent on proton transport and ATP export/ADP import by the ANT, suggesting that the $\Delta\psi_m$ of cancer cells and normal cells will often overlap.

Despite differences in susceptibility to mitochondrial dysfunction compared to HepG2 cells, platelets still have utility in providing information regarding the relative differences between haplogroups. In addition, some basal parameters of platelet mitochondrial function, namely spare respiratory capacity were found to be strongly correlated with the EC_{50} of ATP-linked respiration in flutamide and 2-hydroxyflutamide-treated cells. This demonstrated the utility of platelets for the prediction of dysfunction based on basal state measurements.

A significant limitation of the research described in this chapter was the assumption that the mtDNA variation present in the platelets used for functional analysis would be present in the same abundance as in the whole blood used to extract DNA for genotyping of the volunteers. The whole blood used to obtain the initial DNA sample for each volunteer contained mtDNA from a variety of cell types; the mutational load of platelets could conceivably deviate from the mutational load of the mixed cell population of whole blood. The tenploidy nature of the variant calling performed in Section 3.2.8.2 has also meant that variants present at a 10 % frequency have been detected in volunteer DNA samples, it is possible that the abundance

of these mutations could have significantly changed in the five years since samples were donated for genotyping. Longitudinal studies to monitor changes in mtDNA variation of a selection of the volunteers in this study are planned to address this ambiguity.

4.5 CONCLUSION

To conclude, this research has indicated that platelets offer a viable *ex vivo* model of interindividual variation in mtDNA and susceptibility to drug-induced mitochondrial dysfunction induced by compounds associated with iDILI. Specifically, platelets from donors of haplogroup J have been found to have increased susceptibility to the inhibition of complex I activity by 2-hydroxyflutamide, whereas haplogroup U appeared to confer a degree of protection.

Clear differences between platelets and HepG2 cells however, including the absence of a nuclear genome in platelets (which means differences in mtDNA replication and biogenesis cannot be considered) has meant that the final chapters of this thesis describe work which aims to generate a hepatic *in vitro* model which uses platelets only as a vector of mtDNA. This would enable the impact of mtDNA variation to be studied in a model which is amenable to long term culture and is more representative of the complex architecture of the liver.

Chapter 5

Generation and Characterisation of HepG2 Rho Zero cells and Transmitochondrial Cybrids

CONTENTS

5.1 INTRODUCTION

The investigations detailed in the previous chapter have demonstrated that platelets can be used to provide a rapid assessment of the differences in mitochondrial function between individuals of different mitochondrial haplogroups. Nonetheless, these anucleate cells are not viable for long-term cell culture and it is unknown whether they are representative of mitochondrial function in the hepatocytes of these volunteers. It is also feasible that their anucleate nature may cause an overestimation of toxicity in cases where a nuclear-initiated response may have enabled the activation of compensatory mechanisms and at least a partial alleviation of drug-induced dysfunction.

Transmitochondrial cybrids offer an alternative model which can serve to determine the impact of variation in mtDNA upon mitochondrial, and ultimately cellular function. Typically, cybrids are generated by the fusion of an enucleated cell (cytoplast) with a cell which has been depleted of its mtDNA (ρ0 cell). An alternative is the fusion of platelets (naturally anucleate) with ρ0 cells. Platelets were first reported as mtDNA-donor cells in cybrid generation by Chomyn *et al.,* (Chomyn *et al.*, 1994) and have since been utilised in multiple cases of cybrid generation (Pello *et al.*, 2008; Swerdlow *et al.*, 1996; Silva *et al.*, 2013).

In either case, the cybrids generated provide a controlled nuclear genome background, enabling the attribution of functional changes to variation in the mitochondrial genome (Wilkins *et al.*, 2014).

Since first reported by King and Attardi in 1989 (King and Attardi, 1989), there has been a wealth of literature regarding the generation of cybrids from multiple different cell lines, however there have been no reports of the generation of cybrids derived from a HepG2 ρ0 cell line (Table 1.6). Considering that the HepG2 cell line is one of the most commonly used in preclinical testing for DILI, a HepG2 cell line offering improved representation of the variation in the mitochondrial genome seen in the clinic may offer greater predictivity of iDILI and/or greater mechanistic value (Bale *et al.*, 2014).

It was therefore hypothesised that HepG2 cells are a suitable parental cell line for the generation of transmitochondrial cybrids. Therefore the aim of the experiments reported in this chapter was to generate HepG2 transmitochondrial cybrids using a two-step process 1) depletion of HepG2 mtDNA to generate HepG2 ρ0 cells 2) repopulation of HepG2 ρ0 cells with mtDNA from the platelets of mtDNA-genotyped volunteers.

HepG2 cells were depleted of their mitochondrial genome by long term treatment with the DNA intercalator, ethidium bromide (EtBr).

Mitochondrial genome sequencing of 384 healthy volunteers (Chapter 4) provided a pool of individuals whom could be recalled to donate platelets. Platelets from these individuals were isolated from whole blood before fusion with HepG2 ρ0 cells. Subsequent incubation in a selection medium allowed cultivation of successfully fused cells. The resultant cells were subject to characterisation using real-time PCR (RT-PCR), western blotting, XF analysis and fluorescence imaging; collectively ensuring expression and function of mtDNA-encoded proteins. These analyses were used to confirm the successful repopulation of HepG2 ρ0 cells with volunteer mtDNA to generate HepG2 transmitochondrial cybrids.

5.2 MATERIALS AND METHODS

5.2.1 Materials

All forms of DMEM and real-time PCR (RT-PCR) reagents were purchased from Life Technologies (Paisley, UK) unless stated otherwise. HepG2 WT cells were purchased from European Collection of Cell Cultures (ECACC, Salisbury, UK). All XF assay consumables were purchased from Agilent Technologies (CA, USA). All other reagents and chemicals were purchased from Sigma Aldrich (Dorset, UK) unless stated otherwise.

5.2.2 Cell culture

HepG2 ρ0 cells and EtBr-treated HepG2 cells were maintained in DMEM/F-12 + GlutaMAX™ supplemented with FBS (10 % v/v), L-glutamine (4 mM), sodium pyruvate (1 mM), HEPES (2 mM) and uridine (500 µM).

During selection for successfully fused HepG2 ρ0 cells and platelets, cells were maintained in high-glucose DMEM (glucose; 25 mM) supplemented with dialysed FBS (10 % v/v), amphotericin B (1.35 µM) and antibiotic/antimycotic solution (100 units penicillin/mL, 170 µM streptomycin and 270 nM amphotericin B).

Following selection and during testing, cybrids were maintained in DMEM high-glucose medium (glucose; 25 mM) supplemented with FBS (10 % v/v), L-glutamine (4 mM), sodium pyruvate (1 mM), and HEPES (1 mM). All cells were incubated at 37 °C and 5 % CO_2.

5.2.3 Generation of HepG2 rho zero cells

5.2.3.1. The use of ethidium bromide to deplete mitochondrial DNA

There are multiple proposed mechanisms of mtDNA depletion via EtBr exposure, including direct inhibition of DNA polymerase γ, the mtDNA polymerase (Tarrago-Litvak *et al.*, 1978). The most widely accepted mechanism however is based on the ability of EtBr to intercalate the mtDNA, disrupting tertiary structure, thereby inhibiting both transcription and replication of mtDNA (Zylber *et al.*, 1969).

5.2.3.2. Experimental set up

HepG2 cells (≤ passage 7) were cultured and passaged as required in the presence of EtBr (1 µM). A range of concentrations between 125 nM and 5 µM were tested based on published recommendations, but lower concentrations failed to deplete mtDNA, whilst at higher concentrations a large scale loss of cell viability was evident (Hashiguchi and Zhang-Akiyama, 2009; King and Attardi, 1989). During treatment with EtBr (1 µM), the chemical was removed for 48 h every two weeks to help maintain cell viability. Following eight weeks exposure, EtBr was removed from a subset of cells for one week prior to characterisation (detailed in Section 5.2.5). If a ρ0 cell phenotype was not evident, cells were returned to EtBr treatment (1 µM) prior to removal for another week and re-testing, until a ρ0 cell population was observed.

5.2.4 Generation of HepG2 transmitochondrial cybrids

5.2.4.1 Platelet isolation

Platelets were isolated from 50 mL of whole blood from healthy volunteers as described in Section 4.2.3.

5.2.4.2 Platelet fusion with HepG2 rho zero cells

5.2.4.2.1 Polethylene glycol

Polethylene glycol (PEG), a polymer of ethylene oxide was used for the fusion of platelets and HepG2 ρ0 cells. The proposed mechanism of fusion is via the dehydration of the lipid membranes by the binding of water molecules, this initiates membrane disruption and fusion via osmotic forces (Nagler *et al.*, 2011).

5.2.4.2.2 Experimental set up

During the final centrifugation step of platelet isolation, HepG2 ρ0 cells were collected by trypsinisation and resuspended in HepG2 ρ0 culture medium. Following cell viability assessment (trypan blue; all viabilities were recorded at > 90 %), ρ0 cells (6 x 10^6 cells) were centrifuged (1000 g, 5 min) and resuspended in Ca^{2+}-free DMEM (2 mL; supplemented with 1 mM PGI_2). This cell suspension was added to isolated platelets using a Pasteur pipette so as to minimise disruption to the platelet pellet. The cell mixture was then centrifuged (180 g, no brake, 10 min) to form a multi-layered pellet of platelets and HepG2 ρ0 cells (Figure 5.1).

Following centrifugation, the supernatant was removed and PEG (250 µL; 50 %) was added before resuspending the cell pellet (30 s) followed by a 1 min incubation period. At the end of the incubation period, HepG2 ρ0 cell medium (30 mL) was added and a further 10-fold or 2-fold dilution with HepG2 ρ0 cell medium was performed before seeding into 96-well, 12-well and 6-well plates (Figure 5.1). Details of alternative methods tested during optimisation of this process are described in Table 5.1.

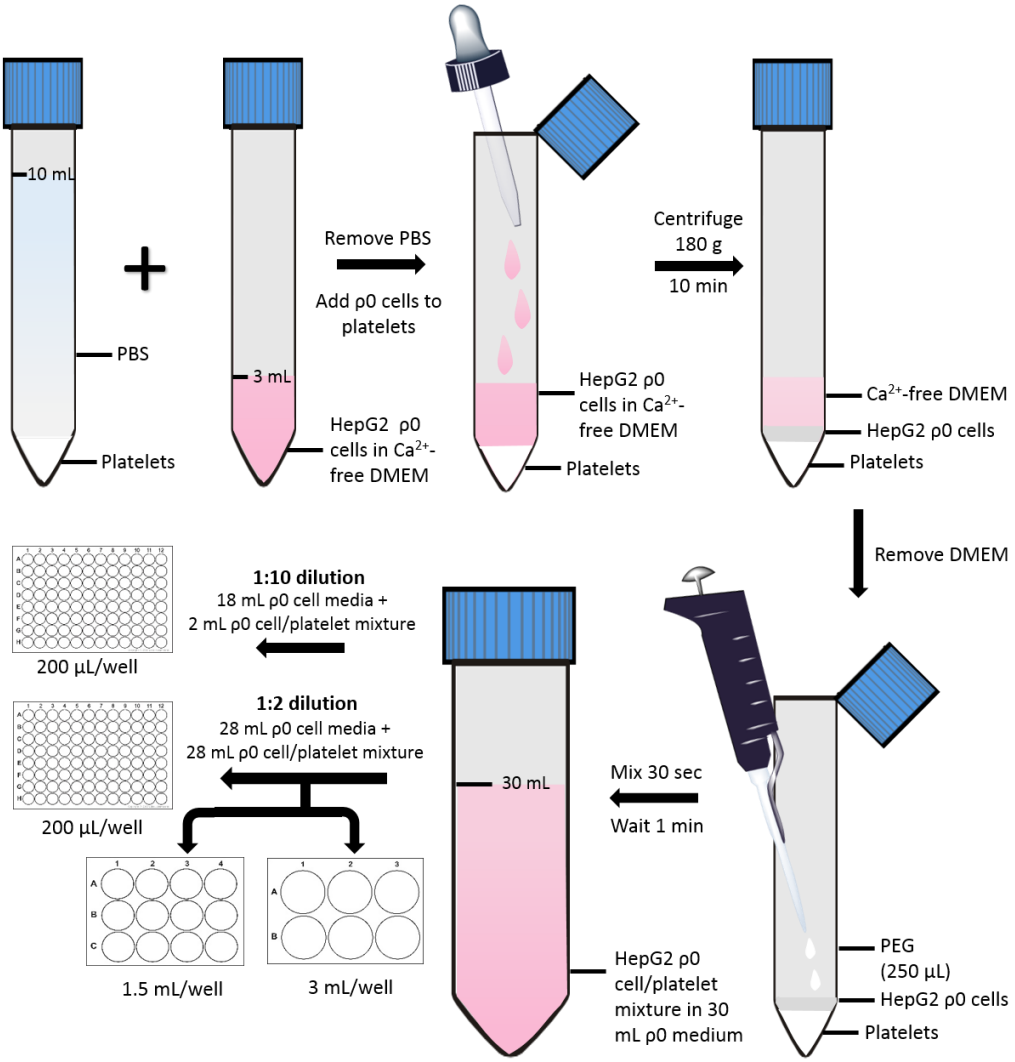

Figure 5.1. Schematic representation of platelet fusion with HepG2 rho zero (ρ0) cells to generate transmitochondrial cybrids. HepG2 ρ0 cells were added to platelets and centrifuged (180 g, 10 min) to generate a multi-layered pellet. Following removal of the supernatant, polyethylene glycol (PEG, fusion reagent) was added and suspended with the cell mixture. After incubation with PEG for 1 min, 30 mL of HepG2 ρ0 cell media was added (containing uridine and pyruvate) before further dilutions into a range of cell culture vessel sizes. Abbreviations: DMEM, Dulbecco's Modified Eagle's Medium; ρ0, rho zero.

Table 5.1. Summary of parameters tested during the optimisation of transmitochondrial cybrid generation. Details of parameters tested to optimise cybrid generation. Highlighted methods were used during the successful generation of cybrids.

Parameter	Methods tested
Reagent for the prevention of platelet activation	PGE_2
	PGI_2
Size of cybrid culture vessel	100 mm petri dish
	Multi-well plates
Density of cybrid culture	1:20
	1:10
	1:2
Pipette size for fusion procedure	p200
	p1000
PEG amount	200 µL
	250 µL

Abbreviations: prostaglandin I_2/E_2, PGI_2/PGE_2; polyethylene glycol, PEG.

5.2.4.3 Selection for successively fused HepG2 rho zero cells/platelets

Two days post-fusion, media were replaced with fresh HepG2 ρ0 media. After a further two days, this was replaced with media consisting of HepG2 ρ0 media and cybrid selection media in equal volumes, before finally switching to 100 % cybrid selection media (summarised in Figure 5.2).

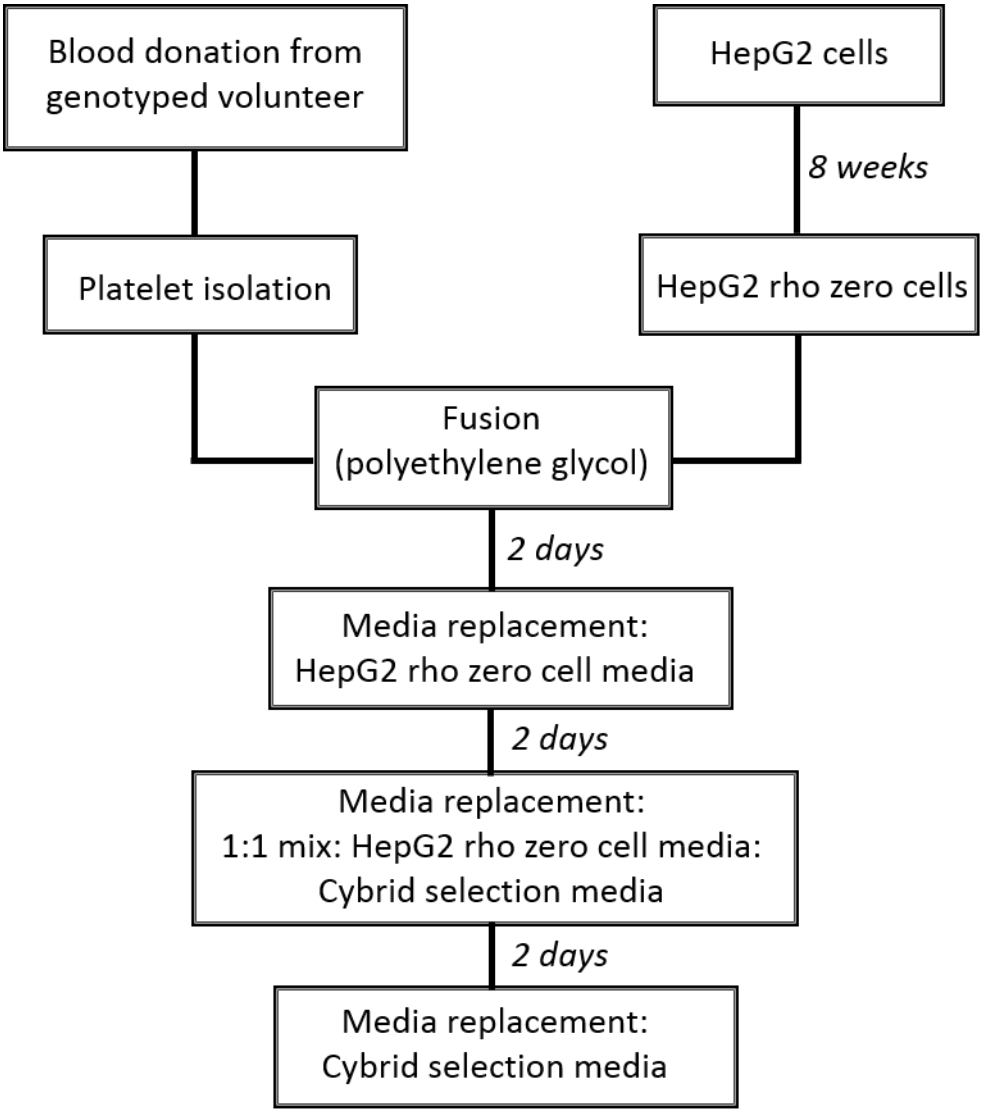

Figure 5.2. Generation of HepG2 transmitochondrial cybrids. Outline of workflow to generate transmitochondrial cybrids derived from the platelets of volunteers with known mitochondrial genotype (Chapter 3). Where there is a significant time lag between consecutive steps the length of this is stated.

5.2.5 Characterisation of HepG2 rho zero cells and cybrids

5.2.5.1 Cell doubling time

WT and ρ0 HepG2 cells were seeded at 30 000 cells/well in a 24-well plate in either ρ0 cell media or selection media (devoid of pyruvate and uridine). On days 1, 3, 5 and 7 of culture, cells were collected by trypsinisation and counted, following which growth rates were calculated. The absence of growth in selection media indicated the complete loss of mtDNA.

5.2.5.2 DNA extraction and real-time PCR

DNA extraction from HepG2 WT, HepG2 ρ0 and HepG2 cybrid cells was performed using a DNA mini kit (Qiagen, Manchester, UK) according to the manufacturer's instructions. Sample DNA concentrations and quality were then quantified using a Quant-iT™ PicoGreen™ dsDNA Assay Kit and nanodrop spectrophotometry respectively (Fischer Scientific, Loughborough, UK).

RT-PCR was carried out using two primers for regions of mtDNA; a custom sequence and ND-1 (complex I subunit) and two primers for regions of nuclear DNA; telomerase reverse transcriptase (TERT) and ribonuclease P RNA component H1 (RNase P) (Applied Biosystems, California, USA) (Table 5.2) (Malik *et al.*, 2011). The use of VIC dye-labelled nuclear DNA primers and FAM-labelled mtDNA primers allowed the simultaneous use of these primers in a single well, reducing variation due to well-loading error.

Table 5.2. Details of real-time PCR primers used to amplify regions of mitochondrial and nuclear DNA.

Gene	Dye/probe	Additional information
RNase P (nDNA)	VIC®dye-labelled TAMRA™ probe	Location: chromosome 14, cytoband 14q11.2
TERT (nDNA)	VIC®dye-labelled TAMRA™ probe	Location: chromosome 5, cytoband 5p15.33
Custom sequence (mtDNA)	FAM®dye-labelled MGB probe	Oligonucleotide sequences: **hmito F5** CTTCTGGCCACAGCACTTAAAC **hmito R5** GCTGGTGTTAGGGTTCTTTGTTTT
ND-1 (mtDNA)	FAM®dye-labelled MGB probe	Location: mtDNA 3307-4262

Abbreviations: FAM, carboxyfluorescein; MGB, minor groove binder; ND-1, NADH dehydrogenase-1; mtDNA, mitochondrial DNA; nDNA, nuclear DNA; RNase P, ribonuclease P RNA component H1; TAMRA, 6-carboxytetramethyl-rhodamine; TERT, telomerase reverse transcriptase; VIC, 2'-chloro-7'phenyl-1,4-dichloro-6-carboxy-fluorescein.

During sample preparation, 2X Taqman® genotyping master mix (5 µL), a nuclear DNA primer (0.5 µL), mtDNA primer (0.5 µL), dH_20 (2 µL) and 10 ng DNA (2 µL) from each sample were combined to give a final sample concentration of 1 ng/µL in each well. RT-PCR was then carried out using the viiA7 RT-PCR system (Life Technologies, UK). MtDNA copies per cell were calculated on the basis that each nuclear DNA primer was present in diploid copies per

cell and used the following formula, where x_1= nuclear DNA primer cycle threshold (C_t) value, x_2=mtDNA primer C_t value: mtDNA copies per cell = $2(2^{(x_1-x_2)})$ (Schäfer, 2016).

5.2.5.3 Detection of mitochondrial/nuclear DNA-encoded mitochondrial proteins

HepG2 ρ0, HepG2 WT or HepG2 cybrid cells were lysed using sonication and 10 µg of lysate protein was resolved by sodium dodecyl sulphate-polyacrylamide gel electrophoresis (SDS-PAGE) using 4-12 % Bis-Tris gel (Invitrogen, UK) in MOPS buffer (MOPS; tris-base; 1.21 % w/v, sodium dodecyl sulphate; 0.20 % w/v, EDTA; 0.06 % w/v in distilled water (dH_20)).

This gel was then transferred to a nitrocellulose membrane (GE Healthcare, Buckinghamshire, UK) in transfer buffer (tris-base; 0.30 % w/v, glycine; 1.5 % w/v, methanol; 20 % v/v in dH_20) and blocked using 10 % non-fat dried milk in Tris Buffered Saline-Tween (TBS-T: TBS; 0.50 % v/v, tween; 0.10 % v/v in dH_20).

Blocking solution was removed using TBS-T and the membrane probed for CI-20, CII-30, CIII-core2, CIV-I and CV-alpha subunits of complexes I-V of the ETC using MitoProfile® Total OXPHOS Human WB Antibody Cocktail (Abcam, Cambridgeshire, UK) (0.20 % v/v in 10 % non-fat dried milk in TBS-T). This was followed by anti-mouse secondary antibody (0.01 % v/v in 10 % non-fat dried milk in TBS-T) before visualisation using an ECL™ system (GE Healthcare, Buckinghamshire, UK).

5.2.5.4 Detection of electron transport chain function

5.2.5.4.1 Mitochondrial stress test

HepG2 WT, HepG2 ρ0 and HepG2 cybrid cells were collected by trypsinisation and plated on a collagen-coated XFe96 cell culture microplate (25 000 cells/100 µL medium/well) and incubated (37 °C, 5 % CO_2) overnight. Cells were then subject to a mitochondrial stress test the following day (Section 2.2.4.3) but without acute injections of the five test compounds.

5.2.5.4.2. Calculation of PPR_{gly}

XF analysis produced two raw outputs, OCR and extracellular acidification rate (ECAR). ECAR can be indicative of the glycolytic rate of the cell, however it also takes into account changes in ECAR due to oxidative phosphorylation. Therefore glycolytic production rate (PPR_{gly}), was used to quantify glycolysis, this was calculated by subtracting respiratory acidification contributions from the total proton production rate (Figure 5.3).

$$\boldsymbol{PPR_{gly} = PPR_{tot} - PPR_{resp}}$$

$$\textbf{Where } \boldsymbol{PPR_{tot} = \frac{ECAR}{BP}}$$

$$PPR_{resp} = \left(\frac{10^{pH-6.093}}{1+10^{pH-6.093}}\right)\left(\frac{\max H^{+}}{O_2}\right)(OCR_{tot} - OCR_{rot})$$

Figure 5.3. Equations for the calculation of PPR_{gly} from mitochondrial stress tests. Abbreviations: PPR_{gly}, proton production rate attributed to glycolysis; PPR_{resp}, proton production rate attributed to respiration; PPR_{tot}, total proton production rate; ECAR, extracellular acidification rate; BP, buffering power; max H^+/O_2, derived acidification for the metabolic transformation of glucose oxidation; OCR_{tot}, total oxygen consumption rate; OCR_{rot}, oxygen consumption rate following rotenone injection; 6.093, PK_1 at 37 °C (Kelly, 2018).

5.2.5.5 Fluorescence imaging of mitochondrial DNA

HepG2 WT, HepG2 ρ0 and HepG2 cybrid cells were collected by trypsinisation and seeded in glass-bottomed 6-well plates in DMEM high-glucose media (200 000 cells/well) and incubated (24 h, 37 °C, 5 % CO_2). Cells were then stained with MitoTracker™ Red CMXRos (200 nM) and PicoGreen™ (0.3 %) and incubated (20 min). Stains were then removed and cells were washed twice in PBS. Cells were imaged with an inverted confocal laser scanning microscope TCS SP5 (Leica Microsystems, Wetzlar, Germany. To avoid a cross talk in excitation of 488 and 561 nm, a sequential scanning mode was performed. Images were acquired with photomultipliers and micrographs were processed and analysed with the software Leica Application Suite Advanced Fluorescence 2.6.0 (Leica Microsystems, Wetzlar, Germany), Adobe Photoshop CS (Adobe Systems, Munich, Germany), ImageJ 1.45s (NIH, Bethesda, MD, USA) and Huygens Professional 4.2.1 (SVI, Hilversum, Netherlands).

5.2.6 Statistical analysis

Unless referred to as a representative figure, all results are representative of n = 3 experiments and are expressed as mean ± SEM.

5.3 RESULTS

5.3.1 Cell doubling rate

The dependence of HepG2 ρ0 cells on pyruvate and uridine meant that culture media devoid of these constituents was able to select for the successful depletion of mtDNA and the resultant non-functional ETC in EtBr-treated cells. Concordantly, HepG2 WT cells had a similar doubling time in media with or without these additives, averaging 26.2 h. In contrast, HepG2 ρ0 cells exhibited no growth without uridine and pyruvate and an average doubling time of 27.6 h when in media containing these two constituents (Figure 5.4).

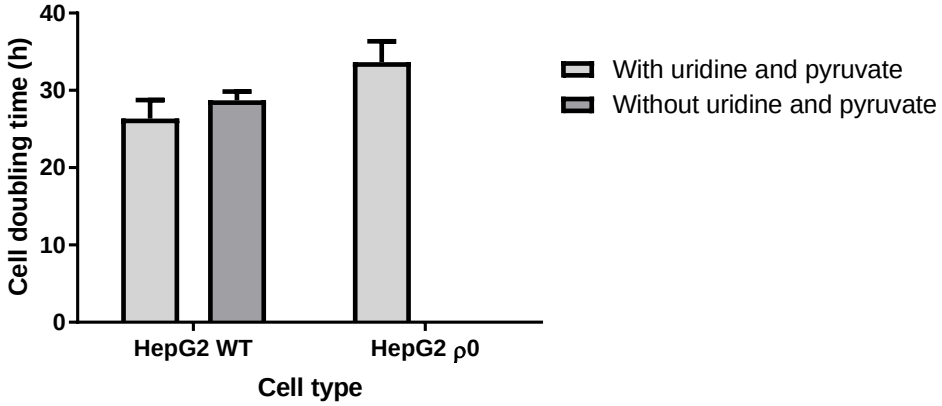

Figure 5.4. Growth rates of HepG2 wild-type (WT) and HepG2 rho zero (ρ0) cells. The two cell types were cultured in media with or without uridine and pyruvate and growth rate calculated. Data are presented as mean + SEM of n=3 experiments.

5.3.2 Real-time PCR characterisation of HepG2 wild-type, rho zero and cybrid cells

The number of mtDNA copies per cell in HepG2 WT, ρ0 and cybrid cells was determined using RT-PCR with primers designed to amplify two regions of nuclear DNA (TERT and RNase P) and two regions of mtDNA (ND-1 and custom 129 bp sequence) culminating in four different combinations of primers. The C_t value of both mtDNA primers increased dramatically in ρ0 compared to WT cells whilst nuclear DNA C_t values remained consistent across all three cell lines. Concordantly, both HepG2 WT and cybrid cells had thousands of mtDNA copies/cell in contrast to the ρ0 cells which had less than one copy/cell (Table 5.3).

Table 5.3. Assessment of cellular mitochondrial DNA (mtDNA) content in HepG2 wild-type (WT), HepG2 rho zero (ρ0) and HepG2 cybrids. Regions of nuclear DNA and mtDNA were amplified using real-time PCR to calculate the number of mtDNA copies per cell.

Sample	Primer C_t value				mtDNA copies/cell			
	TERT	**RNase P**	**ND-1**	**Custom**	**TERT/ ND-1**	**TERT/ custom**	**RNase P/ ND-1**	**RNase P/ custom**
HepG2 WT	30.6 (1.00)	31.3 (1.11)	18.5 (0.120)	18.9 (0.140)	9280	6985	14563	10960
HepG2 ρ0	27.7 (0.0600)	27.2 (0.0700)	34.7 (0.740)	32.0 (0.180)	0.00400	0.0240	0.00300	0.0170
HepG2 cybrid	29.8 (1.10)	30.4 (0.550)	18.9 (0.730)	19.0 (0.0900)	3875	3590	5673	5256

Abbreviations: C_t, cycle threshold; ND-1, NADH dehydrogenase-1; RNase, ribonuclease P RNA component H1; TERT, telomerase reverse transcriptase; WT, wild-type; ρ0, rho zero. C_t values are displayed as mean (SEM).

5.3.3 Protein characterisation of HepG2 wild-type, rho zero and cybrid cells

Western blot analysis (Figure 5.5) showed expression of all nuclear DNA and mtDNA-encoded subunits of the ETC which were probed for in HepG2 WT and cybrid cells. However, ρ0 cells did not express the mtDNA-encoded subunit of complex IV. Notably, despite all the other subunits being encoded in the nuclear DNA, it was only the alpha subunit of ATP synthase which was retained in the ρ0 cells.

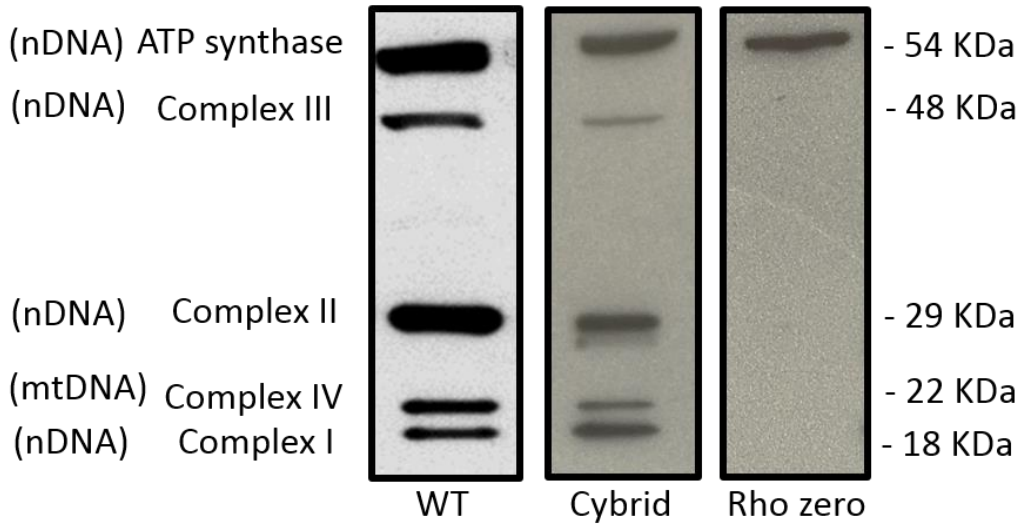

Figure 5.5. Representative western blots of HepG2 wild-type (WT), rho zero (ρ0) and cybrid cell lysates. 10 µg of lysate protein was resolved by SDS-PAGE and probed for subunits of complexes I

(NDUFB8), II (Iron-sulphur protein (IP) 30 KDa), III (Core 2), IV (II), V (alpha). Abbreviations: mtDNA, mitochondrial DNA; nDNA, nuclear DNA.

5.3.4 Functional characterisation of HepG2 wild-type, rho zero and cybrid cells

XF analysis of ρ0 cells and cybrids and comparison to WT HepG2 cells provided information on both PPR_{gly} and OCR. HepG2 WT and cybrid cells exhibited a classic response to the series of mitochondrial inhibitors used to perform the mitochondrial stress test (Figure 5.6C, Table 5.4) whereas the ρ0 cells did not respond to these inhibitors and had very low basal OCR, all of which was due to non-mitochondrial oxygen consumption (Figure 5.6A, Table 5.4). WT cells increased ECAR in response to mitochondrial inhibitors, while ρ0 cells did not respond and had no spare glycolytic capacity (Figure 5.6B). The PPR_{gly} /OCR ratio was also substantially higher in ρ0 cells compared to WT and cybrid cells (Figure 5.6D, Table 5.4).

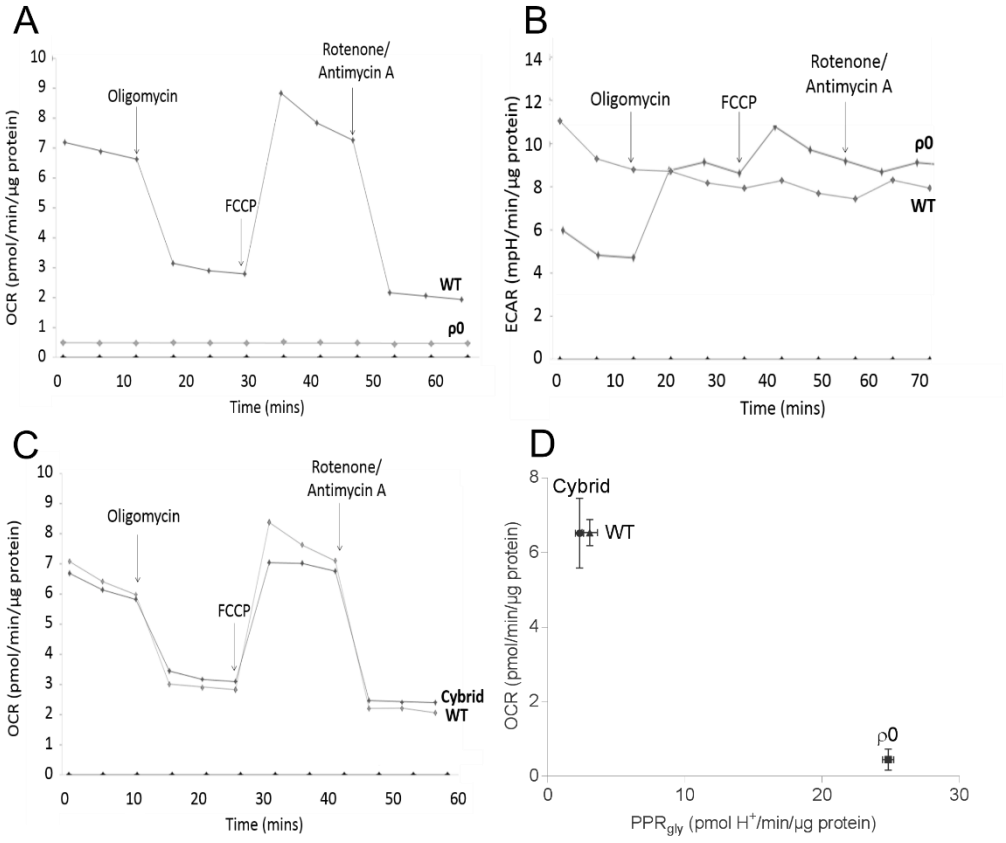

Figure 5.6. Representative extracellular flux analysis traces of HepG2 WT, rho zero (ρ0) and cybrid cells. HepG2 WT, ρ0 and cybrid cells were subject to a mitochondrial stress test (A, C) during which changes in ECAR were also measured (B). This enabled the comparison of PPR_{gly} and OCR in a phenogram (D). Abbreviations: ECAR, extracellular acidification rate; OCR, oxygen consumption rate; PPR_{gly}, proton production rate attributed to glycolysis; WT, wild-type; ρ0, rho zero.

Table 5.4. Differences in parameters of mitochondrial function in HepG2 wild-type (WT), rho zero (ρ0) and cybrid cells. Measurement of both oxygen consumption rate (OCR) and extracellular acidification rate (ECAR) during a mitochondrial stress test allowed comparison of basal OCR, glycolytic proton production rate (PPR_{gly})/OCR and % non-mitochondrial OCR in HepG2 WT, rho zero and cybrid cells.

HepG2 cell type	Basal OCR (pmol/min/µg protein)	PPR_{gly}/OCR	% Non-mitochondrial OCR
WT	6.52 (0.350)	0.354 (0.0900)	28.4 (0.310)
Rho zero	0.450 (0.100)	55.5 (0.930)	102 (4.33)
Cybrid	6.53 (0.400)	0.466 (0.660)	24.3 (0.510)

Abbreviations: OCR, oxygen consumption rate; PPR_{gly}, proton production rate attributed to glycolysis.

5.3.5 Fluorescence imaging of mtDNA in HepG2 wild-type, rho zero and cybrid cells

MtDNA content was visualised by confocal imaging of HepG2 WT, ρ0 and cybrid cells stained with PicoGreen™ (DNA stain) and MitoTracker™ Red CMXRos (mitochondrial network stain). Overlaid images of the two stains show the yellow colour produced from the overlap of PicoGreen™-stained mtDNA with MitoTracker™-stained mitochondria in HepG2 WT and cybrid cells (Figure 5.7A, C). In ρ0 cells there was MitoTracker™ staining of the mitochondria but no staining of mtDNA, with PicoGreen™ staining only evident in the nuclei of cells (Figure 5.7B).

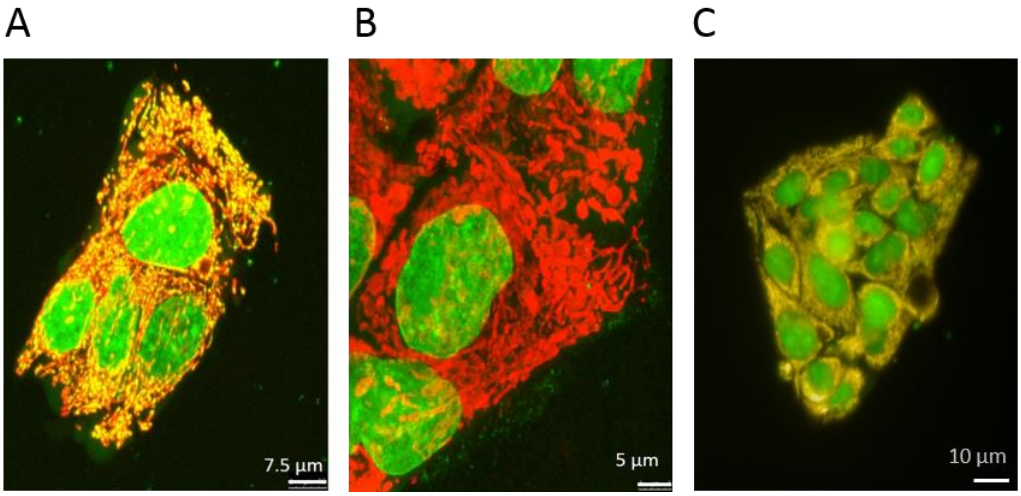

Figure 5.7. Representative images of HepG2 wild-type (WT), rho zero (ρ0) and cybrid cells. HepG2 WT (A), HepG2 ρ0 (B) and HepG2 cybrid cells (C) were incubated with PicoGreen™ (in green) to stain DNA. The mitochondrial network was stained with MitoTracker™ Red CMXRos (in red). Overlay of both fluorescent stains appears as yellow.

5.4 DISCUSSION

HepG2 cells, a commonly used preclinical cell line for the assessment of drug-induced hepatotoxicity, do not represent the mitochondrial genome variation present in patient populations (Godoy *et al.*, 2013). This variation has been evidenced to alter mitochondrial function, which itself is implicated in the onset of iDILI (Kenney *et al.*, 2014; Boelsterli and Lim, 2007). It is therefore the fundamental proposal of this thesis that a failure to account for mitochondrial genome variation may contribute towards the limited prediction of iDILI. As a result, the research described in this chapter aimed to generate HepG2 transmitochondrial cybrids, an *in vitro* model which may be able to better account for mtDNA variation preclinically. The method development required to generate this model is the first of its kind and specific techniques required for successful generation are summarised in Figure 5.8.

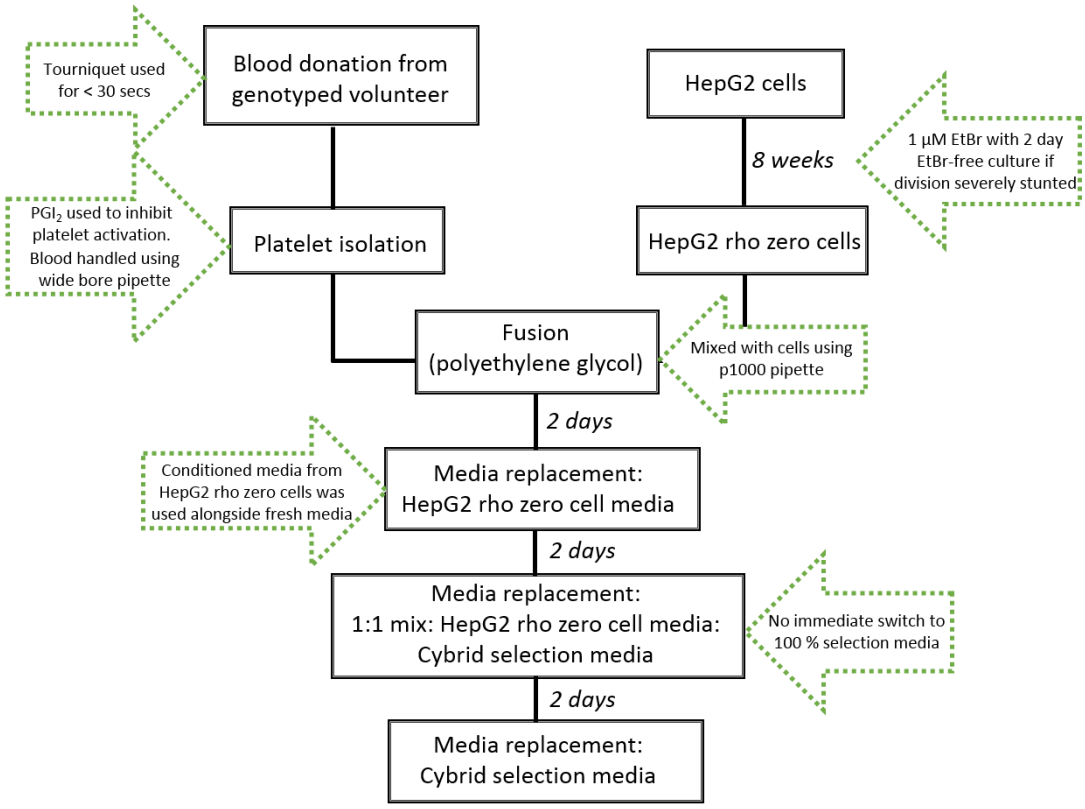

Figure 5.8. Optimised protocol for the generation of HepG2 transmitochondrial cybrids. Black boxes depict the work flow to generate HepG2 transmitochondrial cybrids. Green arrows describe specific adaptations of methods which were found to be crucial for the successful generation of the *in vitro* model. Abbreviations: EtBr, ethidium bromide; PGI_2, prostaglandin I_2.

In order to generate cybrids from a HepG2 cell line it was first necessary to deplete the HepG2 cells of their own mtDNA (to generate HepG2 ρ0 cells), before a donor's mtDNA could be incorporated. Given reports of the effect of EtBr on the nuclear DNA, as well as its inability

to directly eradicate mtDNA (approximately eight weeks treatment is required), alternative methods of mtDNA depletion were tested during this work (Ferraresi *et al.*, 2008; Schubert *et al.*, 2015). For example, the mtDNA polymerase γ inhibitor, ditercalinium or expression of a dominant negative mtDNA polymerase γ construct have been used successfully to create ρ0 cell lines but the success of this technique in a HepG2 cell line is not documented (Jazayeri *et al.*, 2003; Inoue *et al.*, 1997). Alternatively, the transfection of cell lines with mtDNA depletion vectors containing the EcoRI restriction enzyme has also been successfully used, however this was not successful in HepG2 cell lines after multiple attempts due to a loss of viability following transfection (Heller *et al.*, 2013).

On occasion during the expansion of EtBr-treated HepG2 cells in this work, XF analysis revealed a low level of mitochondrial function. This could be indicative of small amounts of mtDNA remaining, though from XF analysis alone it was not clear whether this was due to a low mtDNA copy number in all cells or, a high mtDNA copy number in a proportion of the tested cells. The latter scenario would generate a sub-population of cells which may have enhanced proliferation and the potential to become the dominant population upon cessation of EtBr treatment. Resultantly, when low-level mitochondrial function was identified, cells were re-exposed to EtBr before re-testing for ρ0 status. This risk for small amounts of mtDNA to remain and potentially replicate prompted the thorough characterisation of ρ0 cells described in this chapter.

RT-PCR was employed to confirm the absence of the mitochondrial genome and used multiple nuclear DNA and mtDNA primers. Both nuclear DNA primers, TERT and RNAse P generated similar C_t values, however it should be noted that there are reports of the TERT gene being expressed at greater than diploid copies per cell in some cell lines and therefore values from this primer should be interpreted with caution (Cao *et al.*, 2008). Given the absence of the mtDNA in ρ0 cells, it was unexpected that C_t values were obtained from primers for the mtDNA (ND-1 and custom sequence). Importantly though, these values did not differ from the no-template controls, indicating primer amplification as the source of signal generation. Furthermore, by comparing mtDNA and nuclear DNA primer C_t values, the approximate number of mtDNA copies per cell could be calculated; all fell below one copy of mtDNA per cell, confirming ρ0 cell status (Schäfer, 2016).

Characterisation using confocal imaging did not identify any cells which still contained copies of mtDNA, a possibility that could not be ruled out using PCR methods, in which the presence of mtDNA in sporadic cells could be below the lower limit of detection. Images of ρ0 cells did

show the presence of a small amount of extra-nuclear DNA however this could be from multiple alternative sources, for example DNA from necrotic cells. Importantly this DNA did not overlap with MitoTracker™ Red staining, suggesting that it was not localised to the mitochondria.

Given the absence of the mitochondrial genome in ρ0 cells, an absence of mtDNA-encoded proteins is to be expected. This was indeed the case in this work, with the absence of mtDNA-encoded complex IV subunit II shown by western blotting. However, multiple nuclear DNA-encoded subunits were also absent despite the presence of a nuclear genome in these cells. A limited amount is known regarding the exact underlying mechanism of this absence, though it can be proposed to be due to protein complex instabilities conferred by the absence of mtDNA-encoded subunits in respiratory complexes I and III, of which there are seven and one respectively (Figure 1.8) (Mineri *et al.*, 2009).

Unlike complexes I and III, complex II (succinate dehydrogenase) is entirely encoded in the nuclear DNA, therefore the absence of succinate dehydrogenase subunit B (SDHB) was unanticipated (Schon *et al.*, 2012). Interestingly, succinate dehydrogenase subunit A (SDHA) has in fact been identified in HepG2 ρ0 cells (unpublished data). SDHA is required in ρ0 cells for a functional TCA cycle, the function of which is implied by the fact that ρ0 cells do not require non-essential amino acids for growth (Chevallet *et al.*, 2006). This supports findings that SDHA can remain intact even though overall complex II function is disabled (Guzy *et al.*, 2008). In this situation it is proposed that the oxidation of succinate and electron transfer to the flavin group on SDHA may be normal, while subsequent transfer to the Fe-S cluster (SDHB) and to ubiquinone is impaired. This impairment has great propensity to promote ROS generation through auto-oxidation of the reduced flavin group. In a ρ0 cell line, in which glycolysis is the exclusive mechanism of ATP generation, it could be postulated that this increase in ROS generation which can cause activation of hypoxia-inducible factor 1-alpha (HIF-1α) could be beneficial via HIF-1α-induced activation of several glycolytic transporters and enzymes (Guzy *et al.*, 2008; Marin-Hernandez *et al.*, 2009).

Not all nuclear DNA-encoded ETC subunits were absent in ρ0 cells however, the ATP5A subunit was present, a logical finding as ATP hydrolysis is carried out via the functional F_1 ATPase portion of ATP synthase in ρ0 cells. Despite the absence of mtDNA-encoded F_O subunits ATP6 and 8, ADP^{3-} and Pi are still generated and are exchanged for ATP (from glycolysis) by ANTs. This exchange generates a sufficient $\Delta\psi_m$ to prevent osmotic swelling of the mitochondrial matrix in ρ0 cells (Buchet and Godinot, 1998).

During XF analysis, HepG2 ρ0 cells exhibited low OCR and high ECAR, with both rates insensitive to classical mitochondrial toxins, this reflects the expected bioenergetic state of ρ0 cells in that there is a non-functional ETC and maximal glycolysis to generate ATP. Low OCR which is insensitive to mitochondrial toxins is presumed to be due to the consumption of oxygen by cytosolic oxidases.

These methods of characterisation have provided in-depth information on the phenotype of EtBr-treated cells. However they all share a common limitation, the requirement of a negative result to confirm ρ0 cell status, thus meaning a reliance upon the sensitivity of the method used. In consideration of this, a final characterisation method was used which saw EtBr-treated cells divided into two media: standard ρ0 cell medium (containing pyruvate and uridine) and ρ0 cell selection medium (devoid of pyruvate and uridine). In this selection medium, true ρ0 cells are unable to divide and so this differentiation was used to support findings from other characterisation methods.

The same myriad of methods were employed to ensure the successful reintroduction of an individual's mtDNA into these ρ0 cells during cybrid generation. During incubation of platelets and HepG2 ρ0 cells in selection media, high rates of cell death were visible, implying a low rate of successful ρ0 cell/platelet fusion, possibly due to PEG usage which is known to have a narrow efficacious window (Gottesman *et al.*, 2010). Alternative methods of generation were considered such as electrofusion, a technique based on the reversible membrane breakdown between adjacent cells before reforming where membranes coalesce. However this is reported to induce platelet activation and consequential expulsion of platelet contents, inclusive of the mtDNA (Rems *et al.*, 2013; Torres *et al.*, 2014). Recent research however, has shown the transformation of isolated mitochondria with recipient cells via micropinocytosis-like mechanisms. This poses an alternative to the use of PEG which has a narrow therapeutic window; mitochondria could be isolated from the blood of genotyped volunteers prior to co-incubation with HepG2 ρ0 cells (Patel *et al.*, 2017; Kitani *et al.*, 2014).

The probability that many platelets and ρ0 cells would not fuse meant that these cells needed to be eliminated from culture in order to successfully generate a population of cybrids. Due to the 7-10 day lifespan of platelets *in vivo*, it was not deemed necessary to specifically eliminate unfused platelets. Contrastingly, ρ0 cells can be maintained in culture, but are auxotrophic for uridine and pyruvate (Section 1.5.2.3.3), so the absence of these two additives from culture medium enabled the elimination of ρ0 cells. The absence of these two

constituents does not cause the death of ρ0 cells however, merely the prevention of growth and division and so this is not an instantaneous selection process.

Following six weeks in selection media the remaining cells were expanded and tested for mtDNA presence (RT-PCR, fluorescence imaging), mtDNA-encoded protein expression (western blot) and mitochondrial function (XF analysis). Together, these methods indicated the presence, transcription and translation of the newly introduced mtDNA, alongside the collective function of multiple mitochondrial proteins in the cybrids. Though there were minor deviations between the results of HepG2 WT cells and cybrids, they were considered to be no greater than the variation seen between multiple populations of HepG2 WT cells.

Following the fusion of platelets and ρ0 cells there must be the expression of genes required for mtDNA transcription and translation to enable mitochondrial activity and biogenesis. This mitonuclear communication must be reprogrammed in cybrids derived from cytoplasts (enucleated cells) as a donor cell, but in the case of platelet-derived cybrids, it must be considered that mitonuclear communication has not previously existed in these anucleate cell fragments.

This intergenomic relationship also raises questions about the introduction of "new" mtDNA to a nucleus after Mendelian selection, whereby allelic selection and gene expression have been calibrated by a different mitochondrial genome (Dunham-Snary and Ballinger, 2015). Dependent on the mitochondrial haplogroup of an individual and the consequent mitochondrial function, it is feasible to suggest that the endogenous nuclear signalling may have adapted to this, whether it be by increased mitochondrial biogenesis or increased production/stimulation of cellular antioxidant systems such as Nrf2. The absence of this endogenous signalling in cybrids may result in a misrepresentation of the function of the mitochondria in an individual where endogenous nuclei are present.

Another limitation to consider is the high passage of cells upon cybrid generation and establishment of mitonuclear communication. This is due to the length of time required to generate ρ0 cells (approx. 8 weeks) and cybrids (approx. 6 weeks). Nonetheless, features of high passage cell lines include increased cell senescence which has not been observed during this work, though it may become a problem in future studies using these cybrids (Sikora *et al.*, 2016).

Despite these potential limitations, the cybrids represent a significant advance from the use of homogenous HepG2 cells in preclinical testing and many limitations can be addressed by

testing the mtDNA genotype of cybrids at the start and end of use to ensure they still represent the mtDNA genotype of the individual platelet donor.

5.5 CONCLUSION

To conclude, the work described in this chapter has demonstrated the successful generation of HepG2 ρ0 cells and HepG2 transmitochondrial cybrids for the first time. These cybrids may now be used to identify correlations between mtDNA haplogroup, mitochondrial function and susceptibility to iDILI via mitochondrial dysfunction; utilities which will be explored in the final chapter of this thesis.

Chapter 6

Assessment of the Impact of Mitochondrial DNA Variation upon Mitochondrial (Dys)Function Using HepG2 Transmitochondrial Cybrids

CONTENTS

6.1 INTRODUCTION

Unlike the use of platelets alone, HepG2 transmitochondrial cybrids allow the consequences of mtDNA variation upon mitochondrial (dys)function to be tested in a cell line which has longevity in culture (enabling experimental repeats) and consideration of mitochondrial (dys)function in a situation of mitonuclear communication. In addition, platelets have been found to exhibit significant differences in susceptibility to drug-induced mitochondrial dysfunction compared to HepG2 cells, with the direction of the difference dependent on whether dysfunction is induced by uncoupling or respiratory complex inhibition (Section 4.4). The development of a method to successfully generate HepG2 transmitochondrial cybrids (Chapter 5) has enabled the following hypothesis to be tested in an *in vitro* setting: differential mtDNA haplogroups confer variation in basal mitochondrial function and susceptibility to drug-induced mitochondrial dysfunction.

The aim of the research described in this chapter was therefore to generate ten populations of HepG2 transmitochondrial cybrids, five using platelets derived from volunteers of haplogroup H and five from haplogroup J. This was followed by experiments to identify any differences in basal mitochondrial function and/or susceptibility to compound-induced dysfunction. Haplogroup H was chosen as it is the most common haplogroup in the UK (Eupedia, 2016) (Table 6.1). Haplogroup J on the other hand is less common but is characterised by SNPs including non-synonymous mutations in the region encoding NADH dehydrogenase subunit 3 and 5 (complex I subunit ND3, ND5) (Van Oven and Kayser, 2009; Eupedia, 2016) (Table 6.1). A secondary hypothesis was therefore formulated: mutations in these regions in haplogroup J cybrids confer increased susceptibility to complex I inhibition induced by flutamide and 2-hydroxyflutamide.

The cybrids generated were then subject to testing using methods optimised in Section 2.2, namely ATP quantification in acutely galactose-conditioned cells (Section 2.2.3) and XF analysis using mitochondrial stress tests (Section 2.2.4.3) and complex assays (Section 2.2.4.4). This enabled the assessment of overall mitochondrial respiratory function and the activity of specific respiratory complexes (Ball *et al.*, 2016).

The use of healthy volunteers (i.e. no phenotype of mitochondrial dysfunction) for platelet donation to generate cybrids meant it was possible that any differences observed between haplogroups, particularly at a basal level, would be marginal (Chinnery and Gomez-Duran, 2018). Therefore high throughput imaging was used as an additional tool of mitochondrial health assessment. Changes in mitochondrial morphology and dynamics can be an early

indicator of stress and advances in high throughput imaging and associated machine-learning have enabled the fast and reliable quantification of such changes (Section 1.2.5). Collectively, these techniques were used to determine basal mitochondrial function as well as differences in responses to flutamide, 2-hydroxyflutamide, bicalutamide, tolcapone and entacapone (mechanisms of mitochondrial dysfunction investigated in Chapter 2).

Table 6.1. SNPs and associated proteins of the four most common haplogroups in the UK.

Haplogroup	Frequency in cohort (%)	Non-synonymous (NS) SNPs	Gene(s) affected by NS SNP(s)
H	39.1	_	N/A
J	12.0	A10398G (Thr – Ala) G13708A (Ala – Thr)	MT-ND3 (complex I) MT-ND5 (complex I)
T	7.60	A4917G (Asn – Asp)	MT-ND2 (complex I)
U	16.4	_	N/A

Abbreviations: SNP, single nucleotide polymorphism; NS, non-synonymous; N/A, not applicable.

6.2 MATERIALS AND METHODS

6.2.1 Materials

All forms of DMEM were purchased from Life Technologies (Paisley, UK). HepG2 WT cells were purchased from European Collection of Cell Cultures (ECACC, Salisbury, UK). All XF assay consumables were purchased from Agilent Technologies (CA, USA). All Operetta consumables were purchased from PerkinElmer (MA, USA). All other reagents and chemicals were purchased from Sigma Aldrich (Dorset, UK) unless stated otherwise.

6.2.2 Cohort

Healthy volunteers (n=10) of mitochondrial haplogroups H and J were recruited from the cohort described in Section 3.2.2. Subhaplogroups and SNPs present in DNA isolated from each individual are described in Table 6.2. This project was approved by the North West of England Research Ethics Committee and all participants gave written informed consent. Volunteer confidentiality was maintained by double coding DNA samples and by restricting access to participant's personal data to trained clinical personnel.

Table 6.2. Mitochondrial DNA variation of 10 healthy volunteers whose platelets were used to generate cybrids.

Donor number	Macrohaplogroup	Subhaplogroup	SNPs characteristic of assigned haplogroup	Additional SNPs
2	H	H1c3	257G 263G 477C 750G 1438G 3010A 4769G 8473C 8860G 15326G	195C 12966T 16519C

3	H	H1bb	152C 263G 750G 1438G 3010A 4769G 8860G 11864C 15326G	16519C
4	H	H1a1	73G 263G 750G 1438G 3010A 4769G 6365C 8860G 15326G 16162G	152C 3483A 16360T 16519C
5	H	H1c	263G 477C 750G 1438G 3010A 4769G 8860G 15326G	10646A 16519C
27	H	H2a1e1a1	263G 575T 750G 751G 951A 8860G 15326G 16124C 16148T 16166G 16354T	
6	J	J2b1g	73G 150T 152C 263G 489C 750G 1438G 4769G 5633T 7028T 8860G 9872G 10172A 10398G 11251G 11719A 12612G 13708A 14766T 15257A 15326G 15452A 15812A 16069T 16126C 16193T	2789T 13821T
7	J	J1c+16261	73G 185A 228A 263G 295T 462T 489C 750G 1438G 3010A 4216C 4769G 7028T 8860G 10398G 11251G 11719A 12612G 13708A 14766T 14798C 15326G 15452A 16069T 16126C 16261T	4113A 6554T 10915C 16316G
9	J	J1c1c	185A 228A 462T 482C 489C 750G 1438G 3010A 3394C 4216C 4769G 7028T 8860G 10398G 11251G 11719A 13708A 14766T 14798C 15326G 15452A 16069T 16126C 16145A	188G 13943T 14552G
20	J	J1c2h	185A 188G 222T 228A 263G 295T 462T 489C 750G 1438G 3010A 4216C 4769G 7028T 8860G 10398G 11251G 11719A 12612G 13708A 14766T 14798C 15326G 15452A 16069T 16126C	16189C 16519C 16527T
30	J	J1c1e	185A 228A 263G 295T 462T 482C 489C 750G 1438G 3010A 3394C 4216C 4769G 7028T 8860G 10398G 10454C 11251G 11719A 12612G 13708A 14766T 14798C 15326G 15452A 16069T 16126C 16368C	13889A

Donor numbers align with those stated in Chapter 4 (Table 4.1). Additional SNPs refers to SNPs that were present in the sample but were not characteristic of the assigned haplogroup. Abbreviations: SNP, single nucleotide polymorphism.

6.2.3 Cybrid generation

HepG2 transmitochondrial cybrids were generated as described in Section 5.2.4. A summary of the optimised cybrid generation process is depicted in Figure 6.1.

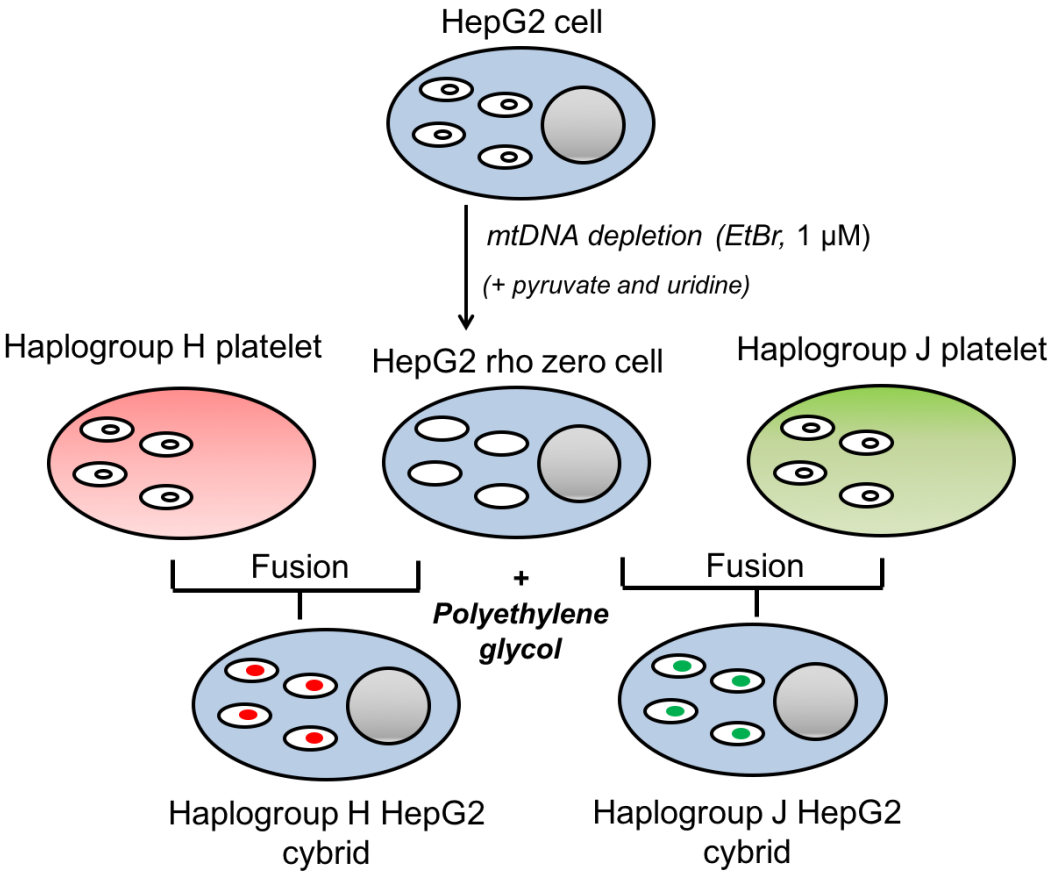

Figure 6.1. Schematic representation of optimised HepG2 transmitochondrial cybrid generation (Chapter 5). HepG2 rho zero cells were generated by HepG2 cell exposure to 1 µM ethidium bromide for approximately eight weeks. HepG2 rho zero cells were then fused with platelets from healthy volunteers of haplogroups H and J using polyethylene glycol. Successfully generated cybrids were selected for by growth in media devoid of pyruvate and uridine (unfused rho zero cells are unable to survive in this media). The cybrids (haplogroup H and J) contain the mitochondrial DNA of the volunteer who donated platelets but have the same HepG2 nuclear DNA background.

6.2.4 Dual assessment of mitochondrial function (ATP content) alongside cytotoxicity (lactate dehydrogenase release)

Following a two hour incubation of the cybrids in galactose media with each of the five test compounds (flutamide, 2-hydroxyflutamide, bicalutamide, tolcapone, entacapone, 0.05 - 500 µM), cell supernatant was extracted and cells were lysed using somatic ATP releasing agent (50 µL) before simultaneous assessment of ATP content, cytotoxicity and protein content as described in Section 2.2.3.

6.2.5 Extracellular flux analysis

HepG2 cybrids were collected by trypsinisation and seeded on a collagen-coated XFe96 cell culture microplate (25 000 cells/100 µL medium/well) and incubated (37 °C, 5 % CO_2) overnight. Following this, mitochondrial stress tests and complex assays were performed according to methods described in Sections 2.2.4.3 and 2.2.4.4 respectively.

6.2.6 Mitochondrial dynamics assessment using high throughput imaging

6.2.6.1 High throughput imaging technology

Automated microscope-based screening (e.g. Operetta CLS (PerkinElmer)) enables the rapid measurement of mitochondrial dynamics under a multitude of conditions when combined with suitable cell permeable dyes. There are multiple dyes available for monitoring mitochondrial dynamics, not all of which depend on $\Delta\psi_m$, enabling the detection of mitochondria with various $\Delta\psi_m$.

In the case of the Operetta platform, high throughput screening is enabled via a fast switching eight position excitation wheel with a four position objective turret and a fast switching 8XLED core. This platform can also host 96- and 384-well plates to enable simultaneous assessment of multiple conditions/cell types.

Confocal imaging on this platform uses a spinning pinhole disk which reduces background, whilst pulses of light reduce photo bleaching, enabling high quality imaging of the same sample at multiple time points. Imaging of the same live sample at multiple time points is also possible due to temperature and CO_2 controls in the sample chamber. Importantly, this enables the effect of treatment cessation or increased treatment times to be assessed. The use of a water objective during imaging can also be used to provide a clearer image due to the similar refractive index of water and the cytosol. Following screening, analysis of mitochondrial and cellular health can be rapidly quantified using PhenoLOGIC™ machine learning (Buchser *et al.*, 2014; Zanella *et al.*, 2010).

6.2.6.2 Cybrid imaging

HepG2 cybrids were collected by trypsinisation and seeded on a flat, clear-bottomed 96-well cell carrier plate in DMEM high-glucose media (15 000 cells/100 µL/well) and incubated (24 h, 37 °C, 5 % CO_2). Glucose media was then removed and cells were washed three times with galactose media before a final addition of galactose media (50 µL) and incubation (2 h, 37 °C, 5 % CO_2). Test compounds were prepared in galactose media to generate final concentrations of 0, 30, 60, 125 and 250 µM when added (50 µl) at the end of the incubation period. Cybrids were treated according to conditions 1, 2, 3 or 4 (described in Table 6.3) and

stained with MitoTracker™ Green (20 min, 129.1 nM) and Hoechst (7 min, 4.05 µM) (LifeTechnologies, Paisley, UK). Care was taken to avoid exposure of cells to light during dye incubation. Following dye incubation, media (containing dyes) was removed and cells were washed twice with PBS (250 µL) before addition of FluoroBrite™ DMEM (100 µL). Imaging was then performed using confocal 63x Water Immersion Objective: binning, 2; numerical aperture, 1.15; working distance, 0.6 mm (field of view: approx. 205 µm x 205 µm).

Table 6.3. Details of test compound incubations performed on HepG2 transmitochondrial cybrids prior to high throughput imaging. E.g. condition 1 consisted of 2 h compound treatment then imaging followed by 2 h treatment-free then imaging.

Condition	Incubation 1 (h)	Incubation 2 (h)	Imaging times (h)
1	2	None	2, 4
2	24	None	24, 26
3	2	2	2, 4
4	24	2	24, 26

6.2.6.3 Image analysis

Images were analysed using Harmony software (1.0) with PhenoLOGIC™ (PerkinElmer). The following analysis sequence was used, directions are defined with [ ] and adjustable parameters in italics:

1. [Input Image] – *Individual planes, FFC Basic*
2. [Find Nuclei] – Channel: *Hoechst 33342; Method: C; Output Population: Nuclei*
3. [Calculate Morphology Properties] – Population: Nuclei, Region: Cell; Method: Standard.
4. [Find Cytoplasm] – Channel: Digital Phase Contrast *Method: A*
5. [Find Spots (2)] – Channel: MitoTracker™ Green Method: B; ROI: Nuclei, Cytoplasm, Output Population; Mitochondria
6. [Find Texture Regions] – Channel: MitoTracker™ Green: Method; Linear classifier training. Output; Population 1: Fission state Population 2: Fusion (representative images shown in Figure 6.6)

6.2.7 Statistical analysis plan

A data analysis plan was formulated based on the specific hypotheses below, all analyses were performed blinded.

1) Haplogroup H and J cybrids have differential mitochondrial function.
2) Haplogroup H and J cybrids have differential susceptibility to drug-induced mitochondrial dysfunction.

To address each question, cybrids were generated using material derived from five haplogroup H volunteers and five haplogroup J volunteers. For both 1) and 2) results from mitochondrial stress tests and complex assays (basal and drug-treated) were to be assessed for a statistically significant difference between the haplogroups. The following parameters were chosen for comparison based on findings from Chapter 2: basal, maximum and ATP-linked respiration, spare respiratory capacity, proton leak and complex I-IV activity (maximal respiration). As each cybrid acted as its own control, maximal and basal respiration were assessed as raw values as oppose to percentage of control. Mitochondrial dynamics were also measured via high throughput imaging. EC_{50} data were determined by nonlinear regression analysis using GraphPad Prism 7.0 following mean centering using SPSS v24 (to account for cases where the control value was 0 for the parameter of interest). Normality was assessed using a Shapiro-Wilk test. Statistical significance was determined by a one-way ANOVA for parametric data followed by a Dunnett's post-hoc test using StatsDirect 2.7.9. Significance was determined from a $p\ value < 0.05$.

6.3 RESULTS

6.3.1 Basal mitochondrial function

Assessment of basal mitochondrial function using a mitochondrial stress test showed no significant difference between haplogroup H and J cybrids in multiple parameters of mitochondrial ETC function (Figure 6.2). Haplogroup J cybrids displayed a significantly increased basal proton leak, however only by a small margin (0.41 pmol O_2/min/μg protein) (Figure 6.2A). Contrastingly, assessment of the activity of individual respiratory complexes revealed a higher activity in haplogroup J cybrids which reached significance in complex I and II activity (Figure 6.3). High throughput imaging to assess the mitochondrial dynamics of cybrids from each haplogroup at basal state revealed no significant difference in the proportion of mitochondria in a fission state between haplogroups H and J (Figure 6.4). Basal mitochondrial function data from each cybrid population is presented in Appendix 4 (4A: data points categorised as either genotypes or as samples which did or did not contain SNPs (16192T, 16189C, 295T) associated with increased mtDNA copy number, 4B: data points individually labelled for ten cybrids generated using material from donors 1-30) (Ebner *et al.*, 2011; Suissa *et al.*, 2009).

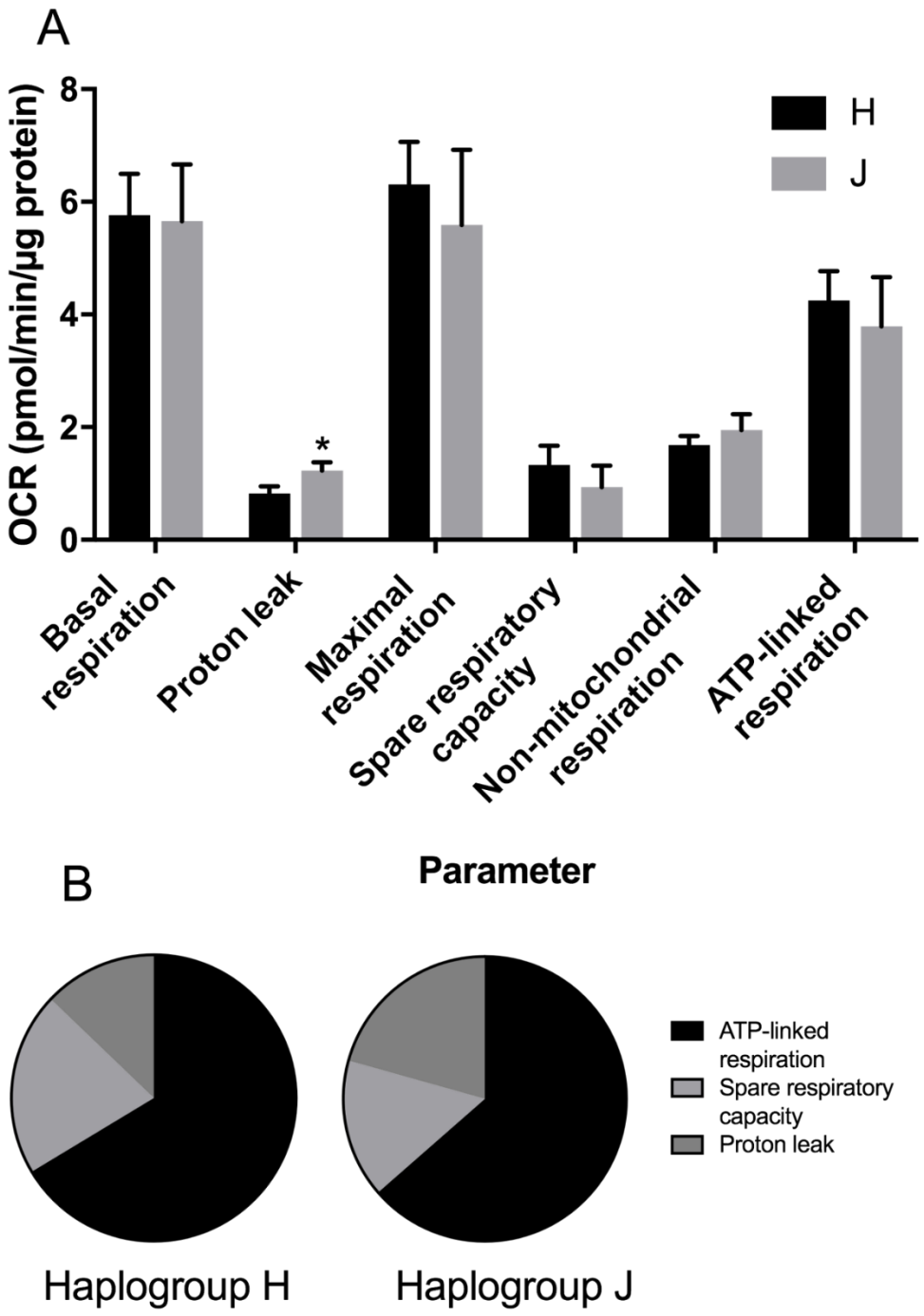

Figure 6.2. Basal parameters of mitochondrial function. Untreated haplogroup H and J cybrids were assessed using extracellular flux analysis and a mitochondrial stress test to determine parameters: basal respiration, maximal respiration, ATP-linked respiration, spare respiratory capacity and proton leak. A: raw values B: values as a proportion of maximal respiration. Statistical significance between haplogroup H and J cybrids: * $p < 0.05$, ** $p < 0.01$, *** $p < 0.001$. Data are presented as mean + SEM of n = 5 experiments.

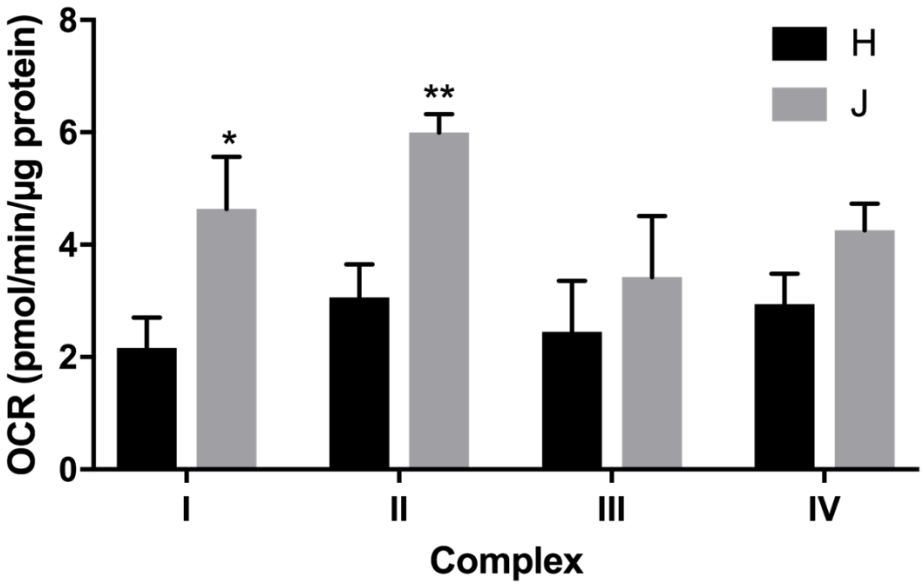

Figure 6.3. Basal respiratory complex activity. Untreated haplogroup H and J cybrids were assessed using extracellular flux analysis and respiration was stimulated by the supply of respiratory complex-specific substrates. Complex I-IV activity was defined as complex I-IV mediated maximal respiration. Statistical significance between haplogroup H and J cybrids: * $p < 0.05$, ** $p < 0.01$, *** $p < 0.001$. Data are presented as mean + SEM of n = 5 experiments.

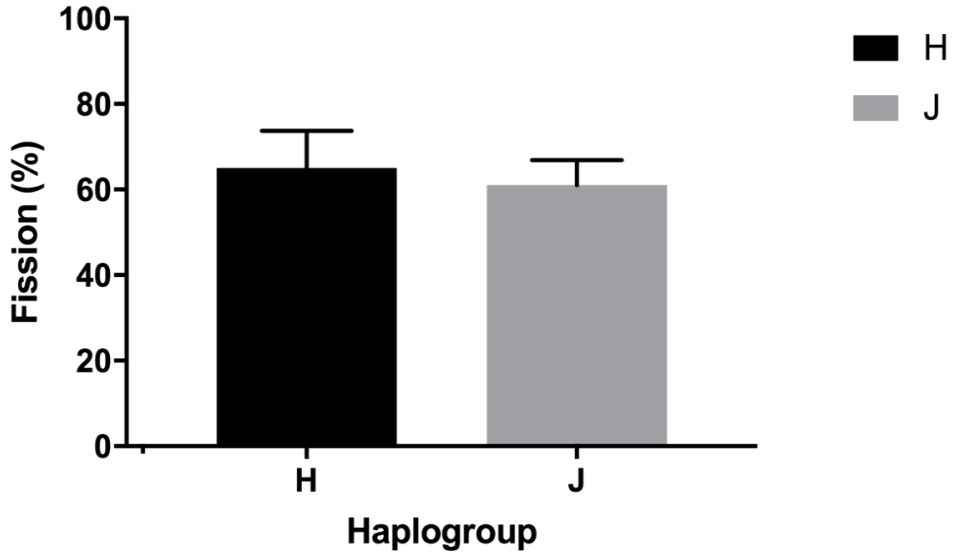

Figure 6.4. Basal mitochondrial dynamics. Untreated haplogroup H and J cybrids were assessed using the Operetta CLS system and PhenoLOGIC™ machine learning to detect mitochondria in a fused or fissioned state. Statistical significance between haplogroup H and J cybrids: * $p < 0.05$, ** $p < 0.01$, *** $p < 0.001$. Data are presented as mean + SEM of n = 5 experiments.

6.3.2 The effect of flutamide upon haplogroup H and J transmitochondrial cybrids

Acute treatment of cybrids with flutamide did not induce significant LDH release at any of the concentrations used. A substantial depletion in ATP was evident but was not significantly different between haplogroup H and J transmitochondrial cybrids (Figure 6.5A). Similarly, there was no significant difference in parameters of mitochondrial respiration between the two cybrid haplogroups when treated with flutamide, though haplogroup J cybrids did exhibit a higher proton leak at all concentrations (Figure 6.5B-F).

Assessment of complex I-IV activity in cybrids revealed haplogroup J cybrids had greater respiratory complex I-IV activity, with the difference reaching significance in complexes I and II, where haplogroup J cybrids had up to two times greater activity (Figure 6.5G, H). Changes in mitochondrial dynamics upon flutamide treatment (Figure 6.6) were not consistently different between the two haplogroups, however haplogroup J did show significantly higher levels of fission following treatment with 63 μM flutamide for 24 h (Figure 6.7D). Notably, when treated with mid-range concentrations of flutamide, haplogroup H cybrids showed a reduction in fission state mitochondria (Figure 6.7B, D). This was not the case with haplogroup J; fission either did not change or increased in a dose-dependent manner.

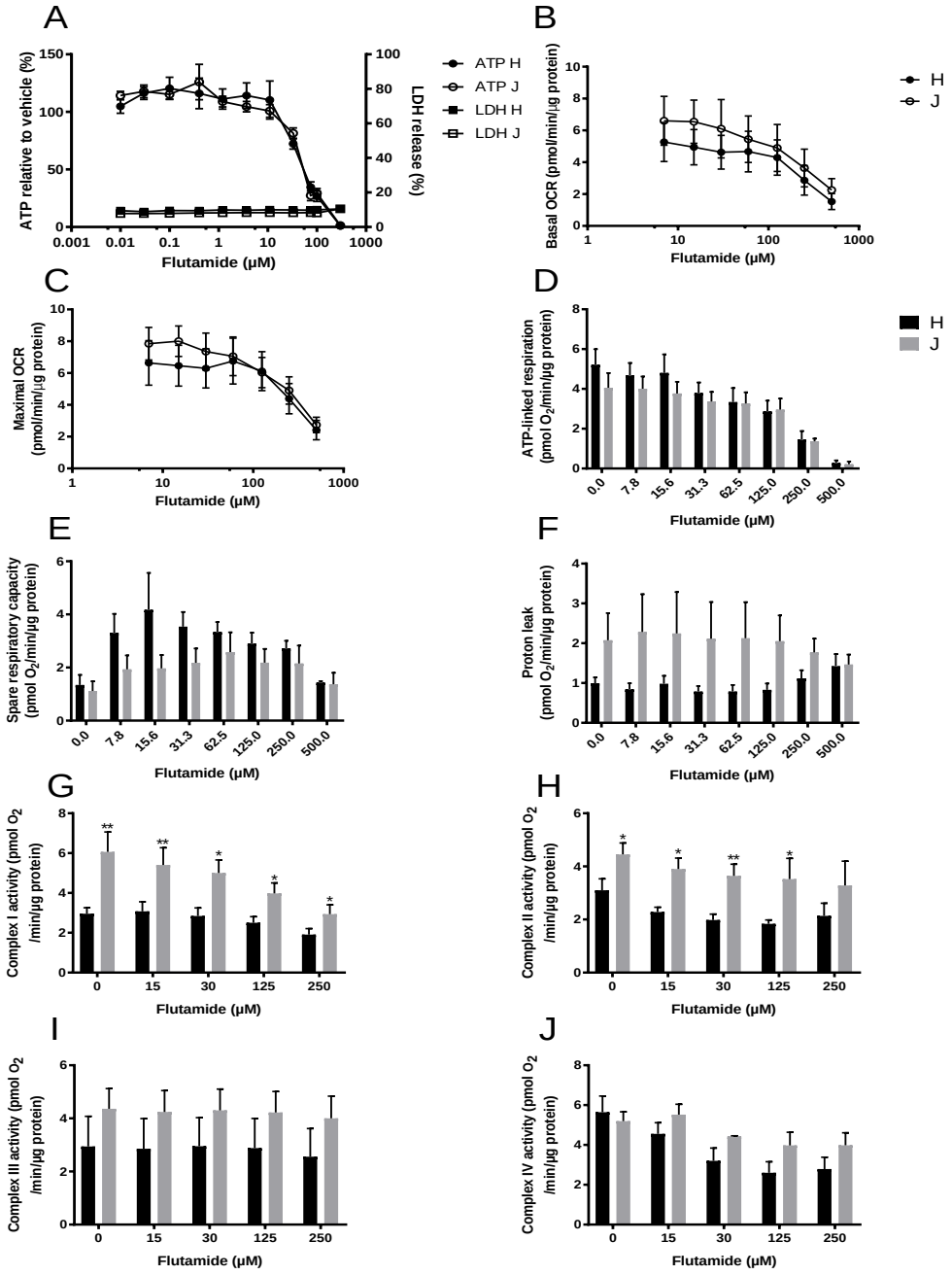

Figure 6.5. The effect of flutamide upon ATP levels, mitochondrial respiratory function and respiratory complex activity in haplogroup H and J HepG2 transmitochondrial cybrids. A: cybrids were treated (2 h) with serial concentrations of flutamide up to 300 μM in glucose or galactose media. ATP values are expressed as a percentage of those of the vehicle control. Lactate dehydrogenase (LDH) release is expressed as extracellular LDH as a % of total LDH. B-F: extracellular flux (XF) analysis-detected changes in basal and maximal respiration, ATP-linked respiration, spare respiratory capacity and proton leak induced by flutamide (up to 500 μM). G-J: Permeabilised cybrids were acutely treated with flutamide (10-250 μM) before a mitochondrial stress test using XF analysis. Complex I, II, III or IV activity was defined as maximal respiration. Statistical significance between haplogroup H and J cybrids: * $p < 0.05$, ** $p < 0.01$, *** $p < 0.001$. Data are presented as mean ± SEM of n = 5 experiments.

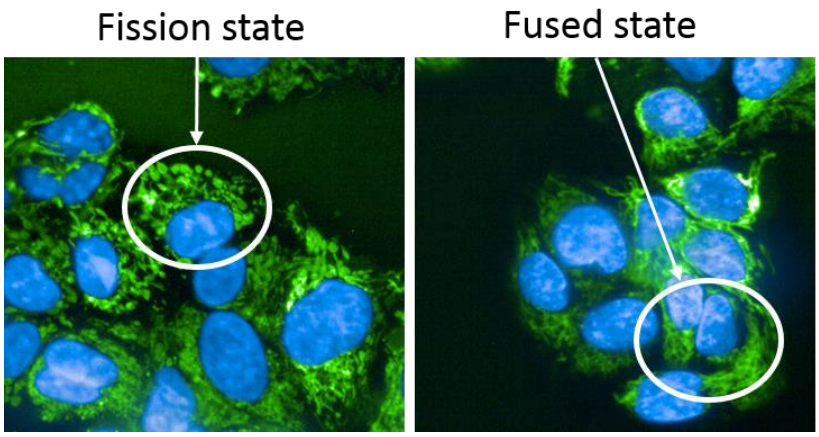

Figure 6.6. Representative images of mitochondria labelled as a fused or fissioned state using PhenoLOGIC™ machine learning.

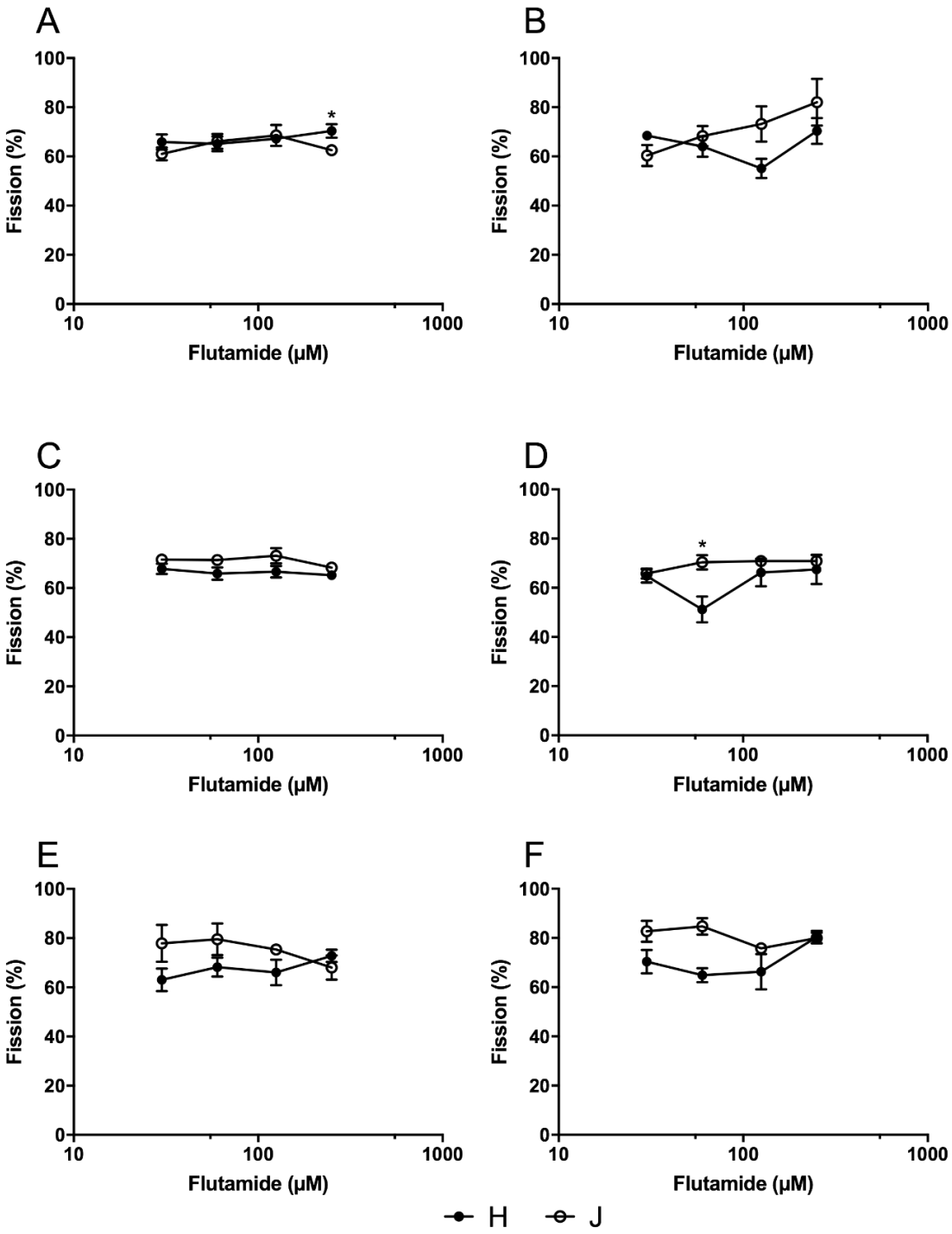

Figure 6.7. Mitochondrial fission in flutamide-treated haplogroup H and J cybrids. Haplogroup H and J cybrids were treated with flutamide for one of the following time points A: 2 h B: 2 h + 2 h compound-free C: 4 h D: 24 h E: 24 h + 2 h compound-free F: 26 h before high throughput imaging. Mitochondria were detected using MitoTracker™ Green and imaging was performed using the Operetta CLS system followed by PhenoLOGIC™ machine learning to detect mitochondria in a fused or fissioned state. Statistical significance compared to other haplogroup: * $p < 0.05$, ** $p < 0.01$, *** $p < 0.001$, 2 h compound-free vs no compound-free incubation: $^{+}p<0.05$, $^{++}p<0.01$, $^{+++}p<0.001$. Data are presented as mean ± SEM of n = 5 experiments.

6.3.3 The effect of 2-hydroxyflutamide upon haplogroup H and J transmitochondrial cybrids

There was no significant difference between cellular ATP depletion in response to 2-hydroxyflutamide in haplogroup H or J cybrids but both displayed a significant reduction in ATP in the absence of significant LDH release (Figure 6.8A). Parameters assessed during mitochondrial stress tests also did not significantly differ between the two haplogroups (Figure 6.8B-F).

Haplogroup J cybrids had higher complex I-IV activity upon 2-hydroxyflutamide treatment, which reached significance in complex I and complex II activity (Figure 6.8G, H). Levels of fission in the two populations of cybrids remained relatively similar, though there was a clearer dose-dependent increase in fission in haplogroup J cybrids following 2 h treatment with 2-hydroxyflutamide (Figure 6.9B).

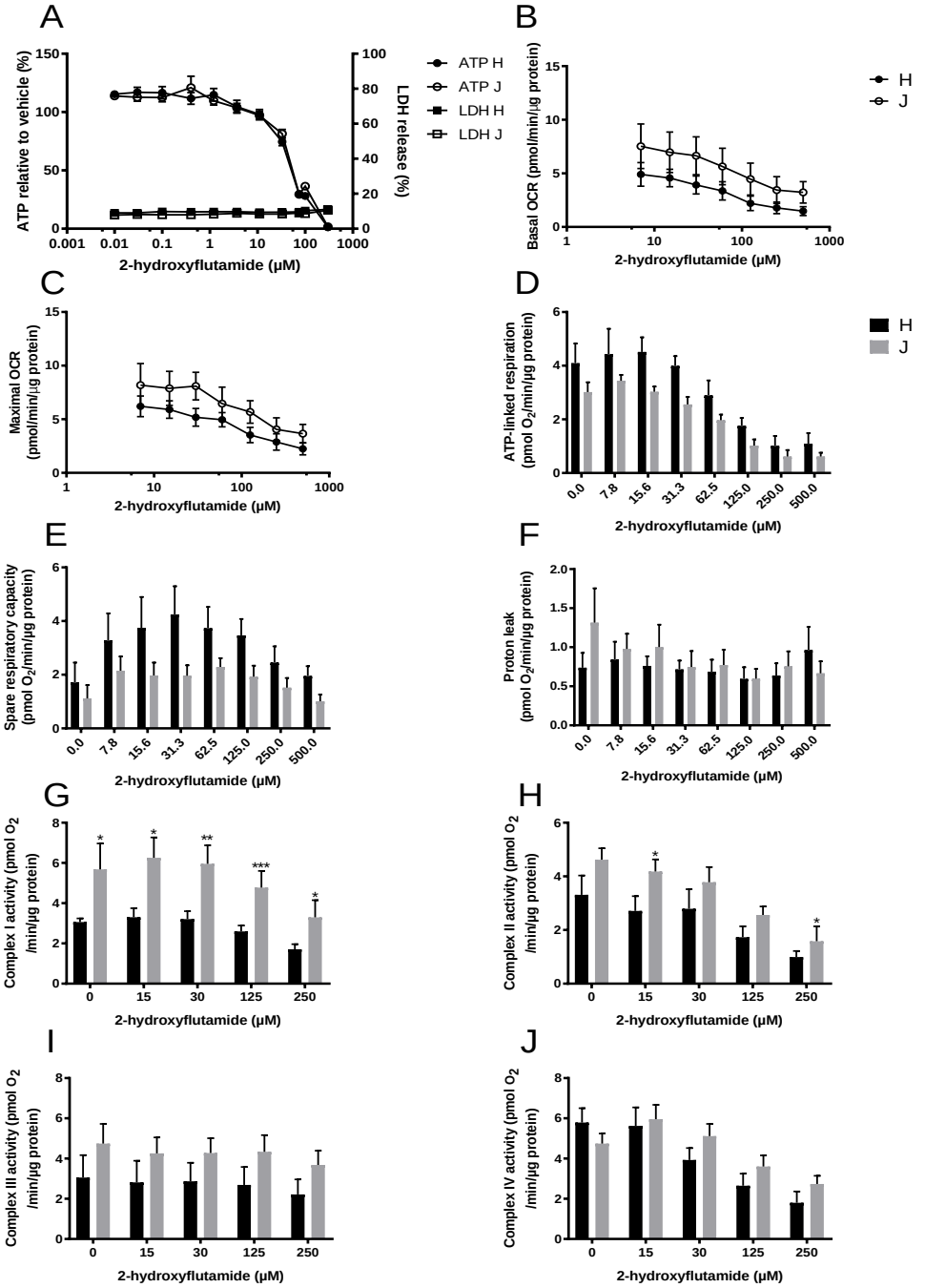

Figure 6.8. The effect of 2-hydroxyflutamide upon ATP levels, mitochondrial respiratory function and respiratory complex activity in haplogroup H and J HepG2 transmitochondrial cybrids. A: cybrids were treated (2 h) with serial concentrations of 2-hydroxyflutamide up to 300 μM in galactose media. ATP values are expressed as a percentage of those of the vehicle control. Lactate dehydrogenase (LDH) release is expressed as extracellular LDH as a % of total LDH. B-F: extracellular flux (XF) analysis-detected changes in basal and maximal respiration, ATP-linked respiration, spare respiratory capacity and proton leak by 2-hydroxyflutamide (up to 500 μM). G-J: Permeabilised cybrids were acutely treated with 2-hydroxyflutamide (10-250 μM) before a mitochondrial stress test using XF analysis. Complex I, II, III or IV activity was defined as maximal respiration. Statistical significance between haplogroup H and J cybrids: * $p < 0.05$, ** $p < 0.01$, *** $p < 0.001$. Data are presented as mean ± SEM of n = 5 experiments.

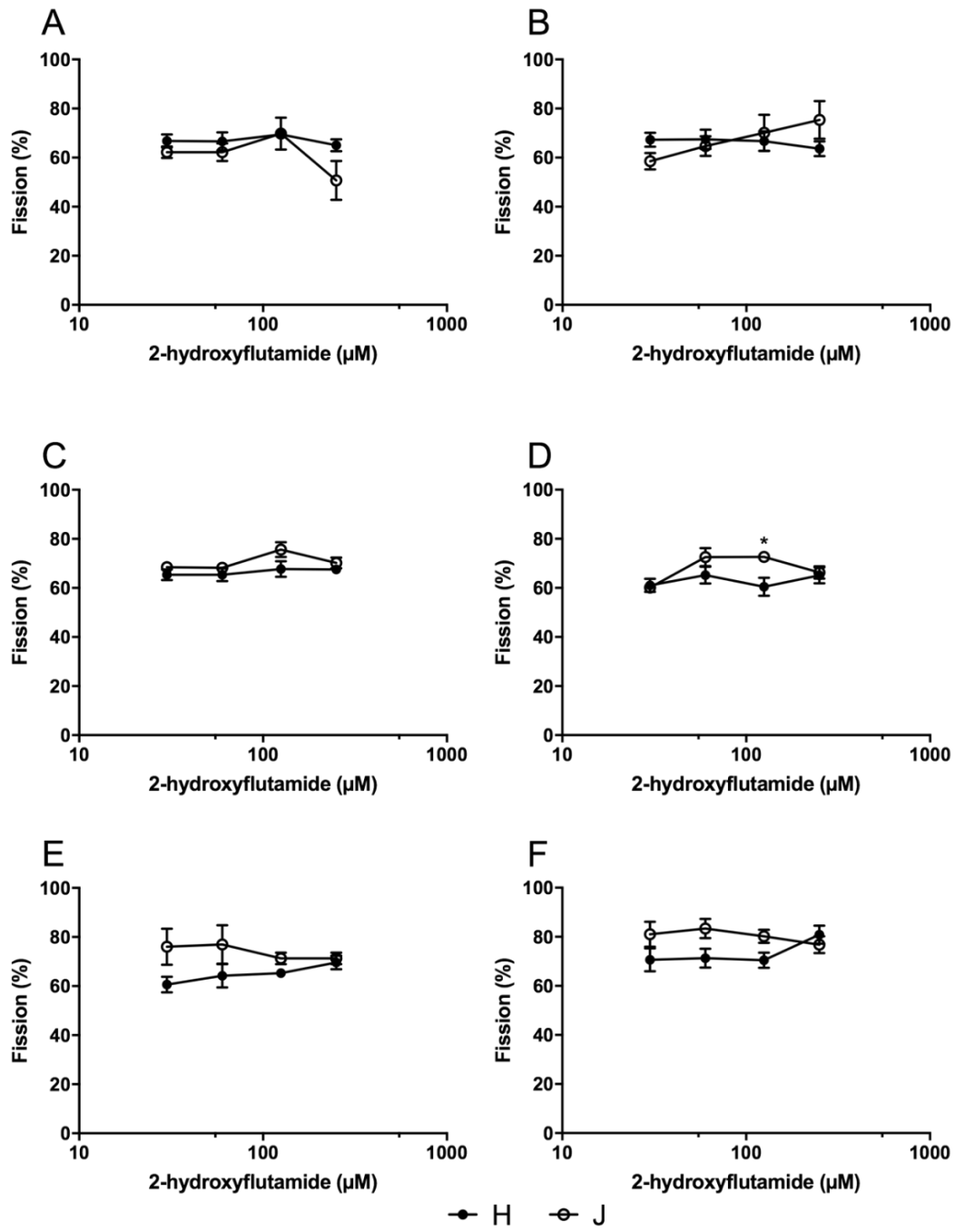

Figure 6.9. Mitochondrial fission in 2-hydroxyflutamide-treated haplogroup H and J cybrids. Haplogroup H and J cybrids were treated with 2-hydroxyflutamide for one of the following time points A: 2 h B: 2 h + 2 h compound-free C: 4 h D: 24 h E: 24 h + 2 h compound-free F: 26 h before high throughput imaging. Mitochondria were detected using MitoTracker™ Green and imaging was performed using the Operetta CLS system followed by PhenoLOGIC™ machine learning to detect mitochondria in a fused or fissioned state. Statistical significance compared to other haplogroup: * $p < 0.05$, ** $p < 0.01$, *** $p < 0.001$, 2 h compound-free vs no compound-free incubation: $^{+}p < 0.05$, $^{++}p < 0.01$, $^{+++}p < 0.001$. Data are presented as mean ± SEM of n = 5 experiments.

6.3.4 The effect of bicalutamide upon haplogroup H and J transmitochondrial cybrids

Bicalutamide-treated cybrids of each haplogroup exhibited a similar decline in ATP content until the highest concentration used (300 µM), when haplogroup J cybrids had significantly less ATP (Figure 6.10A). As with flutamide and 2-hydroxyflutamide treatment, the decline in ATP was in the absence of significant LDH release. No significant differences were evident between the two cybrid groups in parameters of mitochondrial function using XF analysis, however as was the case with flutamide, haplogroup J exhibited higher proton leak in both control and treated cybrids (Figure 6.10B-F). Mitochondrial fission levels in the two cybrid populations did not change substantially upon bicalutamide-treatment, however following 26 h treatment, haplogroup J cybrids had increased fission compared to haplogroup H at all concentrations used (Figure 6.11F).

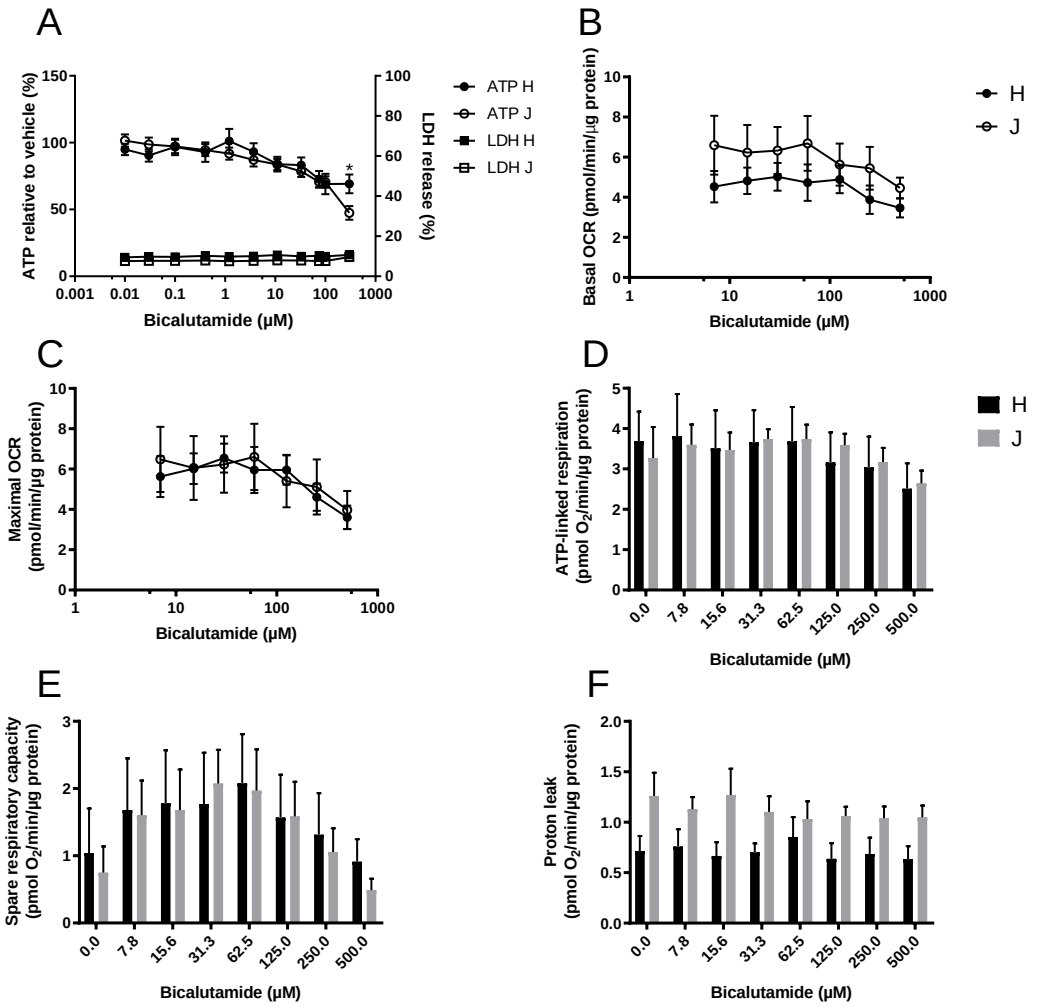

Figure 6.10. The effect of bicalutamide upon ATP levels and mitochondrial respiratory function in haplogroup H and J HepG2 transmitochondrial cybrids. A: cybrids were treated (2 h) with serial concentrations of bicalutamide up to 300 µM in galactose media. ATP values are expressed as a percentage of those of the vehicle control. Lactate dehydrogenase (LDH) release is expressed as extracellular LDH as a % of total LDH. B-F: extracellular flux analysis-detected changes in basal and maximal respiration, ATP-linked respiration, spare respiratory capacity and proton leak induced by bicalutamide (up to 500 µM). Statistical significance between haplogroup H and J cybrids: * $p < 0.05$, ** $p < 0.01$, *** $p < 0.001$. Data are presented as mean ± SEM of n = 5 experiments.

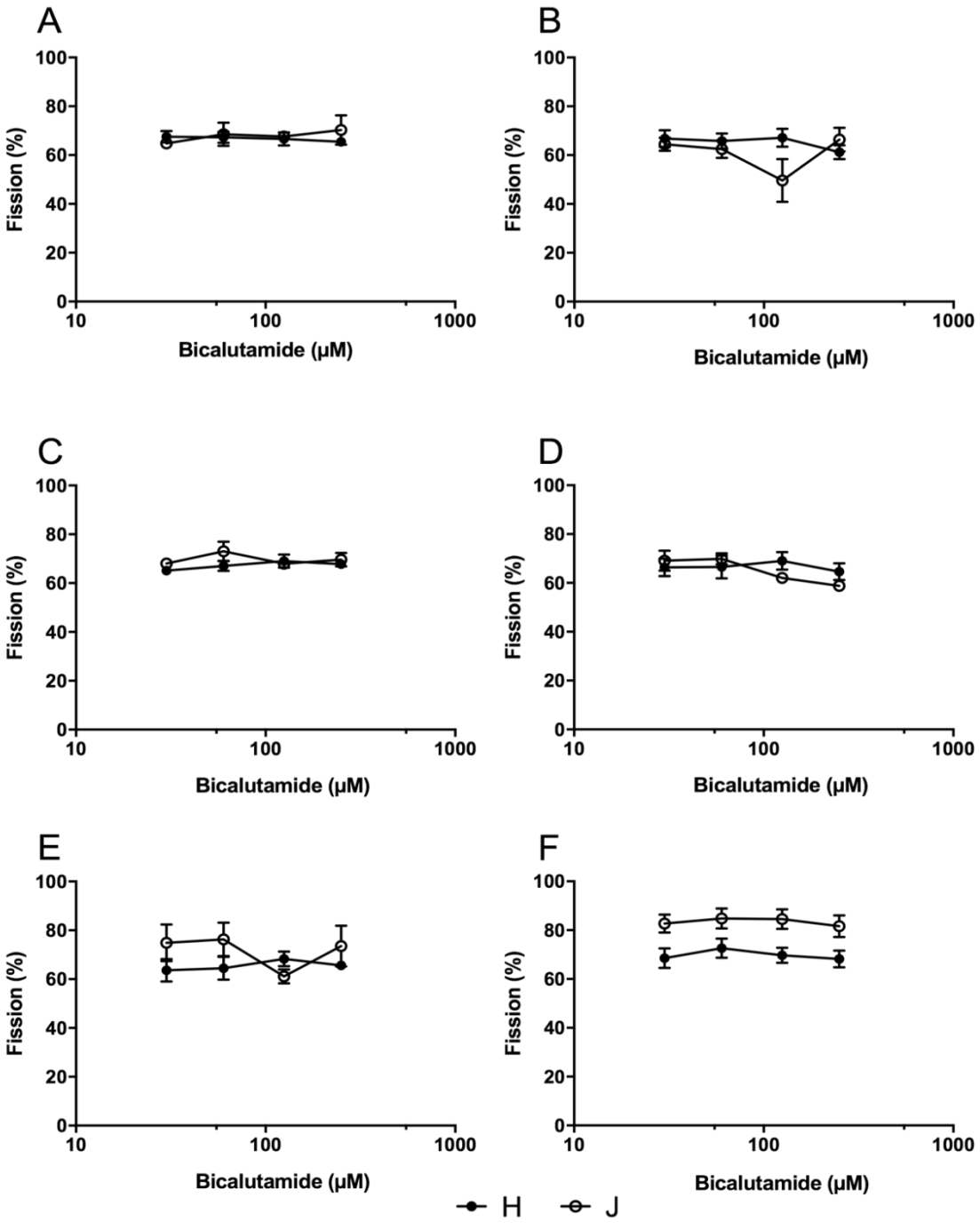

Figure 6.11. Mitochondrial fission in bicalutamide-treated haplogroup H and J transmitochondrial cybrids. Haplogroup H and J cybrids were treated with bicalutamide for one of the following time points A: 2 h B: 2 h + 2 h compound-free C: 4 h D: 24 h E: 24 h + 2 h compound-free F: 26 h before high throughput imaging. Mitochondria were detected using MitoTracker™ Green and imaging was performed using the Operetta CLS system followed by PhenoLOGIC™ machine learning to detect mitochondria in a fused or fissioned state. Data are presented as mean ± SEM of n=5 experiments. Statistical significance compared to other haplogroup: * $p < 0.05$, ** $p < 0.01$, *** $p < 0.001$, 2 h compound-free vs no compound-free incubation: $^{+}p<0.05$, $^{++}p<0.01$, $^{+++}p<0.001$. Data are presented as mean ± SEM of n = 5 experiments.

6.3.5 The effect of tolcapone upon haplogroup H and J transmitochondrial cybrids

ATP levels following treatment with tolcapone were significantly different between the two haplogroups; haplogroup H cybrids exhibited an increase in cellular ATP level at lower tolcapone concentrations before a decline at concentrations of 75 µM and above (Figure 6.12A). At the highest concentrations of tolcapone there was no significant difference between the two haplogroups. XF analysis showed a significantly higher basal respiration in haplogroup J compared to haplogroup H cybrids when treated with 15 µM tolcapone (Figure 6.12B). At higher concentrations of tolcapone and for remaining parameters assessed during XF analysis there was no significant difference between the two haplogroups (Figure 6.12C-F).

Mitochondrial fission in haplogroup J cybrids was significantly more than in haplogroup H cybrids after 2 h treatment (Figure 6.13A-C), however after 24 h treatment there was no difference between the two populations (Figure 6.13D-F). In both haplogroups, fission increased more than with anti-androgen compounds.

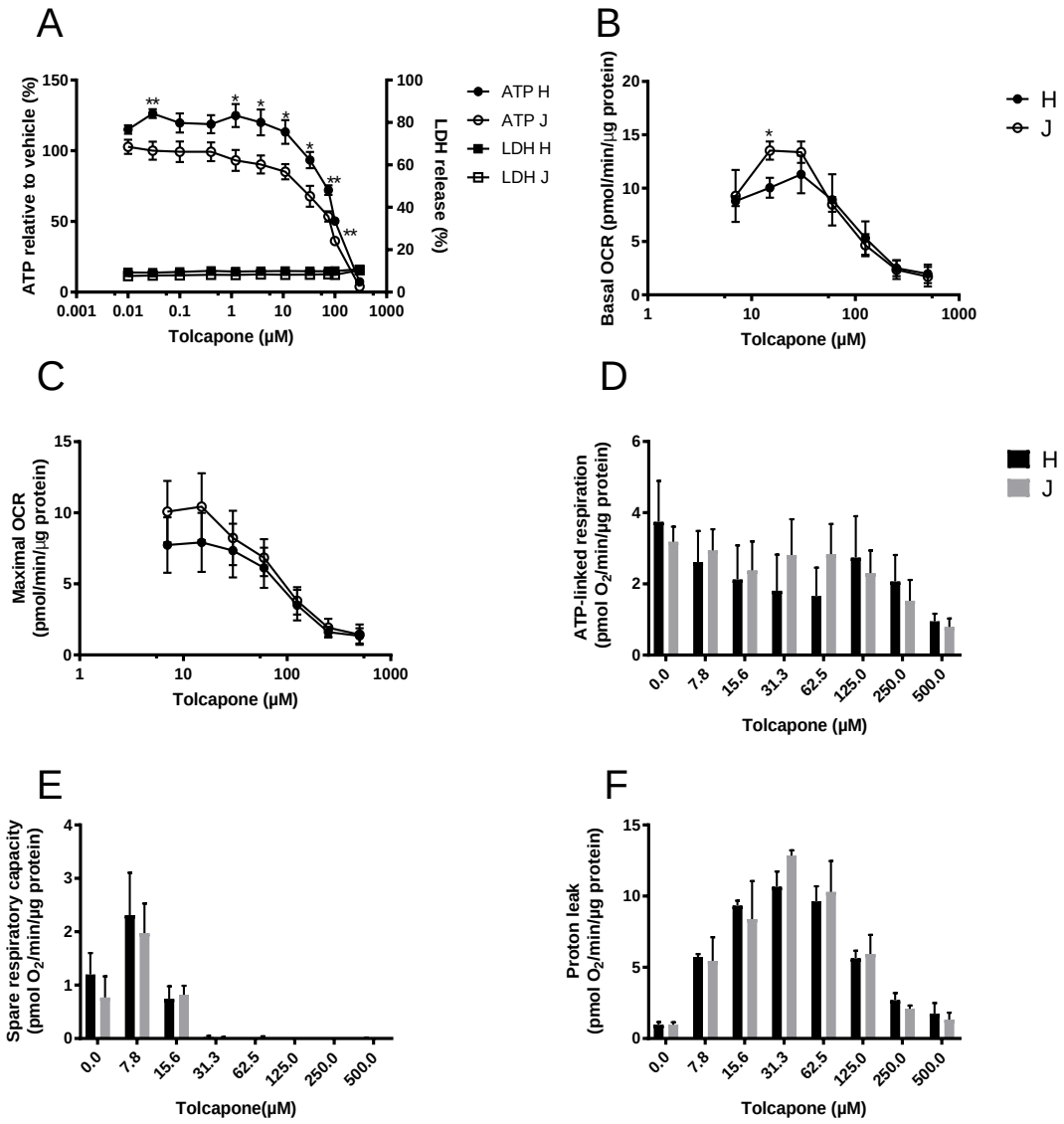

Figure 6.12. The effect of tolcapone upon ATP levels and mitochondrial respiratory function in haplogroup H and J HepG2 transmitochondrial cybrids. A: cybrids were treated (2 h) with serial concentrations of tolcapone up to 300 μM in galactose media. ATP values are expressed as a percentage of those of the vehicle control. Lactate dehydrogenase (LDH) release is expressed as extracellular LDH as a % of total LDH. B-F: extracellular flux analysis-detected changes in basal respiration, maximal respiration, ATP-linked respiration, spare respiratory capacity and proton leak induced by tolcapone (up to 500 μM). Statistical significance between haplogroup H and J cybrids: * $p < 0.05$, ** $p < 0.01$, *** $p < 0.001$. Data are presented as mean ± SEM of n = 5 experiments.

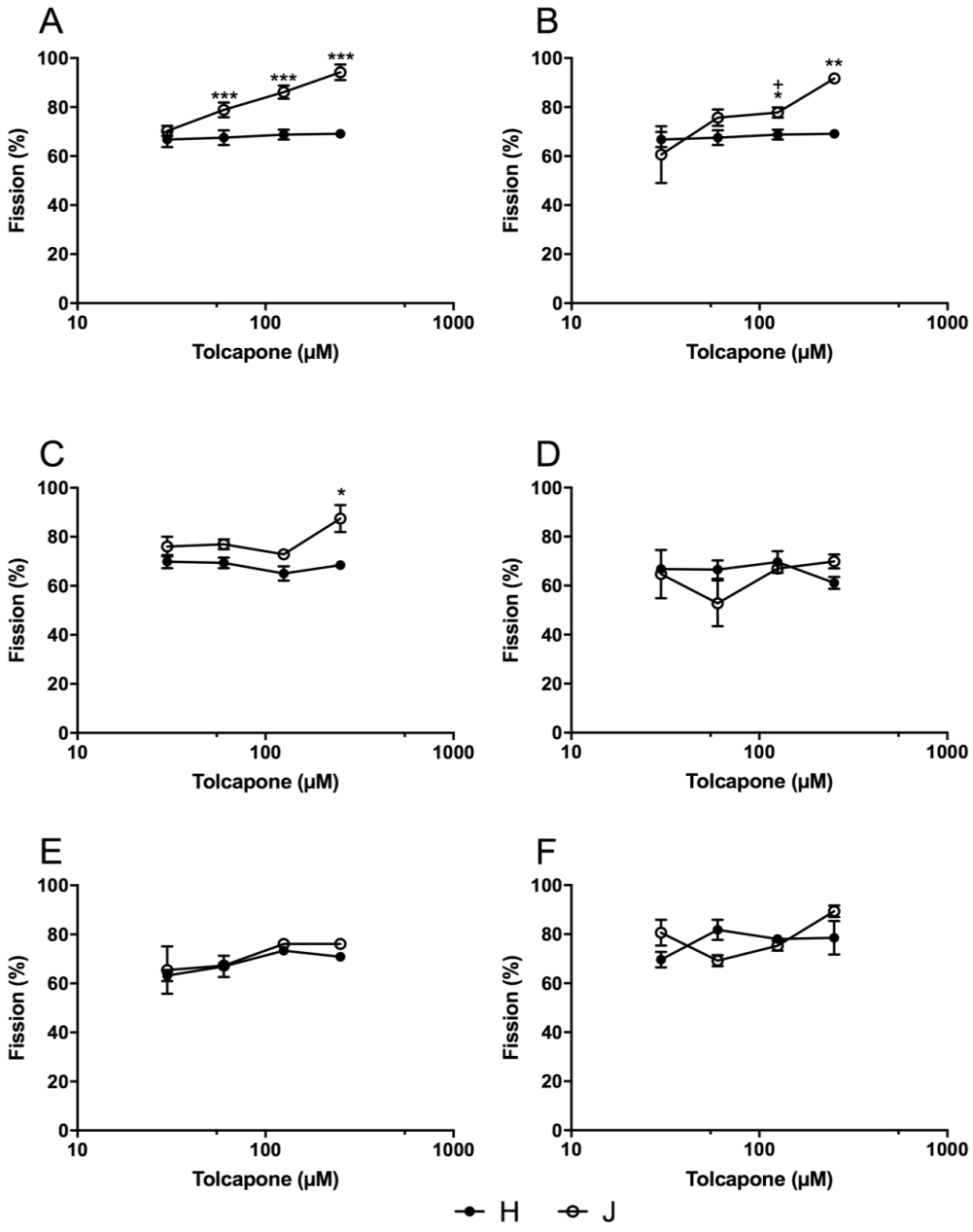

Figure 6.13. Mitochondrial fission in tolcapone-treated haplogroup H and J cybrids. Haplogroup H and J cybrids were treated with tolcapone for one of the following time points A: 2 h B: 2 h + 2 h compound-free C: 4 h D: 24 h E: 24 h + 2 h compound-free F: 26 h before high throughput imaging. Mitochondria were detected using MitoTracker™ Green and imaging was performed using the Operetta CLS system followed by PhenoLOGIC™ machine learning to detect mitochondria in a fused or fissioned state. Statistical significance compared to other haplogroup: * $p < 0.05$, ** $p < 0.01$, *** $p < 0.001$, 2 h compound-free vs no compound-free incubation: $^{+}p < 0.05$, $^{++}p < 0.01$, $^{+++}p < 0.001$. Data are presented as mean ± SEM of n = 5 experiments.

6.3.6 The effect of entacapone upon haplogroup H and J transmitochondrial cybrids

Entacapone induced a smaller decline in ATP levels compared to tolcapone (Figure 6.14A). There was no significant difference in ATP levels between the two haplogroups and also no significant difference in parameters of mitochondrial function, though haplogroup H cybrids had consistently higher ATP-linked respiration and spare respiratory capacity which tended towards significance (Figure 6.14D, E). Only haplogroup J cybrids exhibited significantly increased fission following 2 h treatment with 250 µM entacapone (Figure 6.15A-C). Following 26 h treatment, all concentrations of entacapone induced a higher level of fission in haplogroup J vs H (Figure 6.15F), but there was not a dose-dependent increase in fission unlike at the earlier time points.

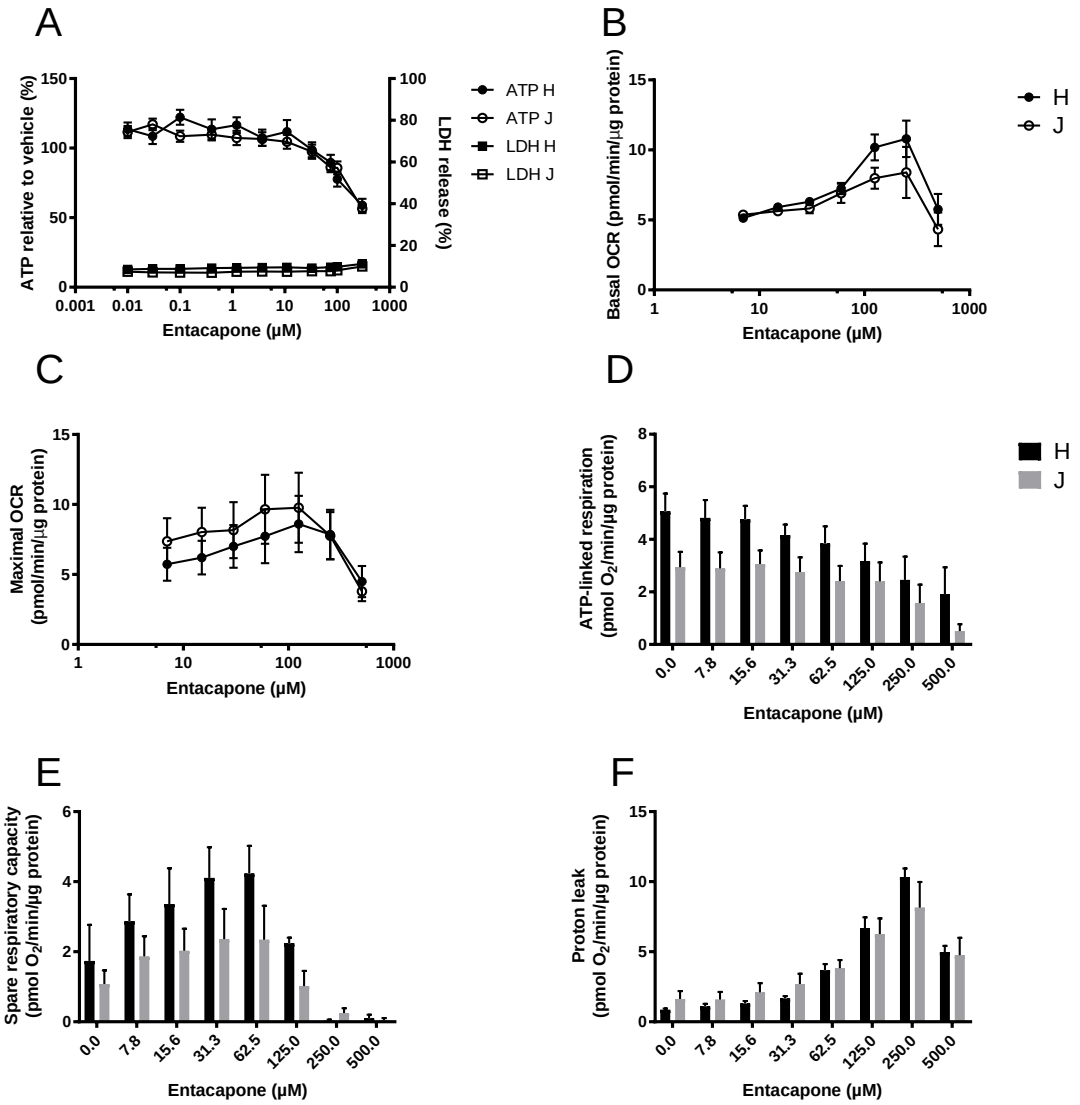

Figure 6.14. The effect of entacapone upon ATP levels and mitochondrial respiratory function in haplogroup H and J HepG2 transmitochondrial cybrids. A: cybrids were treated (2 h) with serial concentrations of entacapone up to 300 µM in galactose media. ATP values are expressed as a percentage of those of the vehicle control. Lactate dehydrogenase (LDH) release is expressed as extracellular LDH as a % of total LDH. B-F: extracellular flux analysis-detected changes in basal respiration, maximal respiration, ATP-linked respiration, spare respiratory capacity and proton leak induced by entacapone (up to 500 µM). Statistical significance between haplogroup H and J cybrids: * $p < 0.05$, ** $p < 0.01$, *** $p < 0.001$. Data are presented as mean ± SEM of n = 5 experiments.

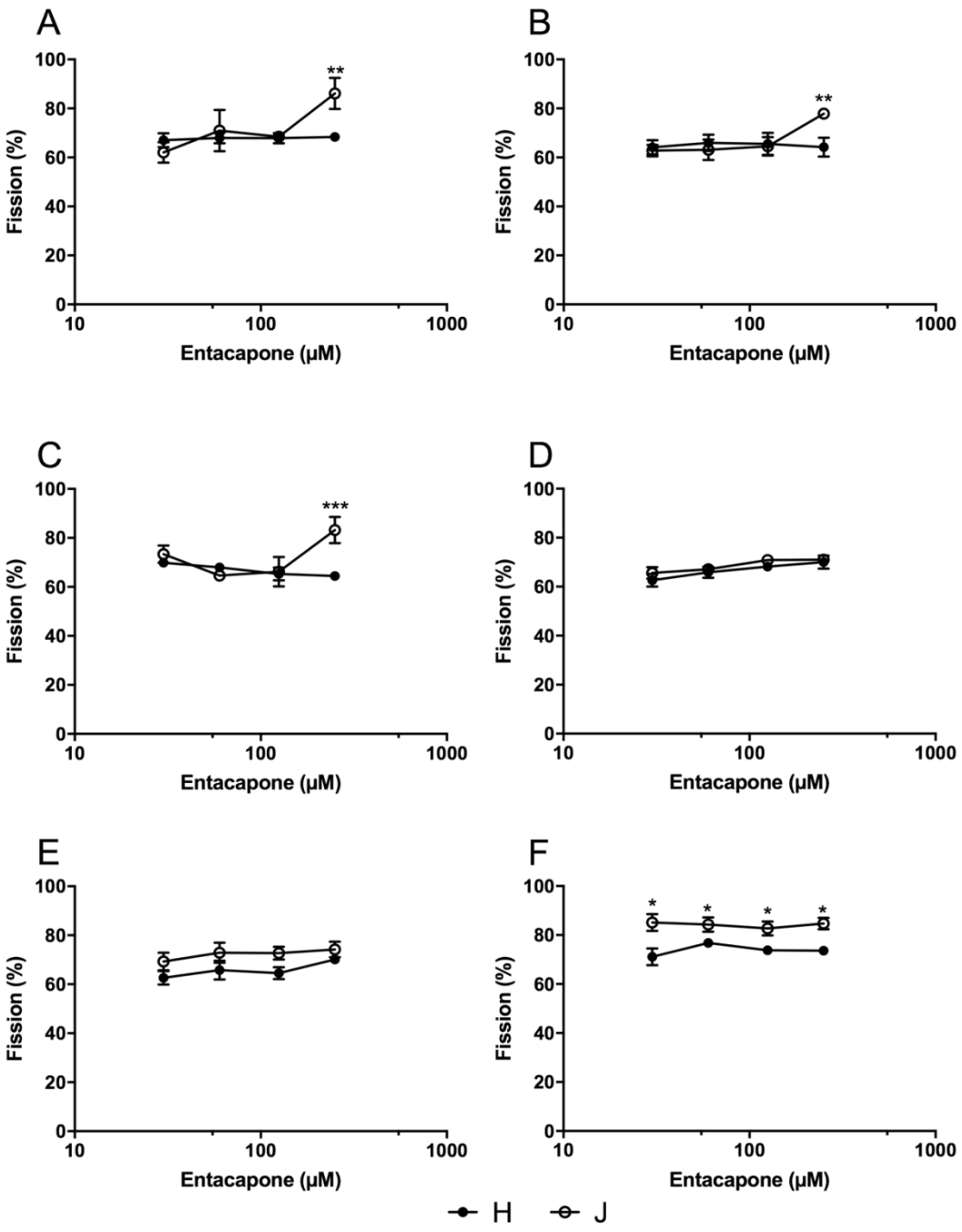

Figure 6.15. Mitochondrial fission in entacapone-treated haplogroup H and J cybrids. Haplogroup H and J cybrids were treated with entacapone for one of the following time points A: 2 h B: 2 h + 2 h compound-free C: 4 h D: 24 h E: 24 h + 2 h compound-free F: 26 h before high throughput imaging. Mitochondria were detected using MitoTracker™ Green and imaging was performed using the Operetta CLS system followed by PhenoLOGIC™ machine learning to detect mitochondria in a fused or fissioned state. Statistical significance compared to other haplogroup: * $p < 0.05$, ** $p < 0.01$, *** $p < 0.001$, 2 h compound-free vs no compound-free incubation: $^{+}p < 0.05$, $^{++}p < 0.01$, $^{+++}p < 0.001$. Data are presented as mean ± SEM of n = 5 experiments.

6.3.7 Comparison of test compound EC_{50}ATP values in haplogroup H and J cybrids

Comparison of test compound EC_{50}ATP values between the two cybrid haplogroups revealed no significant difference in flutamide EC_{50}ATP. The EC_{50}ATP values of bicalutamide and entacapone were not compared between haplogroups as in both cases the concentration range used did not result in a 50 % reduction in ATP level (Table 6.4). 2-hydroxyflutamide displayed a significantly lower EC_{50}ATP in haplogroup H vs haplogroup J cybrids, however the difference was minor (55.7 μM vs 62.2 μM), Figure 6.8A highlights this negligible difference. Consistent with the differences evident in dose-response curves (Figure 6.12A), haplogroup J cybrids had a significantly reduced tolcapone EC_{50}ATP (72.5 μM vs 131 μM) (Table 6.4).

Table 6.4. The effect of flutamide, 2-hydroxyflutamide, bicalutamide, tolcapone and entacapone exposure on intracellular ATP content in haplogroup H and J cybrids.

Compound	EC_{50}ATP (μM)		*P* value
	H	J	
Flutamide	61.1 (3.90)	62.9 (7.90)	0.693
2-hydroxyflutamide	55.7 (2.60)	62.2 (0.690)	0.00300
Bicalutamide	> 300 (n/d)	> 300 (n/d)	n/d
Tolcapone	131 (10.0)	72.5 (8.83)	< 0.000100
Entacapone	> 300 (n/d)	> 300 (n/d)	n/d

EC_{50}ATP refers to the concentration of compound required to cause a 50 % reduction in ATP content; n/d, not determined. *P* value indicates the significance of haplogroup H vs haplogroup J EC_{50}ATP. Data are presented as mean (SEM).

6.3.8 Comparison of haplogroup H and J cybrids with the parental HepG2 cell line

A comparison of EC_{50} values for various parameters of mitochondrial function between the HepG2 parental cell line (haplogroup B2c2), haplogroup H and J HepG2 transmitochondrial cybrids (Table 6.5) when treated with test compounds showed a general reduction in EC_{50} for the parental HepG2 cell line for parameters including basal respiration following flutamide or 2-hydroxyflutamide treatment. Haplogroup H cybrids on the other hand had a higher EC_{50} value for complex I activity following flutamide treatment and ATP level/ATP-linked respiration following tolcapone treatment (Table 6.5). Data used to calculate EC_{50} values are presented in Appendix 5.

Table 6.5. Comparison of EC_{50} values of test compounds in the HepG2 parental cell line (haplogroup B) and haplogroup H and J HepG2 transmitochondrial cybrids. Data are presented as mean (SEM).

Parameter	Haplogroup			Significance		
	B	H	J	B	H	J
Flutamide basal respiration EC_{50}	167.6 (3.02)	315.3 (3.68)	313.2 (3.07)	***		
2-hydroxyflutamide basal respiration EC_{50}	145.9 (1.31)	326.7 (3.40)	300.6 (2.77)	***		
Bicalutamide basal respiration EC_{50}	> 500 (n/d)	> 500 (n/d)	> 500 (n/d)			
Flutamide maximal respiration EC_{50}	100.4 (1.99)	333.1 (5.11)	302.9 (6.94)	***		
2-hydroxyflutamide maximal respiration EC_{50}	22.57 (2.31)	386.2 (6.03)	387.7 (4.02)	**		
Bicalutamide maximal respiration EC_{50}	> 500 (n/d)	> 500 (n/d)	> 500 (n/d)			
Flutamide complex I activity EC_{50}	225.6 (3.22)	496.5 (3.22)	243.5 (1.94)		**	
2-hydroxyflutamide complex I activity EC_{50}	87.06 (3.74)	440.1 (3.56)	559.1 (3.92)	***		
Flutamide complex II activity EC_{50}	287.3 (4.14)	286.4 (4.95)	235 (3.39)			
2-hydroxyflutamide complex II activity EC_{50}	65.42 (3.28)	126.2 (4.10)	136.4 (2.71)	*		
Flutamide complex III activity EC_{50}	> 250 (n/d)	> 250 (n/d)	> 250 (n/d)			
2-hydroxyflutamide complex III activity EC_{50}	> 250 (n/d)	> 250 (n/d)	> 250 (n/d)			
Flutamide complex IV activity EC_{50}	> 250 (n/d)	> 250 (n/d)	> 250 (n/d)			
2-hydroxyflutamide complex IV activity EC_{50}	> 250 (n/d)	125.2 (0.51)	> 250 (n/d)			
Flutamide ATP content EC_{50}	43.9 (1.05)	61.1 (2.78)	62.9 (3.58)			
2-hydroxyflutamide ATP content EC_{50}	48.5 (1.09)	55.7 (1.53)	62.2 (1.34)			
Bicalutamide ATP content EC_{50}	103.1 (0.80)	>300 (n/d)	220.70 (0.67)			
Tolcapone ATP content EC_{50}	74.1 (1.62)	131 (0.41)	72.5 (1.77)		**	
Entacapone ATP content EC_{50}	>300 (n/d)	>300 (n/d)	>300 (n/d)			
Flutamide ATP-linked respiration EC_{50}	198.9 (2.90)	117.1 (3.37)	180.2 (3.79)			
2-hydroxyflutamide ATP-linked respiration EC_{50}	124.5 (1.49)	146.9 (4.88)	111.3 (4.00)			
Bicalutamide ATP-linked respiration EC_{50}	n/d	862.7 (2.89)	n/d			
Tolcapone ATP-linked respiration EC_{50}	57.4 (4.37)	205.9 (7.29)	64.43 (2.58)		**	
Entacapone ATP-linked respiration EC_{50}	206.2 (2.41)	> 500 (n/d)	227.6 (4.85)			

Flutamide spare respiratory capacity EC_{50}	285.2 (4.43)	> 500 (n/d)	> 500 (n/d)			
2-hydroxyflutamide spare respiratory capacity EC_{50}	301.7 (5.72)	> 500 (n/d)	> 500 (n/d)			
Bicalutamide spare respiratory capacity EC_{50}	> 500 (14.66)	> 500 (n/d)	> 500 (n/d)			
Tolcapone spare respiratory capacity EC_{50}	32.0 (0.59)	101.3 (5.10)	27.42 (5.01)		**	
Entacapone spare respiratory capacity EC_{50}	96.9 (1.13)	> 500 (n/d)	> 500 (n/d)	***		

Statistical significance compared to two remaining haplogroups: * $p < 0.05$, ** $p < 0.01$, *** $p < 0.001$. Abbreviations: n/d, value not determined. Data are presented as mean (SEM) of n = 5 experiments.

6.4 DISCUSSION

Haplogroups H and J are two of the most common UK mitochondrial haplogroups (Table 6.1) (Eupedia, 2016). Previous investigations have found that mitochondrial haplogroup can confer changes in mitochondrial function and differential response to drugs (Kenney *et al.*, 2014; Wallace, 2015; Pello *et al.*, 2008; Marcuello *et al.*, 2009; Kallianpur and Hulgan, 2009; Di Lorenzo *et al.*, 2009). The aim of this chapter was therefore to generate HepG2 transmitochondrial cybrids, an *in vitro* model derived from healthy volunteers of haplogroups H and J to determine changes in mitochondrial (dys)function conferred by haplogroup

There were marginal differences in most parameters of mitochondrial function between haplogroup H and J cybrids at basal state. Concordantly, coupling efficiency, the proportion of the oxygen consumed to drive ATP synthesis was not significantly different between cybrids of the two haplogroups (data not shown). Basal activity of specific respiratory complexes however showed a significantly greater complex I and II activity in haplogroup J cybrids.

The fact that these differences were observed despite the division of cybrids into two macrohaplogroups which encompass much variation, suggests that the comparison of more homogenous mtDNA groups may provide further, more valuable insight into the differences conferred by a change in mtDNA background. For example, haplogroup J cybrids generated from donors 9 and 30 both had additional non-synonymous SNPs not characteristic of the assigned haplogroup (Table 6.2) (Van Oven and Kayser, 2009). In addition, a study by Pacheu Grau *et al.,* has demonstrated a significant reduction in the expression of cytochrome *c* oxidase in cybrids containing the m.3018A allele (Pacheu-Grau *et al.*, 2012). This allele was present in cybrids from both haplogroup H and J volunteers in this work, demonstrating the importance of considering all SNPs, even those which are not characteristic of the assigned

haplogroup as they too may have an effect. Considering all SNPs should not be mistaken for a focus upon the effect of just one SNP however, as several linked alleles are likely to interact (Chinnery and Gomez-Duran, 2018). Therefore for future studies using this model, generation of cybrids which are identical at the subhaplogroup level would provide reduced variation within test groups and enable the comparison of, for example, J1 and J2 subhaplogroups, which was not possible in this research as there was only one cybrid of J2 origin.

When the overall respiratory function of cybrids was measured upon treatment with anti-androgenic compounds (flutamide, bicalutamide), both compounds induced higher proton leak in haplogroup J cybrids. Changes in mitochondrial fission associated with these compounds did not significantly differ between each haplogroup however.

When the activity of individual respiratory complexes was measured upon flutamide/2-hydroxyflutamide treatment, haplogroup J conferred significantly higher complex I activity, the opposite to the effect seen in platelets (Section 4.3.3), where haplogroup J conferred a significantly lower complex I activity at a basal and treated state. This disproves the secondary hypothesis of this work; that haplogroup J increases susceptibility to complex I inhibition by flutamide/2-hydroxyflutamide.

In contrast to complex I, complex II is entirely encoded in the nuclear genome. Significant differences in complex II activity dependent on cybrid haplogroup also contrast with platelet studies in which complex II activity following 2-hydroxyflutamide treatment was not significantly different between haplogroups (Section 4.3.3). These inconstancies between the two models were also evidenced in correlation analyses between the 2-hydroxyflutamide complex I and II activity EC_{50} for each donor in platelets or cybrids, this showed a weak correlation between the two models (complex I: $R = 0.01$, $p = 0.98$; complex II, $R = -0.07$, $p = 0.84$). The mitonuclear communication present in cybrids, but not in platelets likely accounts for these differences between the two cell models.

Upon the introduction of the mitochondrial genome in cybrids, the initiation of retrograde responses to the nucleus must ensue, primarily via calcium signalling, which would enable regulation of the nuclear-encoded mitochondrial proteome and perhaps enhanced biogenesis of respiratory complexes in haplogroup J which could account for the increased complex activity seen (Section 1.2.6). Western blotting for respiratory complexes would provide clarification of this, although previous studies have reported a higher mtDNA copy number in haplogroup J cybrids which may translate into a greater protein abundance (Suissa

et al., 2009). Cybrids, unlike platelets also enable the improved study of the effect of mitochondrial haplogroup beyond the mitochondria. Haplogroups have been found to confer changes including differential expression of interleukins, methionine adenosyltransferase and complement factor H (Bellizzi *et al.*, 2012, 2006).

Treatment of cybrids with the catechol-methyltransferase inhibitors, tolcapone and entacapone also displayed differences between cybrids of the two haplogroups. Haplogroup H cybrids exhibited milder uncoupling (indicated by an increase in basal respiration and decrease in ATP-linked respiration) than haplogroup J cybrids when treated with 15 µM tolcapone, but within the same concentration range, cellular ATP content increased in haplogroup H cybrids. This does not align with the concept that mild uncoupling can be beneficial via the reduction of ROS production, but at the expense of a small decrease in ATP production. One study by Naven *et al.,* has reported an increased ATP content following uncoupling however this was via the overexpression of uncoupling protein 4 (UCP4) and not by chemical uncoupling induced by tolcapone, therefore elucidation of this mechanism in haplogroup H cybrids in the future is of interest (Naven *et al.*, 2012).

Identification of enhanced uncoupling in haplogroup J cybrids agrees with findings reported by Ghelli *et al.,* 2014 in which a cybrid model was used to determine that haplogroup J (vs haplogroups H and U) was more susceptible to uncoupling by the neurotoxic metabolite, 2,5-hexanediol (Ghelli *et al.*, 2009). Concordantly, tolcapone and entacapone treatment induced an increase in fission in haplogroup J cybrids, which was significantly more than observed in haplogroup H cybrids. However, unlike parameters measured during XF analysis, mitochondrial dynamics did not change in a clear dose-dependent manner; following 24 h treatment with lower concentrations of tolcapone there was a decrease in the proportion of mitochondria in a fission state, but an increase in fission at a higher concentrations. This is reflective of the complex nature of the mitochondrial network; a fused mitochondrial network is advantageous for efficient ATP production, however, hyperfusion can be indicative of mitochondrial stress. On the other hand, increased fission of mitochondria can be indicative of dysfunction, but fission is also important in enabling mitophagy and the efficient turnover of mitochondria to maintain a healthy population. Given the complex nature of these dynamics, it would be beneficial to use a more quantitative method of mitochondrial dynamics assessment such as the co-localisation algorithm applied to flow cytometry images of mitochondrially-targeted red and yellow fluorescent proteins (Nascimento *et al.*, 2016).

The characterisation of tolcapone and entacapone as uncouplers of respiration was supported by findings of increased fission in the research described in this chapter, however the effect of these compounds upon specific respiratory complexes was not investigated (Miyazono *et al.*, 2018). Since this work was performed however, there has been evidence of the inhibition of specific respiratory complexes by these compounds. This highlights the potential multi-mechanistic nature of compounds and given the haplogroup-associated differences in response to tolcapone treatment, future work should be performed to examine the effect that tolcapone and entacapone have upon specific respiratory complexes using the methods described in this chapter for flutamide/2-hydroxyflutamide (Grünig *et al.*, 2017).

The endpoints assessed in this chapter represent a fraction of the functions which may be affected by mitochondrial haplogroup. ROS generation for example could be a significant factor in assessing the influence of these haplogroups upon mitochondrial health (Chen *et al.*, 2012). In addition, secondary outcomes of perturbations in the ETC such as a decrease in NAD^+/NADH ratio could be measured to assess any further impact of the difference in complex I activity seen in haplogroup H and J cybrids. Finally, although intermitochondrial dynamics have been considered in this research, intramitochondrial dynamics and plasticity such as the assembly of respiratory supercomplexes have not (Section 1.2.3.4). For example, the 3697G>A mutation in mitochondrial-encoded NADH dehydrogenase 1 (ND1) has been found to effect the assembly of supercomplex I + III + IV. Supercomplex dynamics optimise fuel utilisation and may be critical in overcoming the impact of a drug upon oxidative phosphorylation (Acin-Perez and Enriquez, 2014). In the case of this particular mutation, a reduction in cellular respiration and ATP generation was reported (Sun *et al.*, 2016).

Comparison of haplogroup H and J cybrid results with haplogroup B2c2 parental HepG2 cells (SNPs listed in Table 6.6) enabled an assessment of genotypes beyond those which are common in Europe (haplogroup B2 is common among indigenous American populations) (Starikovskaya *et al.*, 2005). HepG2 parental cells (compared to cybrids) had significantly reduced basal respiration, complex I and complex II activity EC_{50} values following treatment with 2-hydroxyflutamide. On the other hand, ATP content and ATP-linked respiration EC_{50} values were substantially higher in haplogroup H cybrids compared to the parental cell line and haplogroup J cybrids. This highlights that preclinical representation of discrete patient groups not only needs to consider individuals at greater risk, but also individuals with protective characteristics.

Table 6.6. Single nucleotide polymorphisms and gene locations of HepG2 parental cell line (haplogroup B2c2).

SNP	Gene	Synonymous/non-synonymous
73G	Control region	S
146C	Control region	S
263G	Control region	S
827G	rRNA	S
1438G	rRNA	S
2706G	rRNA	S
3547G	MT-ND1	NS (Ile-Val)
4755C	MT-ND2	S
4769G	MT-ND2	S
4820A	MT-ND2	S
4977C	MT-ND2	S
6473T	MT-CO1	S
7028T	MT-CO1	S
7241G	MT-CO1	S
8860G	MT-ATP6	NS (Thr-Ala)
9950C	MT-COIII	S
10373A	MT-ND3	S
11177T	MT-ND4	NS (Pro-Ser)
11719A	MT-ND4	S
13590A	MT-ND5	S
14757C	MT-CYB	NS (Met-Thr)
14766T	MT-CYB	NS (Thr-Ile)
15326G	MT-CYB	NS (Thr-Ala)
15535T	MT-CYB	S
16217C	Control region	S
16295T	Control region	S
16519C	Control region	S

Abbreviations: ND, NADH dehydrogenase; NS, non-synonymous; SNP, single nucleotide polymorphism.

When assessing the limitations of this work, the practicalities of cybrid generation meant that the material collected to determine the haplogroup of each volunteer may have been collected up to five years before cybrids were generated and tested. This lag time provides a window for a shift in the mitochondrial genotype of an individual. In addition, the selective pressure applied during cybrid generation may have induced a shift in heteroplasmy. In this case haplogroup B2c2 also did not represent a cybrid cell line; the parental HepG2 cell line had native mitonuclear communication, had not been exposed to the same selection pressure of cybrid cell lines and was at a much lower passage (< 20) than cybrids. There is

evidence that cells with an increased passage number have an increased $\Delta\psi_m$ which may confer a difference in susceptibility to drug-induced mitochondrial dysfunction (Katajisto *et al.*, 2015).

These limitations could be addressed at least in part by genotyping the cybrids generated so that the current genotype of the model is known. It would also be beneficial to treat the HepG2 cell line at the same time as cybrids so that these parental cells could act as a control for cybrid studies. Given the presence of a non-synonymous SNP in the ATP-6 gene in haplogroup B2c2, it would also be of interest to compare ATP synthase (complex V) activity between the parental cell line and cybrids, as haplogroup H and J do not have SNPs in the region encoding this subunit of ATP synthase.

6.5 CONCLUSION

The work described in this chapter has determined that differential mtDNA haplogroups confer variation in basal mitochondrial function and to a greater extent, changes in susceptibility to drug-induced mitochondrial dysfunction in a HepG2 transmitochondrial cybrid model.

Notably, despite marginal basal differences, haplogroup J conferred a significant impact on the response of cybrids to tolcapone, with mitochondrial dynamics, cellular ATP level and oxidative phosphorylation all found to be more greatly affected in cybrids with this mitochondrial haplogroup. Given the positive effects associated with the use of tolcapone in the treatment of Parkinson's disease, future work in this area has potential clinical translation by examining the effect of tolcapone in the context of J subhaplogroups alongside other potential susceptibility factors.

Chapter 7

Final Discussion

The overall aim of the research in this thesis was to generate an *in vitro* hepatic model which can be used to assess the effect of mtDNA variation upon mitochondrial function and susceptibility to iDILI. The HepG2 transmitochondrial cybrid model generated may enhance the preclinical investigation of susceptibility factors for iDILI, with the ultimate goal of reducing late stage attrition due to this rare, but severe adverse drug reaction. This would increase the safety of individuals enrolled in clinical trials and the wider patient population by the prediction of individuals at potentially greater risk. In addition, the economic burden associated with drug attrition could be reduced.

Establishment of iDILI risk is not only important for the prevention of iDILI in susceptible patients, but also for the identification of tolerant individuals. This is of particular importance when a drug is withdrawn without the availability of an equally, or more effective alternative. For example, tolcapone has been shown to have greater efficacy than entacapone, however four instances of liver failure (among the 100 000 individuals whom were administered the drug at the time) caused its withdrawal from the European market (Watkins, 2000; Benabou and Waters, 2003; Olanow and Watkins, 2007; Olanow, 2000; Rivest *et al.*, 1999; Longo *et al.*, 2016; Lees, 2008). Entacapone is widely used as an alternative to tolcapone, however it has been shown that patients have a 50 % reduction in the length of symptom relief when compared to tolcapone treatment. Outside of this period, patients continue to experience the symptoms associated with Parkinson's disease such as tremors and dyskinesia, causing a significant reduction in the patient's quality of life (Lees, 2008; Ouma *et al.*, 2017).

The research described in this thesis has led to the conclusion that common UK mitochondrial haplogroups affect mitochondrial function, as well as dysfunction induced by flutamide, 2-hydroxyflutamide and tolcapone in a HepG2 transmitochondrial cybrid model. Nonetheless, the extension of this to an altered susceptibility to iDILI requires evidence of a clear relationship between drug-induced mitochondrial dysfunction and iDILI.

This relationship was recently disputed in a review by Kenna *et al.,* 2018 which dismissed mitochondrial dysfunction as a cause of iDILI on the basis of three principal observations: 1) compounds which are known to cause mitochondrial injury are not always recorded as causing iDILI 2) virtually all of the studies which suggest that mitochondrial injury is important in iDILI are *in vitro*; the same association has rarely been found *in vivo* 3) although mitochondrial dysfunction can cause lactic acidosis and microvesicular steatosis, this is not

associated with typical iDILI (Kenna and Uetrecht, 2018). The latter observation however, should be considered in the context of a current lack of clear diagnostic criteria for iDILI.

Some recent opinion also points to mitochondrial dysfunction as a symptom (rather than a cause) of iDILI, however the understanding of the pathogenesis of iDILI and the factors involved in its progression (Figure 7.1) remains incomplete and thus it would be an oversight to cease investigations into mitochondrial dysfunction as a potential mechanism (Roth and Lee, 2017). Despite this incomplete understanding, a leading hypothesis proposes iDILI as an initial, intrinsic insult caused by a drug followed by an adaptive response (Russmann *et al.*, 2009; Greer *et al.*, 2010). According to this hypothesis, the initial insult is minimal and subclinical or transient in the majority of the population, whereas the insult is amplified or the adaptive immune response is inappropriate in susceptible individuals, leading to toxicity (Kaplowitz, 2005; Li and Uetrecht, 2010; Yuan and Kaplowitz, 2013). Based on the findings described in this thesis it can be postulated that susceptible individuals may harbour factors including a mitochondrial haplogroup which confers an increased susceptibility to drug-induced mitochondrial dysfunction. This may cause an inappropriate response which differentiates the individual from a population of patients whom can be safely treated.

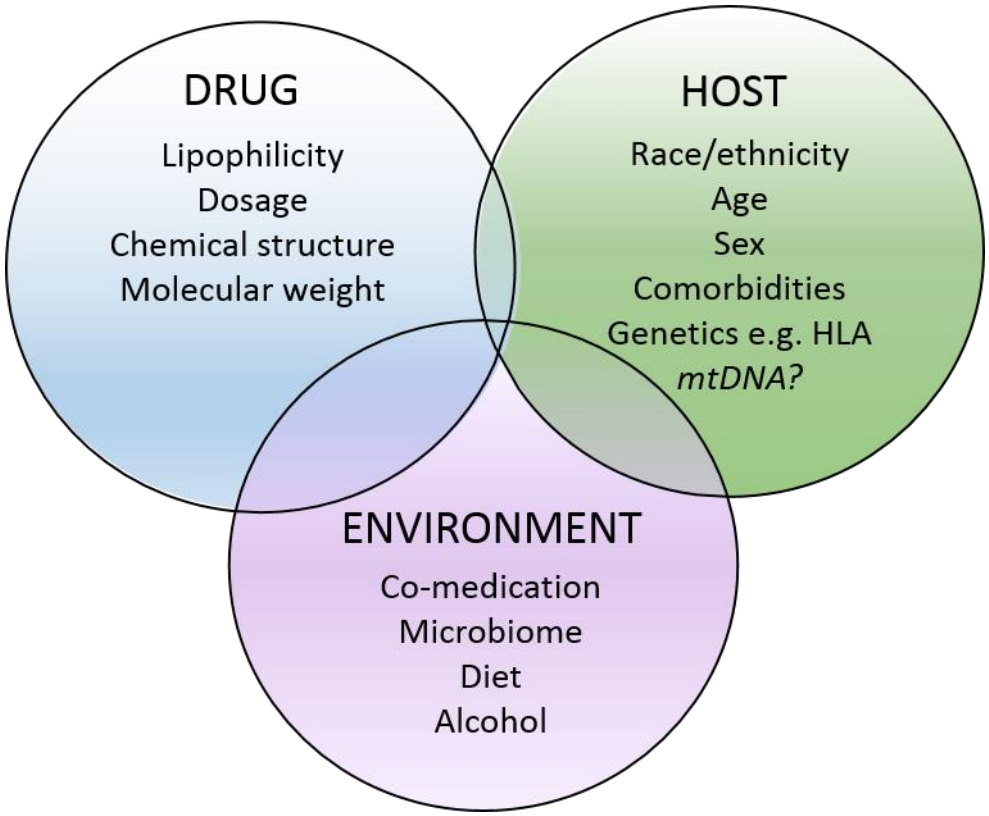

Figure 7.1. Proposed risk factors for idiosyncratic drug-induced liver injury (iDILI). iDILI is a complex interplay of host factors (genetic and environmental) as well as compound-specific risk factors (Fontana, 2014; Chalasani and Bjornsson, 2010).

A principal factor in the concept of immune-mediated iDILI is the effect of human leukocyte antigen (HLA) genotypes upon the recognition of immune cells presenting damaged motifs (Roth and Lee, 2017). However, although HLA genotype can provide a high negative predictive value for certain adverse drug reactions, used alone, it is not able to predict the occurrence of iDILI and needs to be considered in the context of many other factors. For example, patients with the HLA B*5701 haplotype have an 80-fold increased susceptibility to liver injury induced by flucloxacillin, but this still only translates to 1 in 500 individuals with this haplotype developing hepatotoxicity (Han *et al.*, 2013).

An important step in the proposed pathogenesis of iDILI is the release of damage-associated molecular patterns (DAMPs) that activate innate immune cells to release cytokines and chemokines. This draws inflammatory cells to the liver, a prerequisite for the targeted, adaptive, immune attack thought to occur in individuals whom experience iDILI (Li and Uetrecht, 2010). It is possible that mitochondrial dysfunction may enhance immune responses, particularly as many mitochondrial proteins released upon dysfunction can act as potent DAMPs, namely mtDNA, TFAM and cardiolipin. These DAMPs can act individually or in synergy with other DAMPs resulting in responses including increased cytokine production in monocytes and macrophages, neutrophil and inflammasome activation. TFAM and cardiolipin are thought to only be passively released from necrotic cells, however passive and active release (via mitochondria-derived vesicles) of mtDNA has been detected (Grazioli and Pugin, 2018).

One of the most commonly used cell lines in the preclinical assessment of compounds with a propensity to cause iDILI is the HepG2 cell line. This research represents the first time that transmitochondrial cybrids have been generated from this cell line (Gerets *et al.*, 2012). The cybrids generated provide an *in vitro* representation of variation in mtDNA, however the SNPs identified during whole mitochondrial genome sequencing have only been considered alongside other SNPs as part of haplogroups in this project due to sample size restrictions. Currently, there is a wealth of variation between reports of haplogroup-mediated changes in mitochondrial function (Pello *et al.*, 2008; Suissa *et al.*, 2009; Kenney *et al.*, 2013; Bellizzi *et al.*, 2012; Gómez-Durán *et al.*, 2012; Pacheu-Grau *et al.*, 2012). This is likely to be as a result of studies, which like the research described in this thesis, only discriminate at the haplogroup and not the subhaplogroup level, this means that variants in the younger branches of the phylogenetic tree are not accounted for. Equally, this could also be due to differences in the parental cells used to generate cybrids.

In the future it would be beneficial to generate HepG2 cybrids from donors whom are identical at the level of subhaplogroup e.g. J1 and J2 and also from patients whom have experienced iDILI to see if increased susceptibility is evident in a cybrid model. It must also be kept in mind that mitochondrial haplogroup is not the only means of mtDNA-mediated changes in mitochondrial function. For example, mtDNA methylation can affect mtDNA copy number and biogenesis via the modulation of TFAM binding to mtDNA (Van der Wijst and Rots, 2015).

Although HepG2 cells are a commonly used preclinical cell line, their use has many caveats included limited xenobiotic metabolism, no adaptive immune response and aneuploidy, resulting in a potentially unstable nuclear background, when a stable nuclear background is a key requirement for successful cybrid utilisation (Section 1.5.2.2) (Ball *et al.*, 2018). 2D culture of these cells also confers the absence of interactions with extracellular matrix components which contribute to normal hepatocyte function (HepG2.com). The lack of active bile salt export in these cells may also reduce the identification of compounds likely to cause iDILI; dual potency as a mitochondrial and BSEP inhibitor has been highly associated with more severe DILI (Aleo *et al.*, 2014). It may therefore be advantageous to adapt the methods of HepG2 cybrid generation described in this thesis for multiple other cell types such as HepaRG cells, or HepG2 cells with augmented metabolic capacity, such as those generated by Tolosa *et al.,* (Tolosa *et al.*, 2018). It would also be of interest in future studies to test the amenability of cybrids to 3D spheroidal culture to further improve *in vivo* applicability (Gaskell *et al.*, 2016; Fang and Eglen, 2017).

Many of the limitations of the cybrid model generated in this project stem from a lack of knowledge of the exact genotype of the cybrids tested. The mtDNA perpetuated in the cybrids is of platelet origin, yet there are many differences between hepatocytes and platelets, not least the difference in lifespan; 7-10 days for platelets and 200-300 days for hepatocytes (Machlus and Italiano, 2013; Duncan *et al.*, 2009). Given the longer lifespan of hepatocytes it is reasonable to suggest that the propensity to accumulate somatic mutations is higher in their mitochondrial genome, especially given the role of these cells in xenobiotic metabolism. In contrast, platelets are derived from haematopoietic stem cells, which contain few and inactive mitochondria; the lower ROS production associated with inactive mitochondria may reduce the accumulation of mtDNA aberrations (Rimmelé *et al.*, 2015). This may result in significant discrepancies between the mtDNA in cybrids and the mtDNA in the participants' hepatocytes and could have a profound effect on the ability of cybrids to represent an individual's response to potential hepato-mito toxicants.

It would also be of interest to determine the nuclear genotype of cybrids, theoretically this should be the same across cybrids of multiple mitochondrial genotypes, however upon platelet and HepG2 ρ0 cell fusion there must be the establishment of mitonuclear communication. Interestingly, as platelets have been used as mitochondrial donor cells rather than enucleated cells, the mitochondria have not previously been in a situation of mitonuclear communication. Mitonuclear communication is vital for mitochondrial function, especially given the dual genome origin of four of the five enzyme complexes required for oxidative phosphorylation. This intergenomic relationship is an area of intense research and further details continue to be elucidated, including the presence of synchronised mitochondrial and cytosolic translation programmes (Ingolia *et al.*, 2009; Couvillion *et al.*, 2016). Continued improved understanding of these mechanisms is key in comprehending the reprogramming that must take place during cybrid generation. This is particularly important whilst the double mitochondrial membrane continues to prevent site-directed mutagenesis of the mitochondrial genome, meaning functional studies are likely to remain reliant upon the use of cybrid models for some time (Wilkens *et al.*, 2012; Chinnery and Gomez-Duran, 2018).

The use of platelets alone (Chapter 4) to test mitochondrial function offers an alternative which would mitigate the ambiguous impact of the nuclear genome, however the replicative machinery of mitochondria relies upon proteins encoded by the nuclear genome, meaning that platelets cannot account for haplogroup-induced differences in mtDNA replication and mitochondrial biogenesis (Holt and Reyes, 2012).

In conclusion, this work has achieved its aim of generating a novel, personalised *in vitro* model of mtDNA variation. In order to advance its utility, cybrids should be generated from a greater number of mitochondrial subhaplogroups and also from cell types which can better recapitulate complex liver architecture to enhance *in vivo* applicability. The impact of J subhaplogroups upon tolcapone-induced mitochondrial dysfunction would also be of particular interest based on the clinical efficacy of tolcapone and the findings of increased dysfunction conferred by haplogroup J described in this thesis. Finally, it is important to state that although the generation of such models represents a significant advance in the area of iDILI research, the effects of mitochondrial genome variation should always be placed in the context of the broad range of factors implicated in the onset of iDILI if the pathogenesis of this costly adverse drug reaction is to be fully understood.

Appendices

Appendix 1

Phylogenetic tree of 383 genotyped samples: see USB File 1.

Appendix 2

Gender, ethnicity and haplogroups of 384 volunteer samples subject to whole mitochondrial genome sequencing.

Sequencing ID	Subject ID	Gender	Ethnicity	Haplogroup
1	417	Female	White	H104
2	438	Female	White	U3a1c1
3	440	Female	White	J1c3g
4	463	Male	White	X2c
5	497	Male	White	U3a1c1
6	552	Female	White	T1a1a1
7	567	Female	White	HV0
8	622	Female	White	H2a
9	623	Female	White	J1c2q
10	624	Female	White	H4a1c
11	625	Female	White	U5a1a1
12	626	Female	White	H1c
13	627	Female	White	H3aq
14	628	Male	White	U1a1a1
15	629	Female	White	T2e
16	630	Male	White	K2a
17	631	Female	White	H
18	632	Female	White	U5a1a1
19	633	Female	White	H4a1a1a
20	634	Female	White	K1a4a1d
21	635	Female	White	J1c3a2
22	636	Female	White	J1c2m
23	637	Female	White	V10a
24	638	Female	White	H13a1a
25	639	Female	White	V+@16298
26	640	Female	Black African	L0a2a
27	641	Female	White	H6a1b4
28	642	Female	White	H1
29	643	Male	White	T1a1
30	644	Female	Malay	M21b
31	645	Female	White	H5s
32	646	Female	White	U4b1b1b
33	647	Male	White	U4b1a2b
34	648	Male	White	H5+16311
35	649	Female	White	U5a2a2
36	650	Female	White	U1a1a1
37	651	Male	White	V9a2
38	652	Female	White	J1c2h
39	653	Female	White	H2
40	654	Female	White	T2b28

41	655	Female	White	H1bb
42	656	Female	White	H6a1b
43	657	Female	White	J1c3g
44	658	Female	White	T1a1
45	659	Female	White	H58a
46	660	Female	White	U4a3a
47	661	Female	White	W5a1a
48	662	Female	White	H1bs
49	663	Female	White	K1a4a1c
50	664	Male	White	J1c5
51	665	Female	White	U5a1b1
52	666	Female	White	H10e1
53	667	Female	White	J1c1a
54	668	Female	White	H42a
55	669	Female	White	H6a1a3
56	671	Male	White	U8a1a3
57	672	Female	White	J1c7a
58	673	Female	White	K2a3
59	674	Female	Caribbean	J1b1a1a
60	675	Male	White	H3
61	676	Male	White	T2b21
62	677	Female	White	J2a1a1a
63	678	Male	White	H13a1a
64	679	Male	White	H7a1b
65	680	Male	White	U3a1c
66	681	Male	White	K1a4a1a
67	682	Female	White	K1c1b
68	683	Female	White	U5b2b4a
69	684	Female	White	H5a1
70	685	Male	White	K1a4a1b
71	686	Male	White	T1a1
72	687	Female	White	T2e1a
73	688	Female	White	T2b3
74	689	Male	White	U5b1d1c
75	690	Female	White	J2b1g
76	691	Female	White	H3g
77	692	Female	White	V15a
78	694	Female	White	U5a1i1
79	695	Female	White	K1a3a2
80	696	Female	White	F1e3
81	697	Male	White	H2a1e1a1
82	698	Male	White	H49a1
83	699	Male	White	J1c5
84	700	Male	White	T2b4

85	701	Male	White	K1a4a1e
86	702	Male	White	H+195
87	703	Male	Anglo Latin American	B2d
88	704	Female	White	H2
89	705	Male	White	H2
90	706	Female	White	J1c1e
91	707	Female	White	U4c1
92	708	Female	Bangladeshi	M35b
93	709	Male	White	R5a2
94	710	Female	Filipino	R9c1a
95	711	Female	White	H39
96	712	Female	White	U3a1
97	713	Female	Black African	H27
98	714	Female	White	T2a1b1a
99	715	Female	White	U4b1a1a1
100	716	Female	White	J1c+16261
101	717	Male	White	J1c8a1
102	718	Female	White	H5a1
103	719	Female	White	H1q3
104	720	Male	White	H2a2a1
105	721	Female	White	U5b2a2b1
106	722	Male	White	A12a
107	723	Male	White	H4a1a1a
108	724	Male	White	H4a1
109	725	Male	White	T2b
110	726	Female	White	X2b+226
111	727	Male	White	H1m1
112	728	Female	White	H2a2b1a1
113	729	Male	White	K1
114	730	Male	White	J1c3b
115	731	Male	White	U4b1b1a
116	732	Male	White	X2b+226
117	733	Male	White	J2b2
118	734	Male	White	J2a1a1a
119	735	Female	White	H7
120	736	Male	White	H7h
121	737	Female	White	W5a2
122	738	Male	White	J2b1g
123	739	Female	White	J1c5e
124	740	Male	White	U
125	741	Male	White	H+152
126	742	Male	White	A2v
127	743	Male	White	H5a1
128	744	Male	Chinese	R31

129	745	Male	White	V12
130	746	Male	White	H101
131	747	Male	Chinese	M7c
132	748	Female	White	N1b1b1
133	749	Female	Chinese	R
134	750	Female	White	J1c3b
135	751	Female	Hispano Latino	D4h3a6
136	752	Female	Chinese	D4b1b
137	753	Female	Chinese	M8a2c
138	755	Female	White	X2b+226
139	756	Female	Turkish	T2a
140	757	Female	White	U5b2c2a
141	758	Female	White	H1b1+16362
142	759	Female	White	J1c3e2
143	760	Female	Bangladeshi	X2p
144	761	Male	White	H1a1
145	762	Female	White	K1b1a1d1
146	763	Female	White	V8
147	764	Male	White	T2b+152
148	765	Female	White	H13a1a
149	766	Female	British Black	H3k1
150	767	Female	White	HV0d
151	768	Male	White	I2
152	769	Female	White	U4a1
153	770	Female	White	T2b
154	771	Female	White	J1c5f
155	772	Male	White	H10a1a
156	773	Male	White	H1n1b
157	774	Female	White	H5
158	775	Female	White	J2a1a1a
159	776	Male	White	G2a5
160	777	Female	White	H1bi
161	778	Female	White	V
162	779	Male	White	H4a1a1a
163	780	Female	White	U5a2a1
164	781	Male	White	K1b
165	782	Female	White	H1+16189
166	783	Male	White	J1b1a1
167	784	Female	White	I1a1
168	785	Male	White	H1e2
169	786	Female	White	K2a
170	787	Female	White	J1c8a1
171	788	Female	White	T2b2b
172	789	Female	White	J2a1a1a2

173	790	Female	Mixed Race	K2a1
174	791	Female	White	H13a1a1
175	792	Male	White	H13a1a1
176	793	Female	White	J1c1e
177	794	Male	White	H6b2
178	795	Female	White	H1a1a1
179	796	Male	White	H59a
180	797	Female	White	H3a1a
181	798	Female	White	H1c1
182	799	Female	White	J1c+16261
183	800	Female	White	U5b2a3a
184	801	Male	Black African	L3f1a1
185	802	Female	Indian	U7a3a
186	803	Male	Chinese	N9a1
187	804	Female	White	U3b1
188	805	Male	White	U5a1a1
189	806	Male	White	U5a1a1
190	807	Female	White	HV9
191	808	Male	Iranian	N1a3
192	809	Female	White	J1c1b2a
193	810	Female	White	X2c1a
194	811	Female	White	H6c
195	812	Male	White	H3ap
196	813	Female	White Asian	K2a
197	814	Male	White	J1c3b
198	815	Female	Chinese	F1e3
199	816	Female	White	J1c2l
200	817	—	—	—
201	818	Female	White	H39b
202	819	Male	White	K1a+195
203	820	Female	White	J1c2r
204	821	Female	White	H27c
205	822	Female	White	U5a2a2
206	823	Female	White	H1e1b1
207	824	Female	White	HV0+195
208	825	Female	White	H
209	826	Male	White	K1c2
210	827	Male	White	H1c
211	828	Female	White	H1a1
212	829	Male	Indian	U2c1b
213	830	Male	White	H1b1+16362
214	831	Female	White	U5a1b1
215	832	Female	White	U5b3b1
216	833	Male	Indian	R6a2

217	834	Male	White	H3ap
218	835	Female	White	H11a2a1
219	836	Female	White	H11a2a
220	837	Female	White	H3
221	838	Female	White	H70
222	839	Male	White	H56
223	840	Male	White	V2c
224	841	Female	White	K1a4a1a2b
225	842	Female	White	J1c2
226	843	Male	White	T2c1+146
227	844	Female	White mixed	U5b1d1b
228	845	Female	White	U4a2b
229	846	Female	White	U5a1i1
230	847	Female	White	H1au1a
231	848	Female	Asian European	R0a1a
232	849	Female	White	X2b+226
233	850	Female	White	H
234	851	Female	White	V15a
235	852	Female	White	T2e
236	853	Male	White	K1a1b1f
237	854	Female	Bangladeshi	H14a+146
238	855	Female	White	H2a2a1
239	856	Female	White	U5a1b1g
240	857	Female	White	U5b2a1b
241	858	Male	White	M1a3b
242	859	Female	White	U5a1f1a1
243	860	Female	White	U5b1+16189+@16192
244	861	Male	White	T2a1b1a1b
245	862	Male	White	H5a1c1a
246	863	Female	White	T2b
247	864	Female	White	T2b17a
248	865	Male	White	U5a1+@16192
249	866	Male	White	I1a1
250	867	Male	White	T2a1a
251	868	Male	White	H
252	869	Female	White	H1c3
253	870	Female	White	U5a1f1a1
254	871	Male	White	U3a1
255	872	Female	White	I5a2
256	873	Male	White	T1a1
257	874	Male	White	X2b5
258	875	Male	White	H3aq
259	876	Female	White	U5b1c1
260	877	Female	White	H45b

261	878	Female	White	U5a1h
262	879	Male	White	H6a1b3
263	880	Female	Portuguese, Black, Indian	L3d5a
264	881	Male	White	K1c1
265	882	Female	White	K1c2
266	883	Male	White	K1c1
267	884	Male	White	U4b1b1a
268	885	Female	White	V19
269	886	Female	Mixed	H3
270	887	Male	White	U4b1b1
271	889	Male	White	U8b
272	890	Female	White	H1af1b
273	891	Female	White	K2a
274	892	Female	White	H31a
275	893	Female	White	W1+119
276	894	Female	White	X2c1
277	895	Female	White	V15a
278	896	Female	Indian Malaysian	R30b2
279	897	Female	White	H13a
280	898	Female	White	H6a2a
281	899	Female	White	H1bs
282	900	Female	White	H8c2
283	901	Female	White	U5a2a1+152
284	902	Female	White	H1+16239
285	903	Female	Indian	R5a2b4
286	904	Female	White	J2a1a1a2
287	905	Female	White	H24a
288	906	Male	White	H6c
289	907	Female	White	K1a4a1a2b
290	908	Female	White	J1c1c
291	909	Female	White	H10a1a
292	910	Male	White	H5a1g1
293	911	Female	White	T1a1a1
294	912	Female	White	U5b2a1a+16311
295	913	Male	White	J1c3g
296	914	Female	White	H16
297	915	Male	Black African	L2a1b1a
298	916	Male	White	U5a2+16362
299	918	Female	White	U5a1h
300	919	Female	White	H1bz
301	920	Female	Mixed	W5
302	921	Female	White	H1c
303	922	Female	White	H1
304	923	Female	White	U5a1a1

305	924	Female	White	H1m
306	925	Male	White	J1c2
307	926	Male	White	H5a
308	927	Male	White	U5b
309	928	Male	White	K1d
310	929	Female	White	U1b3
311	930	Female	White	H7
312	931	Female	White	H5
313	932	Female	White	H1n3
314	933	Female	White	K1a4a1
315	934	Female	White	K1a30a
316	935	Female	White	J1c1c
317	936	Female	White	U4b1b1a
318	937	Female	White	H3b1a
319	938	Female	White	H3ar
320	939	Female	White	H5b4
321	940	Female	White	H3
322	941	Male	Indian	HV2
323	942	Female	White	K1a1b1a
324	943	Female	White	X2+225+@16223
325	944	Female	White	H1b1e
326	945	Male	White	H5b1
327	946	Male	Indian	H
328	947	Male	White	T2e
329	948	Male	White	J1c8a
330	949	Male	White	U5a1d1
331	950	Female	White	T2a1b1a
332	951	Female	White	H8+(114)+152
333	952	Female	Indian	W6
334	953	Male	White	J1c3
335	954	Female	White	H11a1
336	955	Male	White	H11a1
337	956	Female	White	H1am
338	957	Male	Indian	R5a2b
339	958	Male	White	V15a
340	959	Male	White	HV0d
341	960	Female	White	H1a
342	961	Female	White	H17
343	962	Female	White	J1c3f
344	963	Male	Chinese White	J1c3f
345	964	Female	White	HV4a1
346	965	Female	White	H4a1a2a
347	966	Male	White	H1j
348	967	Male	White	T2b

349	968	Female	White	H65a
350	969	Male	White	H2
351	970	Male	White	H2a2a2
352	971	Male	White	A2+(64)
353	972	Male	White	H1+16189
354	973	Female	White	V15a
355	974	Female	White	D1
356	975	Male	White	U5b2a1a1
357	976	Male	White	H14b1
358	977	Female	White	K2a3
359	978	Female	White	J1c2c1
360	979	Male	White	HV0a
361	980	Male	White	L3e5
362	981	Male	White	H5
363	982	Female	White	H1au1a
364	983	Male	White	HV9a
365	984	Female	White	H1j
366	985	Male	White	U2e1a1
367	986	Male	White	H1g1
368	987	Female	White	K1a+150
369	988	Male	White	T2b2b1
370	989	Female	White	I2a2
371	990	Male	Chinese	R9c1a
372	991	Female	White	H2
373	992	Female	White	H1ai
374	994	Male	Indian	M30c
375	995	Female	White	V10a
376	996	Female	White	J1c1a
377	997	Female	White	H1c3
378	998	Female	White	H1g1
379	999	Female	White	T2
380	000	Female	White	H11a+152
382	617	Male	White	H7b
381	618	Female	White	U2e2a1a
383	620	Male	White	U5a1i1
384	621	Female	White	U2e1'2'3

Appendix 3

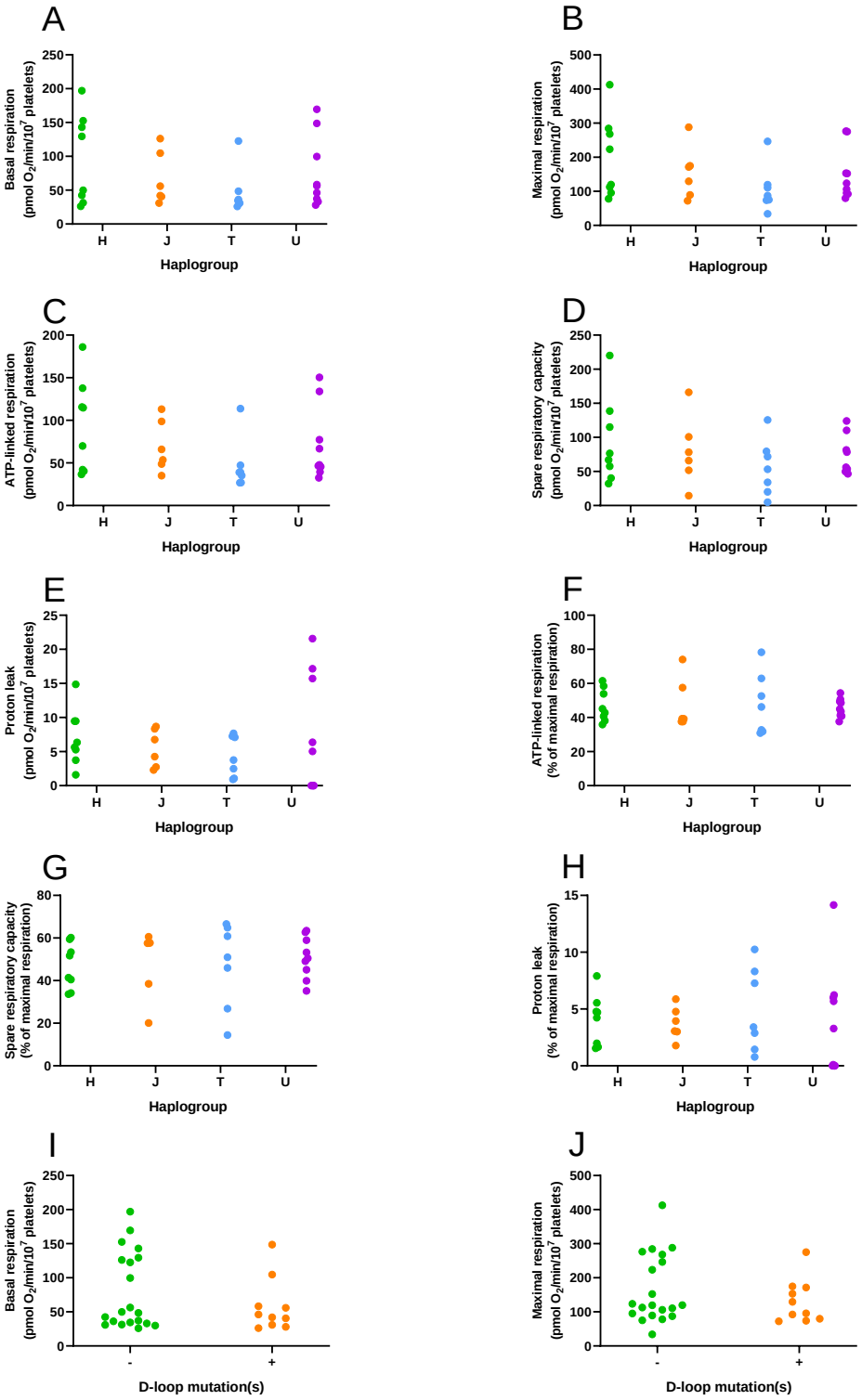

Appendix 3A. Basal platelet mitochondrial function. Extracellular flux analyses of platelets from 30 donors of haplogroups H, J, T and U were performed. A-H: variation in basal mitochondrial function parameters between haplogroups. I-J: Variation in basal (I) and maximal (J) respiration between platelets from donors with (+) and without (-) D-loop mutations cited to effect mtDNA copy number (16192T, 16189C, 295T) (Ebner *et al.*, 2011; Suissa *et al.*, 2009).

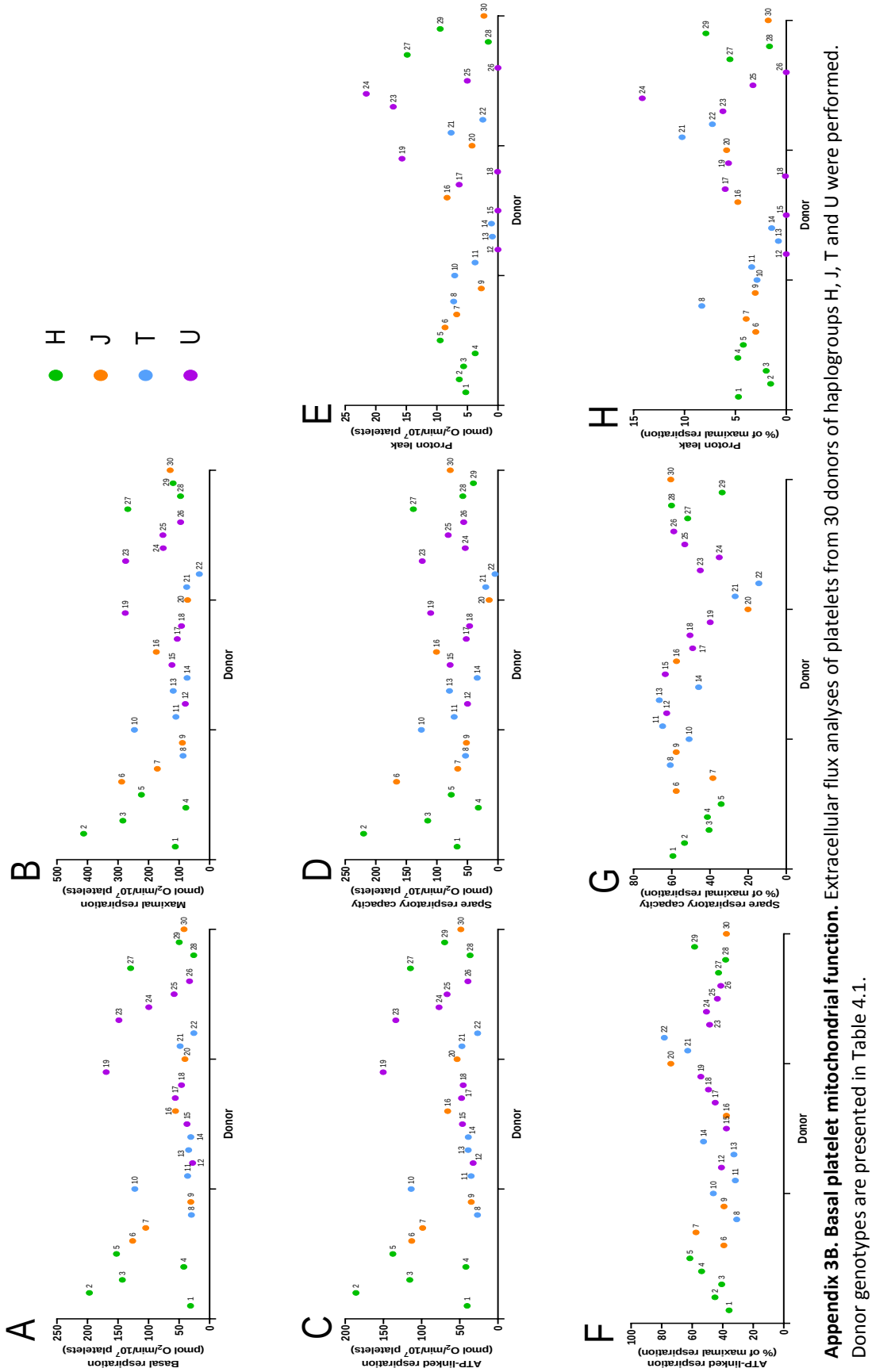

Appendix 3B. Basal platelet mitochondrial function. Extracellular flux analyses of platelets from 30 donors of haplogroups H, J, T and U were performed. Donor genotypes are presented in Table 4.1.

Appendix 4

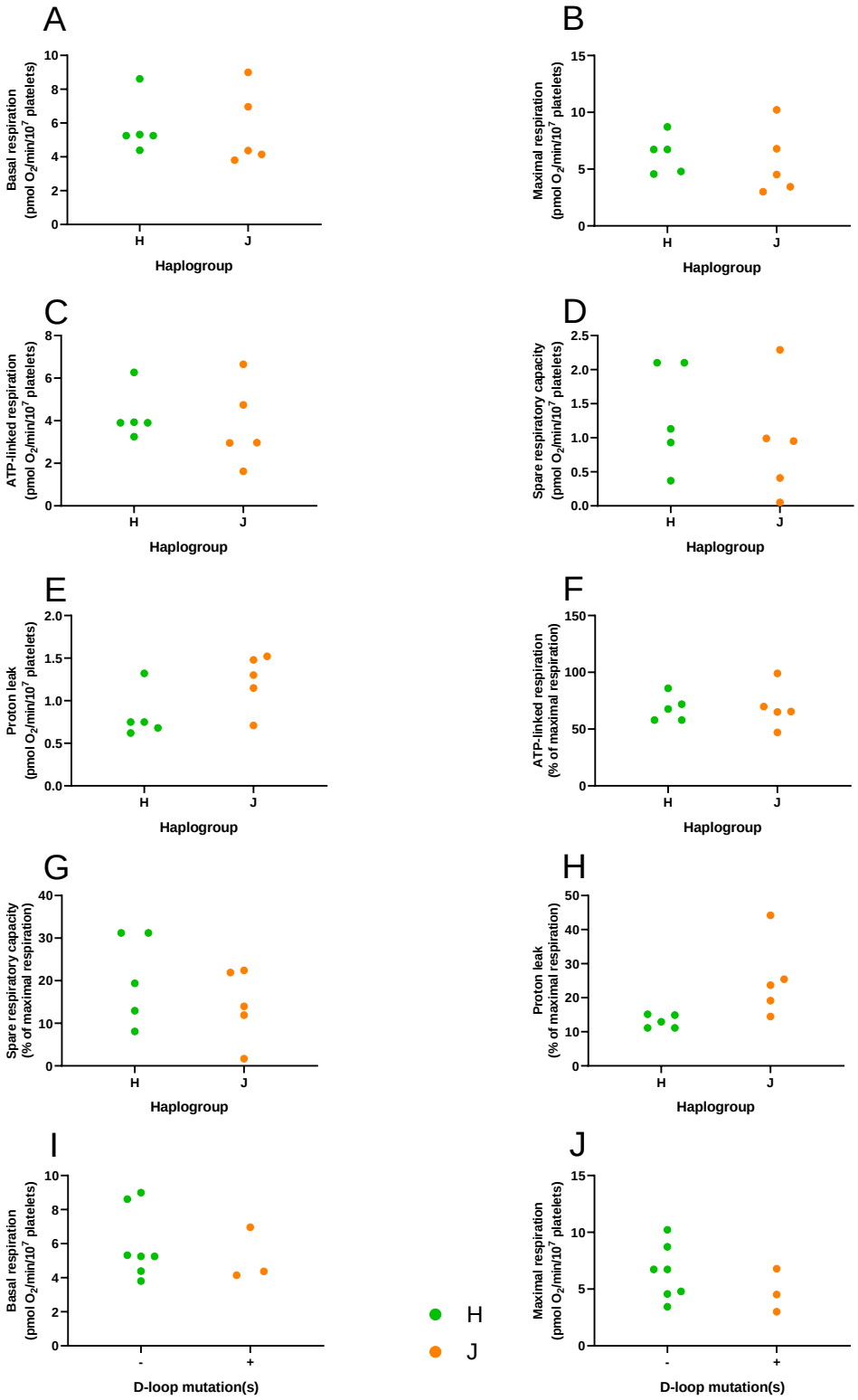

Appendix 4A. Basal cybrid mitochondrial function. A-H: Extracellular flux analyses of five cybrid populations derived from volunteer platelets of haplogroup H and five cybrid populations derived from volunteer platelets of haplogroup J. I-J: Variation in basal (I) and maximal (J) respiration between cybrids derived from donors with (+) and without (-) D-loop mutations cited to effect mtDNA copy number (16192T, 16189C, 295T) (Ebner *et al.*, 2011; Suissa *et al.*, 2009).

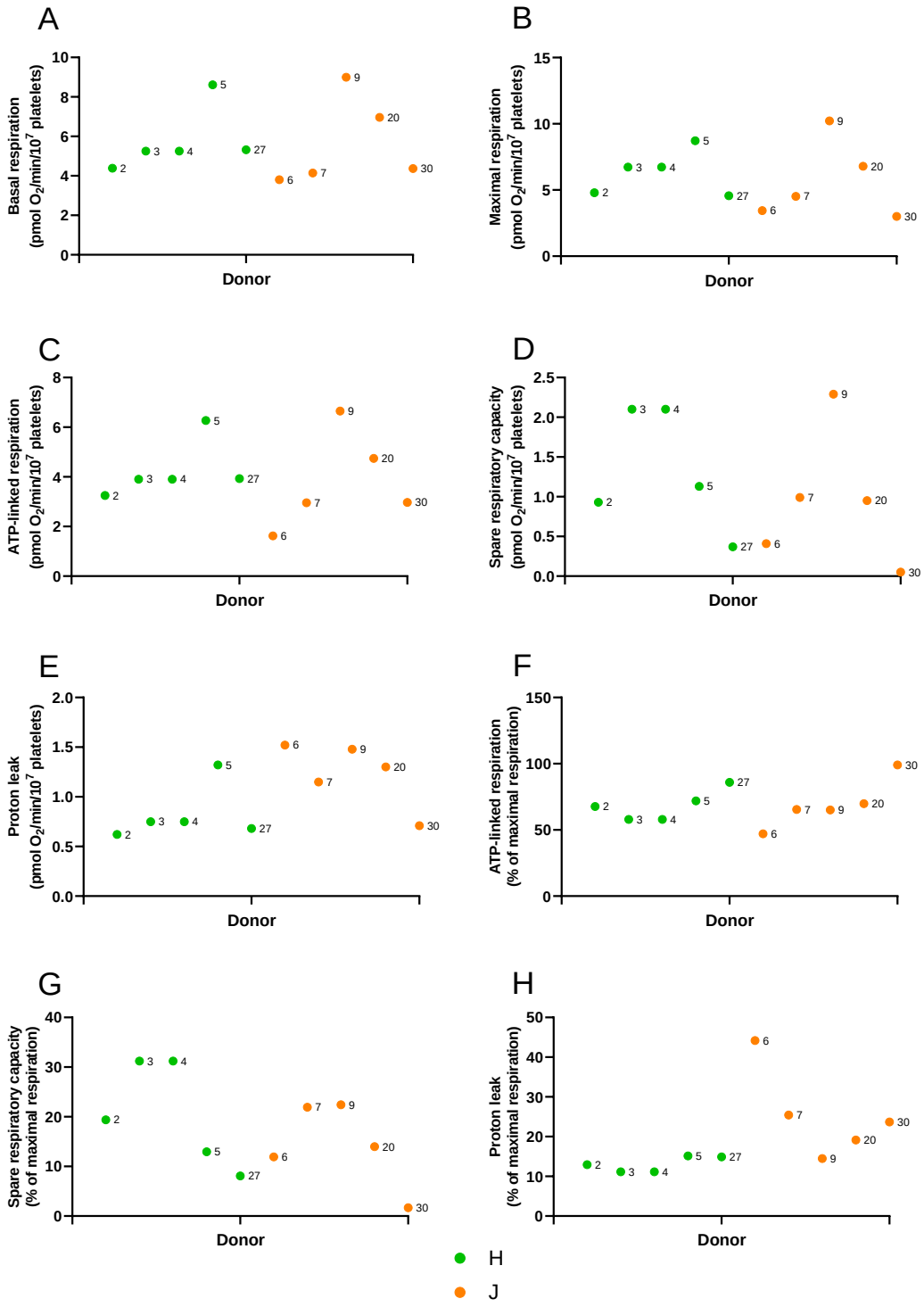

Appendix 4B. Basal cybrid mitochondrial function. Extracellular flux analyses of five cybrid populations derived from volunteer platelets of haplogroup H and five cybrid populations derived from volunteer platelets of haplogroup J. Donor genotypes are presented in Table 6.2.

Appendix 5

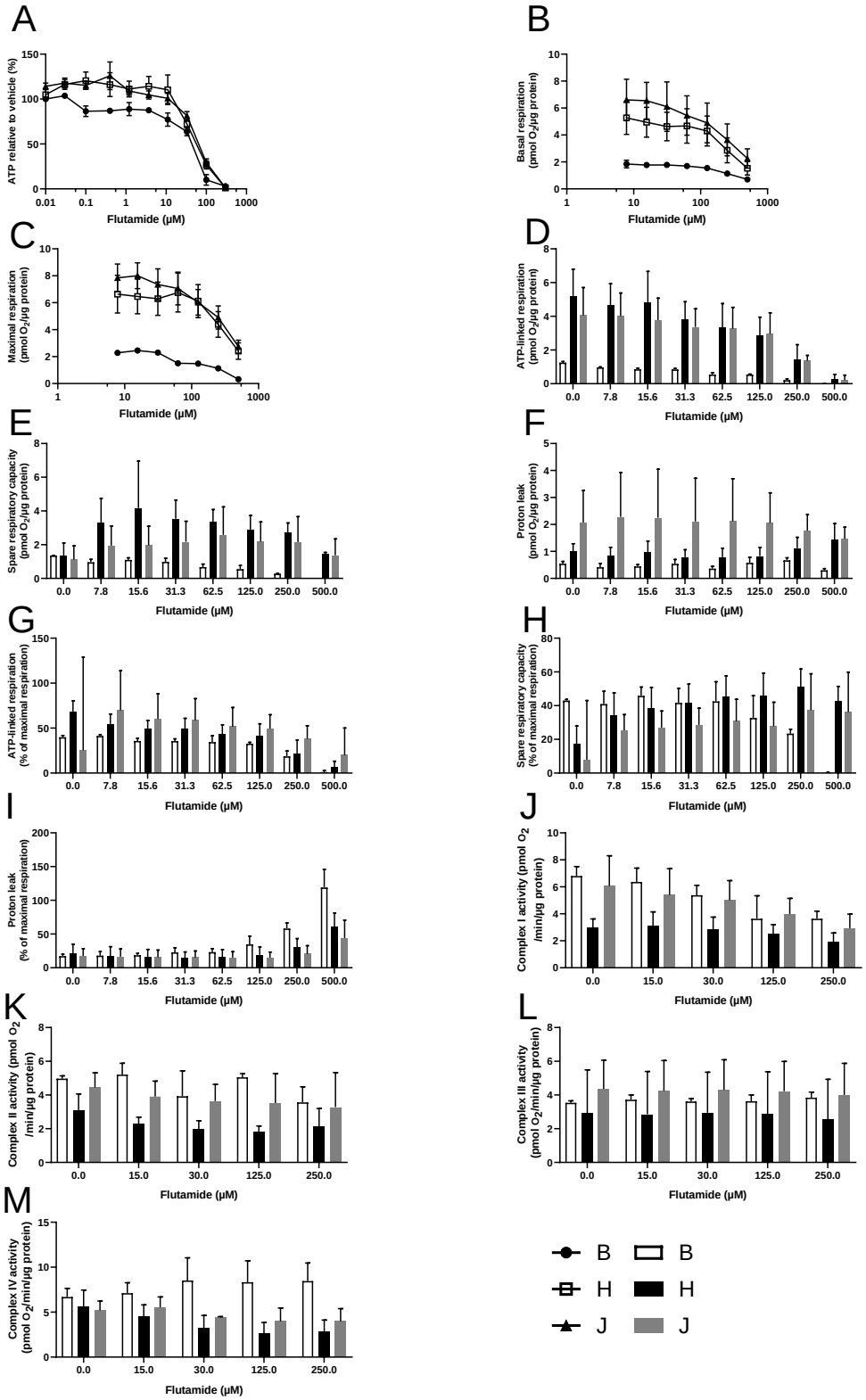

Appendix 5A. Comparison of flutamide-induced changes in mitochondrial function between the parental HepG2 cell line (haplogroup B) and haplogroup H and J HepG2 cybrids. A: ATP assay following 2 h flutamide treatment in galactose medium (Section 6.2.4). B-I: mitochondrial stress test using extracellular flux analysis. J-M: respiratory complex activity measured using extracellular flux analysis (Section 6.2.5).

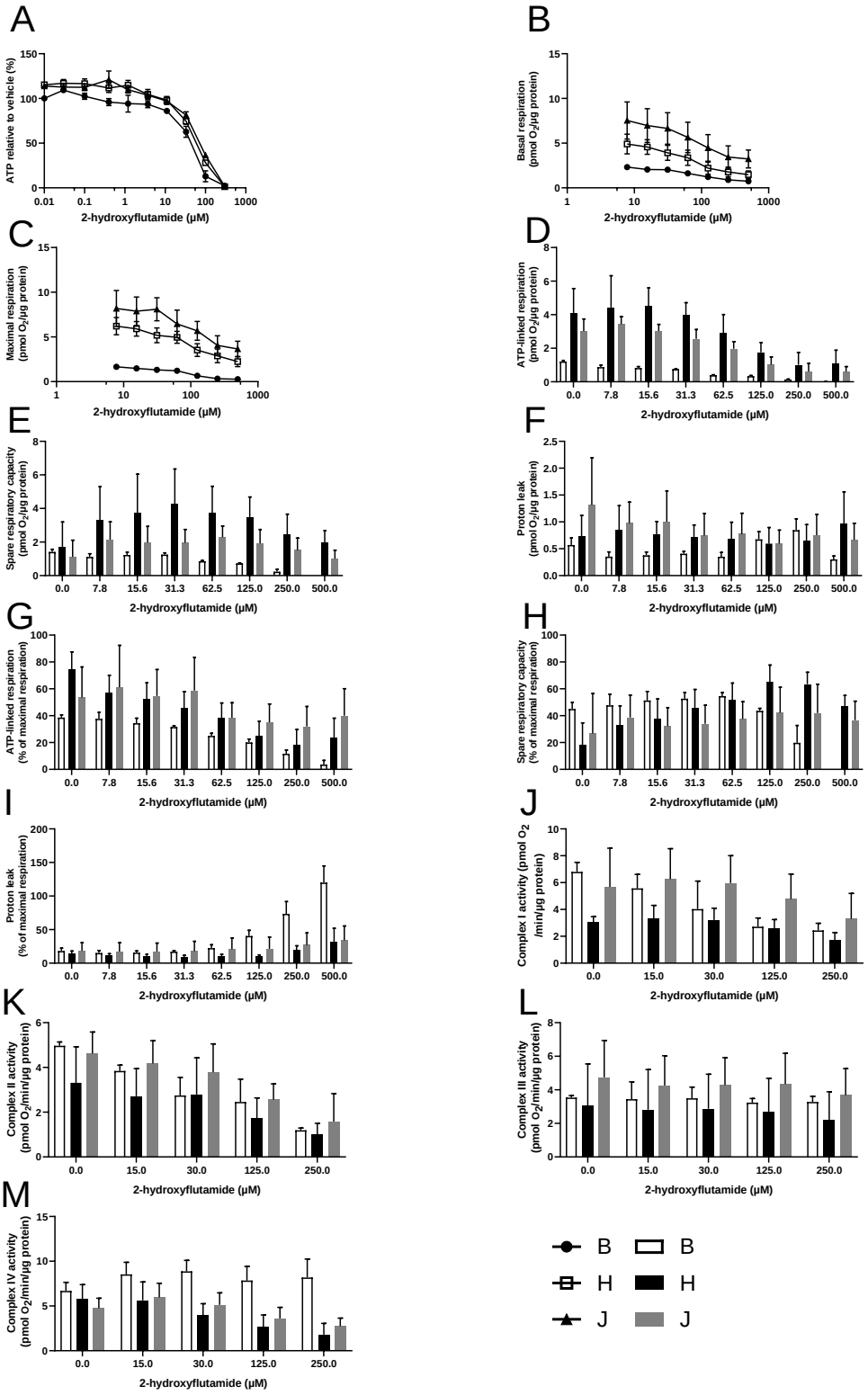

Appendix 5B. Comparison of 2-hydroxyflutamide-induced changes in mitochondrial function between the parental HepG2 cell line (haplogroup B) and haplogroup H and J HepG2 cybrids. A: ATP assay following 2 h 2-hydroxyflutamide treatment in galactose medium (Section 6.2.4). B-I: mitochondrial stress test using extracellular flux analysis. J-M: respiratory complex activity measured using extracellular flux analysis (Section 6.2.5).

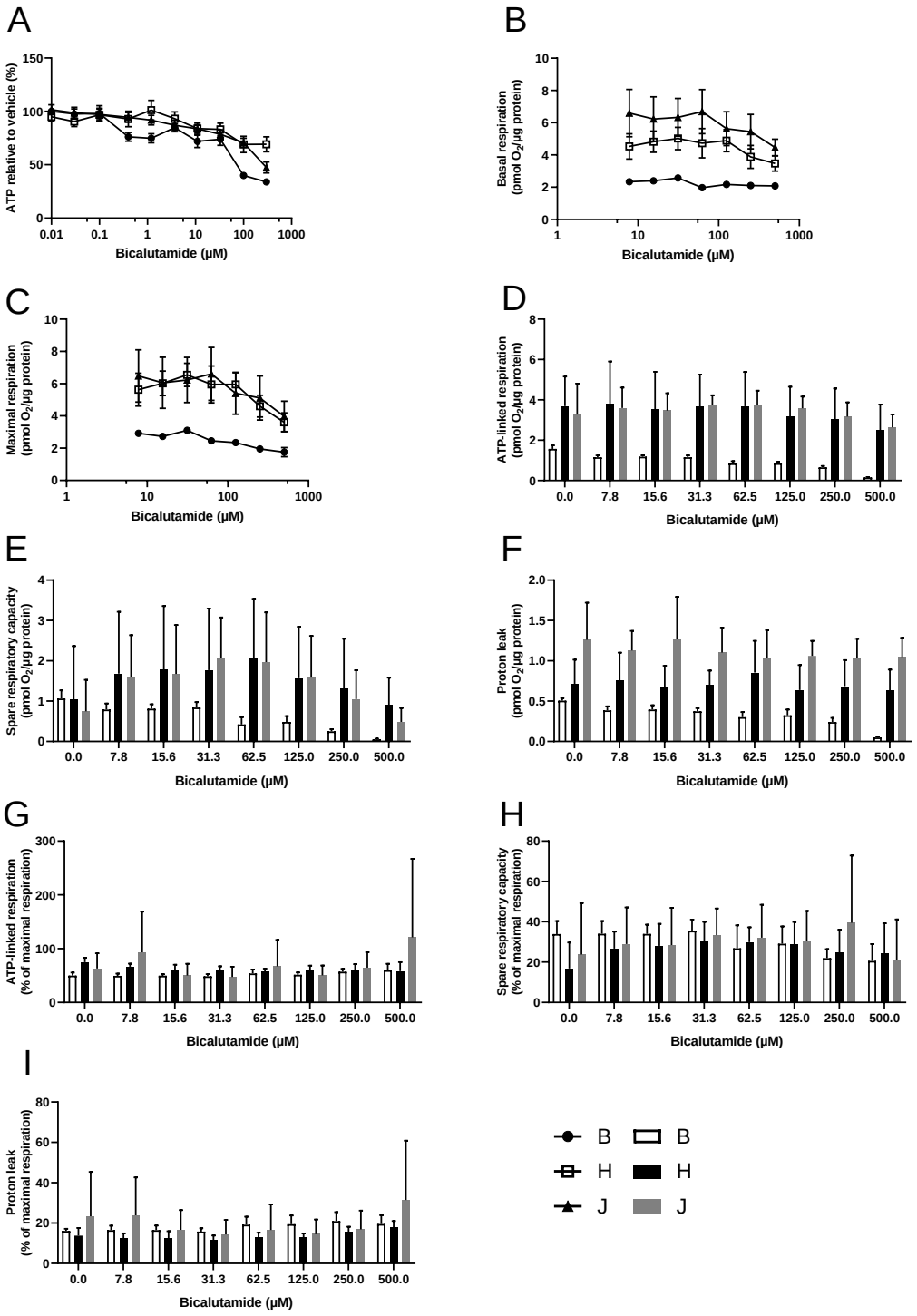

Appendix 5C. Comparison of bicalutamide-induced changes in mitochondrial function between the parental HepG2 cell line (haplogroup B) and haplogroup H and J HepG2 cybrids. A: ATP assay following 2 h bicalutamide treatment in galactose medium (Section 6.2.4). B-I: mitochondrial stress test using extracellular flux analysis (Section 6.2.5).

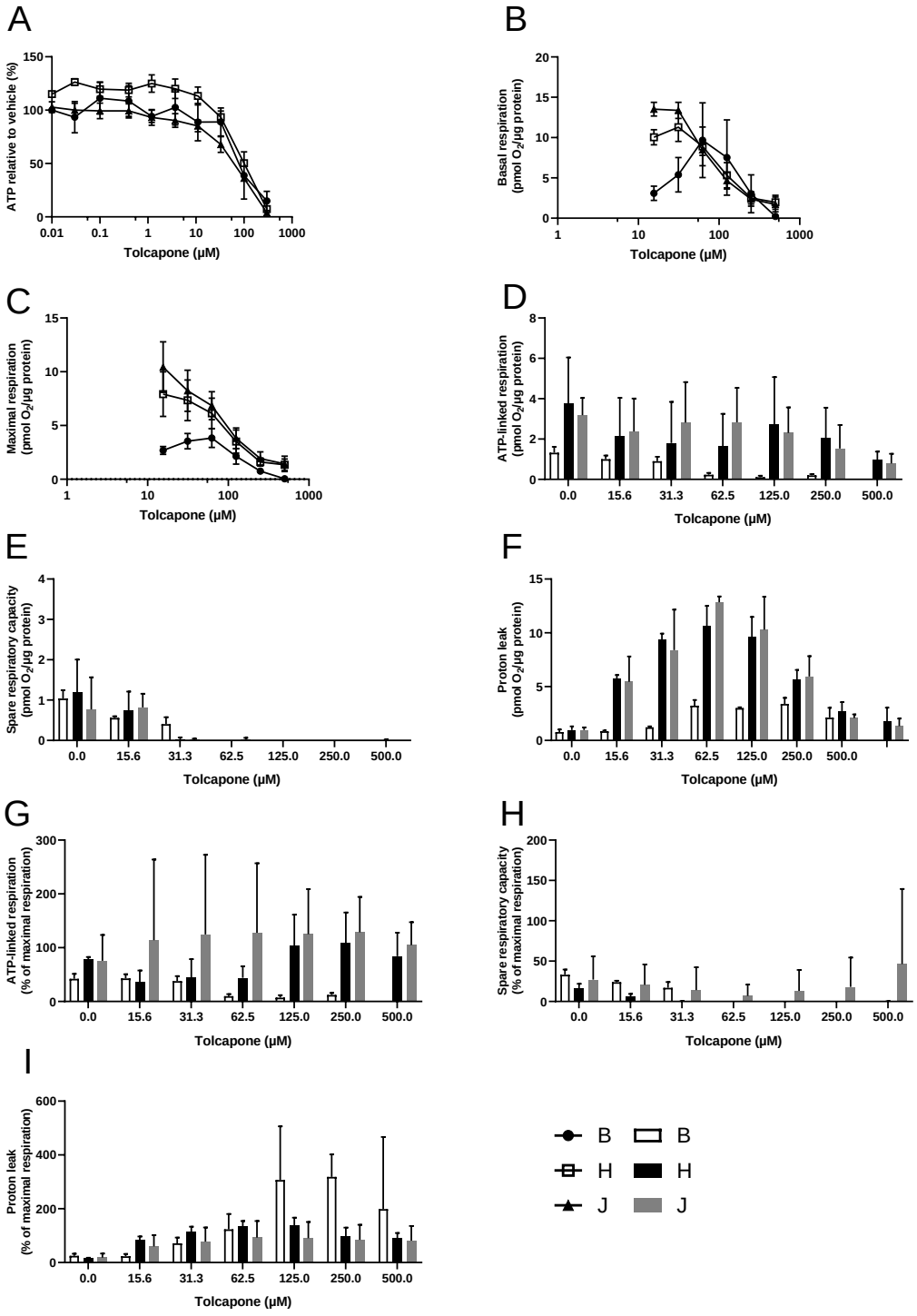

Appendix 5D. Comparison of tolcapone-induced changes in mitochondrial function between the parental HepG2 cell line (haplogroup B) and haplogroup H and J HepG2 cybrids. A: ATP assay following 2 h tolcapone treatment in galactose medium (Section 6.2.4). B-I: mitochondrial stress test using extracellular flux analysis (Section 6.2.5).

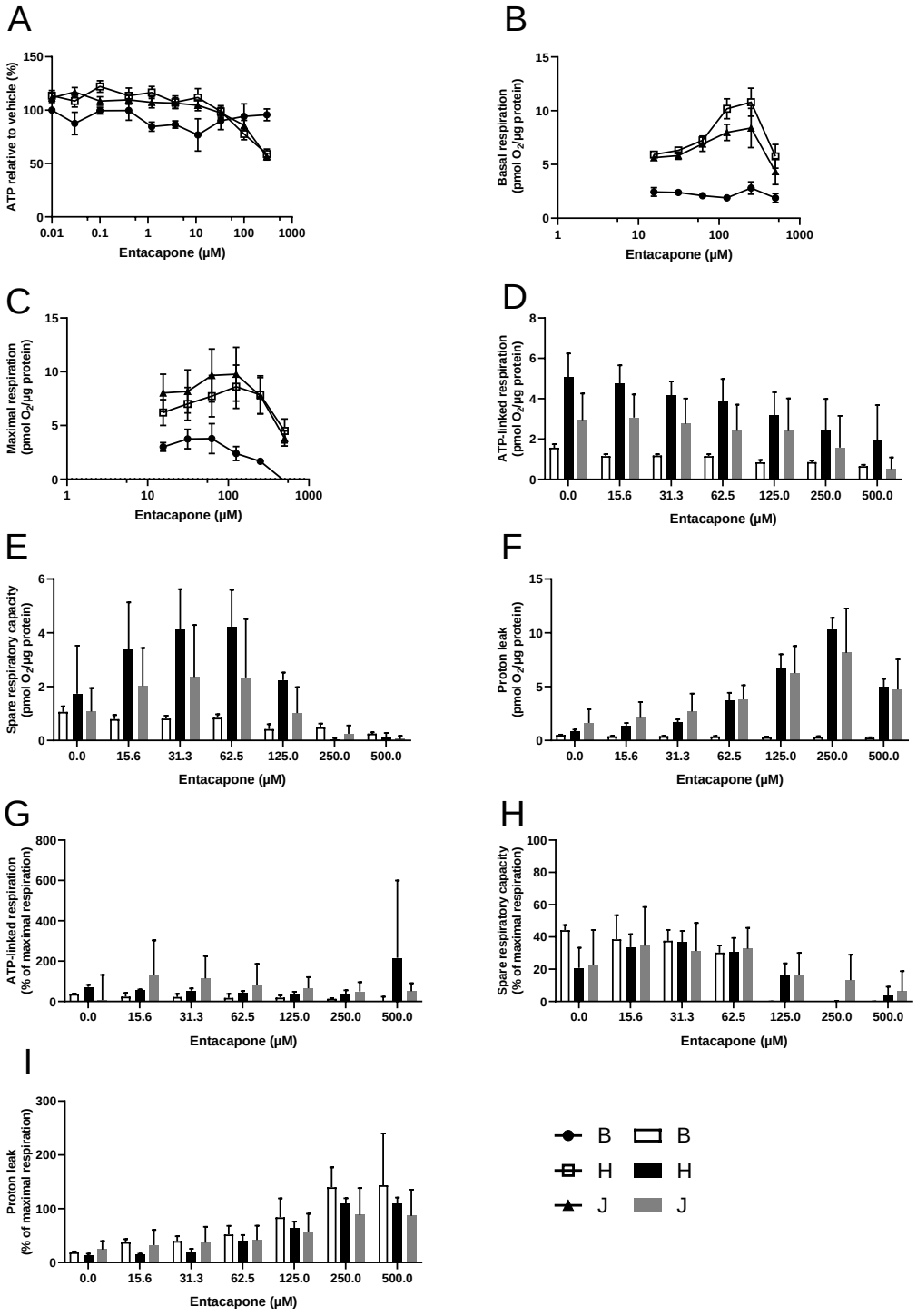

Appendix 5E. Comparison of entacapone-induced changes in mitochondrial function between the parental HepG2 cell line (haplogroup B) and haplogroup H and J HepG2 cybrids. A: ATP assay following 2 h entacapone treatment in galactose medium (Section 6.2.4). B-I: mitochondrial stress test using extracellular flux analysis (Section 6.2.5).

Bibliography

Acin-Perez, R. and Enriquez, J.A. (2014) The function of the respiratory supercomplexes: The plasticity model. *Biochim. Biophys. Acta - Bioenerg.*, **1837**, 444–450.

Agilent How Seahorse Analyzers Measure Extracellular Flux. *Agil. [date accessed 23-07-2018]*.

Alberts, B., Johnson, A., Lewis, J., Walter, P., Raff, M., and Roberts, K. (2002) Molecular Biology of the Cell 4th Edition: International Student Edition.

Aleo, M.D., Luo, Y., Swiss, R., Bonin, P.D., Potter, D.M., and Will, Y. (2014) Human drug-induced liver injury severity is highly associated with dual inhibition of liver mitochondrial function and bile salt export pump. *Hepatology*, **60**, 1015–1022.

Alexeyev, M.F. (2009) Is there more to aging than mitochondrial DNA and reactive oxygen species? *FEBS J.*, **276**, 5768–5787.

Amo, T., Yadava, N., Oh, R., Nicholls, D.G., and Brand, M.D. (2008) Experimental assessment of bioenergetic differences caused by the common European mitochondrial DNA haplogroups H and T. *Gene*, **411**, 69–76.

Amuthan, G., Biswas, G., Ananadatheerthavarada, H.K., Vijayasarathy, C., Shephard, H.M., and Avadhani, N.G. (2002) Mitochondrial stress-induced calcium signaling, phenotypic changes and invasive behavior in human lung carcinoma A549 cells. *Oncogene*, **21**, 7839–7849.

Analytical, A. (2017) Fragment Analyzer. *https://www.aati-us.com/documents/brochures/fragment-analyzer-brochure.pdf [date accessed: 10-10-2018]*.

Andreyev, A.Y., Kushnareva, Y.E., and Starkov, A.A. (2005) Mitochondrial metabolism of reactive oxygen species. *Biochemistry. (Mosc).*, **70**, 200–214.

Archer, S.L. (2013) Mitochondrial dynamics—mitochondrial fission and fusion in human diseases. *N. Engl. J. Med.*, **369**, 2236–2251.

Arduíno, D.M., Esteves, A.R., Swerdlow, R.H., and Cardoso, S.M. (2015) A Cybrid Cell Model for the Assessment of the Link Between Mitochondrial Deficits and Sporadic Parkinson's Disease. *Methods Mol. Biol.*, **1265**, 415–424.

Arias, I.M., Wolkoff, A.W., Boyer, J.L., Shafritz, D.A., Fausto, N., Alter, H.J., and Cohen, D.E. (2011) The liver: biology and pathobiology John Wiley & Sons.

Attardi, G., King, M.P., Chomyn, A., and Loguercio-Polosa, P. (1991) Novel genetic and molecular approaches to the study of mitochondrial biogenesis and mitochondrial diseases in human cells. *Prog Neuropathol*, **7**, 75–92.

Bacon, B.R., O'Grady, J.G., Di Bisceglie, A.M., and Lake, J.R. (2006) Comprehensive clinical hepatology Elsevier Ltd.

Baldwin, G.S., Murphy, V.J., Yang, Z., and Hashimoto, T. (1998) Binding of nonsteroidal antiinflammatory drugs to the alpha-subunit of the trifunctional protein of long chain fatty acid oxidation. *J. Pharmacol. Exp. Ther.*, **286**, 1110–1114.

Bale, S.S. *et al.* (2014) In Vitro Platforms for Evaluating Liver Toxicity. *Exp. Biol. Med. (Maywood).*, **239**, 1180–1191.

Ball, A.L., Kamalian, L., Alfirevic, A., Lyon, J.J., and Chadwick, A.E. (2016) Identification of the Additional Mitochondrial Liabilities of 2-Hydroxyflutamide When Compared With its Parent Compound, Flutamide in HepG2 Cells. *Toxicol Sci*.

Ball, A.L., Kamalian, L., E, J.C., and Chadwick, A.E. (2018) Evaluating Mitotoxicity as Either a Single or Multi-Mechanistic Insult in the Context of Hepatotoxicity. *Mitochondrial Dysfunct. Caused by Drugs Environ. Toxicants*.

Begriche, K., Massart, J., Robin, M.-A., Borgne-Sanchez, A., and Fromenty, B. (2011) Drug-induced toxicity on mitochondria and lipid metabolism: mechanistic diversity and deleterious consequences for the liver. *J. Hepatol.*, **54**, 773–794.

Bellizzi, D., D'Aquila, P., Giordano, M., Montesanto, A., and Passarino, G. (2012) Global DNA methylation levels are modulated by mitochondrial DNA variants. *Epigenomics*, **4**, 17–27.

Bellizzi, D., Cavalcante, P., Taverna, D., Rose, G., Passarino, G., Salvioli, S., Franceschi, C., and De Benedictis, G. (2006) Gene expression of cytokines and cytokine receptors is modulated by the common variability of the mitochondrial DNA in cybrid cell lines. *Genes Cells*, **11**, 883–891.

Benabou, R. and Waters, C. (2003) Hepatotoxic profile of catechol-O-methyltransferase inhibitors in Parkinson's disease. *Expert Opin. Drug Saf.*, **2**, 263–267.

Berg, J.M., Tymoczko, J.L., Stryer, L., and Stryer, L. (2002) Biochemistry, Ed 5th.

Boelsterli, U.A. and Lim, P.L.K. (2007) Mitochondrial abnormalities—a link to idiosyncratic drug hepatotoxicity? *Toxicol. Appl. Pharmacol*, **220**, 92–107.

Bogenhagen, D. and Clayton, D.A. (1977) Mouse L cell mitochondrial DNA molecules are selected randomly for replication throughout the cell cycle. *Cell*, **11**, 719–727.

Boudreau, L.H. *et al.* (2014) Platelets release mitochondria serving as substrate for bactericidal group IIA-secreted phospholipase A_2 to promote inflammation. *Blood*, **124**, 2173–2183.

Brand, M.D. and Nicholls, D.G. (2011) Assessing mitochondrial dysfunction in cells. *Biochem. J.*, **435**, 297–312.

Brand, M.D. (2010) The sites and topology of mitochondrial superoxide production. *Exp. Gerontol.*, **45**, 466–472.

Buchet, K. and Godinot, C. (1998) Functional F1-ATPase essential in maintaining growth and membrane potential of human mitochondrial DNA-depleted rho degrees cells. *J. Biol. Chem.*, **273**, 22983–22989.

Buchser, W., Collins, M., Garyantes, T., Guha, R., Haney, S., Lemmon, V., Li, Z., and Trask, O.J. (2014) Assay development guidelines for image-based high content screening, high content analysis and high content imaging.

Calabrese, C., Simone, D., Diroma, M.A., Santorsola, M., Gutta, C., Gasparre, G., Picardi, E., Pesole, G., and Attimonelli, M. (2014) MToolBox: a highly automated pipeline for heteroplasmy annotation and prioritization analysis of human mitochondrial variants in high-throughput sequencing. *Bioinformatics*, **30**, 3115–3117.

Calvo, S.E. and Mootha, V.K. (2010) The mitochondrial proteome and human disease. *Annu. Rev. Genomics Hum. Genet.*, **11**, 25–44.

Canter, J.A., Haas, D.W., Kallianpur, A.R., Ritchie, M.D., Robbins, G.K., Shafer, R.W., Clifford, D.B., Murdock, D.G., and Hulgan, T. (2007) The mitochondrial pharmacogenomics of haplogroup T: MTND2[ast]LHON4917G and antiretroviral therapy-associated peripheral neuropathy. *Pharmacogenomics J*, **8**, 71–77.

Canter, J.A. *et al.* (2010) African mitochondrial DNA subhaplogroups and peripheral neuropathy during antiretroviral therapy. *J Infect Dis*, **201**, 1703–1707.

Cao, Y., Bryan, T.M., and Reddel, R.R. (2008) Increased copy number of the TERT and TERC telomerase subunit genes in cancer cells. *Cancer Sci.*, **99**, 1092–1099.

Carr, I.M., Robinson, J.I., Dimitriou, R., Markham, A.F., Morgan, A.W., and Bonthron, D.T. (2009) Inferring relative proportions of DNA variants from sequencing electropherograms. *Bioinformatics*, **25**, 3244–3250.

Chacko, B.K., Kramer, P.A., Ravi, S., Johnson, M.S., Hardy, R.W., Ballinger, S.W., and Darley-Usmar, V.M. (2013) Methods for defining distinct bioenergetic profiles in platelets, lymphocytes, monocytes, and neutrophils, and the oxidative burst from human blood. *Lab. Invest.*, **93**, 690–700.

Chalasani, N. and Bjornsson, E. (2010) Risk Factors for Idiosyncratic Drug-Induced Liver Injury. *Gastroenterology*, **138**, 2246–2259.

Chen, A., Raule, N., Chomyn, A., and Attardi, G. (2012) Decreased reactive oxygen species production in cells with mitochondrial haplogroups associated with longevity. *PLoS One*, **7**.

Chen, H., Detmer, S.A., Ewald, A.J., Griffin, E.E., Fraser, S.E., and Chan, D.C. (2003) Mitofusins Mfn1 and Mfn2 coordinately regulate mitochondrial fusion and are essential for embryonic development. *J. Cell Biol.*, **160**, 189–200.

Chen, J. *et al.* (2007) Maternally inherited aminoglycoside-induced and nonsyndromic hearing loss is associated with the 12S rRNA C1494T mutation in three Han Chinese pedigrees. *Gene*, **401**, 4–11.

Chevallet, M., Lescuyer, P., Diemer, H., Van Dorsselaer, A., Leize-Wagner, E., and Rabilloud, T. (2006) Alterations of the mitochondrial proteome caused by the absence of mitochondrial DNA: A proteomic view. *Electrophoresis*, **27**, 1574–1583.

Chinnery, P.F. and Gomez-Duran, A. (2018) Oldies but Goldies mtDNA Population Variants and Neurodegenerative Diseases. *Front. Neurosci.*, **12**, 682.

Chinnery, P.F. and Hudson, G. (2013) Mitochondrial genetics. *Br. Med. Bull.*, **106**, 135–159.

Chomyn, A., Lai, S.T., Shakeley, R., Bresolin, N., Scarlato, G., and Attardi, G. (1994) Platelet-mediated transformation of mtDNA-less human cells: analysis of phenotypic variability among clones from normal individuals--and complementation behavior of the tRNALys mutation causing myoclonic epilepsy and ragged red fibers. *Am. J. Hum. Genet.*, **54**, 966–974.

Chu, C.W., Hwang, S.J., Luo, J.C., Tsay, S.H., Li, C.P., Huang, Y.S., Chang, F.Y., and Lee, S.D. (1998) Flutamide-induced liver injury: a case report. *Chin. Med. J*, **61**, 678–682.

Cockshott, I.D. (2004) Bicalutamide: clinical pharmacokinetics and metabolism. *Clin Pharmacokinet*, **43**, 855–878.

Coe, K.J. *et al.* (2007) Comparison of the cytotoxicity of the nitroaromatic drug flutamide to its cyano analogue in the hepatocyte cell line TAMH: evidence for complex I inhibition

and mitochondrial dysfunction using toxicogenomic screening. *Chem Res Toxicol*, **20**, 1277–1290.

Coe, K.J. (2008) Metabolism and Cytotoxicity of the Nitroaromatic Drug Flutamide and Its Cyano Analog in Hepatocyte Cell Lines ProQuest.

Couvillion, M.T., Soto, I.C., Shipkovenska, G., and Churchman, L.S. (2016) Synchronized mitochondrial and cytosolic translation programs. *Nature*, **533**, 499–503.

Czarnecka, A.M. *et al.* (2010) Mitochondrial NADH-dehydrogenase subunit 3 (ND3) polymorphism (A10398G) and sporadic breast cancer in Poland. *Breast Cancer Res. Treat.*, **121**, 511–518.

Deschamps, D., DeBeco, V., Fisch, C., Fromenty, B., Guillouzo, A., and Pessayre, D. (1994) Inhibition by perhexiline of oxidative phosphorylation and the beta-oxidation of fatty acids: possible role in pseudoalcoholic liver lesions. *Hepatology*, **19**, 948–961.

Devlin, T.M. (2011) Textbook of biochemistry John Wiley & Sons,.

Dickinson, A., Yeung, K.Y., Donoghue, J., Baker, M.J., Kelly, R.D.W., McKenzie, M., Johns, T.G., and St. John, J.C. (2013) The regulation of mitochondrial DNA copy number in glioblastoma cells. *Cell Death Differ.*, **20**, 1644–1653.

Ding, W.-X. and Yin, X.-M. (2012) Mitophagy: mechanisms, pathophysiological roles, and analysis. *Biol. Chem.*, **393**, 547–564.

Duncan, A.W., Dorrell, C., and Grompe, M. (2009) Stem Cells and Liver Regeneration. *Gastroenterology*, **137**, 466–481.

Dunham-Snary, K.J. and Ballinger, S.W. (2015) GENETICS. Mitochondrial-nuclear DNA mismatch matters. *Science*, **349**, 1449–1450.

Duvezin-Caubet, S. *et al.* (2006) Proteolytic processing of OPA1 links mitochondrial dysfunction to alterations in mitochondrial morphology. *J. Biol. Chem.*, **281**, 37972–37979.

Dykens, J.A., Jamieson, J.D., Marroquin, L.D., Nadanaciva, S., Xu, J.J., Dunn, M.C., Smith, A.R., and Will, Y. (2008) In vitro assessment of mitochondrial dysfunction and cytotoxicity of nefazodone, trazodone, and buspirone. *Toxicol. Sci.*, **103**, 335–345.

Dykens, J.A. and Will, Y. (2007) The significance of mitochondrial toxicity testing in drug development. *Drug Discov. Today*, **12**, 777–785.

Ebner, S. *et al.* (2011) Mitochondrial haplogroups, control region polymorphisms and malignant melanoma: a study in middle European Caucasians. *PLoS One*, **6**, e27192.

Elmore, S. (2007) Apoptosis: a review of programmed cell death. *Toxicol. Pathol.*, **35**, 495–516.

Ermak, G. and Davies, K.J.A. (2002) Calcium and oxidative stress: from cell signaling to cell death. *Mol. Immunol.*, **38**, 713–721.

Espinosa-Diez, C., Miguel, V., Mennerich, D., Kietzmann, T., Sánchez-Pérez, P., Cadenas, S., and Lamas, S. (2015) Antioxidant responses and cellular adjustments to oxidative stress. *Redox Biol.*, **6**, 183–197.

Eupedia (2016) European MtDNA Haplogroups Frequency. *http://www.eupedia.com/europe/european_mtdna_haplogroups_frequency.shtml*

[date accessed: 07-07-2016].

Fang, Y. and Eglen, R.M. (2017) Three-Dimensional Cell Cultures in Drug Discovery and Development. *Slas Discov.*, **22**, 456–472.

Fau, D., Eugene, D., Berson, A., Letteron, P., Fromenty, B., Fisch, C., and Pessayre, D. (1994) Toxicity of the antiandrogen flutamide in isolated rat hepatocytes. *J Pharmacol Exp Ther*, **269**, 954–962.

Faulkner, L., Gibson, A., Sullivan, A., Tailor, A., Usui, T., Alfirevic, A., Pirmohamed, M., Naisbitt, D.J., and Kevin Park, B. (2016) Detection of Primary T Cell Responses to Drugs and Chemicals in HLA-Typed Volunteers: Implications for the Prediction of Drug Immunogenicity. *Toxicol. Sci.*, **154**, 416–429.

Fernandez-Marcos, P.J. and Auwerx, J. (2011) Regulation of PGC-1alpha, a nodal regulator of mitochondrial biogenesis. *Am. J. Clin. Nutr.*, **93**, 88–90.

Ferraresi, R. *et al.* (2008) Resistance of mtDNA-depleted cells to apoptosis. *Cytometry. A*, **73**, 528–537.

Fillmore, N., Alrob, O.A., and Lopaschuk, G.D. (2011) Fatty Acid Beta-Oxidation. *AOCS Lipid Libr. doi*, **10**.

Fontana, R.J. (2014) Pathogenesis of Idiosyncratic Drug-Induced Liver Injury and Clinical Perspectives. *Gastroenterology*, **146**, 914–928.

Fromenty, B., Fisch, C., Labbe, G., Degott, C., Deschamps, D., Berson, A., Letteron, P., and Pessayre, D. (1990) Amiodarone inhibits the mitochondrial beta-oxidation of fatty acids and produces microvesicular steatosis of the liver in mice. *J. Pharmacol. Exp. Ther.*, **255**, 1371–1376.

Fromenty, B. and Pessayre, D. (1995) Inhibition of mitochondrial beta-oxidation as a mechanism of hepatotoxicity. *Pharmacol. Ther.*, **67**, 101–154.

Gamen, S., Anel, A., Montoya, J., Marzo, I., Piñeiro, A., and Naval, J. (1995) mtDNA-depleted U937 cells are sensitive to TNF and Fas-mediated cytototxicity. *FEBS Lett.*, **376**, 15–18.

Gao, W., Kim, J., and Dalton, J.T. (2006) Pharmacokinetics and Pharmacodynamics of Nonsteroidal Androgen Receptor Ligands. *Pharm. Res.*, **23**, 1641–1658.

Garcia-Ruiz, I., Solis-Munoz, P., Fernandez-Moreira, D., Munoz-Yague, T., and Solis-Herruzo, J.A. (2013) Pioglitazone leads to an inactivation and disassembly of complex I of the mitochondrial respiratory chain. *BMC Biol.*, **11**, 88.

Gaskell, H., Sharma, P., Colley, H.E., Murdoch, C., Williams, D.P., and Webb, S.D. (2016) Characterization of a functional C3A liver spheroid model. *Toxicol. Res. (Camb).*, **5**, 1053–1065.

Gellerich, F.N., Gizatullina, Z., Trumbeckaite, S., Nguyen, H.P., Pallas, T., Arandarcikaite, O., Vielhaber, S., Seppet, E., and Striggow, F. (2010) The regulation of OXPHOS by extramitochondrial calcium. *Biochim. Biophys. Acta - Bioenerg.*, **1797**, 1018–1027.

Gerets, H.H.J., Tilmant, K., Gerin, B., Chanteux, H., Depelchin, B.O., Dhalluin, S., and Atienzar, F.A. (2012) Characterization of primary human hepatocytes, HepG2 cells, and HepaRG cells at the mRNA level and CYP activity in response to inducers and their predictivity for the detection of human hepatotoxins. *Cell Biol. Toxicol.*, **28**, 69–87.

Ghelli, A. *et al.* (2009) The background of mitochondrial DNA haplogroup J increases the

sensitivity of Leber's hereditary optic neuropathy cells to 2,5-hexanedione toxicity. *PLoS One*, **4**, e7922.

Giorgio, V., Bisetto, E., Soriano, M.E., Dabbeni-Sala, F., Basso, E., Petronilli, V., Forte, M.A., Bernardi, P., and Lippe, G. (2009) Cyclophilin D Modulates Mitochondrial F(0)F(1)-ATP Synthase by Interacting with the Lateral Stalk of the Complex. *J. Biol. Chem.*, **284**, 33982–33988.

Godoy, P. *et al.* (2013) Recent advances in 2D and 3D in vitro systems using primary hepatocytes, alternative hepatocyte sources and non-parenchymal liver cells and their use in investigating mechanisms of hepatotoxicity, cell signaling and ADME. *Arch. Toxicol.*, **87**, 1315–1530.

Gomez-Duran, A., Pacheu-Grau, D., Martinez-Romero, I., Lopez-Gallardo, E., Lopez-Perez, M.J., Montoya, J., and Ruiz-Pesini, E. (2012) Oxidative phosphorylation differences between mitochondrial DNA haplogroups modify the risk of Leber's hereditary optic neuropathy. *Biochim. Biophys. Acta*, **1822**, 1216–1222.

Gómez-Durán, A., Pacheu-Grau, D., López-Gallardo, E., Díez-Sánchez, C., Montoya, J., López-Pérez, M.J., and Ruiz-Pesini, E. (2010) Unmasking the causes of multifactorial disorders: OXPHOS differences between mitochondrial haplogroups. *Hum. Mol. Genet.*, **19**, 3343–3353.

Gómez-Durán, A., Pacheu-Grau, D., Martínez-Romero, Í., López-Gallardo, E., López-Pérez, M.J., Montoya, J., and Ruiz-Pesini, E. (2012) Oxidative phosphorylation differences between mitochondrial DNA haplogroups modify the risk of Leber's hereditary optic neuropathy. *Biochim. Biophys. Acta - Mol. Basis Dis.*, **1822**, 1216–1222.

Gottesman, A., Milazzo, J., and Lazebnik, Y. (2010) V-fusion: a convenient, nontoxic method for cell fusion. *Biotechniques*, **49**, 747–750.

Grazioli, S. and Pugin, J. (2018) Mitochondrial Damage-Associated Molecular Patterns: From Inflammatory Signaling to Human Diseases. *Front. Immunol.*, **9**.

Greer, M.L., Barber, J., Eakins, J., and Kenna, J.G. (2010) Cell based approaches for evaluation of drug-induced liver injury. *Toxicology*, **268**, 125–131.

Gregoire, M., Morais, R., Quilliam, M.A., and Gravel, D. (1984) On auxotrophy for pyrimidines of respiration-deficient chick embryo cells. *Eur. J. Biochem.*, **142**, 49–55.

Grover, N. (2006) Principles of biochemistry.

Grünig, D., Felser, A., Bouitbir, J., and Krähenbühl, S. (2017) The catechol-O-methyltransferase inhibitors tolcapone and entacapone uncouple and inhibit the mitochondrial respiratory chain in HepaRG cells. *Toxicol. Vitr.*, **42**, 337–347.

Guzman-Fulgencio, M. *et al.* (2014) European mitochondrial haplogroups are not associated with hepatitis C virus (HCV) treatment response in HIV/HCV-coinfected patients. *HIV Med*, **15**, 425–430.

Guzy, R.D., Sharma, B., Bell, E., Chandel, N.S., and Schumacker, P.T. (2008) Loss of the SdhB, but Not the SdhA, subunit of complex II triggers reactive oxygen species-dependent hypoxia-inducible factor activation and tumorigenesis. *Mol. Cell. Biol.*, **28**, 718–731.

Halestrap, A.P. (2009) What is the mitochondrial permeability transition pore? *J. Mol. Cell. Cardiol.*, **46**, 821–831.

Hallberg, B.M. and Larsson, N.-G. (2014) Making proteins in the powerhouse. *Cell Metab.*,

20, 226–240.

Han, D., Dara, L., Win, S., Than, T.A., Yuan, L., Abbasi, S.Q., Liu, Z.-X., and Kaplowitz, N. (2013) Regulation of drug-induced liver injury by signal transduction pathways: critical role of mitochondria. *Trends Pharmacol. Sci.*, **34**, 243–253.

Heller, S., Schubert, S., Krehan, M., Schäfer, I., Seibel, M., Latorre, D., Villani, G., and Seibel, P. (2013) Efficient Repopulation of Genetically Derived Rho Zero Cells with Exogenous Mitochondria. *PLoS One*, **8**, e73207.

Hendrickson, S.L., Kingsley, L.A., Ruiz-Pesini, E., Poole, J.C., Jacobson, L.P., Palella, F.J., Bream, J.H., Wallace, D.C., and O'Brien, S.J. (2009) Mitochondrial DNA Haplogroups influence lipoatrophy after Highly Active Anti-retroviral Therapy. *J. Acquir. Immune Defic. Syndr.*, **51**, 111–116.

Herst, P.M., Tan, A.S., Scarlett, D.-J.G., and Berridge, M. V (2004) Cell surface oxygen consumption by mitochondrial gene knockout cells. *Biochim. Biophys. Acta (BBA)-Bioenergetics*, **1656**, 79–87.

Hewitt, N.J. *et al.* (2007) Primary hepatocytes: current understanding of the regulation of metabolic enzymes and transporter proteins, and pharmaceutical practice for the use of hepatocytes in metabolism, enzyme induction, transporter, clearance, and hepatotoxicity studies. *Drug Metab. Rev.*, **39**, 159–234.

Holt, I.J. and Jacobs, H.T. (2014) Unique features of DNA replication in mitochondria: a functional and evolutionary perspective. *Bioessays*, **36**, 1024–1031.

Holt, I.J. and Reyes, A. (2012) Human Mitochondrial DNA Replication. *Cold Spring Harb. Perspect. Biol.*, **4**.

Hussain, S., Haidar, A., Bloom, R.E., Zayouna, N., Piper, M.H., and Jafri, S.M. (2014) Bicalutamide-induced hepatotoxicity: A rare adverse effect. *Am J Case Rep*, **15**, 266–270.

Hutchinson, T. (2010) Glossary. *Int. Soc. Genet. Geneal.*

Hüttemann, M., Lee, I., Samavati, L., Yu, H., and Doan, J.W. (2007) Regulation of mitochondrial oxidative phosphorylation through cell signaling. *Biochim. Biophys. Acta (BBA)-Molecular Cell Res.*, **1773**, 1701–1720.

Ingolia, N.T., Ghaemmaghami, S., Newman, J.R.S., and Weissman, J.S. (2009) Genome-wide analysis in vivo of translation with nucleotide resolution using ribosome profiling. *Science*, **324**, 218–223.

Inoue, K., Ito, S., Takai, D., Soejima, A., Shisa, H., LePecq, J.B., Segal-Bendirdjian, E., Kagawa, Y., and Hayashi, J.I. (1997) Isolation of mitochondrial DNA-less mouse cell lines and their application for trapping mouse synaptosomal mitochondrial DNA with deletion mutations. *J. Biol. Chem.*, **272**, 15510–15515.

Jastroch, M., Divakaruni, A.S., Mookerjee, S., Treberg, J.R., and Brand, M.D. (2010) Mitochondrial proton and electron leaks. *Essays Biochem.*, **47**, 53–67.

Jazayeri, M., Andreyev, A., Will, Y., Ward, M., Anderson, C.M., and Clevenger, W. (2003) Inducible expression of a dominant negative DNA polymerase-gamma depletes mitochondrial DNA and produces a rho0 phenotype. *J. Biol. Chem.*, **278**, 9823–9830.

Jeong, J.-H., Yum, K.S., Chang, J.Y., Kim, M., Ahn, J., Kim, S., Lapchak, P.A., and Han, M.-K. (2015) Dose-specific effect of simvastatin on hypoxia-induced HIF-1α and BACE

expression in Alzheimer's disease cybrid cells. *BMC Neurol.*, **15**.

Jing, W. *et al.* (2015) Mitochondrial mutations associated with aminoglycoside ototoxicity and hearing loss susceptibility identified by meta-analysis. *J. Med. Genet.*, **52**, 95–103.

Jonckheere, A.I., Smeitink, J.A.M., and Rodenburg, R.J.T. (2012) Mitochondrial ATP synthase: architecture, function and pathology. *J. Inherit. Metab. Dis.*, **35**, 211–225.

Jorga, K., Fotteler, B., Heizmann, P., and Gasser, R. (1999) Metabolism and excretion of tolcapone, a novel inhibitor of catechol-O-methyltransferase. *Br. J. Clin. Pharmacol.*, **48**, 513–520.

Kallianpur, A.R. and Hulgan, T. (2009) Pharmacogenetics of nucleoside reverse-transcriptase inhibitor-associated peripheral neuropathy. *Pharmacogenomics*, **10**, 623–637.

Kalow, W. (2006) Pharmacogenetics and pharmacogenomics: origin, status, and the hope for personalized medicine. *Pharmacogenomics J.*, **6**, 162–165.

Kamalian, L., Chadwick, A.E., Bayliss, M., French, N.S., Monshouwer, M., Snoeys, J., and Park, B.K. (2015) The utility of HepG2 cells to identify direct mitochondrial dysfunction in the absence of cell death. *Toxicol. Vitr.*, **29**, 732–740.

Kampira, E., Kumwenda, J., van Oosterhout, J.J., and Dandara, C. (2013) Mitochondrial DNA subhaplogroups L0a2 and L2a modify susceptibility to peripheral neuropathy in malawian adults on stavudine containing highly active antiretroviral therapy. *J Acquir Immune Defic Syndr*, **63**, 647–652.

Kaplowitz, N. (2005) Idiosyncratic drug hepatotoxicity. *Nat. Rev. Drug Discov.*, **4**, 489–499.

Katajisto, P. *et al.* (2015) Asymmetric apportioning of aged mitochondria between daughter cells is required for stemness. *Science*, **348**, 340–343.

Kelly, R. (2018) Biochemical Thermodynamic Modelling of Cellular Bioenergetics: A Quantitative Systems Pharmacology Approach.

Kenna, J.G. and Uetrecht, J. (2018) Do In Vitro Assays Predict Drug Candidate Idiosyncratic Drug-Induced Liver Injury Risk? *Drug Metab. Dispos.*

Kennedy, J.A., Unger, S.A., and Horowitz, J.D. (1996) Inhibition of carnitine palmitoyltransferase-1 in rat heart and liver by perhexiline and amiodarone. *Biochem. Pharmacol.*, **52**, 273–280.

Kenney, M.C. *et al.* (2014) Molecular and bioenergetic differences between cells with African versus European inherited mitochondrial DNA haplogroups: implications for population susceptibility to diseases. *Biochim. Biophys. Acta (BBA)-Molecular Basis Dis.*, **1842**, 208–219.

Kenney, M.C. *et al.* (2013) Mitochondrial DNA variants mediate energy production and expression levels for CFH, C3 and EFEMP1 genes: implications for age-related macular degeneration. *PLoS One*, **8**, e54339.

Keränen, T., Gordin, A., Karlsson, M., Korpela, K., Pentikäinen, P.J., Rita, H., Schultz, E., Seppälä, L., and Wikberg, T. (1994) Inhibition of soluble catechol-O-methyltransferase and single-dose pharmacokinetics after oral and intravenous administration of entacapone. *Eur. J. Clin. Pharmacol.*, **46**, 151–157.

Khazaria (2000) No Title. *http://www.khazaria.com/genetics/irish.html [date accessed: 26-*

04-2018].

Khetani, S.R., Kanchagar, C., Ukairo, O., Krzyzewski, S., Moore, A., Shi, J., Aoyama, S., Aleo, M., and Will, Y. (2013) Use of micropatterned cocultures to detect compounds that cause drug-induced liver injury in humans. *Toxicol Sci*, **132**, 107–117.

King, M.P. and Attardi, G. (1989) Human cells lacking mtDNA: repopulation with exogenous mitochondria by complementation. *Science (80-.).*, **246**, 500–503.

Kitani, T., Kami, D., Matoba, S., and Gojo, S. (2014) Internalization of isolated functional mitochondria: involvement of macropinocytosis. *J. Cell. Mol. Med.*, **18**, 1694–1703.

Kloss-Brandstatter, A. *et al.* (2015) Validation of Next-Generation Sequencing of Entire Mitochondrial Genomes and the Diversity of Mitochondrial DNA Mutations in Oral Squamous Cell Carcinoma. *PLoS One*, **10**.

Knerr, S., Wayman, D., and Bonham, V.L. (2011) Inclusion of Racial and Ethnic Minorities in Genetic Research: Advance the Spirit by Changing the Rules? *J. Law. Med. Ethics*, **39**, 502–512.

Koboldt, D.C., Chen, K., Wylie, T., Larson, D.E., McLellan, M.D., Mardis, E.R., Weinstock, G.M., Wilson, R.K., and Ding, L. (2009) VarScan: variant detection in massively parallel sequencing of individual and pooled samples. *Bioinformatics*, **25**, 2283–2285.

Koboldt, D.C. *et al.* (2012) VarScan 2: somatic mutation and copy number alteration discovery in cancer by exome sequencing. *Genome Res.*, **22**, 568–576.

Konkel, L. (2015) Racial and Ethnic Disparities in Research Studies: The Challenge of Creating More Diverse Cohorts. *Environ. Health Perspect.*, **123**, 297–302.

Korlipara, L. V, Cooper, J.M., and Schapira, A.H. (2004) Differences in toxicity of the catechol-O-methyl transferase inhibitors, tolcapone and entacapone to cultured human neuroblastoma cells. *Neuropharmacology*, **46**, 562–569.

Kramer, P.A., Ravi, S., Chacko, B., Johnson, M.S., and Darley-Usmar, V.M. (2014) A review of the mitochondrial and glycolytic metabolism in human platelets and leukocytes: Implications for their use as bioenergetic biomarkers. *Redox Biol.*, **2**, 206–210.

Kühlbrandt, W. (2015) Structure and function of mitochondrial membrane protein complexes. *BMC Biol.*, **13**, 1–11.

Kukat, C., Wurm, C.A., Spahr, H., Falkenberg, M., Larsson, N.-G., and Jakobs, S. (2011) Super-resolution microscopy reveals that mammalian mitochondrial nucleoids have a uniform size and frequently contain a single copy of mtDNA. *Proc. Natl. Acad. Sci. U. S. A.*, **108**, 13534–13539.

Kunau, W.H., Dommes, V., and Schulz, H. (1995) beta-oxidation of fatty acids in mitochondria, peroxisomes, and bacteria: a century of continued progress. *Prog. Lipid Res.*, **34**, 267–342.

Kushnareva, Y., Murphy, A.N., and Andreyev, A. (2002) Complex I-mediated reactive oxygen species generation: modulation by cytochrome c and NAD(P)+ oxidation-reduction state. *Biochem. J.*, **368**, 545–553.

Kussmaul, L. and Hirst, J. (2006) The mechanism of superoxide production by NADH:ubiquinone oxidoreductase (complex I) from bovine heart mitochondria. *Proc. Natl. Acad. Sci. U. S. A.*, **103**, 7607–7612.

Kuznetsov, A. V, Veksler, V., Gellerich, F.N., Saks, V., Margreiter, R., and Kunz, W.S. (2008) Analysis of mitochondrial function in situ in permeabilized muscle fibers, tissues and cells. *Nat. Protoc*, **3**, 965–976.

Labbe, G., Pessayre, D., and Fromenty, B. (2008) Drug-induced liver injury through mitochondrial dysfunction: mechanisms and detection during preclinical safety studies. *Fundam. Clin. Pharmacol.*, **22**, 335–353.

Larosche, I., Letteron, P., Fromenty, B., Vadrot, N., Abbey-Toby, A., Feldmann, G., Pessayre, D., and Mansouri, A. (2007) Tamoxifen inhibits topoisomerases, depletes mitochondrial DNA, and triggers steatosis in mouse liver. *J. Pharmacol. Exp. Ther.*, **321**, 526–535.

Larsson, N.-G. and Clayton, D.A. (1995) Molecular genetic aspects of human mitochondrial disorders. *Annu. Rev. Genet.*, **29**, 151–178.

LeCluyse, E.L., Witek, R.P., Andersen, M.E., and Powers, M.J. (2012) Organotypic liver culture models: meeting current challenges in toxicity testing. *Crit. Rev. Toxicol.*, **42**, 501–548.

Lees, A.J. (2008) Evidence-based efficacy comparison of tolcapone and entacapone as adjunctive therapy in Parkinson's disease. *CNS Neurosci. Ther.*, **14**, 83–93.

Lewis, W., Levine, E.S., Griniuviene, B., Tankersley, K.O., Colacino, J.M., Sommadossi, J.P., Watanabe, K.A., and Perrino, F.W. (1996) Fialuridine and its metabolites inhibit DNA polymerase gamma at sites of multiple adjacent analog incorporation, decrease mtDNA abundance, and cause mitochondrial structural defects in cultured hepatoblasts. *Proc. Natl. Acad. Sci. U. S. A.*, **93**, 3592–3597.

Li, H. and Durbin, R. (2009) Fast and accurate short read alignment with Burrows-Wheeler transform. *Bioinformatics*, **25**.

Li, J. and Uetrecht, J.P. (2010) The danger hypothesis applied to idiosyncratic drug reactions. *Handb. Exp. Pharmacol.*, 493–509.

Li, N., Ragheb, K., Lawler, G., Sturgis, J., Rajwa, B., Melendez, J.A., and Robinson, J.P. (2003) Mitochondrial complex I inhibitor rotenone induces apoptosis through enhancing mitochondrial reactive oxygen species production. *J. Biol. Chem.*, **278**, 8516–8525.

Liang, M. *et al.* (2009) Leber's hereditary optic neuropathy is associated with mitochondrial ND1 T3394C mutation. *Biochem. Biophys. Res. Commun.*, **383**, 286–292.

Lim, M.S., Lim, P.L.K., Gupta, R., and Boelsterli, U.A. (2006) Critical role of free cytosolic calcium, but not uncoupling, in mitochondrial permeability transition and cell death induced by diclofenac oxidative metabolites in immortalized human hepatocytes. *Toxicol. Appl. Pharmacol.*, **217**, 322–331.

Longo, D.M., Yang, Y., Watkins, P.B., Howell, B.A., and Siler, S.Q. (2016) Elucidating Differences in the Hepatotoxic Potential of Tolcapone and Entacapone With DILIsym((R)), a Mechanistic Model of Drug-Induced Liver Injury. *CPT pharmacometrics Syst. Pharmacol.*, **5**, 31–39.

Di Lorenzo, C. *et al.* (2009) Mitochondrial DNA haplogroups influence the therapeutic response to riboflavin in migraineurs. *Neurology*, **72**, 1588–1594.

Luo, Y., Bond, J.D., and Ingram, V.M. (1997) Compromised mitochondrial function leads to increased cytosolic calcium and to activation of MAP kinases. *Proc. Natl. Acad. Sci.*, **94**,

9705–9710.

Machlus, K.R. and Italiano, J.E. (2013) The incredible journey: From megakaryocyte development to platelet formation. *J. Cell Biol.*, **201**, 785–796.

MacVicar, T.D.B. and Lane, J.D. (2014) Impaired OMA1-dependent cleavage of OPA1 and reduced DRP1 fission activity combine to prevent mitophagy in cells that are dependent on oxidative phosphorylation. *J. Cell Sci.*, **127**, 2313–2325.

Maddukuri, V.C. and Bonkovsky, H.L. (2014) Herbal and dietary supplement hepatotoxicity. *Clin. Liver Dis.*, **4**, 1–3.

Malik, A.N., Shahni, R., Rodriguez-de-Ledesma, A., Laftah, A., and Cunningham, P. (2011) Mitochondrial DNA as a non-invasive biomarker: Accurate quantification using real time quantitative PCR without co-amplification of pseudogenes and dilution bias. *Biochem. Biophys. Res. Commun.*, **412**, 1–7.

Marcuello, A., Martinez-Redondo, D., Dahmani, Y., Casajus, J.A., Ruiz-Pesini, E., Montoya, J., Lopez-Perez, M.J., and Diez-Sanchez, C. (2009) Human mitochondrial variants influence on oxygen consumption. *Mitochondrion*, **9**, 27–30.

Marin-Hernandez, A., Gallardo-Perez, J.C., Ralph, S.J., Rodriguez-Enriquez, S., and Moreno-Sanchez, R. (2009) HIF-1alpha modulates energy metabolism in cancer cells by inducing over-expression of specific glycolytic isoforms. *Mini Rev. Med. Chem.*, **9**, 1084–1101.

Marroquin, L.D., Hynes, J., Dykens, J.A., Jamieson, J.D., and Will, Y. (2007) Circumventing the Crabtree effect: replacing media glucose with galactose increases susceptibility of HepG2 cells to mitochondrial toxicants. *Toxicol. Sci*, **97**, 539–547.

Micheloud, D. *et al.* (2011) European mitochondrial DNA haplogroups and metabolic disorders in HIV/HCV-coinfected patients on highly active antiretroviral therapy. *J Acquir Immune Defic Syndr*, **58**, 371–378.

Michikawa, Y., Mazzucchelli, F., Bresolin, N., Scarlato, G., and Attardi, G. (1999) Aging-dependent large accumulation of point mutations in the human mtDNA control region for replication. *Science*, **286**, 774–779.

Miller, J.H., Lewontin, R.C., Gelbart, W.M., and Griffiths, A.J.F. (2002) Molecular Cell Biology 4th Edition & Cd-rom Macmillan Higher Education.

Miller, S.W., Trimmer, P.A., Parker Jr, W.D., and Davis, R.E. (1996) Creation and characterization of mitochondrial DNA-depleted cell lines with “neuronal-like” properties. *J. Neurochem.*, **67**, 1897–1907.

Mineri, R., Pavelka, N., Fernandez-Vizarra, E., Ricciardi-Castagnoli, P., Zeviani, M., and Tiranti, V. (2009) How do human cells react to the absence of mitochondrial DNA? *PLoS One*, **4**, e5713.

Mishmar, D. *et al.* (2003) Natural selection shaped regional mtDNA variation in humans. *Proc Natl Acad Sci U S A*, **100**.

Miyazono, Y., Hirashima, S., Ishihara, N., Kusukawa, J., Nakamura, K., and Ohta, K. (2018) Uncoupled mitochondria quickly shorten along their long axis to form indented spheroids, instead of rings, in a fission-independent manner. *Sci. Rep.*, **8**, 350.

Mookerjee, S.A., Divakaruni, A.S., Jastroch, M., and Brand, M.D. (2010) Mitochondrial uncoupling and lifespan. *Mech. Ageing Dev.*, **131**, 463–472.

Morozov, Y.I., Agaronyan, K., Cheung, A.C.M., Anikin, M., Cramer, P., and Temiakov, D. (2014) A novel intermediate in transcription initiation by human mitochondrial RNA polymerase. *Nucleic Acids Res.*, **42**, 3884–3893.

Mueller, E.E. (2012) Functional Differences between Mitochondrial Haplogroup T and Haplogroup H in HEK293 Cybrid Cells. **7**.

Murphy, M.P. (2009) How mitochondria produce reactive oxygen species. *Biochem. J.*, **417**, 1–13.

Nagler, C., Zanker, K.S., and Dittmar, T. (2011) Cell Fusion, Drug Resistance and Recurrence CSCs. *Adv. Exp. Med. Biol.*, **714**, 173–182.

Nascimento, A., Lannigan, J., and Kashatus, D. (2016) High-throughput detection and quantification of mitochondrial fusion through imaging flow cytometry. *Cytometry. A*, **89**, 708–719.

Nass, M.M. and Nass, S. (1963) Intramitochondrial Fibers with DNA Characteristics. I. Fixation and Electron Staining Reactions. *J Cell Biol*, **19**, 593–611.

Naven, R.T., Swiss, R., Mcleod, J.K., Will, Y., and Greene, N. (2012) The Development of a Structure-Activity Relationships for Mitochondrial Dysfunction: Uncoupling of Oxidative Phosphorylation. *Toxicol. Sci.*, kfs279.

Nicholls, D.G. and Ferguson, S.J. (2003) 5 - Respiratory chains. In, Nicholls,D.G. and Ferguson,S.J.B.T.-B. (Third E. (eds). Academic Press, London, p. 89–XIII.

Olanow, C.W. (2000) Tolcapone and hepatotoxic effects. Tasmar Advisory Panel. *Arch. Neurol.*, **57**, 263–267.

Olanow, C.W. and Watkins, P.B. (2007) Tolcapone: an efficacy and safety review. *Clin. Neuropharmacol.*, **30**, 287–294.

Ouma, S. *et al.* (2017) The Risk Factors for the Wearing-off Phenomenon in Parkinson's Disease in Japan: A Cross-sectional, Multicenter Study. *Intern. Med.*, **56**, 1961–1966.

Van den Ouweland, J.M., Maechler, P., Wollheim, C.B., Attardi, G., and Maassen, J.A. (1999) Functional and morphological abnormalities of mitochondria harbouring the tRNA(Leu)(UUR) mutation in mitochondrial DNA derived from patients with maternally inherited diabetes and deafness (MIDD) and progressive kidney disease. *Diabetologia*, **42**, 485–492.

Van den Ouweland, J.M., Lemkes, H.H., Ruitenbeek, W., Sandkuijl, L.A., de Vijlder, M.F., Struyvenberg, P.A., van de Kamp, J.J., and Maassen, J.A. (1992) Mutation in mitochondrial tRNA(Leu)(UUR) gene in a large pedigree with maternally transmitted type II diabetes mellitus and deafness. *Nat. Genet.*, **1**, 368–371.

Van Oven, M. and Kayser, M. (2009) Updated comprehensive phylogenetic tree of global human mitochondrial DNA variation. *Hum Mutat*, **30**.

Pacheu-Grau, D., Gómez-Durán, A., Iglesias, E., López-Gallardo, E., Montoya, J., and Ruiz-Pesini, E. (2012) Mitochondrial antibiograms in personalized medicine. *Hum. Mol. Genet.*, dds517.

Pandit, A., Sachdeva, T., and Bafna, P. (2012) Drug-induced hepatotoxicity: A review.

Paradies, G., Paradies, V., De Benedictis, V., Ruggiero, F.M., and Petrosillo, G. (2014) Functional role of cardiolipin in mitochondrial bioenergetics. *Biochim. Biophys. Acta* -

Bioenerg., **1837**, 408–417.

Patel, D., Rorbach, J., Downes, K., Szukszto, M.J., Pekalski, M.L., and Minczuk, M. (2017) Macropinocytic entry of isolated mitochondria in epidermal growth factor-activated human osteosarcoma cells. *Sci. Rep.*, **7**.

Patel, S.R., Hartwig, J.H., and Italiano, J.E. (2005) The biogenesis of platelets from megakaryocyte proplatelets. *J. Clin. Invest.*, **115**, 3348–3354.

Pello, R. *et al.* (2008) Mitochondrial DNA background modulates the assembly kinetics of OXPHOS complexes in a cellular model of mitochondrial disease. *Hum. Mol. Genet.*, **17**, 4001–4011.

Perry, C.G.R., Kane, D.A., Lanza, I.R., and Neufer, P.D. (2013) Methods for assessing mitochondrial function in diabetes. *Diabetes*, **62**, 1041–1053.

Perry, S.W., Norman, J.P., Barbieri, J., Brown, E.B., and Gelbard, H.A. (2011) Mitochondrial membrane potential probes and the proton gradient: a practical usage guide. *Biotechniques*, **50**, 98–115.

Pignataro, D., Francia, S., Zanetta, F., Brenna, G., Brandini, S., Olivieri, A., Torroni, A., Biamonti, G., and Montecucco, A. (2017) A missense MT-ND5 mutation in differentiated Parkinson Disease cytoplasmic hybrid induces ROS-dependent DNA Damage Response amplified by DROSHA. *Sci. Rep.*, **7**, 9528.

Poillet-Perez, L., Despouy, G., Delage-Mourroux, R., and Boyer-Guittaut, M. (2015) Interplay between ROS and autophagy in cancer cells, from tumor initiation to cancer therapy. *Redox Biol.*, **4**, 184–192.

Porras, C.A. and Bai, Y. (2015) Respiratory supercomplexes: plasticity and implications. *Front. Biosci. (Landmark Ed.*, **20**, 621–634.

Rachek, L.I., Yuzefovych, L. V, Ledoux, S.P., Julie, N.L., and Wilson, G.L. (2009) Troglitazone, but not rosiglitazone, damages mitochondrial DNA and induces mitochondrial dysfunction and cell death in human hepatocytes. *Toxicol. Appl. Pharmacol.*, **240**, 348–354.

Ravi, S., Chacko, B., Kramer, P.A., Sawada, H., Johnson, M.S., Zhi, D., Marques, M.B., and Darley-Usmar, V.M. (2015) Defining the effects of storage on platelet bioenergetics; the role of increased proton leak. *Biochim. Biophys. Acta*, **1852**, 2525–2534.

Regev, A. (2014) Drug-induced liver injury and drug development: industry perspective. *Semin. Liver Dis.*, **34**, 227–239.

Reitzer, L.J., Wice, B.M., and Kennell, D. (1979) Evidence that glutamine, not sugar, is the major energy source for cultured HeLa cells. *J. Biol. Chem.*, **254**, 2669–2676.

Rems, L., Usaj, M., Kanduser, M., Rebersek, M., Miklavcic, D., and Pucihar, G. (2013) Cell electrofusion using nanosecond electric pulses. *Sci. Rep.*, **3**, 3382.

Rimmelé, P. *et al.* (2015) Mitochondrial metabolism in hematopoietic stem cells requires functional FOXO3. *EMBO Rep.*, **16**, 1164–1176.

Rivest, J., Barclay, C.L., and Suchowersky, O. (1999) COMT inhibitors in Parkinson's disease. *Can. J. Neurol. Sci.*, **26 Suppl 2**, S34-8.

Rodriguez, R.J. and Acosta, D.J. (1996) Inhibition of mitochondrial function in isolated rate liver mitochondria by azole antifungals. *J. Biochem. Toxicol.*, **11**, 127–131.

Roth, A.D. and Lee, M.-Y. (2017) Idiosyncratic Drug-Induced Liver Injury (IDILI): Potential Mechanisms and Predictive Assays. *Biomed Res. Int.*, **2017**.

Ruiz-Pesini, E., Mishmar, D., Brandon, M., Procaccio, V., and Wallace, D.C. (2004) Effects of purifying and adaptive selection on regional variation in human mtDNA. *Science (80-.).*, **303**.

Russmann, S., Kullak-Ublick, G.A., and Grattagliano, I. (2009) Current concepts of mechanisms in drug-induced hepatotoxicity. *Curr. Med. Chem*, **16**, 3041.

Saelens, X., Festjens, N., Vande Walle, L., van Gurp, M., van Loo, G., and Vandenabeele, P. (2004) Toxic proteins released from mitochondria in cell death. *Oncogene*, **23**, 2861–2874.

Salabei, J.K., Gibb, A.A., and Hill, B.G. (2014) Comprehensive measurement of respiratory activity in permeabilized cells using extracellular flux analysis. *Nat. Protoc*, **9**, 421–438.

Scaduto, R.C. and Grotyohann, L.W. (1999) Measurement of mitochondrial membrane potential using fluorescent rhodamine derivatives. *Biophys. J.*, **76**, 469–477.

Scatena, R., Bottoni, P., Martorana, G.E., Ferrari, F., De Sole, P., Rossi, C., and Giardina, B. (2004) Mitochondrial respiratory chain dysfunction, a non-receptor-mediated effect of synthetic PPAR-ligands: biochemical and pharmacological implications. *Biochem. Biophys. Res. Commun.*, **319**, 967–973.

Schäfer, I. (University of L. (2016) Personal Communication.

Scheffler, I.E. (2008) Basic Molecular Biology of Mitochondrial Replication. In, *Drug-Induced Mitochondrial Dysfunction*. Wiley-Blackwell, pp. 37–70.

Scheibye-Knudsen, M., Fang, E.F., Croteau, D.L., and Bohr, V.A. (2014) Contribution of defective mitophagy to the neurodegeneration in DNA repair-deficient disorders. *Autophagy*, **10**, 1468–1469.

Schirris, T.J.J. *et al.* (2015) Statin-Induced Myopathy Is Associated with Mitochondrial Complex III Inhibition. *Cell Metab.*, **22**, 399–407.

Schon, E.A., DiMauro, S., and Hirano, M. (2012) Human mitochondrial DNA: roles of inherited and somatic mutations. *Nat Rev Genet*, **13**, 878–890.

Schubert, S., Heller, S., Löffler, B., Schäfer, I., Seibel, M., Villani, G., and Seibel, P. (2015) Generation of Rho Zero Cells: Visualization and Quantification of the mtDNA Depletion Process. *Int. J. Mol. Sci.*, **16**, 9850–9865.

Schulz, M., Schmoldt, A., Donn, F., and Becker, H. (1988) The pharmacokinetics of flutamide and its major metabolites after a single oral dose and during chronic treatment. *Eur J Clin Pharmacol*, **34**, 633–636.

Shet, M.S., McPhaul, M., Fisher, C.W., Stallings, N.R., and Estabrook, R.W. (1997) Metabolism of the antiandrogenic drug (Flutamide) by human CYP1A2. *Drug Metab. Dispos*, **25**, 1298–1303.

Sikora, E., Mosieniak, G., and Sliwinska, M.A. (2016) Morphological and Functional Characteristic of Senescent Cancer Cells. *Curr. Drug Targets*, **17**, 377–387.

Silva, D.F. *et al.* (2013) Bioenergetic flux, mitochondrial mass and mitochondrial morphology dynamics in AD and MCI cybrid cell lines. *Hum. Mol. Genet.*, **22**, 3931–3946.

Sison-Young, R.L. *et al.* (2015) Comparative Proteomic Characterization of 4 Human Liver-Derived Single Cell Culture Models Reveals Significant Variation in the Capacity for Drug Disposition, Bioactivation, and Detoxication. *Toxicol Sci*, **147**, 412–424.

Smits, P., Smeitink, J., and van den Heuvel, L. (2010) Mitochondrial Translation and Beyond: Processes Implicated in Combined Oxidative Phosphorylation Deficiencies. *J. Biomed. Biotechnol.*, **2010**, 24.

Song, S., Pursell, Z.F., Copeland, W.C., Longley, M.J., Kunkel, T.A., and Mathews, C.K. (2005) DNA precursor asymmetries in mammalian tissue mitochondria and possible contribution to mutagenesis through reduced replication fidelity. *Proc. Natl. Acad. Sci. U. S. A.*, **102**, 4990–4995.

Srinivasan, S., Guha, M., Dong, D.W., Whelan, K.A., Ruthel, G., Uchikado, Y., Natsugoe, S., Nakagawa, H., and Avadhani, N.G. (2015) Disruption of cytochrome c oxidase function induces the Warburg effect and metabolic reprogramming. *Oncogene*.

Starikovskaya, E.B. *et al.* (2005) Mitochondrial DNA Diversity in Indigenous Populations of the Southern Extent of Siberia, and the Origins of Native American Haplogroups. *Ann. Hum. Genet.*, **69**, 67–89.

Stein, L.R. and Imai, S. (2012) The dynamic regulation of NAD metabolism in mitochondria. *Trends Endocrinol. Metab.*, **23**, 420–428.

Stewart, J.B. and Chinnery, P.F. (2015) The dynamics of mitochondrial DNA heteroplasmy: implications for human health and disease. *Nat Rev Genet*, **16**, 530–542.

Suissa, S., Wang, Z., Poole, J., Wittkopp, S., Feder, J., Shutt, T.E., Wallace, D.C., Shadel, G.S., and Mishmar, D. (2009) Ancient mtDNA Genetic Variants Modulate mtDNA Transcription and Replication. *PLoS Genet.*, **5**.

Sun, D., Li, B., Qiu, R., Fang, H., and Lyu, J. (2016) Cell Type-Specific Modulation of Respiratory Chain Supercomplex Organization. *Int. J. Mol. Sci.*, **17**.

Swerdlow, R.H., Parks, J.K., Miller, S.W., Tuttle, J.B., Trimmer, P.A., Sheehan, J.P., Bennett, J.P.J., Davis, R.E., and Parker, W.D.J. (1996) Origin and functional consequences of the complex I defect in Parkinson's disease. *Ann. Neurol.*, **40**, 663–671.

Taddeo, E.P. *et al.* (2014) Opening of the mitochondrial permeability transition pore links mitochondrial dysfunction to insulin resistance in skeletal muscle(). *Mol. Metab.*, **3**, 124–134.

Tarrago-Litvak, L., Viratelle, O., Darriet, D., Dalibart, R., Graves, P. V, and Litvak, S. (1978) The inhibition of mitochondrial DNA polymerase gamma from animal cells by intercalating drugs. *Nucleic Acids Res.*, **5**, 2197–2210.

Thon, J.N. and Italiano, J.E. (2012) Platelets: production, morphology and ultrastructure. *Handb. Exp. Pharmacol.*, 3–22.

Tolosa, L., Jiménez, N., Pérez, G., Castell, J. V, Gómez-Lechón, M.J., and Donato, M.T. (2018) Customised in vitro model to detect human metabolism-dependent idiosyncratic drug-induced liver injury. *Arch. Toxicol.*, **92**, 383–399.

Torres, A.S. *et al.* (2014) Platelet activation using electric pulse stimulation: growth factor profile and clinical implications. *J. Trauma Acute Care Surg.*, **77**, S94–S100.

Trounce, I., Neill, S., and Wallace, D.C. (1994) Cytoplasmic transfer of the mtDNA nt 8993 T->G (ATP6) point mutation associated with Leigh syndrome into mtDNA-less cells

demonstrates cosegregation with a decrease in state III respiration and ADP/O ratio. *Proc. Natl. Acad. Sci. U. S. A.*, **91**, 8334–8338.

Turrens, J.F. (2003) Mitochondrial formation of reactive oxygen species. *J. Physiol.*, **552**, 335–344.

Vinogradov, A.D. and Grivennikova, V.G. (2016) Oxidation of NADH and ROS production by respiratory complex I. *Biochim. Biophys. Acta - Bioenerg.*, **1857**, 863–871.

Vithayathil, S.A., Ma, Y., and Kaipparettu, B.A. (2012) Transmitochondrial cybrids: tools for functional studies of mutant mitochondria. *Methods Mol. Biol.*, **837**, 219–230.

Vuda, M. and Kamath, A. (2016) Drug induced mitochondrial dysfunction: Mechanisms and adverse clinical consequences. *Mitochondrion*, **31**, 63–74.

Walker, U.A. *et al.* (2004) Depletion of mitochondrial DNA in liver under antiretroviral therapy with didanosine, stavudine, or zalcitabine. *Hepatology*, **39**, 311–317.

Wallace, D.C. (2015) Mitochondrial DNA Variation in Human Radiation and Disease. *Cell*, **163**, 33–38.

Wallace, D.C. and Chalkia, D. (2013) Mitochondrial DNA genetics and the heteroplasmy conundrum in evolution and disease. *Cold Spring Harb. Perspect. Biol.*, **5**, a021220.

Wallace, K.B. and Starkov, A.A. (2000) Mitochondrial targets of drug toxicity. *Annu. Rev. Pharmacol. Toxicol.*, **40**, 353–388.

Wanders, R.J.A., Komen, J., and Kemp, S. (2011) Fatty acid omega-oxidation as a rescue pathway for fatty acid oxidation disorders in humans. *FEBS J.*, **278**, 182–194.

Warden, C.D., Adamson, A.W., Neuhausen, S.L., and Wu, X. (2014) Detailed comparison of two popular variant calling packages for exome and targeted exon studies. *PeerJ*, **2**, e600.

Watkins, P. (2000) COMT inhibitors and liver toxicity. *Neurology*, **55**, S51-2; discussion S53-6.

Weissensteiner, H., Pacher, D., Kloss-Brandstatter, A., Forer, L., Specht, G., Bandelt, H.-J., Kronenberg, F., Salas, A., and Schonherr, S. (2016) HaploGrep 2: mitochondrial haplogroup classification in the era of high-throughput sequencing. *Nucleic Acids Res.*, **44**, W58-63.

Westerink, W.M.A. and Schoonen, W.G.E.J. (2007) Cytochrome P450 enzyme levels in HepG2 cells and cryopreserved primary human hepatocytes and their induction in HepG2 cells. *Toxicol. In Vitro*, **21**, 1581–1591.

Westermann, B. (2012) Bioenergetic role of mitochondrial fusion and fission. *Biochim. Biophys. Acta - Bioenerg.*, **1817**, 1833–1838.

Wiesner, R.J., Zsurka, G., and Kunz, W.S. (2006) Mitochondrial DNA damage and the aging process: facts and imaginations. *Free Radic. Res.*, **40**, 1284–1294.

Van der Wijst, M.G.P. and Rots, M.G. (2015) Mitochondrial epigenetics: an overlooked layer of regulation? *Trends Genet.*, **31**, 353–356.

Wilkens, L., Hammer, C., Glombitza, S., and Muller, D.-E. (2012) Hepatocellular and cholangiolar carcinoma-derived cell lines reveal distinct sets of chromosomal imbalances. *Pathobiology*, **79**, 115–126.

Wilkins, H.M., Carl, S.M., and Swerdlow, R.H. (2014) Cytoplasmic hybrid (cybrid) cell lines as a practical model for mitochondriopathies. *Redox Biol.*, **2**, 619–631.

Will, Y. and Dykens, J. (2014) Mitochondrial toxicity assessment in industry--a decade of technology development and insight. *Expert Opin. Drug Metab. Toxicol.*, **10**, 1061–1067.

Wintrobe, M.M. (2009) Wintrobe's clinical hematology Lippincott Williams & Wilkins.

Wojtczak, L. and Zabłocki, K. (2008) Basic Mitochondrial Physiology in Cell Viability and Death. In, *Drug-Induced Mitochondrial Dysfunction*. John Wiley & Sons, Inc., pp. 1–35.

Wu, M., Kalyanasundaram, A., and Zhu, J. (2013) Structural and biomechanical basis of mitochondrial movement in eukaryotic cells. *Int. J. Nanomedicine*, **8**, 4033–4042.

Wysowski, D.K. and Fourcroy, J.L. (1996) Flutamide hepatotoxicity. *J. Urol.*, **155**, 209–212.

Xu, J.J., Henstock, P. V, Dunn, M.C., Smith, A.R., Chabot, J.R., and de Graaf, D. (2008) Cellular imaging predictions of clinical drug-induced liver injury. *Toxicol. Sci.*, **105**, 97–105.

Yuan, L. and Kaplowitz, N. (2013) Mechanisms of Drug Induced Liver Injury. *Clin. Liver Dis.*, **17**, 507–518.

Zanella, F., Lorens, J.B., and Link, W. (2010) High content screening: seeing is believing. *Trends Biotechnol.*, **28**, 237–245.

Zylber, E., Vesco, C., and Penman, S. (1969) Selective inhibition of the synthesis of mitochondria-associated RNA by ethidium bromide* 1.

MITOMAP *https://www.mitomap.org/foswiki/bin/view/MITOMAP/MitoPolypeptide [date accessed: 07-09-2018]*.

HepG2.com *[date accessed: 26-09-2018]*.